SBUF

ID: 13842

NCC

# DESIGN OF FOUNDATIONS FOR HIGH-SPEED RAILWAY EMBANKMENTS

*A methodology for setting-up and performing numerical calculations of ground vibrations*

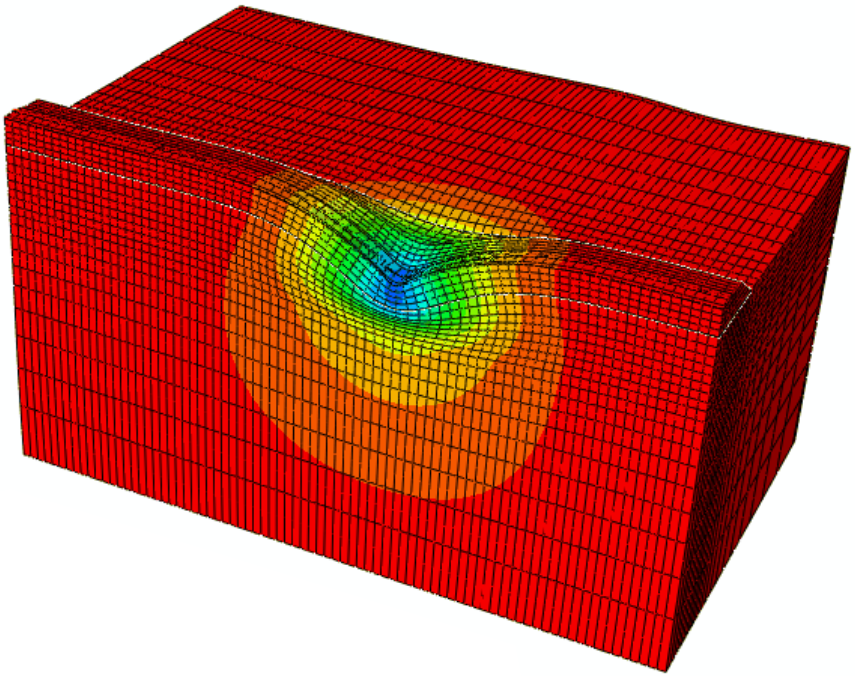

**Lars Hall, Jou-Yi Shih, Jesus Armesto Barros, Abbas Zangeneh, Costin Pacoste, Jörgen Johansson & Amir M Kaynia**

**2022-02-28**

# PREFACE

This project was carried out during the period between February 2020 to February 2022 and concerned calculation of train-induced ground vibrations in railway embankments. The work was performed in two working groups. – where one group was focusing on developing numerical calculations, while the other group was focusing on developing simplified calculation tools. The following people have worked in this project:

- Lars Hall (NCC Sverige) – was project manager for the work group of numerical calculation. It is Lars' idea that lies behind the basic model methodology. Lars has been responsible for setting up the input file concerning embankment materials, soil properties and ground reinforcement to the developed base model program. He is also the main author of chapters 1, 2, 3, 7.1, 8 and co-author to chapter 7.2 and 7.4.
- Jou-Yi Shih (NCC Sverige/ Zynamic AB) – was the main designer in the work group of numerical calculation and thereby was responsible in the programming of the developed shell program in base model methodology. Jou-Yi also provided valuable input in the optimization of the numerical modeling and how to control that the calculations behaves correctly. Jou-Yi also verified the developed base model program against a published reference case and against the Ledsgård case history. She is the main author of chapter 5 and co-author of chapter 7.2 and 7.4.
- Jesus Armesto Barros (NCC Sverige AB) – provided valuable help in how the in base model methodology could be set-up and has help in the programming of the shell program.
- Abbas Zangeneh (ELU Konsult AB) - performed analyzes in how the numerical calculations could be optimized and is main author of chapter 4 and chapter 5.4.1. Abbas also programmed the equivalent linear subroutine to the base model program.
- Costin Pacoste (ELU Konsult AB) - was our expert in numerical modeling and responsible in the strategy how the numerical calculations could be optimized. Costin's expert knowledge in numerical modeling have been a great resource for developing the base model methodology.
- Jörgen Johansson (NGI) - was the project manager for the work group of simplified calculation tools. He performed the comparison calculation using the VibTrain program and is the main author of chapter 6 and 7.3. Jörgen also provided support in the evaluations of soil properties and is the author of *Appendix A* concerning NGI:s experience on advanced soil modeling.
- Amir M Kaynia (NGI) - was main designer in the work group for simplified calculation tools and the author behind the VibTrain program.

To ensure that the projects were conducted in the right direction, regular meetings were held with a steering group that consisted of Johan Jonsson (Trafikverket), Prof. Stefan Larsson (KTH) and Geir Svanø (BaneNOR). Their support and help during the progresses of this project are greatly appreciated. A reference group was also put together to ensure that the work was carried out with a sufficiently high quality. The reference group consisted of Peter Claesson (Skanska Sverige AB), Karl Lundstedt (Skanska Sverige AB), Prof. Nils Rydén (PEAB), P-E Bengtsson (PEB Geoteknik AB) and Prof. Jelke Dijkstra (Chalmers). Their critical review at the beginning of the project has been a source of further quality improvement of our work.

The project was financed by Trafikverket (Swedish Transport Administration), SBUF (Swedish Construction Industry Development Fund), NCC Sverige AB and BaneNOR (Norwegian Railways Administration). This made it possible to carry out the project and their support is therefore much appreciated. Special thanks also to Staffan Hinzte (formerly at NCC) and prof. Stefan Larsson (KTH) for their help in the process of finding finical support for this project.

# SUMMARY

In this project a user-friendly methodology, for efficient numerical calculations of train-induced ground vibrations in the railway embankments, has been developed. This was made by creating an input file for setting up the problem and a shell program that reads the input file, creates, and runs the model of the problem on a commercial numerical software, and also extracts the results from the calculations to an output file. By this the calculations could be automized and thus become easy to use.

The developed methodology, called the base model methodology, was applied to a published reference case and to a case history with vibrations measurements before and after a ground reinforcement with lime-cement columns. Based on these analyzes, it was concluded that the methodology works well, and good agreements were obtained with the reference case and the case history with vibration measurements. With the base model methodology, the risk for large ground vibrations for planned new and existing railway embankments can be controlled and any required ground reinforcement with lime-cement columns can be designed and optimized based on permissible vibration requirements for planned new railway lines

With this methodology, less time and work is needed in the numerical modeling of the problem. Also, the need to have high knowledge to use advanced numerical computer programs decreases. This form of analyses thus becomes more user-friendly, more people can perform these analyses and thereby increases the understanding the knowledge for this kind of problem. Since the methodology will save both working hours and computing time, this will create more time for optimizing the foundation of railway embankments. This methodology can therefore be very useful in the design of the forthcoming major infrastructure projects of new railways lines in the Nordic countries.



# SAMMANFATTNING

I detta projekt har en användarvänlig metodik, för effektiva numeriska beräkningar av tåginducerade markvibrationer i järnvägsbankar, utvecklats. Detta har utförts genom att skapa en indatafil för att sätta upp problemet och skapa ett skalprogram som läser indatafilen, skapar och kör modellen av problemet på en kommersiell numerisk programvara, extraherar resultaten från beräkningarna av problemet och sparar resultatet i en utdatafil. Genom detta kunde beräkningarna automatiseras och blev därmed lättanvända.

Den utvecklade metodiken, kallad basmodellsmetodiken, tillämpades på ett publicerat referensfall och på en fallstudie med vibrationsmätningar före och efter en grundförstärkning med kalkcementpelare. Utifrån dessa analyser drogs slutsatsen att metodiken fungerar väl och god överensstämmelse erhölls med referensfallet och fallstudien med vibrationsmätningar. Med basmodellsmetodiken kan risken för stora markvibrationer för planerade nya och befintliga järnvägsbankar kontrolleras och eventuell markförstärkning med kalkcementpelare kan utformas och optimeras utifrån tillåtna vibrationskrav för planerade nya järnvägslinjer.

Med denna metodik behövs mindre tid och arbete i den numerisk modellering av problemställningen. Dessutom minskar behovet av att ha hög kunskap av att använda avancerade numeriska datorprogram. Denna analysform blir därmed mer användarvänlig, fler kan utföra dessa analyser och ökar därmed förståelsen för den här typen av problem. Eftersom metodiken kommer att spara både arbetstimmar och beräkningstid, skapas det därmed också mer tid för att optimera grundläggningen av järnvägsbankar. Denna metodik kan därför vara mycket användbar vid utformningen av de kommande stora infrastrukturprojekten med utbyggnaden av de nya planerad stambanorna i de nordiska länderna.

# UTÖKAD SAMMANFATTNING

Rapporten är skriven på engelska. I föreliggande kapitel ges därför en längre sammanfattning av rapporten på svenska.

## Inledning

### Bakgrund

En större satsning pågår idag med att bygga nya stambanor för höghastighetståg i Sverige och i de nordiska länderna. Dessa stambanor har främst som syfte att binda ihop storstadsregionerna med persontrafik och benämns vanligen som höghastighetsbanor. Den första sträckan som avses byggas i Sverige är Ostlänken - en 16 mil lång dubbelspårig höghastighetsjärnväg mellan Stockholm och Linköping. Ostlänken, med planerad byggstart 2024, kommer att bli Sveriges hittills största infrastrukturutvecklingsprojekt.

Järnvägsbanor byggs traditionellt på s.k. järnvägsbankar. Erfarenheten av att bygga järnvägar på järnvägsbankar i Sverige är också lång och denna kunskap har till stor del arbetats in de föreskrifter som Trafikverket publicerar. Geoteknisk dimensionering av järnvägsbankar innebär kontroll av att det inte finns några risker för tjällyft, att stabiliteten i järnvägsbanken och omgivningen är tillfredställande och att långtidssättningar av järnvägsbanken inte överskrider tillåtna deformationer över dess tekniska livslängden. I detta arbete ingår även att kontrollera att tåginducerad markvibrationer inte blir för stora och att de hamnar inom tillåtna krav. Annars kan, framför allt med snabbare och tyngre tåg, markvibrationerna bli för stora för tågets säkerhet och kan då i värsta fall orsaka urspårning.

De geotekniska teorierna, kraven och hur man utför beräkningar för kontroll av säkerheter och för att utforma eventuella nödvändiga och erforderliga åtgärder mot tjällyft, stabilitet och sättning, är välkända och etablerade. Att kunskapen är så god för dessa problemställningar, beror främst på att det finns lättanvända programvaror för att kunna analysera dessa olika geotekniska problem. Så är inte fallet för att utvärdera risker för stora markvibrationer i järnvägsbankar. För att analysera tåginducerade markvibrationer, måste man använda avancerade numeriska programvaror. Förutom att dessa programvaror kan vara svåranvända, måste man även ha god kännedom om de olika krav som finns för att kunna modellera problemställningen på ett korrekt sätt. På grund av problemställningen art (tredimensionalitet och tids-/frekvensberoende), är dessa numeriska beräkningar också mycket tidskrävande avseende både mantimmar och beräkningstid. Att analysera problemet och utforma eventuella förstärkningsåtgärder kan därför bli kostsamt med många potentiella felkällor. Förstärkningsåtgärder, mot eventuella risker för stora markvibrationer i järnvägsbankar, tillämpas därför ofta konservativt istället för att utföra komplicerade och kostsamma beräkningar.

Med tanke på de kommande stora infrastrukturprojekten av nya järnvägslinjer i de nordiska länderna, bör beräkningar för kontroll av risken för stora tåginducerade markvibrationer utföras mer rutinmässigt. Det finns därför ett behov av att göra denna typ av beräkningar både effektivare och lättare att utföra, samt med möjlighet att optimera erforderliga förstärkningsåtgärder.

## Syfte och mål med projektet

Avsikten med detta projekt var att utveckla en användarvänlig metodik, kallad basmodellmetodiken, för effektiva (numeriska) beräkningar av tåginducerade markvibrationer i järnvägsbankar. Detta för olika typer av spårkonstruktioner, bankar och markförhållanden. Syftet med projektet har varit att ta fram en metodik som kan användas både för uppskattningar och detaljprojektering, samt för att kunna analysera och optimera de eventuella förstärkningsåtgärder som krävs.

Motiven till projektet var att göra denna typ av analyser lättare att använda och därmed tillgänglig för fler användare. Ett annat motiv var att, genom att göra denna typ av beräkningar snabbare att utföra, frigöra mer tid för att optimera de förstärkningsåtgärder som krävs. Med en lättanvänd metodik kommer också kunskapen och förståelsen för denna typ av analyser att öka. Med en automatiserad process, för att sätta upp modeller för att analysera denna typ av problem, kommer risken för beräkningsfel och designfel att minska. Detta ger både säkrare konstruktioner och optimerade grundförstärkningar.

# Tåginducerad markvibration

## Huvudkällan och kritisk fart

När ett tåg står stilla på spåret orsakar detta förskjutningar och skapar ett spänningsmönster i marken under hjulen. När tåget rör sig, förflyttar sig förskjutningarna och spänningsmönstret med tåget och inducerar spänningsvågor som sprider sig i marken och vidare ut till i omgivningen. Dessa markrörelser, både i järnvägsbanken och i omgivningen, benämns som tåginducerade markvibrationer. Deformationer under tågets hjul, som ses i *Figur 2.1.1*, kan definieras som **spårdeformationer**. Denna mekanism är huvudkällan till tåginducerade markvibrationer och kommer att inducera stressvågor även i frånvaro av ojämnheter i spåret, järnvägsbanken eller tåget. Huvudkällan till tåginducerade markvibrationer är därmed avståndet mellan hjulaxlarna, axelvikten och tågets fart. Storleken på de inducerade markvibrationerna beror också på styvheten och geometrin för järnvägsbanken och dess grund.

De högre tågfarterna åtföljs vanligen av ökade markvibrationer i järnvägsbanken och större vibrationsstörningar för omgivningen. För så kallade höghastighetståg, kan markrörelserna vara särskilt stora när tågfarten närmar sig den **kritisk farten** för järnvägsbanken. Den kritiska farten definierades, som när den rörliga lasten har en fart som är lika med utbredningsfarten för spänningsvågorna i järnvägsbanken. Energin kan då inte spridas ut från lasten, utan byggs istället upp kring den rörliga lasten och kan då orsaka att mycket stora markvibrationer uppstår.

## Jordegenskapernas skjuvtöjningsberoende

Utöver att tåginducerade markvibrationer är beroende av tågets fart och tyngd, så kompliceras det hela av att fyllningens och jordens styvhet och materialdämpning är skjuvtöjningsberoende. Med ökande skjuvtöjningar, så minskar markens och järnvägsbankens styvhet och materialdämpning ökar. Det betyder spårdeformationer och den kritiska farten ökar respektive minskar, när tåget har en fart som närmar sig järnvägsbankens kritiska fart. Vid beräkning av spårdeformationer och den kritiska farten, är det därför viktigt att beakta både effekterna av tågets fart och att fyllnings- och jordegenskaperna är skjuvtöjningsberoende.

Det finns också risk att, vid stora skjuvtöjningar, att jordens skjuvhållfasthet påverkas, och jordbrott kan uppstå beroende på storleken på lasterna och antalet belastningscykler. Kontroll för risk om skjuvtöjningen är så stor att det finns risk för initiering av porvattenövertryck och nedsatt skjuvhållfasthet, kan göras mot tröskelvärdet för volymetrisk skjuvtöjning ($\gamma_{vt}$) enligt *Figur 3.1.2*. För vidare detaljer om fyllnings och jords skjuvtöjningsberoende, se i *Avsnitt 3.1*.

## Materialmodeller

Analyser av dynamiska problem utförs idag vanligtvis genom beräkningar i numeriska programvaror. För att beskriva jordens beteende när den utsätts för belastningar, används matematiska formler - så kallade materialmodeller. Materialmodellerna är mer eller mindre komplicerade beroende på vilken typ av problem som ska analyseras och vilket materialbeteende som behöver beskrivas. För jorddynamiska problem gäller att, ju högre skjuvtöjningsnivå, desto mer komplex materialmodell behövs för att kunna modellera de olika fenomen som kan uppstå. En sammanställning av sambanden mellan skjuvtöjningsnivån, olika jorddynamiska fenomen och lämpliga materialmodeller för att analysera de olika problemen presenteras i *Figur 3.2.1*.

När en belastning förväntas inducera mycket små skjuvtöjningar i jorden, kan jordens beteende modelleras med linjärelastisk modell. Om små till medelstora skjuvtöjningsamplituder förväntas, blir jordens beteende elastoplastiskt varvid både jordens styvhet och materialdämpningen töjningsberoende måste beaktas. Detta kan utföras genom att använda en olinjär materialmodell där skjuvtöjningsberoendet beaktas direkt i beräkningarna eller genom iterativt sätt med den enklare **ekvivalenta linjära metoden**. För större skjuvtöjningar måste, materialmodellen vara mer komplex för att modellera generering av porvattenöverskott, skjuvhållfasthetsminskningar och brottförhållanden. Dessa modeller kallas cykliska icke-linjära materialmodeller.

De olika materialmodellerna beskrivs översiktligt i *Avsnitt 3.2* och i *Avsnitt 3.3* beskrivs den olinjär materialmodell som används i föreliggande studie, samt empiriska samband för att uppskatta initiella styvheter och materialdämpning för olika jordarter utifrån resultatet från geotekniska undersökningar. I *Avsnitt 3.3* beskrivs även förstärkningsåtgärder med kalkcementpelare, samt hur man kan uppskatta dess materialegenskaper. Kalkcementpelare är den vanligaste förkommande förstärkningsåtgärden mot stora tåginducerade markvibrationer.

# Basmodellmetodiken

## Konceptet

Konceptet med basmodellmetodiken är att en indatafil används för att sätta upp problemet för analys, ett skalprogram som läser indatafilen, skapar och kör en numerisk modellen av problemet på en kommersiell numerisk programvara, samt extraherar resultaten från beräkningen och sparar resultaten i en utdatafil. Strukturen för basmodellmetodiken, som utvecklades i denna studie, visas i *Figur 5.1.1* och inkluderar följande delar:

- En **indatafil** - Ett Excelark skapades med en databas för att systematisera skapandet av den numeriska modellen av problemställningen. Detta inkluderar val av järnvägsbankens geometri, material och egenskaper, jordprofil med egenskaper, eventuella förstärkningsåtgärder och vilka typer av analyser som ska utföras.
- **Basmodellprogrammet** – Ett skalprogram skapades, med hjälp av *Phyton*-skript, för att läsa indatafilen, köra finita-elementprogrammet, samt extrahera resultaten från den numeriska programvaran.
- Ett **numeriskt program** – I detta test användes den kommersiella finta-elementprogrammet *Brigade* och som är en applikation av programvaran *Abaqus*.
- **Utdatafiler -** Från de numeriska beräkningarna extraherar basmodellprogrammet resultat och sparar dem som figurer och textfiler.

## Metodiken

I *Figur 5.1.2* visas ett flödesschema över basmodellmetodiken och de olika stegen i **indatafilen,** som behöva för att definiera problemet som ska analyseras. De olika stegen i indatafilen diskuteras i *Avsnitt 5.1.* I *Bilaga B1* och *Bilaga C1* visas exempel på val i indatafilen för att analysera Ledsgårds fallstudie före, respektive efter utförda förstärkningsåtgärder.

I *Avsnitt 5.2* beskrivs det utvecklade **skalprogrammet** för att automatiserade beräkningar i den numeriska finita-elementprogrammet *Brigade* (eller *Abaqus*). Programmet, här kallade basmodellprogrammet, har programmerats i *Python* och omfattar även bearbetning och analyser av beräkningsresultaten.

Baserat på inmatningsfilen, sätter basmodellprogrammet upp en **numerisk modell** av järnvägsbanken och undergrunden, samt eventuella förstärkningsåtgärden, se *Figur 5.1.3*. Olika kombinationer av spåranläggningar, underballast, jordprofil och förstärkningsåtgärder kan sättas upp. För att öka beräkningseffektiviteten, beaktas därför endast hälften av spår- och jordmodellen i beräkningen (dvs problemet antas vara symmetrisk i horisontalplanet). Simuleringen beräknas i tidsdomänen. I *Figur 5.1.4* visas redovisas konceptet för beräkningen av dynamik för interaktion mellan spår och mark. En av huvudteknikerna för att öka effektiviteten i beräkningarna är **superpositionsmetoden**. Genom att använda data från beräkningen från en enda rörlig last och sedan lägga ihop beräkningsresultaten för att få hela tågets inducerade markvibrationer i järnvägsbanken, kan mycket beräkningstid sparas. Detta är möjligt genom den ekvivalentlinjära metoden för att ta hänsyn till de styrande materialparameternas onlinjära beteende med skjuvtöjningen, se *Avsnitt 5.5.1.* Alla beräkningar inom den numeriska programvaran utförs således med linjära elastiska materialmodeller och materialegenskapernas olinjäritet beaktas istället i skalprogrammet. Detta tillvägagångssätt har visat på betydande förbättringar för simuleringseffektiviteten. Dessutom reduceras den erforderliga modellstorleken, vilket följaktligen minskar beräkningstiden. Subrutinen för den ekvivalentlinjär metodiken i skalprogrammet redovisas i *Avsnitt 5.4.1.*

När en beräkning är klar, så plottas resultatet från de olika analyserna i form av diagram. Exempel på **utdata** redovisas i *Appendix B2* och *Appendix C2* för analyser av Ledsgårds fallstudie före, respektive efter jordförstärkningsåtgärderna.

Tre olika **typer av analyser** kan utföras i det utvecklade programmet: 1. Receptansanalys. 2. Bestämning av kritisk fart och 3. Rörlig lastanalys. I receptansanalysen beräknas den numeriska modellens resonansfrekvenser. Egenfrekvenser beräknas för en cyklisk punktlast applicerad mitt på spåret, se exempel i *Figur 5.1.5.* Vid bestämning av kritisk fart, utförs flera simuleringar med olika tågfarter och resultat sammanställs i form av beräknad maximal top-till-top-deformation mot tågfarter, se exempel i *Figur 5.1.7.* I diagrammet jämför utvädrad kritiska fart ($c_{cr}$) med den lägsta tillåtna kritiska farten enligt *TK Geo* (se *Avsnitt 2.2.2.*), samt högsta tillåtna spårdeformationer förskjutningen vid dimensioners tågfart ($v_{sth}$). Rörlig lastanalys är detsamma som vid beräkning av kritiska fart, men endast med en tågfart analyseras och ingen kritisk fart bestäms.

## Numerisk modellering

I *Kapitel 4* redovisas några andra optimeringstekniker för att öka modelleringseffektivitet och minska beräkningstider till erforderlig noggrannhet i beräkningsresultat. I *Avsnitt 5.2* redovisas de elementtyper som valt att användes för modellera de olika delarna i järnvägsbanken och jord. Här redovisas även belastningsmodellen med rörliga laster och hur de s.k. tysta ränderna har modellerats. I *Avsnitt 5.3* redovisas verifiering av den numeriska modelleringen enligt de rekommendationer som har tagits fram i detta projekt.

# Fallstudie Ledsgård

## Bakgrund

Ledsgårds fallhistorik är en av de mest väldokumenterade fallhistorierna avseende mätningar av tåginducerade markvibrationer. Vibrationsmätningar har utförts här vid olika tidpunkter, både före och efter de installerade markförstärkningarna. Mätningarna utfördes på slipers, i banvallen och på olika djup under järnvägsbanken, samt på markyta på olika avstånd från banvallen. I *Avsnitt 5.1* och *Avsnitt 5.2* sammanfattas tidigare utförda markundersökningar, markförstärkningar och vibrationsmätningar. Fallhistorien har sedan analyserats med basmodellmetodiken, med hjälp av det utvecklade basmodellprogrammet, och resultaten från beräkningarna har jämförts med de tidigare utförda vibrationsmätningarna.

## Beräkningsresultat

Beräkningar med det utvecklade basmodellprogrammet tillämpades på Ledsgårds fallhistorik för de två fallen - före och efter markförstärkningen. Indata och resultat från beräkningarna redovisas i *Appendix B* och *Appendix C* för det oförstärkta och respektive förstärkta fallet. I *Avsnitt 5.3* jämförs resultaten från beräkningarna med motsvarande resultaten från vibrationsmätningarna.

Rörliga lastanalyser har utförts för tågfarter 70, 142 och 204km/h för det oförstärkta fallet och har jämförts med motsvarande mätningar från extensometern. För det förstärkta fallet jämfördes beräkning för en tågfart på 200km/h med motsvarande mätningar från accelerometer. Jämförelserna visas i *Figur 7.2.2*. För det oförstärkta fallet visar beräkningarna och mätningarna god överensstämmelse för tågfarter 70km/h och 142km/h. Vid tågfart 204km/h visar beräkningarna på lite mindre och bredare förskjutning jämfört med mätningarna. För de förstärkta fallet med tågfart 200km/h, visar beräkningarna mycket god överensstämmelse med mätningarna.

I *Figur 7.2.3* jämförs det beräknade och uppmätta maximala topp-till-topp-värdet mot tågfart. För det oförstärkta fallet visar beräkningarna och mätningarna god överensstämmelse upp till en tågfart på cirka 185km/h. Enligt beräkningen med basmodellmetoden erhålls den kritiska farten vid 185km och de beräknade förskjutningarna börjar minska vid högre tågfart. Mätningarna visade att den kritiska farten var högre än 204km/h och detta förklarar skillnaden i förskjutning mellan beräkningarna och mätningarna vid tågfart 204km/h. Den kritiska farten för det förstärkta fallet bestämdes till cirka 405km/h. Således ökade kalkpelarförstärkningen den kritiska farten med en faktor ca 2.

## Diskussion

Den utvecklade basmodellmetodiken verkar fungera bra och beräkningarna ger god överensstämmelse med vibrationsmätningarna. Den stora skillnaden mellan beräkningarna och vibrationsmätningen var att den kritiska farten beräknades till att vara lägre än vad mätningarna indikerade. I den här studien fanns det inte tid att analyser varför den beräknade kritisk farten, enligt basmodelprogrammet, var lägre än vad mätningarna visade. En orsak kan vara att den valda materialmodellen inte beskrev skjuvtöjningsberoendet i gyttjaskiktet på ett korrekt sätt. Ytterligare studier behövs för att undersöka detta

# Slutsatser

Avsikten med detta projekt var att utveckla en användarvänlig metodik för effektiva numeriska beräkningar av tåginducerade markvibrationer i järnvägsbankar. En metodik har utvecklats och det har bevisats att den fungerar. Detta gjordes genom att utveckla en indatafil med en databas för att definiera problemet, utveckla ett skalprogram som läser indatafilen, skapar och kör modellen av problemet på en kommersiell numerisk programvara, samt extraherar resultaten från beräkningen av problemet och sparar resultatet i en utdatafil. Genom detta kunde beräkningarna automatiseras och gjorde dem därmed enkla att använda.

Den utvecklade metodiken tillämpades på publicerat referensfall och på en fallhistorik med vibrationsmätningar före och efter en markförstärkning med kalkcementpelare. Från dessa resultat har det visat sig att den utvecklade metoden:

- kan användas beräkna markvibrationer som visar mycket god överensstämmelse (nästan identisk) med resultat i publicerade analys och god överensstämmelse med vibrationsmätningar för analyserade fallstudier.
- kan användas för att bestämma erforderliga jordförstärkningsåtgärder med kalkcementpelare utifrån vibrationskrav.

I analyser av fallhistorien gjordes också följande observationer:

- I analyserna är det viktigt att ha rätt geometri och goda uppskattningar av material- och jordegenskaper.
- För de dynamiska jordegenskaperna:
    - Är det användbart att använda de starka empiriska sambanden, med odränerad skjuvhållfasthet ($c_u$) plasticitetsindex (PI) och effektiv spänning ($\sigma'$), för att uppskatta de initiella jordegenskaperna,
    - Den ekvivalenta linjära metoden, för att ta hänsyn till jordegenskapernas skjuvtöjningsberoende, verkar fungera mycket bra.

Resultaten i beräkningarna är alltså starkt påverkade av input till analyserna. I denna rapport ges vägledning om hur man utvärderar markegenskaper som är nödvändiga för markdynamiska analyser. Rapporten ger också vägledning om hur man kan optimera de numeriska beräkningarna för att minimera beräkningstiden med tillräcklig noggrannhet i resultaten.

Den utvecklade metoden är självinstruerande och mindre tid och arbete krävs för att utföra numeriska beräkningar av tåginducerade markvibrationer. Behovet av att ha hög kunskap för att använda avancerade numeriska datorprogram minskar. Denna form av analyser blir därmed mer användarvänlig, fler kan utföra dessa analyser och ökar därmed förståelsen för denna typ av problem. Den utvecklade metoden kommer att minska beräknings- och konstruktionsfel, samt skapa mer tid för att optimera eventuella jordförstärkningsåtgärder. Denna metodik kan därför vara mycket användbar vid utformningen av de kommande stora infrastrukturprojekten med utbyggnaden av de nya planerade järnvägslinjerna i Norden.

# TABLE OF CONTENTS

# LIST OF APPENDICES

# 1. INTRODUCTION

## 1.1. Background

In the Nordic countries there are currently major plans to expand the railway network with high-speed lines between its metropolitan regions and for contact with the rest of Europe. High-speed railway lines are planned to connect Sweden's three metropolitan regions (Gothenburg, Malmö and Stockholm) with Jönköping as a hub, and a high-speed railway line through the Baltic countries (called Rail Baltica) is planned to connect the Baltic capitals with Warsaw in the south and Helsinki in the north. There are also desires to build a high-speed railway line between Oslo and Copenhagen (via Gothenburg and Malmö). From Copenhagen, the construction of a high-speed railway line to Hamburg (called the Fehmarn Belt Link) has just begun. In Sweden, it is Ostlänken, a 16-mile long double-track high-speed railway line between Stockholm and Linköping that will be built first. Ostlänken, with a planned start of construction in 2024, will be Sweden's largest infrastructure development project to date and comprises 12 construction contracts. Of these, 4 contracts will be carried out as turnkey contracts and the rest as execution contracts. In total, according to the Swedish Transport Administration, the entire Ostlänken is estimated to cost around SEK 89 milliards to build.

Railway lines are traditionally built on embankments. This method usually has the cheapest construction costs compared to building railway lines only on bridges. Also, the experience of constructing railway lines on embankments in Sweden is long and this knowledge has largely been built in the regulations published by the Swedish Transport Administration. The design of railway embankments, with the geological conditions that exists in the Nordic countries, still can have some geotechnical challenges and ground reinforcement are sometimes necessary to fulfill the requirements in both the ultimate and service limit states. Geotechnical dimensioning of railways embankments involves controlling that there are no risks for frost heave, that the stability of the embankment and the surrounding is sufficient and that long term settlements of the railway embankment are in the limits for allowable deformations for the designed technical lifetime span. This also includes checking that train-induced, so-called, high-speed ground vibrations do not become too large and that they fall within the safe limits of the track. Otherwise, especially with faster and heavier trains, the ground vibrations can become too large for the safety of the traveling train and this can, in worst-case, cause derailment. Large train-induced ground vibrations can also cause degradation of the embankment material, and stability problems for the railway embankment. Stability problems can occur, as larger vibrations may generate excess pore water pressures in the ground and thus impair the shear strength of the soil. Train-induced ground vibration can also cause of comfort-disturbing vibrations in buildings that are in the vicinity (<150m) of the railway lines.

The geotechnical theories, requirements and how to perform calculations for the control of safeties and to design any necessary and required measures against frost heave sensitivity, stability and settlement are well known and established. The knowledge about this, is mainly due to easy-to-use software for each of these problems. This is, however, not the case for evaluating the potential risk of large ground vibrations in railway embankments. The theory behind train-induced ground vibrations is somewhat well known, there are requirements and knowledge in how to design reinforcement measures, but the major problem is that the knowledge about the problem is not very well spread. This is mainly due to the fact that easy-to-use software, for analyses of train induced ground vibrations, does not exist. To analyze the problem, general purposes numerical software are usually used, but there are lots of requirements in the modeling in order to be able to model the problem correctly. Due to the art of the problem (three-dimensionality and time/frequency dependence), the numerical calculations are time-consuming both in terms of man-hours and computing time. Analyzing the

problem and designing any reinforcement measures can therefore be costly with many potential sources of error. Instead performing expensive and complicated calculations, reinforcement measures against possible risks of large ground vibrations in embankments are therefore often instead applied conservatively.

Considering the upcoming large infrastructure project of new railway lines in the Nordic countries, it is believed calculations for the control of the risk of large train induced ground vibrations must be performed more routinely and with a possibility to optimize required ground reinforcement. There is therefore a need to make this type of calculations both more efficient and easier to perform.

## 1.2. Aims and Objectives

The intention with this project was to develop a user-friendly methodology for efficient (numerical) calculations of train-induced ground vibrations in the railway embankment. This for different types of track structures, embankments, and soil conditions. The purpose was to develop a methodology that can be used both for estimates and detailed design of, as well as to be able to analyze and optimize any required reinforcement measures.

The motives to the project were to make this type of analysis easier to use and thereby available for more users. Another motive to this project was to show what could be done to save both man-hours and computing times to a sufficient good accuracy for this kind of calculations. By making this type of analyzes easier to use and faster to perform, more time can be spent on optimizing the required reinforcement measures. Also, with an easy-to-use methodology, the knowledge and understanding for this kind analyses will increase. With an automized process of setting of models for analyzing this kind of problem, the risk of calculations errors and designing mistakes will be reduced. Hence, this will give both safer constructions and optimized ground reinforcement.

## 1.3. Project plan

The project was set-up with the following activities:

1. Optimization of calculations

The activity included the work of evaluating the most appropriate calculation method, and possible ways to optimize the numerical models to minimize computing times to the required accuracy in calculation results. Comparative calculations of some typical cases were performed to find out possible optimization methods, reduce sources of error and find the most suitable calculation methods.

2. Soil modeling

This activity dealt with the soil's behavior under cyclical loads and current material models to describe this. Guidelines for evaluation of soil and material parameter were described and how to consider the shear properties shear dependence in the numerical calculations. The activity also included the design of railway embankments according to requirements and describing ground reinforcement method that was used in this study.

3 Base models methodology

The idea was to create a data base, from which typical soil profile, ground foundation (unreinforced, lime cement column) as well as different types of railway embankment (sleepers, slab track, etc.) and train types, could be chosen. From this data base, a numerical model could be set-up, and calculations were performed in a commercial numerical software. The work also included verification of the numerical calculation against a case history with vibrations measurement.

4. Simplified calculation tools

In this activity, simplified calculation tools were planned to be developed and adapted. The tools aim to be able to perform fast simple calculations of train-induced ground vibrations. The idea was to calibrate these tools against typical cases (benchmarks) with vibration measurement and numerical calculations performed in the project. A previously simplified calculation tool, developed at NGI, was used in this study

5. Reporting

The amount of data created from for this type of analyses can be large. Therefore, it is also necessary to have an activity that deals with how the calculation results should be analyzed and displayed, as well as how the result should be controlled against requirements.

The results from the present project are shown in this report. Here, the so-called base model methodology is described, and recommendations are given for the numerical modeling. Furthermore, the calculations with base model methodology have been verified against a well-known case history with known soil profile, different ground foundation and result from vibrations measurements, Instructions and guidelines have been produced for evaluation of material parameters for material models, as well as for analysis and reporting of calculation results. The simplified calculation tool will be available in the form of executable file. This report also gives a short guideline for using the simplified tool.

## 1.4. Organization

The project was financed by Trafikverket (Swedish Transport Administration), SBUF (Swedish Construction Industry Development Fund) and BaneNOR (Norwegian Railways Administration). NCC Sverige AB has also supported the project with financially. The project owners were KTH (Royal Institute of Technology), NCC Sverige AB and NGI (Norwegian Geotechnical Institute). The project was organized in two parts, were the Swedish part (with NCC as a leading partner) focused on developing the numerical calculations and a Norwegian part that focused on further developing NGI's own analytical calculation tool called VibTrain. The Norwegian part of the project was thus completely run by NGI. The Swedish part of the project consisted of a working group with people from NCC and ELU.

To ensure that the projects were conducted in the right direction, regular meetings were held with the steering group. A reference group was also put together to ensure that the work was carried out with a sufficiently high quality. The steering group included contact persons from the project's owners and financiers, whereas the reference group included experts from universities, research institutes and contractors. *Figure 1.4.1* shows the organization chart and *Table 1.4.1* shows the different people that worked in the project, their group affiliation, the company they represent and their function in the project.

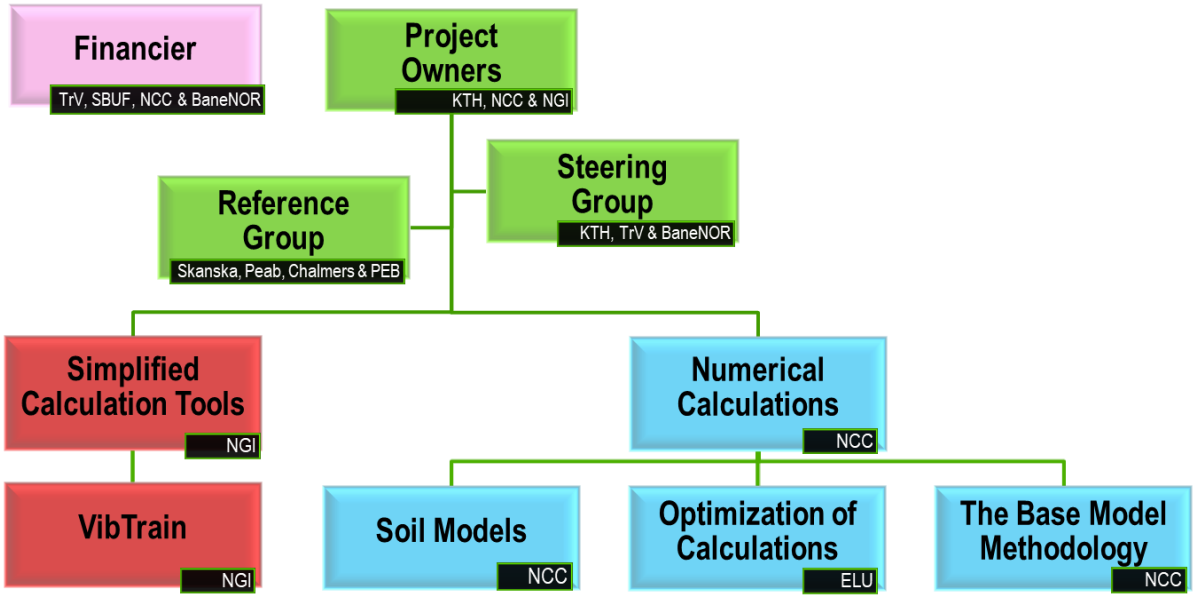


**Figure 1.4.1** Organization of the project with its different groups and activities

**Table 1.4.1** List of people who worked on the project, their role in the project, group affiliation and which company they represent

| **Name** | | | |
|---|---|---|---|
| **Work Group Numerical calculations** | | | |
| Lars Hall | PhD. | Project manager | NCC Sverige AB |
| Jou-Yi Shih | PhD. | Main designer | NCC Sverige AB (Zynamic AB) |
| Jesus Armesto Barros | MSc. | Designer | NCC Sverige AB |
| Abbas Zangeneh | PhD. | Designer | ELU Konsult AB |
| Costin Pacoste | Docent | Expert | ELU Konsult AB |
| **Work Group Simplified Tools** | | | |
| Jörgen Johansson | PhD. | Project manager | NGI-Norwegian Geotechnical Institute |
| Amir M Kaynia | Prof. | Main designer | NGI-Norwegian Geotechnical Institute |
| **Steering Group** | | | |
| Johan Jonsson | PhD. | Expert | Trafikverket-Swedish Transport Administration |
| Stefan Larsson | Prof. | Expert | KTH- Royal Institute of Technology |
| Geir Svanø | MSc. | Expert | BaneNOR-Norwegian Railways Administration |
| **Reference Group** | | | |
| Peter Claesson | PhD. | Expert | Skanska Sverige AB |
| Karl Lundstedt | MSc. | Expert | Skanska Sverige AB |
| Nils Rydén | Adj. Prof. | Expert | PEAB |
| P-E Bengtsson | MSc. | Expert | PEB Geoteknik AB |
| Jelke Dijkstra | Prof. | Expert | Chalmers University of Technology |

# 2. Design of Railway Embankments

Requirements on the design of railway embankments in Sweden are discussed briefly in this chapter and in some more detail concerning requirements on ground vibrations. A brief introduction to train induced ground vibrations is also given.

## 2.1. Definition of train induced ground vibration

When a train is standing still on the track, this causes displacements and produces a stress pattern in the ground beneath wheels. As the train moves, the track displacement and stress pattern moves with the train and induces stress waves that spreads into the ground and further out to the surroundings, see *Figure 2.1.1*. The ground movements, caused by the moving stress pattern and the spreading of stress waves into the ground, can be defined as train-induced ground vibrations and the deflection under the trains wheels, as seen in Figure 2.1.1, can be defined as the **track displacement**. This mechanism, the main source of train-induced ground vibrations, will induce stress waves even in the absence of imperfections or periodic irregularities in the vehicle or the track. The main source of train induced ground vibrations, thereby depends on the spacing of the wheel axles, the axle weight, and the speed of the train. The magnitude of the induced ground vibrations also depends on stiffness and geometry of the railway embankment and its foundation. Generally, larger ground vibrations are induced in soft soils than in stiff soils. Also, in a stiff and large (high) railway embankment - slightly lower ground vibrations will be induced compared to a small (low) railway embankment.

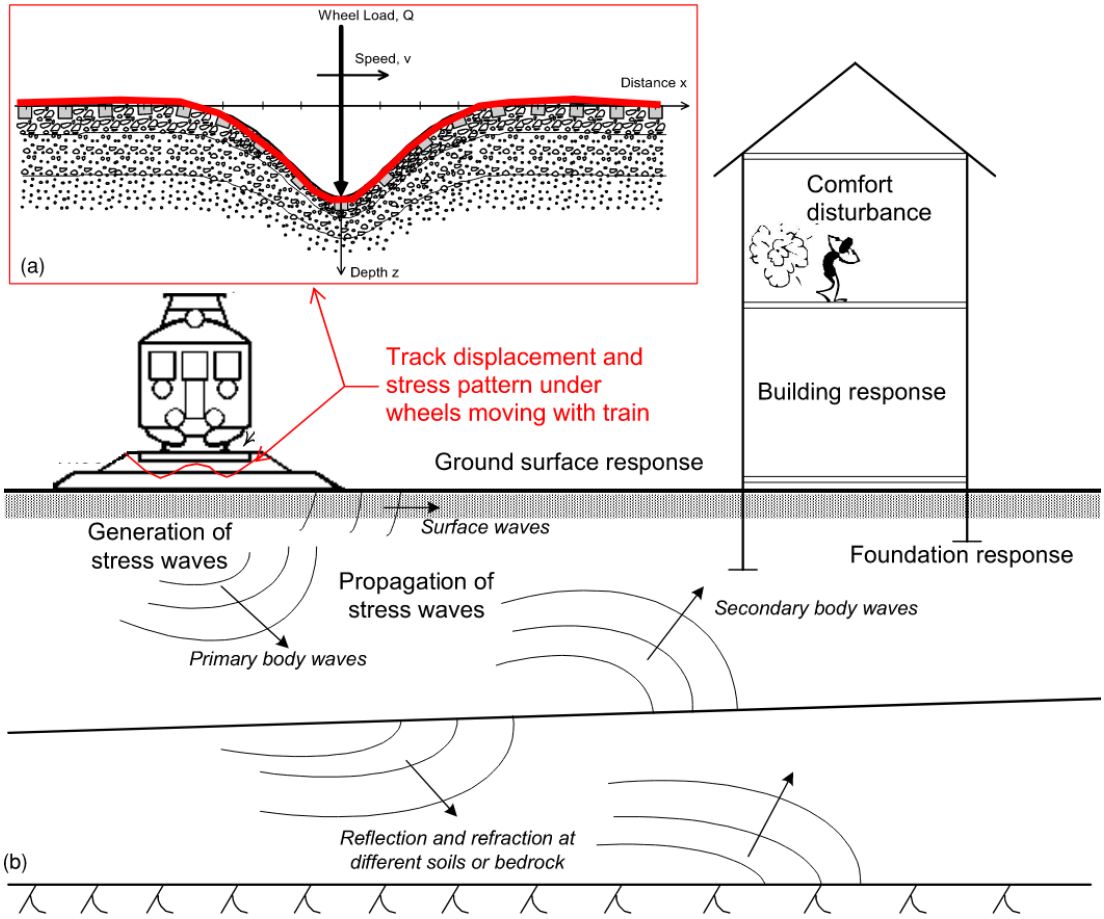


**Figure 2.1.1** The track displacement caused by the main source (i.e. the axle weight of the vehicle and the speed of the train) seen (a) along the track and (b) perpendicular to the track and the spreading of ground vibrations into the surroundings.

Any unsteady riding of the vehicle may cause fluctuating forces on the railway track. Neither does the track itself always provide a uniform support for the train, the ground condition can vary, rails can be of fixed lengths or sleepers may have an insufficient support by the ballast material. Acceleration and retardation of trains, curves, and tilting track, as well as switches and misalignment of motors, may also cause disturbances. All these different vibration sources contribute to the induced ground stresses and to the vibration disturbance that propagates to the surroundings. Some of these sources will only produce local ground vibrations, while others will create a ground stress pattern that moves with the train. However, it has been shown by Hannelius (1978) and others - that the complex induced stress pattern, if measured as forces or movements, can be repeated at a site if the load characteristics (e.g. speed of train, train type, composition of cars etc.) are the same. So for train induced ground vibrations, it is normally only the main source that needs to be considered in the analyses of this problem.

The higher speeds for trains are usually accompanied by increased ground movements in the railway embankment and greater vibration disturbances for the surroundings. For so-called high-speed trains, ground movements can be particularly large when the train speed approaches a critical speed of the railway embankment. The critical speed has been proved mathematically by Kenney (1954) by analyzing a beam on an elastic bed of springs (a so-called Winkler bed) loaded by a point load moving at a constant speed. The first time this high-speed phenomenon was observed in actual measurements of for train-induced ground vibrations, was in 1997 in Ledsgård by Adolfsson et al (1999). The critical speed, according to Kenney (1954), corresponds to the ratio when the moving load has a speed that is equal to the propagation speed of the stress waves in the beam. In that case, the energy cannot be spread out from the load but is instead built up around the moving load, whereby very large movements can occur. The critical speed for a beam on elastic support was defined by *Kenney (1954)* as:

$$c_{cr} = \sqrt[4]{\frac{4\kappa EI}{\rho^2 A^2}} \qquad \textit{(Equation 2.1.1)}$$

where,

$\kappa = \frac{0.82 \cdot E_S}{(1-v_S^2)} \cdot \sqrt[12]{\frac{E_S \cdot b^4}{EI}}$ modulus of foundation and formula by *Vesic (1961)*

$EI$ flexural rigidity of the beam

$EI_s$ flexural rigidity for the foundation

$\rho$ density of the beam

$A$ cross-sectional area of the beam

$v_s$ Poisson's ratio for the foundation

$b$ the half with of the beam

Based on *Kenney's (1954*) mathematical equations, the theoretical response for moving loads can be calculated. *Figure 2.1.2* shows the response of the beam from a moving load at different speeds of the critical speed. In order to be able to apply Kenny's equations for analysis of ground response from railway traffic, the beam can be assumed to be equal to the railway embankment and the modulus of foundation correspond to the ground under the railway embankment. The parameters, *EI,* ρ, *A* and *b* for the beam can then be assumed to be the flexural rigidity, density, and the cross-sectional area and the effective width of the railway embankment.

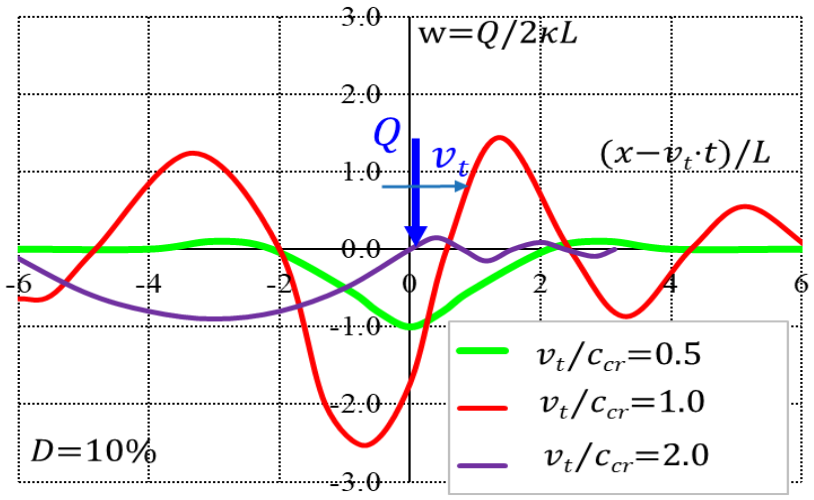


**Figure 2.1.2** The response fore beam on elastic bed according equations by Kenney (1954) for a moving point load at different speeds of the critical speed.

If the material and soil properties in the embankment and ground were linear elastic, the critical speed could be estimated using *Equations 2.1.1*. However, this is not the case - the stiffness of embankment material and the ground is shear strain dependent and decreases with increasing shear strain. The track displacement and the critical speed thus increases and decreases, respectively, as the train approaches the critical speed of the railway embankment. Therefore, when calculating track displacement and the critical speed, it is therefore important to consider both the effects of the speed for the moving loads (i.e. the speed and weight of the train) and that materials and soil properties are shear strain dependent.

## 2.2. Geotechnical requirements

The Swedish Transport Administration (Trafikverket) is responsible for planning, constructing, and managing the Swedish state-owned railway lines. The requirements on constructing these railways lines are regulated by Trafikverket's own standards and guidelines.

### 2.2.1. Standard railway embankments

Most of the Swedish railway lines are built on railway embankments and those are today designed for train speeds up to 250km/h. These railway embankments are constructed with ballast and sleepers. Requirements on the geometry and materials of these embankment are regulated by the following documents:

- *BVS 1585.005* – Typsektioner för banan. (eng. type sections for railway lines). Document number TKOK 2015:0198. Version 2.0. Valid from 2021-05-01. Published by Trafikverket
- *AMA* Anläggning 20. Published by Svensk Byggtjänst.

Document *BVS 1585.005* describes the geometry requirements for railway embankments in both the design of new railways lines and for upgrading existing railways lines. In the document, also the different terms used for describing the different part in a railway embankment are defined (see examples in *Figure 2.1.1*).

AMA is a series of reference documents that is used when setting up documents for the description and execution of construction work for all types of buildings and infrastructure facilities in Sweden. The Swedish Transport Administration's requirements for materials in the railway embankments (ballast, subballast, frost insulation and base material) are incorporated in AMA and are referred to in the Swedish Transport Administration's own documents. AMA also provides guidelines for putting out masses and how the packing work should be carried out. AMA is updated about every third year.

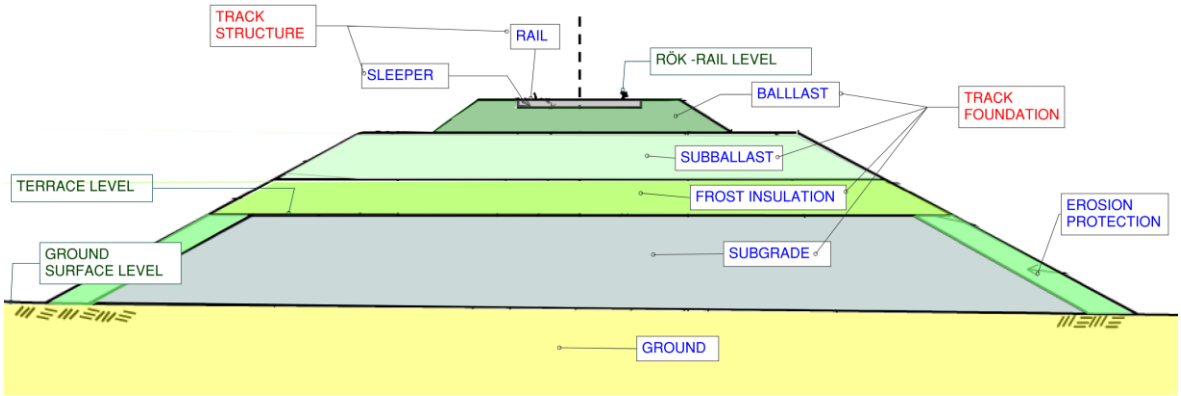


**Figure 2.1.1** Terms used in defining a railway embankment

The railway embankment must be designed to have sufficient safety for itself and the surrounding in both ultimate and serviceability limit states. For railway embankments, this concerns the geotechnical requirements and those are given in the following document by Trafikverket:

- TK Geo 13 – Trafikverkets tekniska krav för geokonstruktioner (eng. Swedish Transport Administration requirements on geotechnical design). Document number TKOK 2013:0667 Version 2.0. Valid from 2016-02-29. Published by Trafikverket

*TK Geo* gives requirements for control of stability, settlements, frost heave and ground vibrations for embankments, as well as in the design of any required ground reinforcement measures ( e.g. lime-cement columns and embankment piles). *TK Geo* is associated to Eurocode and with national choices as given by the Swedish Transport Agency (Transportstyrelsen). TK Geo is also updated about every third year.

### 2.2.2. High-speed railway embankments

In order to handle train speed up to 320km/h for the high-speed railway lines that are being planned in Sweden, the Swedish Transport Administration has produced the following governing document:

- TSS NGJ 4.17 – Teknisk systemstandard för en ny generation järnväg (eng. Technical system standard for a new generation railway). Published by Trafikverket

With this document, also the use of slab-track in the track structure will be allowed as an alternative to sleepers and ballast. The requirements for control of stability and frost heave of the railway embankments are, however, the same as given in *TK Geo*. The requirements on allowable settlements are, however, much stricter. The requirements on ground vibrations are also the same as given in *TK Geo* and are discussed in some more detail in the following chapter.

### 2.2.3. Requirements on Ground Vibrations

In *TK Geo* it is recommended that analyses of the risk damaging ground vibrations in railway embankments, should be performed in two steps. First an initial analysis should be performed. If the requirements are fulfilled in the initial analyses, there are no need for any further analyses, and it can be assumed that there will be no risk for damaging ground vibrations in the railway embankment. If any of the requirements are not met in the initial analyses, a detail analyses shall be performed, and ground reinforcement measure must be designed to meet the requirements.

Train induced ground vibrations do also spread to the surrounding and can in some case causes comfort disturbing vibrations in nearby buildings. Comfort disturbing vibrations in homes and offices are in Sweden regulated in a norm called *SS-4604861*. Comfort disturbing vibrations is not included in the scope of this study.

#### *Initial Analysis*

According to TK Geo, there is no need to consider ground vibration in railway embankment, if one of the following requirements are fulfilled:

$$v_{sth} \leq 160 km/h \qquad \textit{(Equation 2.2.1.a)}$$

$$v_{sth} \leq c_{S0,min}/1.5 \qquad \textit{(Equation 2.2.1.b)}$$

where,

$v_{sth}$ = the designed (highest) train speed for the railway embankment

$c_{S0,min}$ = the minimum shear wave propagation speed (at small strains) for the soil profile under the railway embankment

The above requirements are based on experience. i.e., the vibrations levels in railway embankments are usually small (≤2mm/s peek-to-peek value) when any of the above requirements are fulfilled.

### *Detailed Analysis*

If any of the requirements in *Equation 2.2.1* are not met, the critical speed of the embankment and the vertical displacements of the track must be determined. For existing railway lines, this can be done either by actual measurements of passing trains or by calculations. For new railway lines, calculations must, obviously, be performed. These calculations can be performed using either analytical or numerical methods and must be performed with moving loads of the same magnitude as the axle loads for which the railway is to be dimensioned.

In the detailed analyses, the railway embankment must be designed in such a way that the following requirements, according to TK Geo, are fulfilled:

1. The determined (calculated or measured) **track displacements (**peek-to-peek value) for the designed train speed ($v_{sth}$), shall not exceed 2mm or as agreed with Trafikverket. This can be defined as

   $u(v_{sth})_{calc} \leq u(v_{sth})_{allow}$ *(Equation 2.2.2.a)*

   $u(v_{sth})_{meas} \leq u(v_{sth})_{allow}$ *(Equation 2.2.2.b)*

2. The designed train speed ($v_{sth}$) should be less than the calculated **critical speed** of the railway embankment ($c_{cr}$) multiplied by a factor $C_d$ (i.e.,, $v_{sth} \leq C_d \cdot c_{cr,calc}$). Or it can be done through vibrations measurements at different train speeds up to the design train speed and showed that critical speed of the railway embankment is very high (i.e., measurements shows that there is no increase of deformations with train speed). This can be defined as:

   $c_{cr,calc} > c_{cr,allow} = v_{sth}/C_d$ *(Equation 2.2.3.a)*

   $c_{cr,meas} \gg v_{sth}$ *(Equation 2.2.3.b)*

*TK Geo* gives some guidelines in how the factor $C_d$ can be determined. However, there are some aspects that is not mentioned in *TK Geo*. The calculations must be performed with moving loads and the three-dimensionality of the problem must be considered. In addition, the shear strain dependence on materials and soil properties must be considered. The options in choosing the value $C_d$ can therefore be reduced as shown in *Table 2.2.1*.

If any of the above requirements (*Equation 2.2.2* and *2.2.3*) are not fulfilled, ground reinforcement must be designed. The most used measure is to reinforce the ground and this by using lime-cement columns in rows under and along the embankment, se *Section 3.3.3*. In the example shown in *Figure 2.2.1*, lime-cement column reinforcements (LLC) were required to meet all the requirements. Lime-cement columns are also often used as ground reinforcement for stability and settlements problems. In the case of very weak subsoil, embankment piles or pile decks can be an alternative as ground reinforcement against damaging ground vibrations as well as for stability and settlements problems.

**Table 2.2.1** Determination of the factor $C_d$ depending on the evaluation methods for determining soil properties and their shear dependency (*TK Geo*)

| Method number | A1B3 | A2B3 | A3B3 |
|---|---|---|---|
| Evaluation of the material parameters' initial values | Well established empirical relationships. | Based on seismic field tests | Based on seismic field tests |
| Evaluation of the soil model for the shear-strain dependency | Well established empirical relationships. | Well established empirical relationships. | Based on seismic laboratory tests. |
| Calculation method (B3) | Calculations in 3D models with moving point loads. | | |
| Value of factor $C_d$ | 0.60 | 0.65 | 0.70 |

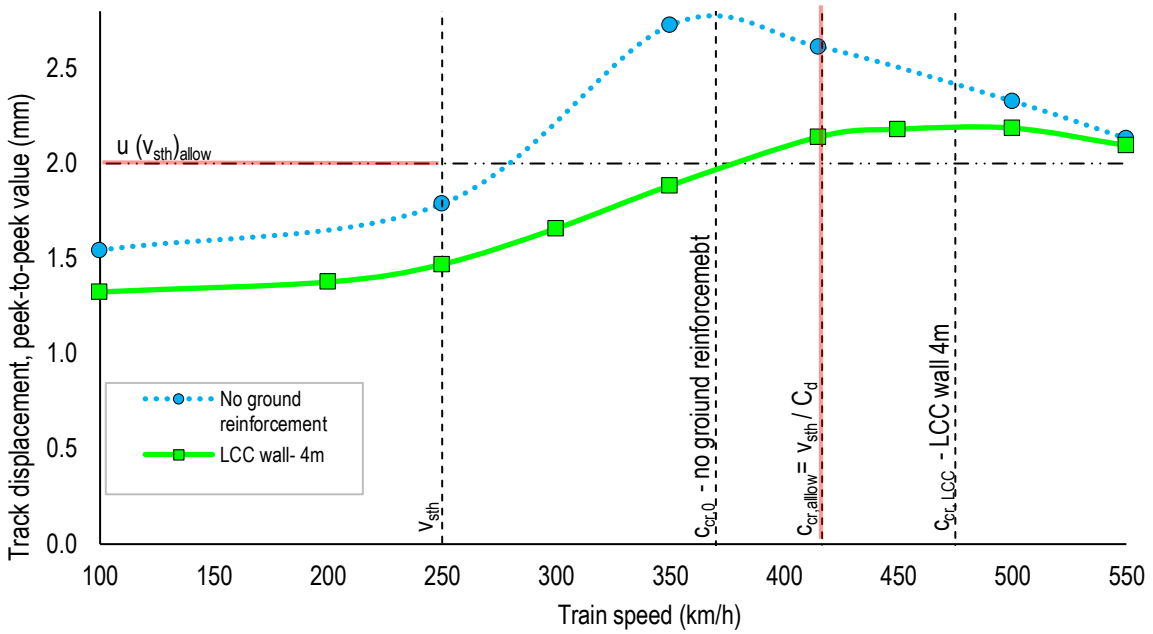


**Table 2.2.1** Calculated track displacement from a detailed analysis of a railway line for high-speed trains over an area with loose clay and the design of required ground reinforcement (Hall et al, 2013)

## 2.3. References


ADOLFSSON, K., ANDREASSON, B., BENGTSSON, P.E. & ZACKRISSON, P. (1999). High speed train X2000 on soft organic clay – measurements in Sweden. *Proc. XIIth Europ. Conf. Soil Mech. Geotech. Engng*, Amsterdam, Netherlands, 3, 1713-1718.

AMA Anläggning 20. Published by *Svensk Byggtjänst*

BVS 1585.005 – Typsektioner för banan. (eng. type sections for railway lines). Document number TKOK 2015:0198. Version 2.0. Valid from 2021-05-01. *Trafikverket*

HANNELIUS, L, (1978), "Vibrationer från tung tågtrafik. Problemställningar vidbyggnadsplanering och grundläggning", Report No. 12, *KTH- Royal Institute of Technology*.

HALL, L., ZANGENEH, A., ANDRÉASSON, B. & PASCOTE, C., (2013), "KC-pelarförstärkning mot höghastighetsvibrationer, Nytt dubbelspår vid Gamla Uppsala". Utförd av *ELU Konsult AB* på uppdrag av Tyréns AB och Trafikverket.

KENNEY, J.T., (1954), "Steady-state vibrations of beam on elastic foundation for moving load", *Journal of Applied Mechanics*, Vol. 76, pp. 359-364

SS 460 48 61 "Vibration och stöt – Mätning och riktvärden för bedömning av komfort i byggnader". *Standardiseringskommissionen i Sverige.*

TK GEO 13 – Trafikverkets tekniska krav för geokonstruktioner (eng. Swedish Transport Administration requirements on geotechnical design). Document number TKOK 2013:0667 Version 2.0. Valid from 2016-02-29. *Trafikverket*

TSS NGJ 4.17 – Teknisk systemstandard för en ny generation järnväg (eng. Technical system standard for a new generation railway). *Trafikverket*

VESIC, A,S., (1961), "Bending of beams resting on isotropic elastic solids", *Journal of Engineering Mechanics Division*, ASCE Vol. 52, pp. 35-53

# 3. DYNAMIC SOIL PROPERTIES

The magnitude and spreading of ground vibrations are strongly dependent on the soil's mechanical properties, where the soils stiffness and material damping are the most important. For very small shear strains, these properties are linear, but for larger shear strains they become non-linear and depend on the magnitude of the shear strain. With even greater shear strains, the strength of the soil can be affected, and soil failure may occur depending on the magnitude and number of load cycles. This section briefly describes the shear strain dependence of the shear modulus and damping ratio, different material models and empirical relationships with other soil properties for good estimations of soil properties used in soil dynamic analyses.

## 3.1. Shear Strain Dependency

The deformation behavior of the soil under cyclic loads is usually described by the **shear modulus**, i.e. the slope between the shear stress and the shear strain. For small strains, the shear modulus can be described as the average slope of the stress-strain curve (see *Figure 3.1.1.a*). For larger shear strains, the stress-strain curve becomes non-linear, and the shear modulus changes from being constant to depend on the magnitude of the shear strains. The shear stress's variation with the shear strain is given by a hysteresis curve, see *Figure 3.1.1.b*. The area within the hysteresis curve is a measure of the energy loss during a load cycle and is referred to as the **damping ratio.** The damping ratio is a measure of the soil's material damping and is, like the shear modulus, shear strain dependent.

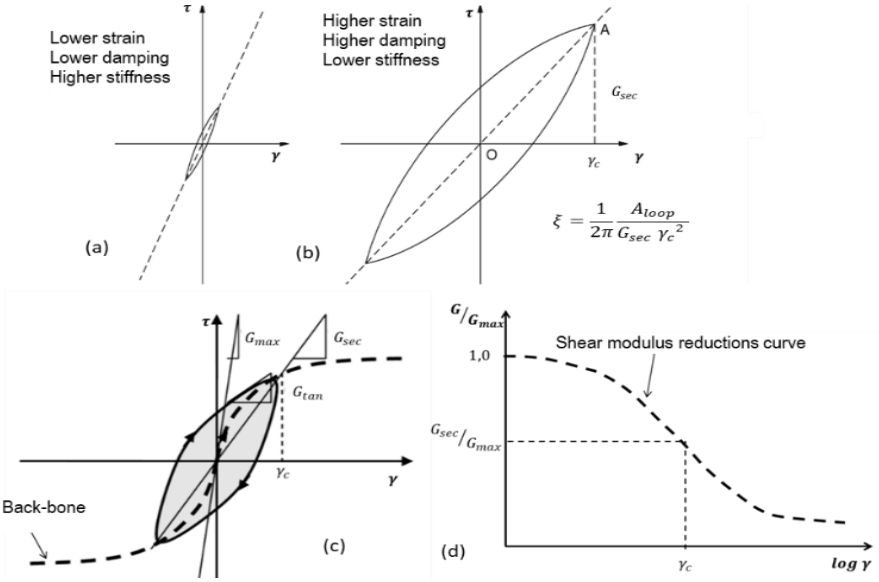


**Figure 3.1.1** a) Illustration of the effect of shear strain on shear modulus and damping ratio for (a) very small strains and (b) medium large strains. Definition of the (c) back-bone curve and the (d) shear modulus reduction curve.

The secant modulus is the most common method for describing the shear modulus variation with the shear strain. The curve that is obtained by this, see *Figure 3.1.1.c*, is called the **back-bone curve**. The largest value of the secant modulus is found at the origin and is the value of the shear modulus at very small shear strains. By drawing the ratio between the secant value of the shear modulus ($G_{sec}$) and the maximum shear modulus at very small strain value ($G_0$) against shear strain, the **shear modulus reductions curve** is obtained, se *Figure 3.1.1.d*. Based on results from laboratory test on many different soil types, it has been found that shear modulus and damping ratio have strong dependency with the soil type and effective stress. One of the most well-known reductions curves and damping ratios relationships with shear strain are those developed by *Vucetic & Dobry (1991*), see *Figure 3.1.2.* Here, the soil type is represented by the plasticity index (PI).

When shear strain becomes larger, the soil tends to contract for a loose deposit. If the cyclic load is fast, or the drainage is limited, an excess pore water pressure is instead built up. If loads continues to build up pore-pressure in the ground, the soil might eventually fail. For more detail description of this phenomena, see *Hall et al (2015).*

According to *Vucetic (1994),* the threshold value for shear strain when the soil becomes non-linear ($G/G_0<0.96$) is around 0.0005% for sand and between 0.0015 and 0.005% for clay. This threshold value is referred to as the **linear cyclic threshold shear strain** ($\gamma_{tl}$) and shear strains lower than this value are referred to as very small shear strains. The threshold value for when shear strain causes the soil to build up excess pore water pressure varies, according to *Mikami et al (2011)*, between about 0.01 and 0.02% for sand and gravel and between about 0.04, 0.08 and 0.14% for low (PI<30%), medium (30≤PI≤50) and high plastic (PI>50%) clay respectively. This threshold value is referred to as the **volumetric cyclic threshold shear strain** ($\gamma_{tv}$) and correspond to a shear modulus reduction ratio ($G/G_0$) around 0.6. Shear strains higher than this value are referred to as medium to large shear strains. Shear strains between the two threshold values, are referred to as small shear strains. The relationship between the plasticity index (PI) and the threshold values for the linear and volumetric cyclic shear strain are shown in *Figure 3.1.2.*

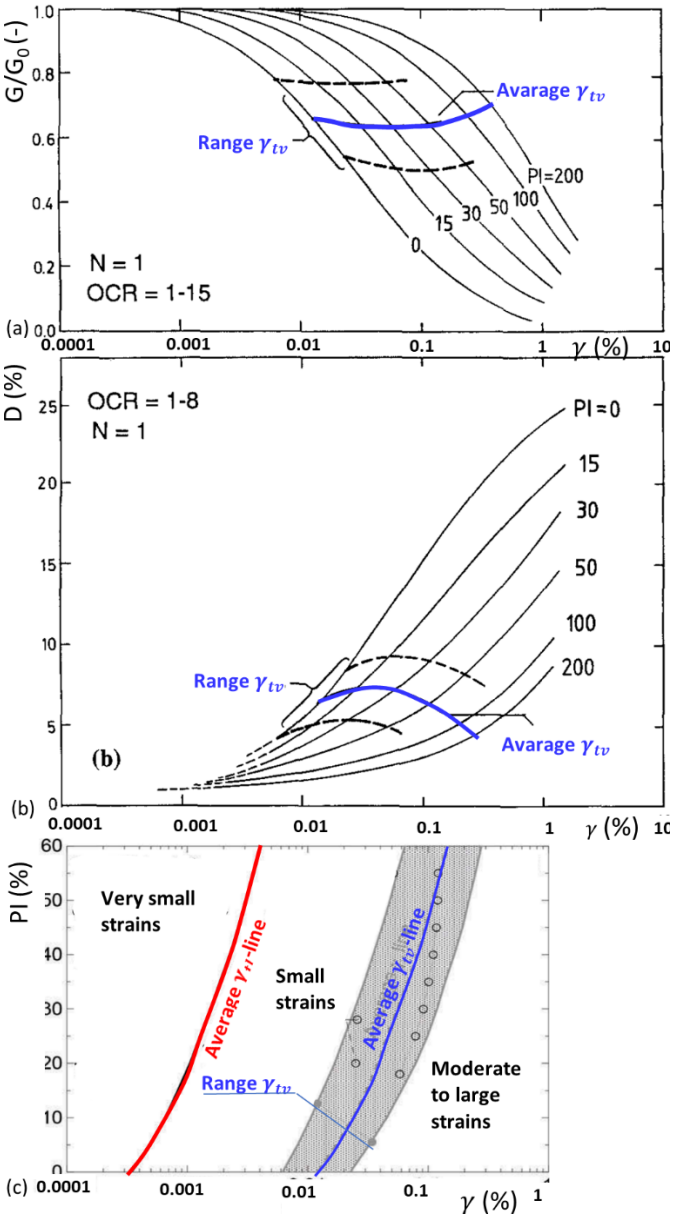


**Figure 3.1.2** a) Shear modulus reduction curve and (b) damping ration for soils of different plasticity indices. (c) The relationship between plasticity index for different soils' threshold values for linear cyclic shear strain and volumetric cyclic shear strain (*Vucetic, 1994*).

## 3.2. Material Models

Analyses of dynamic problems today are usually performed by calculations in numerical software. In order to describe the soil's behavior when exposed to loads, mathematical formulas - so-called material models, are used. The material models must be more and less complicated depending on what kind of the problem that is to be analyzed and what material behavior that is needed to be described. For soil dynamic problems, the higher the shear strain level, the more complex material model is needed to be able to model the various phenomenon that can arise. A summary of the relationships between the shear strain level, different soil behavior and appropriate material models to analyze the problem, is presented in *Figure 3.2.1.*

When a load is expected to induce very small shear strains in the ground, the soil behavior can be modelled by linear elastic model. If small to medium shear strain amplitudes are expected, the soil behavior becomes elasto-plastic. Then the shear strain dependency of the of the stiffness and the material damping needs to be considered. This can be performed by using a non-linear model where the shear strain dependency is considered directly in the calculations or by iterative manner with the simpler equivalent linear method. For larger shear strain, the material model needs to be more complex in order to model generation of excess pore pressure, shear strength reductions and failure conditions. These models are called cyclic non-linear material models.

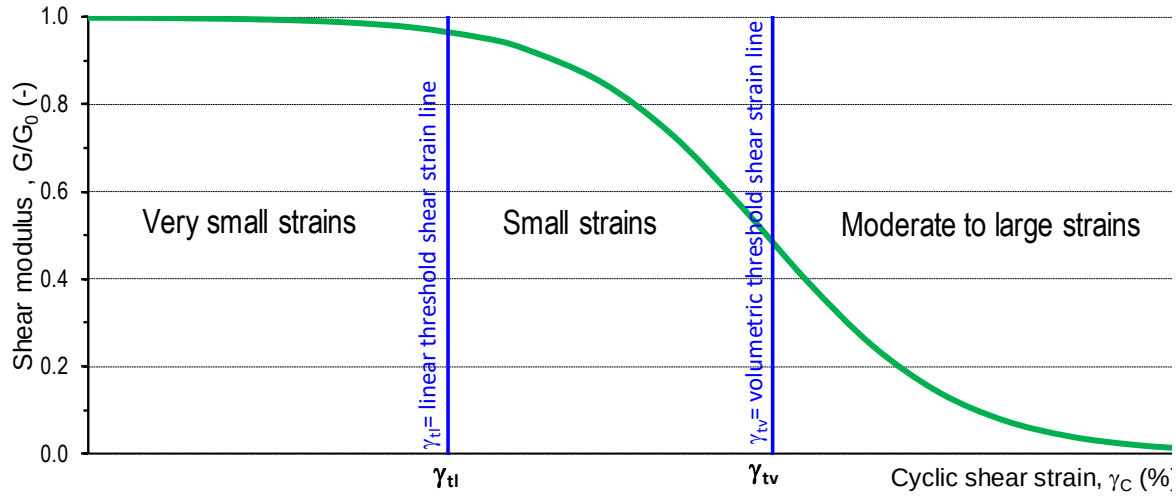


| Shear strains, $\gamma_c$ (-) | Very small ($\gamma_{tl}$) | Small strains | Moderate to large strains ($\gamma_{tv}$) |
|---|---|---|---|
| Stress-strain behavior | Linear | Non-linear | |
| Type of degradation | Constant stiffness | Fully recoverable behavior | Strength degradation |
| Pore water pressure | No pore water generation | No pore water pressure accumulation | Pore water pressure generation and build up with loading cycles |
| Governing soil properties | Stiffness and material damping | | Shear strength |
| Appropriate soil models | Linear model | Non-linear models | Cyclic non-linear models |

**Figure 3.2.1** Variation of dynamic shear modulus with shear strain amplitude with strain range classification, stress-strain behavior, type of degradation and pore pressure state. The figure and the table are created based on information from *Vucetic (1994)* and *Ishihara (1991*).

### 3.2.1. Linear Elastic Material Model

The simplest soil model for describing stress-strain relationships, is an elastic material model where stress and strain are linearly dependent. When a soil's deformation behavior is expected to be within a very small shear strain, the stress-strain ratio is in principle linearly proportional, see *Figure 3.1.1.a.* The use of a linear-elastic material model is then justified (e.g. for calculating wave propagation). In this case, the shear modulus is the most important soil parameter.

In soils with a linear elastic stress-strain behavior, there will theoretically be no energy loss other than the geometric damping. However, experimental evidence (*Hall & Richart, 1963*) shows that some energy is dissipated even at low strain levels, so the material damping is never zero.

### 3.2.2. Non-linear Models

As discussed earlier, both the shear modulus and the material damping are shear strain depended. So, when small and medium shear strain levels are expected, this behavior must be considered in the analyses. Most commercial numerical software have material models available to model this and these non-linear models are usually based on results by *Vucetic & Dobry (1991)* as shown in *Figure 3.1.2.* One of the most commonly used mathematical solutions, in matching the results by *Vucetic & Dobry (1991),* is given by *Darendeli (2001)*. These mathematical models take account for the effective stress and soil type by the plasticity index. In some models, also the overconsolidation ratio is considered. The shear modulus and damping ratio is calculated based on the shear strain level.

If the shear strain dependency of the soil properties is considered directly in the numerical calculations, the calculations can be very computational time consuming. This as the shear strains must be calculated and the material properties must be adjusted on the same time for each element and time-step. A simpler approach is therefore to use the so-called the equivalent linear method to approximate the actual non-linear response of the soil.

#### *The Equivalent Linear Method*

In the equivalent linear approach, linear elastic analyses are performed with soil properties that are iteratively adjusted to be consistent with an effective level of the shear strain that is induced in the ground. Calculations in the numerical software are performed with linear elastic material models, and after each calculation, the parameter values of the soil properties are adjusted to the calculated effective shear strain. The calculation is then repeated with the adjusted soil properties. This process is repeated until the adjusted shear strain depended soil property parameters do not change much from the previous calculation. Usually, the calculations converge, with a less than 5% difference of the soil property parameters, after about 3-5 iterations

The effective shear strain represents the average response to a cyclic load. Usually, the effective shear strain is obtained from the calculated maximum shear strain according the following equation:

$$\gamma_{\text{eff}} = R_{\text{r}}\ \gamma_{\text{max}} \qquad \textit{(Equation 3.2.1)}$$

where $R_r$ is a strain reduction factor and is often chosen to have a value of 0.65 (*Yoshida et al., 2002*). The maximum shear strain ($\gamma_{\text{max}}$) is calculated in the numerical model for a specific layer and region with similar shear strain levels. The iterative process with equivalent material method in a numerical calculation program can be performed as shown in *Figure 3.2.1*

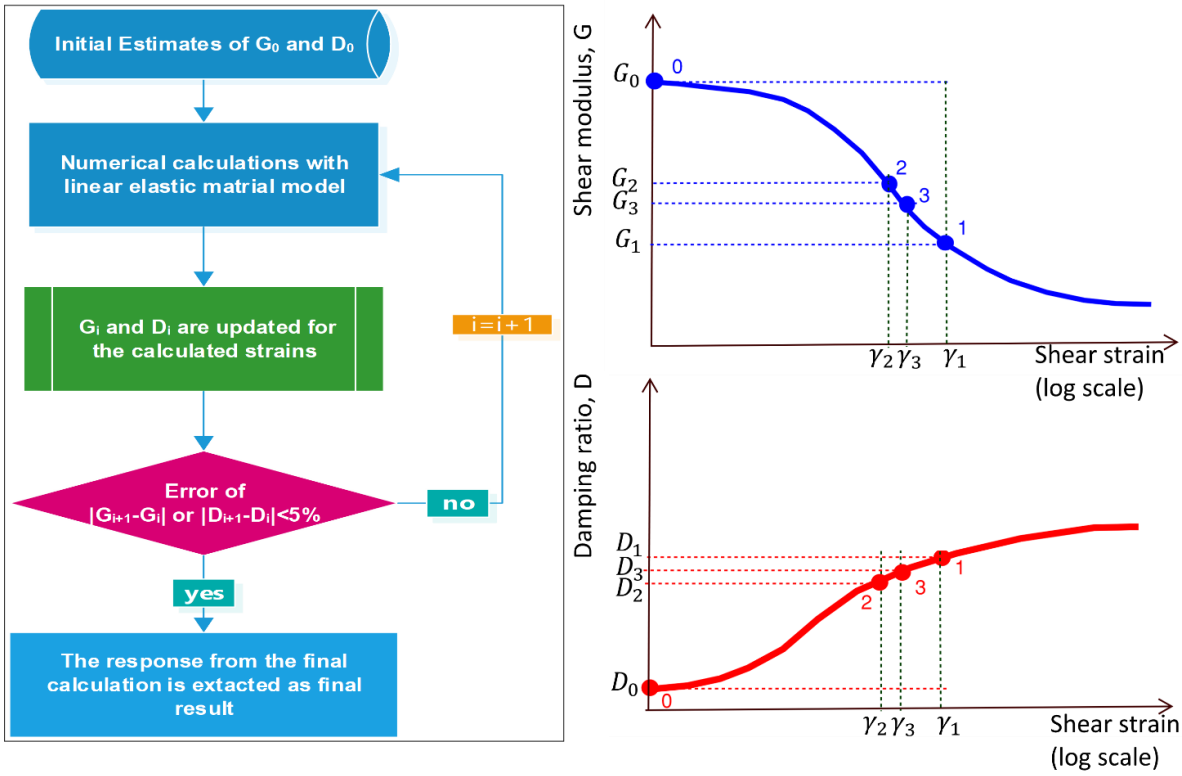


**Figure 3.2.1** The iterative process when using the equivalent material method to consider the soil properties non-linear behavior with shear strain in numerical calculations.

The equivalent linear method was developed for analyses of earthquake induced ground vibrations with the software ProShake. The method has, according to the literature *(Schnabel et al, 1972)*, shown to provide reasonably good estimates of the ground response for many different kinds of geotechnical conditions and ground vibrations. It must, however, be accentuated that strain-compatible shear modulus and damping ratios remains constant through the calculation of the analyzed problem (earthquake or a train traffic induced ground vibrations). Also, when the strains induced in the soil are small and when they are large.

### 3.2.3. Cyclic Non-Linear Material Models

At large shear strains, the soil properties tend to change considerably with the shear strain, but also with the number of load cycles and its frequencies. To model this, the material model must be able follow the actual stress-strain relationship of the soil behavior under a cyclic load. In this way, the shear strength of the soil can be determined with a suitable modeling of the generation of excess pore pressure. The cyclic non-linear models are characterized by a backbone curve and series of rules which govern the unloading-reloading behavior, stiffness degradation, irregular loading, densification, and other effects. The more complex the model, the larger the number of rules is used and the more effects that can be modeled. See *Ishihara (1996)* for further information of these models. See also *Appendix A*, where NGI:s experiences on advanced modeling of soils behavior during cyclic loading are summarized.

## 3.3. Selected Empirical Relationships

This chapter summarize that empirical relationships that was used in the present study. This cover modeling the shear strain-dependency of the soil properties, as well as estimating the initial values of the dynamic soil properties based on the results from commonly used soil investigation methods in Sweden. The chapter also contains a short descriptions of ground reinforcement with lime-cement columns for railway embankment and how the dynamic soil properties of lime-cement columns can be estimated.

### 3.3.1. Shear Strain Dependency

Some numerical software have the material model developed by *Darendeli (2001*) as a choice for modeling the soil properties with shear strain dependency. A similar material model has been developed by *Zhang et al (2005).* Both these two material models show reasonably good agreement with the laboratory tests results as compiled by *Vucetic & Dobry (1991)*. However, as seen in *Figure 3.3.1,* there are some slight differences in the results between the two material models. Darendeli's material model is, however, very complex and especially for the damping ratio. Because of the mathematical simplicity, Zhang's material model was chosen to be used in this study. The equations for shear strain dependency model by *Zhang et al (2005*) are as follow:

$$\frac{G}{G_0} = \frac{1}{1+(\gamma_c/\gamma_r)^{\alpha}} \qquad \textit{(Equation 3.3.1.a)}$$

$$D = D_0 + 10.6(G/G_0)^2 - 31.6(G/G_0) + 21 \qquad \textit{(Equation 3.3.1.b)}$$

Where,

| | |
|---|---|
| $D_0 = (b_7 \cdot PI + b_8) \cdot (\sigma'_m/100kPa)^{-k/2}$ | estimate of the initial (very small strain) damping ratio [%] |
| $\sigma'_{m0} = \sigma'_{v0} \cdot (1 + 2 \cdot K_0)/3$ | average effective stress [kPa] |
| $\sigma'_{v0}$ | initial effective vertical stress [kPa] |
| $PI$ | plasticity index [%] |
| $K_0$ | earth pressure at rest [-] |

Other parameters and constants

| | |
|---|---|
| $\gamma_r = \gamma_{r1} \cdot (\sigma'_m/100kPa)^k$ | $\gamma_{r1} = b_1 PI + b_2$ |
| $\alpha = b_3 PI + b_4$ | $k = b_5 exp\,(-b_6 PI)$ |
| *$b_1$=0.0011 vid PI>10 else 0.0009* | *$b_2$=0.0749 for PI>10 else 0.0385* |
| *$b_3$=0.0021 for PI>10 else 0.0043* | *$b_4$=0.834 for PI>10 else 0.794* |
| *$b_5$=0.316 for PI>10 else 0.420* | *$b_6$=0.0142 for PI>10 else 0.0456* |
| *$b_7$=0.008* | *$b_8$=0.82* |

For more accurate results, the empirical relationship should be correlated with the results from advanced laboratory tests (resonant column tests and/or cyclic triaxial test) on soil samples from the site of the analyses. See *Figure 7.1.2* for the comparisons of *Zheng's* and *Darendeli's* material models with laboratory tests on gyttja specimens from Ledsgård.

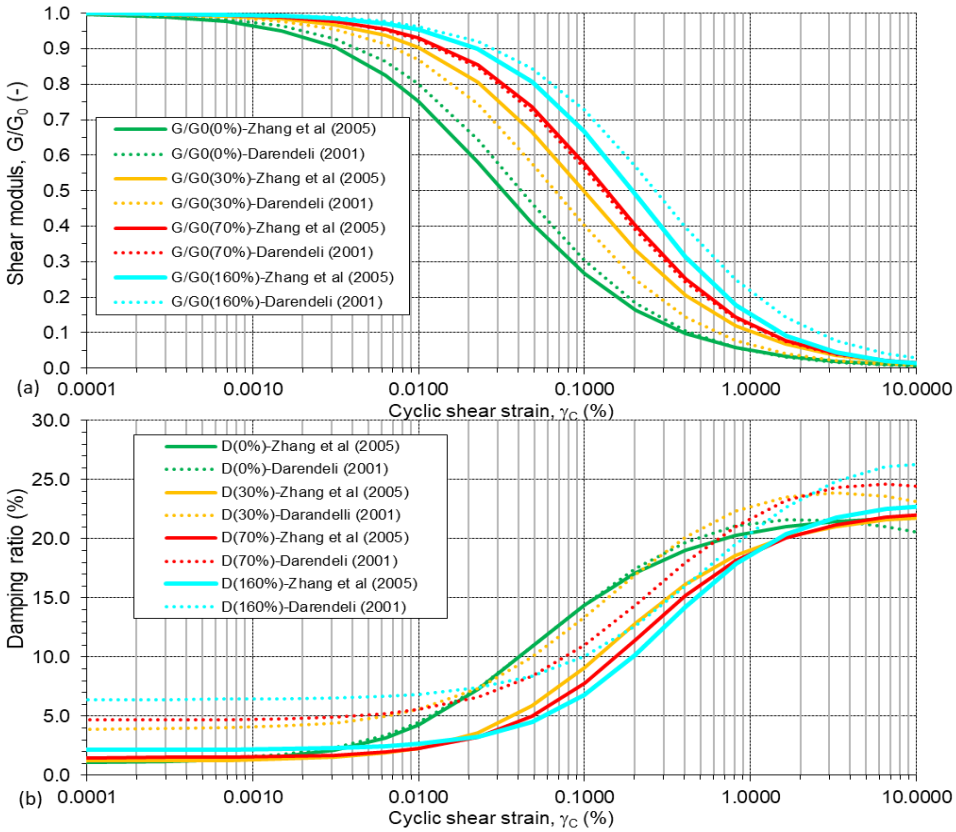


**Figure 3.3.1** Comparison of the shear strain dependency material models by *Zhang et al (2005)* and *Darendeli (2001)* for a confining pressure of 30kPa and different placidity indexes.

## 3.3.2. Initial Shear Modulus

The shear modulus is the single most important soil parameter in influencing the propagation of stress waves and resulting vibrations. The most reliable means of evaluating the in-situ value of the shear modulus is to measure the shear wave velocity directly in the field (e.g., cross-hole tests) or by laboratory tests (e.g., bender element tests) on soil specimens from the site. The initial (very small shear strain) shear modulus $G_0$ can then be calculated as:

$$G_0 = \rho \cdot c_{S0}^2 \qquad \textit{(Equation 3.3.2)}$$

where,

| | |
|---|---|
| $\rho$ | total density [kg/m$^3$] |
| $c_{S0}$ | shear wave propagation speed [m/s] |

For further information concerning determined the initial shear modulus with in-situ and laboratory tests, see *Hall & Bodare (2003)* and *Rydén (2021*), respectively.

The initial shear modulus can also be estimated by empirical relationships with other soil parameters. In cohesionless soils, the shear modulus is mainly affected by the effective stress and to some degree of the compactness of the soil. Most empirical relationships for estimating the initial shear strain shear modulus in cohesionless soil is based on the effective confining pressure and void ratio. There also exist a lot experience in estimating initial shear modulus from effective confining pressure and the N-values from SPT tests. In Sweden, however, both determination of void ratio (e) and soil investigation using the SPT tests is very uncommon in Sweden. The relative density ($D_R$) can, however, be estimated from CPT tests. For **cohesionless soil**, the following empirical expressions can therefore be used (Seed et al 1986):

$$G_0 \approx 220 \cdot K_2 \cdot \sqrt{\sigma'_{m0}} \quad [kPa] \qquad \textit{(Equation 3.3.3)}$$

where,

| | |
|---|---|
| $K_2 \approx C_1 \cdot (16 + 0.6 \cdot D_r)$ | shear modulus coefficient (Seed et al, 1987), [-] |
| $C_1$ | constant with value of 1.0 for sandy soil 1.6 for gravely soil [-] |
| $D_R$ | relative density [%] |
| $D_R \approx 0.478(q_{C1N})^{0.264} - 1.063$ | empirical equation for sand (*Idriss & Boulanger, 2003*) |
| $q_{C1N} = \frac{q_C}{P_{a2}} \cdot \left(\frac{P_a}{\sigma'_{v0}}\right)^{0.5}$ | normalized cone penetration resistance (*Robertson & Wride, 1988*) |
| $q_C$ | cone penetration resistance from CPT [MPa] |
| $P_a$=100kPa | reference pressure |
| $P_{a2}$=0.1MPa | reference pressure |
| $\sigma'_{m0} = \sigma'_{v0} \cdot (1 + 2 \cdot K_0)/3$ | average initial effective stress [kPa] |
| $\sigma'_{v0}$ | initial effective vertical stress [kPa] |
| $K_0 = 1\text{-}sin(\varphi')$ | earth pressure at rest [-] |

For **cohesive soils**, estimates of maximum shear modulus can be obtained from undrained shear strength ($c_u$). For Scandinavian clays, according to *Larsson & Mulabdic (1991)*, the following empirical relationships are recommended to estimate the maximum shear modulus for intermediate plastic to high plastic clay (equation 3.3.4.a), and low plastic clay and clayey gyttja (equation 3.3.4b) respectively:

$$G_0 \approx (207/PI + 250) \cdot c_u \qquad \textit{(Equation 3.3.4.a)}$$

$$G_0 \approx 504/w_L \cdot c_u \qquad \textit{(Equation 3.3.4.b)}$$

where,

| | |
|---|---|
| $PI$ | plasticity index [%] |
| $w_L$ | liquid limit [%] |
| $c_u$ | undrained shear strength [kPa] |

The empirical relation between shear modulus and undrained shear strength is strong and estimates of the initial shear modulus using the above equations usually gives a good agreement with the results from seismic field tests such as cross-hole tests.

### 3.3.3. Initial Damping Ratio

The damping ratio usually varies between 2% and 6% for very small shear strains. The damping ratio is usually lower for ground vibrations in clay and slightly higher in friction soil at the same shear strain level. The damping ratio can be determined in field and laboratory tests as shown in *Hall & Bodare (2000)* and *Rydén (2021),* respectively. For an empirical estimate of the initial damping ratio, the following equations can be used (*Zhang et al, 2005*):

$$D_0 = (0.008 \cdot PI + 0.82) \cdot (\sigma'_m/100kPa)^{-k/2} \qquad \textit{(Equation 3.3.5)}$$

where,

| | |
|---|---|
| $\sigma'_{m0} = \sigma'_{v0} \cdot (1 + 2 \cdot K_0)/3$ | average effective stress [kPa] |
| $\sigma'_{v0}$ | initial effective vertical stress [kPa] |
| $PI$ | plasticity index [%] |
| $k = b_5 exp\,(-b_6 PI)$ | constant |
| $b_5$=0.316 for PI>10 else 0.420 | constant |
| $b_6$=0.0142 for PI>10 else 0.0456 | constant |

### 3.3.4. Properties of Lime-Cement Columns

Lime-cement columns (LCC) is a commonly used ground reinforcement measure in cohesive soils for railway and road embankments in Scandinavia. LCC ground reinforcement consists of stabilized columns of soils that is produced at the site. The columns are **produced** by a rotating mixing tool that is pressed down into the natural soil and binder is discharged and mixed in while stirring the soil mass. Most commonly, the soil is only stirred while pressing down the mixer and binders are discharged and mixed with the soil while rotating the mixer on the way up to the ground surface. The columns in the LCC ground reinforcement normally have with diameters of 0.5, 0.6 or 0.8m and with a maximum length of about 25 m. A diameter of 0.6m is most common. Large diameter columns are often economically advantageous, when a large volume of soil is to be stabilized, e.g., in blocks and continues walls. The installation with large diameters is limited, however, to the required torque to install the columns into the ground.

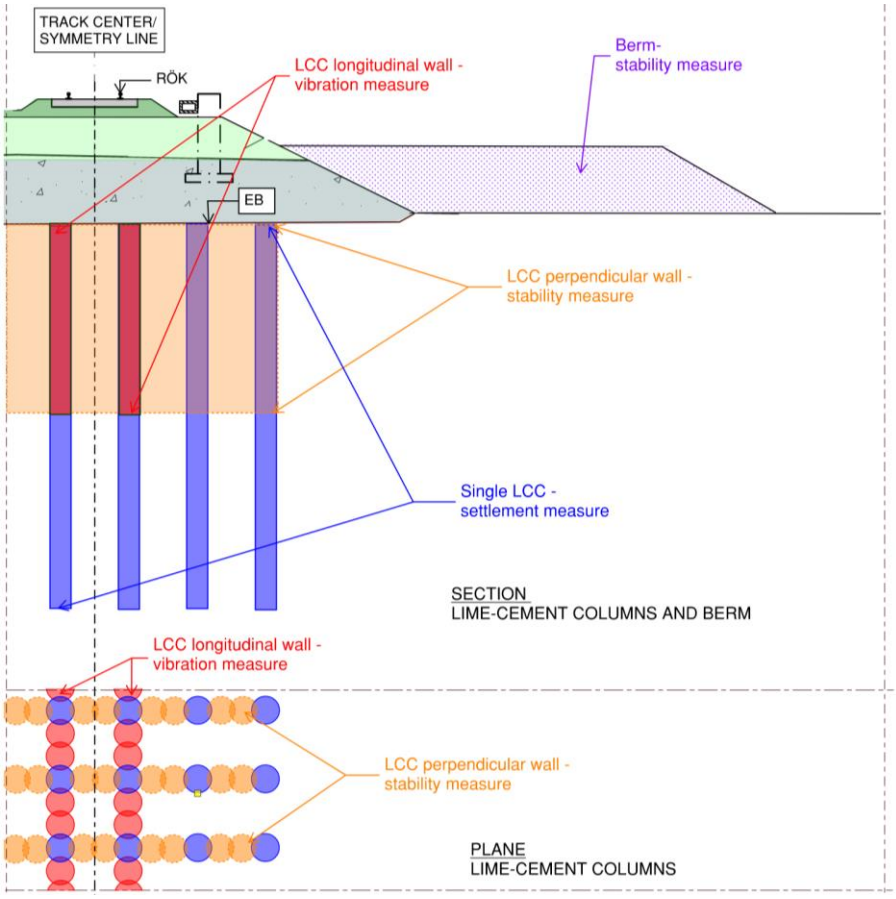


**Figure 3.3.2** Typical patterns of LCC in ground reinforcement of embankments as a measure for settlement, stability, and vibrations problems respectively**.**

The **main application** of lime-cement columns in Sweden is to reduce ground settlements and ensure the stability of loose soils under road and railway embankments. Lime-cement columns is also the main ground reinforcement method against large ground vibrations (so-called high-speed ground vibrations) for railways embankments. When used to reduce settlement, single columns with a certain spacing (1.5 - 2.5m) are installed and columns are usually made as long as possible. To use the method in order to increase the total stability, LCC must be placed in continues walls perpendicular to the slope. This as LCC mainly can take compression loads and has less capacity for shear and tensions forces. In the same way, when LCC is used as a measure against high-speed ground vibrations, the columns must be installed as continues walls along embankment. In the latter case, LCC are placed centrically under the rail. Typical patterns of LCC for ground reinforcement for settlement, stability and vibrations are shown in *Figure 3.3.2*.

The installed lime-cement columns are usually very heterogenous and is not unusual that the columns produced at one site, can have **undrained shear strengths** that varies between 100 and 500kPa. Usually, the binder mix is chosen so that the installed lime-cement columns will have a shear strength of at least 100kPa. To verify the minimum shear strength of the LCC, different types of recipes of the mixing binding with soil from the site is first tested in the laboratory and then a certain number of columns are tested in-situ. For further information on the LCC reinforcement method, see *Larsson (2006*).

*Åhnberg & Holmén (2011)* have conducted a large number of laboratory tests on lime-cement stabilized clay, where the undrained shear strengths ($c_u$) have been determined by unconfined compression test and compared the very small shear strain shear wave ($c_{S0}$) and compression **wave propagation speed** ($c_{P0}$) on the same specimen with bender elements and resonant column tests. In the tests, samples of high plasticity clay were used from 7 different sites in Sweden. Based on these tests, the following correlation between the shear strength and the wave propagation speeds were found (*Åhnberg & Holmén, 2011*):

$$2 \cdot c_{u,LCC} \approx 0.0028 \cdot {c_{S0,LCC}}^2 + 0.29 \cdot c_{S0,LCC} \qquad \textit{(Equation 3.3.6.a)}$$

$$2 \cdot c_{u,LCC} \approx 0.001 \cdot {c_{P0,LCC}}^2 + 0.22 \cdot c_{P0,LCC} \qquad \textit{(Equation 3.3.7.a)}$$

where,

| | |
|---|---|
| $c_{u,\mathrm{LCC}}$ | Undrained shear strength for the lime-cement stabilized soil [kPa] |
| $c_{S0,\mathrm{LCC}}$ | Shear wave propagation speed for the lime-cement stabilized soil [m/s] |
| $c_{S0\mathrm{LCC}}$ | Compression wave propagation speed for the lime-cement stabilized soil [m/s] |

The equations above can be reformulated in terms of wave propagation speeds as functions of the undrained shear strength:

$$c_{S0,kc} \approx 25/14 \cdot \left(\sqrt{224 \cdot c_{u,LCC} + 841)} - 29\right) \qquad \textit{(Equation 3.3.6.b)}$$

$$c_{P0,kc} \approx 10 \cdot \left(\sqrt{20 \cdot c_{u,LCC} + 121)} - 11\right) \qquad \textit{(Equation 3.3.7.b)}$$

*Dannewitz et al (2005)* have determined undrained shear strength and shear wave speed from both field and laboratory test on lime-cement mixed clay in Uppsala. The shear strength was determined by unconfined compression tests and probing test in laboratory and field, respectively. The shear wave propagation speed was determined by bender element and down-hole tests, in laboratory and field, respectively. Good agreement between the shear strength and shear wave propagations speed, was found using the following equations (*Dannewitz et al, 2005*):

$$c_{u,LCC} \approx 0.0424 \cdot {c_{S0,LCC}}^{(1.462)} \qquad \textit{(Equation 3.3.8.a)}$$

$$c_{S0,LCC} \approx 23.585 \cdot {c_{u,LCC}}^{(1/1.462)} \qquad \textit{(Equation 3.3.8.b)}$$

According *Dannewitz et al (2005)*, the above equation showed also good agreement with unstabilized clay. When comparing the *Equation 3.3.6* and *Equation 3.3.8,* they give similar result for typical shear strength values of lime-cement-columns.

## 3.4. References


DANNEWITZ, N. ERIKSSON, H., MATTSSON H., LARSSON, R. HOLM, G, (2005). Seismisk kontrollmetod för kc-pelare. *Svensk Djupstabilisering*. Arbetsrapport 35:

DARENDELI, M. B. 2001. "Development of a new family of normalized modulus reduction and material damping curves." PhD thesis, Dept. of Civil Engineering, *U. Texas at Austin*.

DÍAZ-RODRÍGUEZ, J. A., AND J. A. LÓPEZ-MOLINA (2008). "Strain thresholds in soil dynamics". he 14th *World Conference on Earthquake Engineering. 2008.*

HALL, J.R & RICHART, F.E, (1963), "Dissipation of elastic wave energy in granular soils", *J of Soil Mechanics and Foundations Division*, ASCE, Vol. 89 No. SM6, pp. 27-56

HALL,L, & BODARE, A. (2000). "Analyses of the cross-hole method for determining shear wave velocities and damping ratios". *Soil Dyn & Earthquake En*. Vol.20. pp. 167-173.

HALL, L & WERSÄLL, C. editors (2015). "Markvibrationer". SGF Informationsskrift 1:2012. Reviderad 2015-12-22. Utgiven av *SGF*.

MIKAMI, T., ICHII, K., NISHINA, H., & KITADE, K. (2011) "Effect of variation of determined parameters on numerical analyses for seismic performance evaluations." *Geotechnical and Highway Engineering*- pp. 429-434).

IDRISS, I.M & BOULANGER, R.W., (2006) "Semi-emperical procedure for evaluation liquefaction potential." *Soil Dynamics & Earthquake Engineering*. V26. pp.429-434.

ISHIHARA, K. (1996). Soil behavior in earthquake geotechnics.

LARSSON L. (2006) "Djupstabilisering medbindemedelsstabiliserade pelare och masstabilisering– En vägledning". *Svensk Djupstabilisering*. Rapport 16.

LARSSON, R., & MULABDIC, M. (1991). Shear moduli in Scandinavian clays. Measurement of initial shear modulus with seismic cones. Empirical correlations for the initial shear modulus in clay. Report 40. *SGI.*

RYDÉN, N. (2021) " Maximal dynamisk modul från labratoriemätningar (Skjuvmodul)". Rapport 2:2021. *SGF.*

ROBERTSON, P.K, & WRIDE C.E. (1988). Evaluation cyclic liquefaction potential using cone penetration test. *Can. Geotech. J. 35:442-459.*

SCHNABEL, P., SEED, H. B., & LYSMER, J. (1972). Modification of seismograph records for effects of local soil conditions. *B Seismological Society of America*, 62(6), 1649-1664.

SEED, H. B., WONG, R. T., IDRISS, I. M., & TOKIMATSU, K. (1986). Moduli and damping factors for dynamic analyses of cohesionless soils. *J Geotech Eng* 112(11), 1016-1032.

VUCETIC, M. (1994). Cyclic threshold shear strains in soils. *J Geotech Engi*, 120(12), 2208-2228.

VUCETIC, M., & DOBRY, R., (1991), "Effect of soil plasticity on cyclic response", *J Geotechl Eng*, ASCE, Vol. 117, No. 1, pp. 89-107

YOSHIDA, N.,KOBAYASHIi, S., SUETOMI, I., & MIURA, K. (2002). Equivalent linear method considering frequency dependent characteristics of stiffness and damping. *Soil Dynamic and Earthquake Engineering*, 22(3), 205-222.

ZHANG, J., ANDRUS, R. D., & JUANG, C. H. (2005). Normalized shear modulus and material damping ratio relationships. J *Geotech & Geoenv Eng,* 131(4), 453-464.

ÅHNBERG, H., & HOLMÉN, M. (2011). Assessment of stabilized soil strength with geophysical methods. *Ground Improvement*, V164.I3.pp. 109-116.

# 4. Optimization of Numerical Calculations

## 4.1. Analysis Method

The most straightforward numerical approach to solve the problem under consideration is to develop a full 3D finite element model of the entire track-embankment-ground system (*Hall, 2003; Shih, 2017*). The track-embankment elements and possible reinforcement elements, if needed, are also modeled along with part of the underlying soil. The non-reflecting boundaries can then be implemented at the borders of the near-field soil domain to account for the semi-infinite extend of the truncated far-field soil medium. The main advantage of this approach is that it allows great flexibility in modeling complex geometries (variability in the track-embankment profile, local discontinuities, particular structures, inclined soil layers) and, above all, it can be easily applied using commercial software packages which are widely available in the industry. The 3D FE model can be solved in both time and frequency domain. The frequency domain solution (*Kausel, 2017*) is not as straightforward as the time domain solution in practice as it requires Fourier transform analysis. The frequency domain solution is very efficient in solving linear problems, provided that a limited number of output results are required. In order to include non-linear effects in the track or soil, or transient effects, a time-domain approach will be required. However, this is computationally more expensive. The main weakness of the full 3D approach is the large computational cost.

Generally, there are two other alternative approaches which have been extensively used to solve the problem. Apart the analytical methods (*Kaynia et al., 2000; Sheng et al., 2004; Karlström & Boström, 2006*), the 2.5D approaches (finite /boundary elements methods and/or finite/infinite elements methods) can be also used, assuming the track and soil are invariant along the track direction (*Yang et al., 2003, Costa et al., 2010; François et al., 2010; Galvín et al., 2010; Gao et al., 2012*). The fundamental hypothesis for such a simplification (2D geometry and 3D loading conditions) is the periodic nature of the track along its longitudinal direction. In general, a frequency-wavenumber domain transformation is required for solving the 3D wave propagation problem. Recently, a track modeling approach based on a wave analysis technique for multi-coupled periodic structures has been presented. This approach allows the efficient modeling of a track with varying characteristics in the longitudinal direction (*Germonpré et al., 2018*). Evidently, these rigorous and efficient methods have their own limitations, and, above all, they are not generally available in commercial software.

## 4.2. Modeling of Non-Reflecting Boundaries

In FE modeling, the dimensions of the finite domain of the soil medium in combination with the implemented non-reflecting boundaries should guarantee that the steady state response of the system is not contaminated by wave reflection at the boundaries. Different types of non-reflecting boundaries such as viscous dashpots/infinite elements (*Lysmer & Kuhlemeyer, 1969*) or perfectly matched layers (PML) (*Basu & Chopra, 2003*) are available in commercial finite element software.

Both viscous dashpots and infinite elements perfectly absorb waves at normal incidence while their efficiency exponentially decrease as the wave's impinging angle deviates from the normal direction. Therefore, the size of the near-field soil domain in this case needs to be sufficiently large. These types of absorbing boundaries are not also applicable to static problems. As a more advanced and accurate alternative for the viscous boundaries, the Perfectly Matched Layer (PML) can be used. In this method, an absorbing boundary layer is modeled at the edges of the finite mesh. In order to absorb elastodynamic waves inside the PML buffer zone, the spatial coordinate is artificially extended by applying complex coordinate stretching (*Basu & Chopra, 2003*). The better performance of the PML in comparison to the viscous boundaries, however,

comes at the cost of tuning the attenuation parameters of the PML layer for the frequency range of interest. As a practical alternative, fixed-boundary condition is frequently used for modeling simplicity while it leads to large FE models (*Shih, 2017*).

## 4.3. Size of the computational model

In the following, a 3D FE-PML model in the frequency domain, developed in COMSOL, will be used to study the optimum size of the numerical model. In the analyses, the geometrical and initial material properties of the Ledsgård case study are used, see *Table 5.3.1. Figure 4.3.1* shows the general configuration of the FE-PML model. It should be noted that this model does not include the rail and railpads and moving loads are directly applied at sleepers' locations.

The accuracy of the chosen mesh configuration and PML attenuation parameters in absorbing the scattered outgoing waves in the frequency range of interest has been verified using the Direct Stiffness Method (*Kausel, 2006*) as implemented in the elastodynamics toolbox EDT (*Schevenels et al., 2009*). The implemented FE-PML model will be considered as a reference model for verifying the base model methodology in chapter 5.

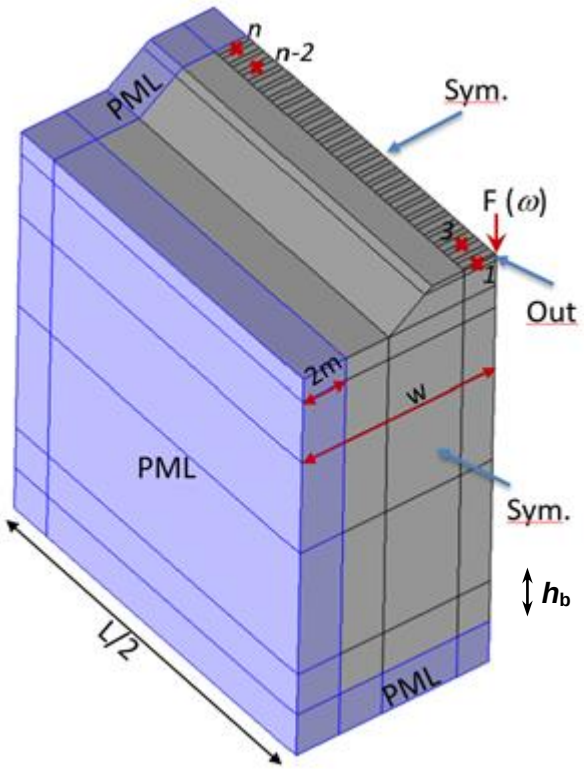


**Figure 4.3.1** General configuration of the FE-PML model in the frequency domain

### 4.3.1. Length of the FE Model

In general, the size of the FE model along the track should be sufficiently long to consider the reaction forces far from the point of interest, providing a non-negligible contribution to the computed vibration levels (*Kouroussis et al., 2019*). Previous studies showed that the response to the moving load requires a certain length of calculation for the waves to develop fully which depends on the geometrical spreading and the propagation velocities of the different waves (*Shih, 2017*). The required length generally varies with the speed of the traveling load as well as the soil properties. *Figure 4.3.2* shows computed max/min mid-point displacement of the numerical model in the case of Ledsgård site, subjected to X2000 train moving load. As can be seen, the required length depends on the proximity of the load speed to the critical speed and

increases considerably in the vicinity of the critical speed. To obtain reasonably good (~ 90%) accuracy in the calculations, the length of the FE-model should be set to $L$ =120 m for train speeds up to 95% of critical speed.

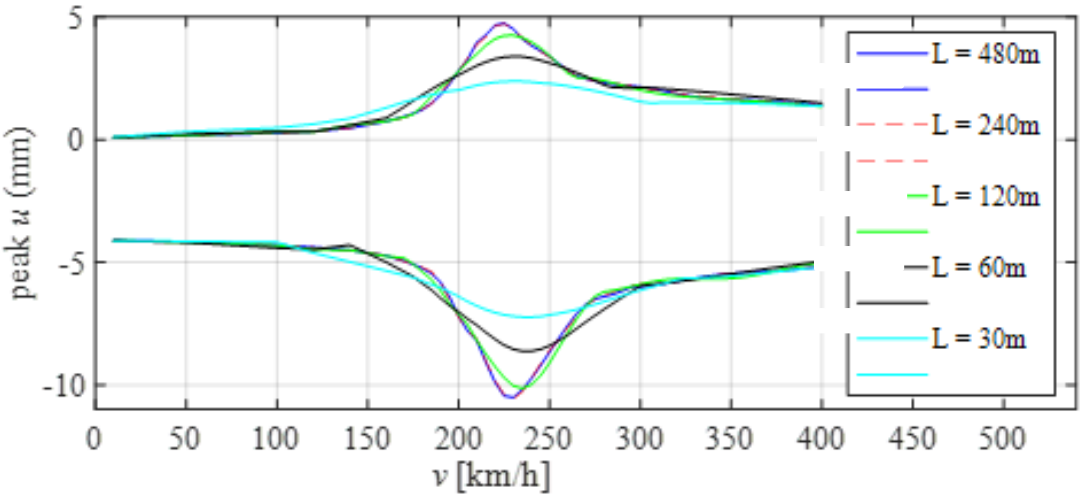


**Figure 4.3.2** Computed max/min mid-point displacement of the numerical model versus train speed, Ledsgård site case study subjected to X2000 train moving load

As shown in *Section 5.3*, the required model length can be obtained for each train speed based on an iterative procedure.

### 4.3.2. Width of the FE Model

In the presence of an efficient non-reflecting boundary condition at the far field side of the FE model, the width of FE model can be kept as small as possible while the computed vibration levels of the track are not contaminated by the spurious wave reflections.

The results of steady-state analyses of the Ledsgård case study in *Figure 4.3.3* have shown that the total width of the FE model in combination with PMLs can be set to 9 m. In the case of using viscous dashpots (or infinite elements) as absorbing boundaries, however, this width should be almost doubled. In the previous numerical analyses of the studied problem (*Hall, 2000; Shih, 2017*), the width of the FE models was set to 23 m and 20 m in which dashpots and infinite elements were respectively used as non-reflecting boundaries.

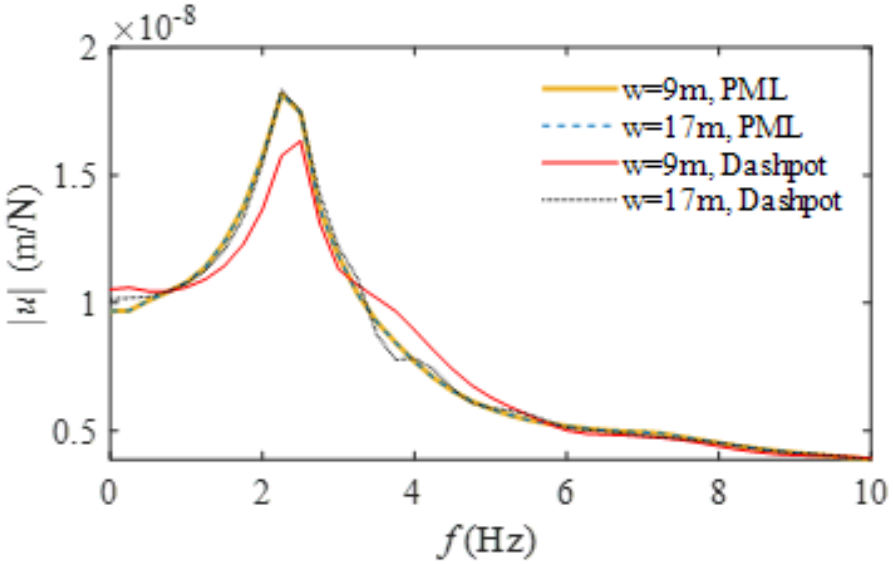


**Figure 4.3.3** Computed frequency response functions at the mid-point of the model for different boundary conditions at the side of the model

In the absence of any non-reflecting boundary condition at the far field side of the FE model, the width of the model should be sufficiently large to ensure that the spurious wave reflections at the side have negligible effect on the computed vibration levels on track. As a practical recommendation, the width of FE model (*W*), can be estimated as per Equation 4.3.1. This was approximated based on 6 dB reduction at the side which gives good agreement with the results of a wave-number FE/BE model (*Shih, 2017*).

$$W \geq 1.38\, c_s/\alpha \qquad \textit{(Equation 4.3.1)}$$

where $c_s$ is the shear wave velocity and $\alpha$ is the Rayleigh's mass proportional damping coefficient as defined in *Chapter 4.4.5*.

Theoretically, the decay with distance for a plane harmonic wave at circular frequency $\omega$ propagating in an elastic medium at a constant wave speed, $c$, can be expressed in dB/m as

$$D = 8.69\omega\xi/c \qquad \textit{(Equation 4.3.2)}$$

where $\xi$ is the damping ratio. *Shih (2017)* showed that when the mass-proportional damping is used, $D$ becomes frequency-independent and a reduction in terms of distance can be estimated for the required width of the model, minimizing the spurious reflection from the side.

### 4.3.3. Effect of Bottom Layers

It is crucial to properly model the soil stratification in a way that the computed resonance frequencies of the underlying ground system are not affected by the modelling simplifications. In the presence of a shallow bedrock at site, the bedrock can be assumed as rigid and thus the bottom nodes of the lowest soil layer be fixed.

In the absence of a shallow bedrock, the lowest soil layer should be modeled as a half-space medium by using proper non-reflecting boundary conditions. However, provided that the FE model is deep enough, a fixed-boundary condition can be used at the bottom of the model for the sake of modeling simplicity. It has been found previously that the computed vibration levels and the estimated range of the critical speed are mainly governed by the properties of the upper ground layers (*Shih, 2017*). As shown in Figure 4.3.4, in the case of Ledsgård site, the computed vibration levels and the estimated critical speed by the FE-PML model subjected to a unit moving load is not noticeably affected by the depth of the lowest clay layer (denoted as $h_b$ in Figure 4.3.1).

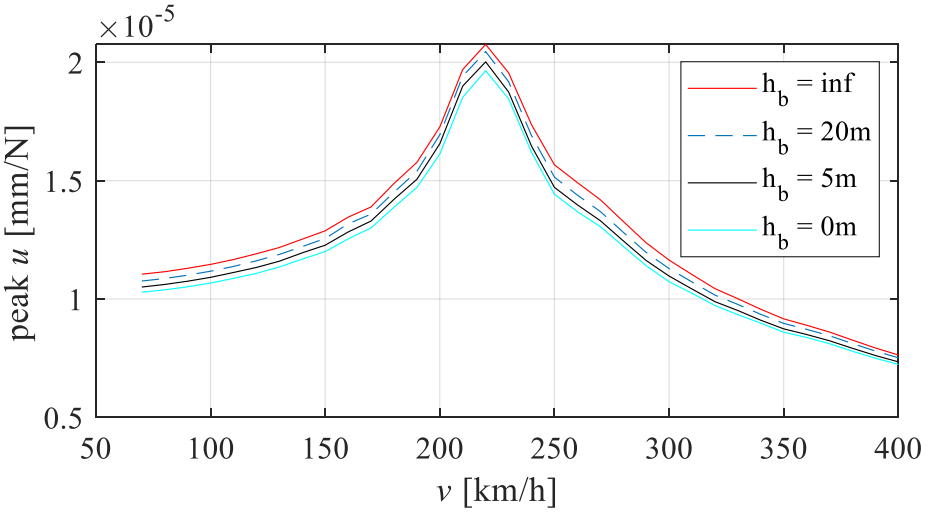


**Figure 4.3.4** Computed mid-point peak displacement of the numerical model versus a moving load speed, Ledsgård site case study subjected to a unit single load

## 4.4. General Recommendations

### 4.4.1. Maximum Frequency of Interest

Since the interest of this work is focused on the region close to the track, the problem under study is generally characterized by a low-frequency content ($f_{max} < 20$ Hz).

Generally, the overall frequency range of interest for the studied problem can be accurately estimated based on the computed frequency response functions through a receptance (steady state) analysis. However, the maximum frequency of interest, $f_{max}$, can be roughly approximated as the first vertical resonant frequency of the layered soil beneath the track, $f_{v,1}$ (*Gazetas, 1998*).

$$f_{v,1} = \frac{c_{La}}{4H} \approx \frac{c_{S0}}{2H} \qquad \textit{(Equation 4.4.1)}$$

where $c_{La}$ and $c_{S0}$ are respectively Lysmer's analog wave velocity (*Lysmer & Richart, 1966*) and shear wave velocity of the softest layer and $H$ is the corresponding depth.

### 4.4.2. Element Size

The maximum element size, $l_{e,max}$, in the soil medium is controlled by the minimum shear wavelength, $\lambda_{min} = c_s/f_{max}$. Nine nodes (eight linear elements/four quadratic elements) per wavelength will provide about 90 % accuracy on wave amplitudes in the highest frequency range of interest, $f_{max}$ (*Kuhlemeyer & Lysmer, 1973*).

### 4.4.3. Volumetric Locking

In the case of fully saturated soil layers, when the material response is nearly incompressible (Poisson's ratio is greater than 0.48), the finite element solution by using fully integrated displacement-based elements may result in volumetric locking (*Cook et al., 2002*). In this case, spurious pressure stresses develop at the integration points, causing an element to behave too stiffly for deformations that should cause no volume changes. Volumetric locking can be avoided by using mixed displacement-pressure formulation (hybrid) elements with the cost of having pressure stress as an independently interpolated basic solution variable. Using linear displacement elements by fully or selectively reduced integration can also remedy the problem (*ABAQUS User's Manual, 2014*). From a practical point of view, however, limiting the Poisson's ratio of the soil layers to a certain maximum value ($\upsilon \leq 0.475$) may not affect the wave propagation.

### 4.4.4. Optimal Time Step

Based on the sampling theory, to avoid aliasing effect which results in a complete loss of the interesting frequencies, the time step should be chosen to be equal to or smaller than half of the smallest period of the interest.

$$\Delta t \leq 0.5/f_{max} \qquad \textit{(Equation 4.4.2)}$$

From the numerical analysis point of view, Newmark's method for implicit dynamic analysis is also stable if the integration time step is lower than a certain limit as following:

$$\Delta t \leq 0.55/f_{max} \qquad \textit{(Equation 4.4.3)}$$

However, normally a shorter time step than above mentioned values should be used to obtain an accurate representation of both the excitation and the response (*Kausel, 2017*).

In the case of moving load analysis, point loads are applied directly on the rail nodes as triangular pulses distributed between three nodes, see *Figure 4.4.1.a*. Then, these triangular pulses are moved from node to node by a time interval equal to $\Delta x/v$, where $\Delta x$ is the node

spacing of the loading nodes and $v$ is the speed of the moving loads. This is schematically described in *Figure 4.4.1.b* (*Hall, 2000*). Consequently, to obtain a proper representation of the load, the analysis time step should be equal to or smaller than $\Delta x/v$.

As a general recommendation, the integration time step for dynamic analysis of the studied problem should be chosen as per *Equation 4.3.3*.

$$\Delta t \leq min\,(0.5/f_{max}\,, \Delta x/v) \qquad \textit{(Equation 4.4.4)}$$

Based on the convergence and verification studies, the recommended time step leads to relatively accurate results for the studied problem while the computational cost is kept as low as possible. Noteworthy to mention, for the range of interesting train speeds and maximum frequencies of interest, the time step is normally controlled by $\Delta x/v$.

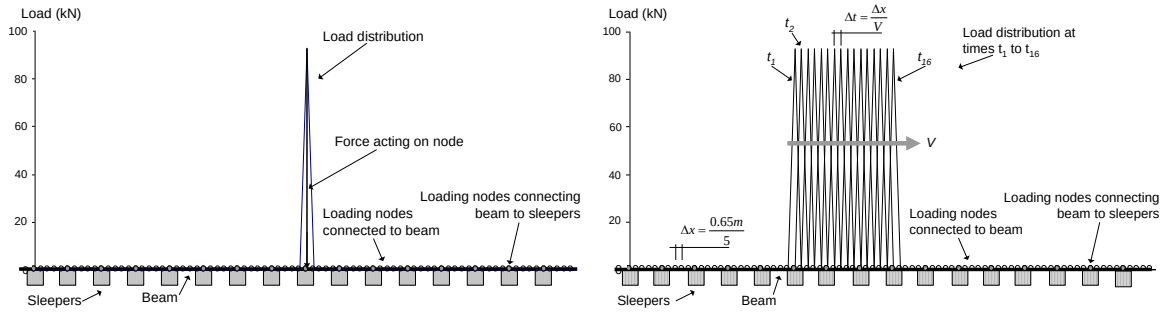


**Figure 4.4.1** Description of the loading model used in the finite element models with a beam simulating the rail. (a) Load distribution for a point load on a beam. (b) Load distribution of a moving point load on a beam traveling at speed $v$ (*Hall, 2000*).

## 4.4.5. Material Damping

In frequency domain analysis, the hysteretic material damping can be accurately modeled by introducing a complex elastic modulus (*Kausel, 2017*) as follow:

$$E^* = E(1 + \eta i) \qquad \textit{(Equation 4.4.5)}$$

where $\eta = 2\xi$ is the loss factor and $\xi$ is the material damping ratio.

In time-domain analysis, the material damping matrix is usually approximated as a combination of mass **M** and stiffness **K** matrices (*Kausel, 2017*).

$$\boldsymbol{C} = \alpha \boldsymbol{M} + \beta \boldsymbol{K} \qquad \textit{(Equation 4.4.6)}$$

where $\alpha$ and $\beta$ are Rayleigh damping coefficients and chosen so to match the damping ratio at two specific frequencies of interest, $\omega_1$ and $\omega_2$.

When damping ratio for both frequencies is set to an equal value, $\xi$, these coefficients can be simply obtained as follow:

$$\begin{cases} \alpha = \omega_1 \omega_2 \beta \\ \beta = 2\xi/(\omega_1 + \omega_2) \end{cases} \qquad \textit{(Equation 4.4.7)}$$

## 4.4.6. Transient Effects

As mentioned in Section 4.4.4, in the case of using triangle load distributions along the rail (beam elements) to model the quasi-static moving loading, the maximum amplitude occurs at the position of the moving wheel. When constant amplitude is used, a small disturbance signal occurs at the beginning of the moving load simulation when the sudden impulse loads apply on the model, as shown in *Figure 4.4.2*. This phenomenon can be improved by introducing a

transition zone, which gradually increases the actual amplitude of the wheel load. *Figure 4.4.2* shows the results when different size of transition zone is applied. As can be seen, when the transition zone sets up to 0.5 second, which is ¼ of the total simulation time, almost no noise can be observed.

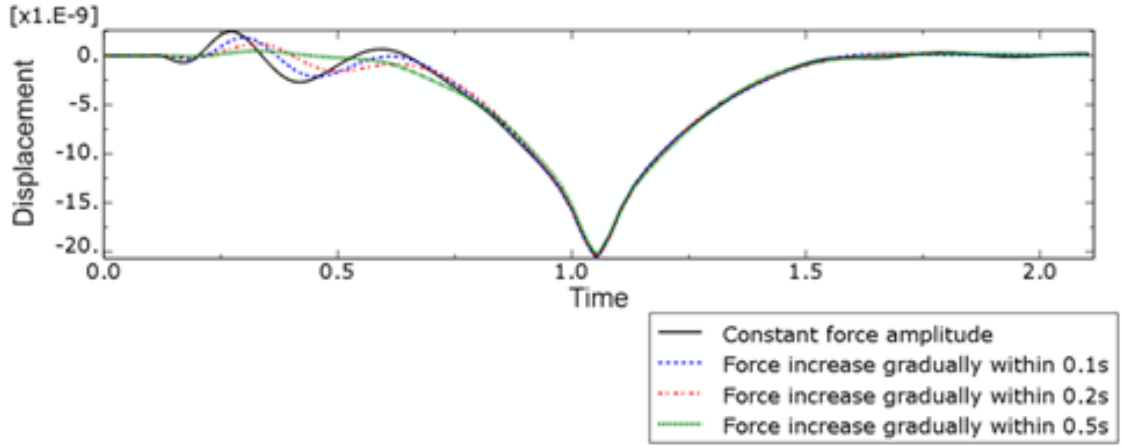


**Figure 4.4.2** Moving load results with different transition zones

## 4.5. Conclusions and Recommendations

Based on this study, the following recommendation can be given for an optimized numerical modeling of train-induced ground vibrations and requirements for calculations for results with sufficient accuracy.

- The frequency domain solution is very efficient in solving linear problems (using the reciprocity principle), provided that a very limited number of output results are required. However, it is not as straightforward as the time domain solution in practice as it requires Fourier transform analysis.

- In order to deal with huge number of output results (e.g., strain levels in all elements) the time-domain approach is more efficient. In case of linear or equivalent linear analysis, the computation time can be reduced by applying the superposition principle.

- As shown, the size of 3D FE model and type of implemented boundary conditions has a great influence on the results.

- The required length of the FE model depends on the proximity of the load speed to the critical speed and increases considerably in the vicinity of the critical speed.

- In the presence of an efficient non-reflecting boundary condition at the far field side of the FE model, the width of FE model can be kept as small as possible. In the absence of any non-reflecting boundary condition, however, the width of the model should be sufficiently large to ensure that the spurious wave reflections at the side have negligible effect on the computed vibration levels on track.

- The computed vibration levels and the estimated range of the critical speed are mainly governed by the properties of the upper ground layers.

## 4.6. References


BASU U., CHOPRA A.K. (2003), Perfectly matched layers for time-harmonic elastodynamics of unbounded domains: theory and finite-element implementation. *Comput. Methods Appl. Mech. Engr*g. 2003; 192: 1337-1375.

COMSOL Multiphysics Reference Manual, version 5.6, COMSOL, Inc, www.comsol.com

COOK R.D., MALKUS D.S., PLESHA M.E. AND WITT R.J., (2002). Concepts and Applications of Finite Element Analysis, 4th Edition, *John Wiley*, 2002.

COSTA P.A., CALÇADA R., CARDOSO A.S., BODARE A., (2010). Influence of soil non-linearity on the dynamic response of high-speed railway tracks. *Soil Dyn Earthq Eng* 2010;30(4):221–35.

DASSAULT SYSTMES. (2014). ABAQUS/Standard User's Manual, 6.14 ed., Providence, RI, USA, 2014.

FRANÇOIS S., SCHEVENELS M., GALVÍN P., LOMBAERT G., DEGRANDE G. (2010). A 2.5D coupled FE–BE methodology for the dynamic interaction between longitudinally invariant structures and a layered halfspace. *Comp Methods Appl Mech Eng*, 2010; (199) 23–24: 1536-48.

GALVÍN P., FRANÇOIS S., SCHEVENELS M., BONGINI E., DEGRANDE G. AND LOMBAERT G., (2010). A 2.5D coupled FE-BE model for the prediction of railway induced vibrations. *Soil Dyn Earth Eng*, 2010; 30(12): 1500–1512.

GAO G.Y., CHEN Q.S., HE J.F. AND LIU F., (2012). Investigation of ground vibration due to trains moving on saturated multi-layered ground by 2.5D finite element method. *Soil Dyn Earth Eng,* 2012; 40(0): 87–98.

GAZETAS G., (1998). Foundation vibrations, in: H. Y. Fang (Eds.), *Foundation Engineering Handboo*k, Springer Science+Business, Newyork 1998, pp. 553-593

GERMONPRÉ M., DEGRANDE G. AND LOMBAERT G.. (2018). Periodic track model for the prediction of railway induced vibration due to parametric excitation. *Transportation Geotechnics,* 17(Part A):98-108, 2018.

HALL, L. (2000). "Simulations and analyses of train-induced ground vibrations". Doctoral Thesis, Division of Soil and Rock Mechanics, *KTH-Royal Institute of Technology*.

HALL L., (2003). Simulations and analyses of train-induced ground vibrations in finite element models. *Soil Dyn Earthq Eng* 2003;23(5):403–13.

KARLSTRÖM A., BOSTRÖM A., (2006).An analytical model for train-induced ground vibrations from railways. *J Sound and Vib*, 2006; (292) 1–2: 221-241.

KAUSEL E., (2017). Advanced Structural Dynamics, *Cambridge University Press*, 2017.

KAUSEL E., (2006).Fundamental solutions in elastodynamics: a compendium. *Cambridge University Press*, New York, 2006.

KAYNIA AM, MADSHUS C, ZACKRISSON P. (2000).Ground vibration from high-speed trains: prediction and countermeasure. *J Geotech Geoenviron Eng* 2000; 126(6): 531–7.

KOUROUSSIS G., (2010). Predicting high speed railway vibration using time-domain numerical engineering approaches, In V. V. Krylov (ed.), *Ground Vibrations from High-Speed Railways: Prediction and Mitigation*, 2019; Chapter 6, pp. 187–216, ISBN 978-0-7277-6379-2.

KUHLEMEYER R.L., LYSMER J., (1973). Finite element method accuracy for wave propagation problems*, Journal of the Soil Mechanics and Foundations Division*, Vol. 99, No. 5. (May 1973), pp. 421-427.

LYSMER J., KUHLEMEYER R.L., (1969). Finite dynamic model for infinite media, *Journal of Engineering Mechanic Division*, ASCE 95 (1969) 859–877.

LYSMER J., RICHART F. E. JR., (1966).Dynamic Response of Footing to Vertical Loading*, J. of the Soil Mechanics and Foundations Division*, 1966, ASCE, Vol. 92, No. SMI, pp. 65-91.

SCHEVENELS M., FRANÇOIS S., DEGRANDE G., (2009). EDT: An ElastoDynamics Toolbox for MATLAB. *Computers & Geosciences*. 2009; 35(8):1752–1754.

SHENG X., JONES C.J.C., THOMPSON D.J., (2004). A theoretical model for ground vibration from trains generated by vertical track irregularities. *J Sound Vib*, 2004; (272) 3–5: 937-965.

SHIH J.Y., THOMPSON D.J., ZERVOS A., (2017).The influence of soil nonlinear properties on the track/ground vibration induced by trains running on soft ground, *Transportation Geotechnics*. 2017 (11),1-16.

SHIH, J.Y., (2017).Models for vehicle/track/ground interaction in the time domain. PhD diss., *University of Southampton*, 2017.

YANG Y.B, HUNG H.H, CHANG D.W., (2003).Train-induced wave propagation in layered soils using finite/infinite element simulation. *Soil Dyn Earthq Eng,* 2003; (23) 4: 263-278.

# 5. THE BASE MODEL METHODOLOGY FOR NUMERICAL CALCULATIONS

## 5.1. General Description of the Methodology

In this chapter, the base model methodology for numerical calculations is introduced. The concept of the methodology is that an input file was used to set-up the problem that is to be analyzed, a shell program reads the input file, creates, and runs the model of the problem on a commercial numerical software, extracts the results from the calculation of the problem and saves the results in an output file. The structure of the base model methodology, that was developed in this study, is shown in *Figure 5.1.1* and included:

- An **input file** - An excel sheet was created with a database for a systematized set-up of the problem to be analyzed. This includes choosing the geometry of the railway embankment, ground condition and any required ground reinforcements, as well of choosing type of analyses.
- The **base model program** – A shell program, using *Phyton* scripts, was created that reads the input file, runs the finite-element software as well as extracts the results from the numerical software.
- A **finite element software** – In this test, the commercial software *Brigade* was used. Brigade is an application of the software *Abaqus*.
- **Output files** -From the numerical calculations, the base model program extracts results and saves them as figures and text files.

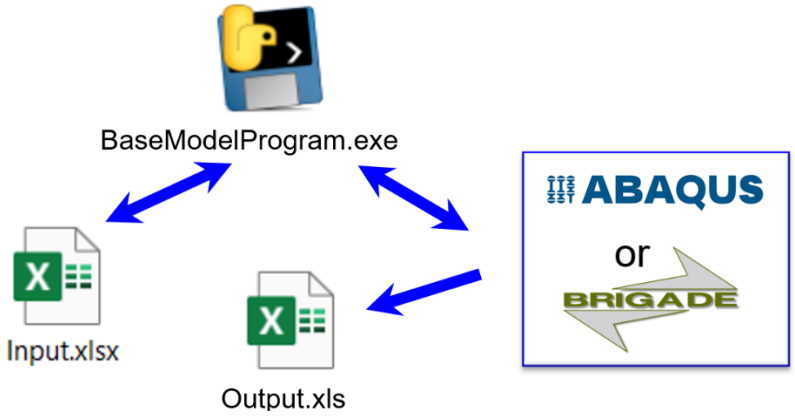


**Figure 5.1.1** The structure of the base model methodology developed in this study.

### 5.1.1. Setting Up the Numerical Analyses (the input file)

Setting up the calculations involves selecting type of railway embankment, give the ground condition and chose any required ground reinforcement measures. Also, to choose what kind of analyses that will be performed. In *Figure 5.1.2*, a flow chart of the base model methodology is shown with the different steps in the input file that is used to define the problem that will be analyzed. The different steps in the input file are shortly discussed in this chapter. In *Appendix B1* and *Appendix C1,* the developed input file is shown with choices concerning the Ledsgård case history prior and after the lime-cement columns reinforcement, respectively.

#### *Vehicle types (A1)*

In the input file, the train set, or a unit load can be selected. At the moment, seven different train set have been incorporated in the input file. The unit load can be chosen according to the allowable axle loads as defined in *TK Geo*.

### *Track structure (A2)*

The track structure involves choosing type of rail, rail pad and track system. In the input file, there are two rail types, commonly used in Sweden (60E1 and 50E3), available, and three different types of rail pads (soft, medium, and stiff) that can be selected. For the track system, one can select concrete sleepers with ballast according to *AMA* or slab track according to the *RHEDA 2000* system. The thickness of ballast together with sleepers or reinforcement layer together with slab track, is chosen default as described in *AMA* or by the *RHEDA 2000* system, receptively. The initial material properties in the railway's embankment are calculated according to *TK Geo*.

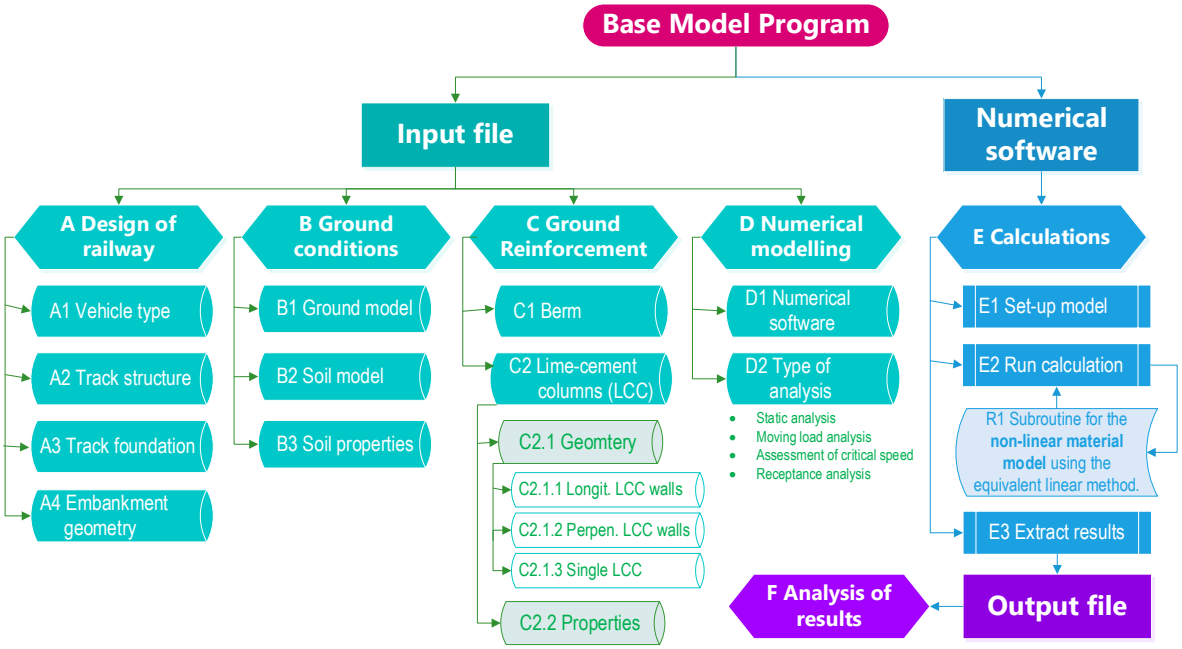


**Figure 5.1.2** Flow chart of the base model methodology with a shell program (base model program that reads data from the input file, set-up the numerical model, perform the calculations in the numerical software and extracts and saves the results in output file. Also, the subroutine for non-linear material model (using the equivalent linear method) is run by the shell program. The numerical model and type of calculations are set-up from choices in the input file.

### *Track foundation (A3)*

For the track foundation, the subballast has default thickness according to *AMA* and the frost insulation thickness is chosen according to the guidelines given in *AMA*. The subgrade thickness is calculated according chosen geometry of the embankment. The material types and the initial material properties are according to *AMA* and *TK Geo*.

### *Embankment geometry (A4)*

The geometry of the embankment is set-up by giving values for the levels of the rail top and the level of the ground surface. Also, the slope of the embankment needs to be selected. Any vegetation removal can also be given. The rest of the embankment geometry is calculated based on selected type of track structure and track foundation, as well as some other requirements according to *BVS 1585.005* and *AMA*.

### *Ground conditions (B)*

In the ground conditions, first select between homogenous half space, layer half space and fixed bottom. If the soft soil depth is less than 30m, then select the fixed bottom option. After that, select between linear or non-linear material model. If linear material model is selected, the

calculations are performed with linear elastic material model. If non-linear model is chosen, the shear strain dependency of the soil properties is considered with the equivalent linear method.

Three soil layers can be chosen. For respectively soil layer, give the values for the total density, the initial shear wave speed ($c_{S0}$) and compression wave propagation speed ($c_{P0}$), initial damping ratio ($D_0$), plasticity index (PI) as well as earth pressure at rest ($K_0$). The total density, shear wave propagation speed and plasticity index can be chosen so that they change with depth. From these parameters, the initial stiffnesses (elasticity modulus and Poisson's ratio) for the different embankment materials and soil layers are derived from the shear wave and compression wave propagation speeds. Poisson's ratio has, to avoid any numerical problems in numerical calculation, set to have a maximum value of 0.475. The compressions wave propagation speed will therefore be changed accordingly. The plasticity index (PI) and the earth pressure at rest ($K_0$), are used in equivalent linear method for adjusting shear strain dependent material properties. The ground water table is set default set to be between the first and second soil layers.

### *Ground reinforcement (C)*

Ground reinforcements can be chosen based on requirements for vibrations, stability, or settlement reasons. In the developed program, a berm and or lime-cement columns can be selected.

For the **berm**, chose height, width and slope and type of material. The different material can be chosen between crushed rock fill, coarse-grain mixed fill soil or a fill of the first soil layer given in the previous section. The material properties are calculated according to *TK Geo* or, for first soil layer, as given in given in the previous section.

**Lime-cement columns** (LCC) can be chosen to be LCC-wall under the rail, LCC-wall perpendicular embankment and/or as single LCC. The diameter of the columns can be selected to be 0.6m or 0.8m. The spacing between the columns, can be selected based on chosen diameters. The length of the columns can be chosen between 3m and up to 25m depth below the ground surface. The material properties of the LCC are calculated from a chosen value of the undrained shear strength according to the strong empirical relationship with shear wave and wave propagation speeds (see *Chapter 3.3.4*).

### *Numerical modeling (D)*

The program includes the following four types of analyses:

- Static analysis
- Moving load analysis
- Assessment of critical speed
- Receptance analysis

In the static analysis, calculation of the deformations is calculated for a still standing train in the middle of the numerical model. Whereas for a moving load analysis, a moving train with a constant speed is simulated with calculations in the time domain. In the analyses of assessments of critical speed, multiple moving load analyses are performed in the time domain with increasing train speed until the critical speed can be evaluated. And finally, in the receptance analysis, the resonance frequencies of the numerical model are calculated. This is useful in determining the Rayleigh damping (see *Equation 4.4.7).* Furthermore, overall track stiffness can also be calculated based on the inverse of the receptance value at the very low frequency.

### 5.1.2. Steering the Analyses (the base model program)

The developed shell program, the base model program, was programmed in Python for automatized calculations in the numerical software Abaqus (or Brigade) as well as the post-processing and analyses of results. The process includes:

- Model development
- Numerical simulation
- Post-processing the output data

Based on the input file, the base model program set-up a numerical model of the railway embankment and ground and any required ground reinforcement measure in the numerical software see *Figure 5.1.3*. In the model, the X-coordinate is in the longitudinal (running) direction, the Y-coordinate is in vertical direction and the Z-coordinate is in the transversal (perpendicular) direction.

Different combination of track foundation layers as well as the reinforcements can be set-up. The model is assumed to be **symmetric** in the horizontal plane. Therefore, to increase the calculation efficiency, only half of the track and ground model is considered in the calculation. The simulation is calculated in the time domain. See also *Chapter 4* for requirements on the numerical modeling and some other optimizations techniques that is incorporated the base model program to increase the computing time efficiency.

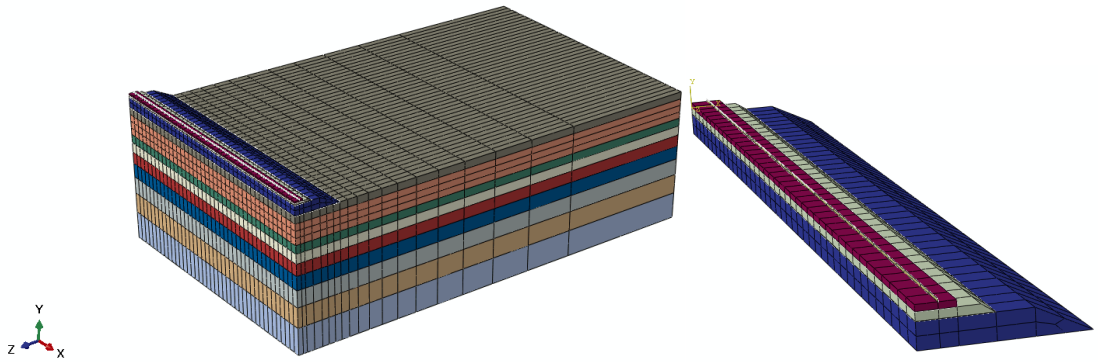


(a) (b)

**Figure 5.1.3** Overview of the numerical Base model; (a) track/ground model; (b) track model

In *Figure 5.1.4* the used concept of the track/ground interaction dynamics calculation is shown. One of the main techniques to increase time computing time efficiency, is the **superposition approach.** By using the data from the calculation from a single moving load, and the add the results to get the whole train results, much computing time can be saved. The program output the maximum rail displacement along the track to identify the converged location and then output the time history results from the numerical software to calculate the whole train results based on superposition approach. This is possible through the **equivalent linear method**, see *Section 5.5.1*, so all the calculations within the numerical software is performed with linear elastic material models and the non-linearity of the material properties are considered outside the numerical software. This approach showed significant improvement for the simulation efficiency. Furthermore, the required model size is also reduced which consequently decrease the computing time. The computing time, using normal laptop with 6 processor, is around 5-10 minutes for a complete linear analysis and around 30-60 minutes when the non-linearity is considered using the equivalent linear method.

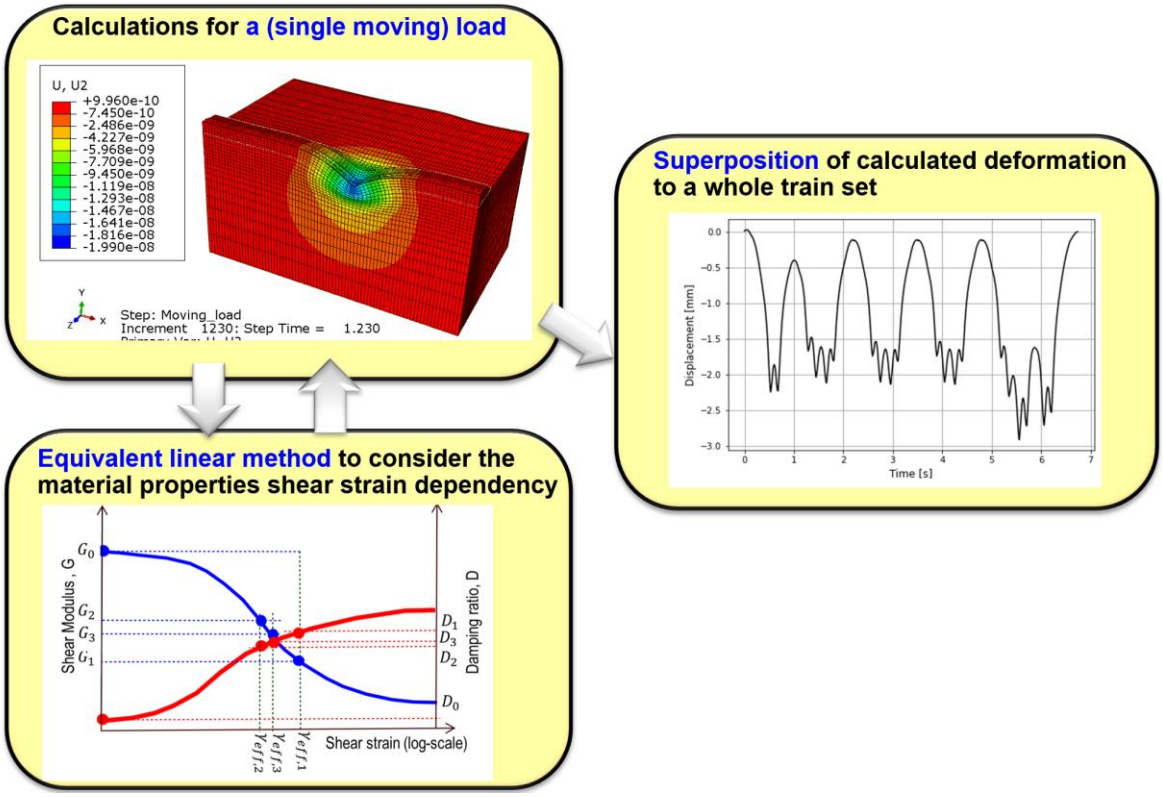


**Figure5.1.4** Track/ground interaction dynamics calculation

## 5.1.3. Analyzing the Results (the output files)

In this chapter, the output from the different analyses (receptance analyses, assessment of critical speed and moving load) are discussed. See also *Appendix B2* and *Appendix C2* for examples of diagrams produced from the developed base model program in analyses of the Ledsgård case history prior and with lime-cement columns reinforcement, respectively.

### *Receptance analysis*

In the receptance analysis, the resonance frequencies of the numerical model are calculated. Results from a rail receptance analysis, for dynamic load applied middle of the track, is shown in *Figure 5.1.5.*

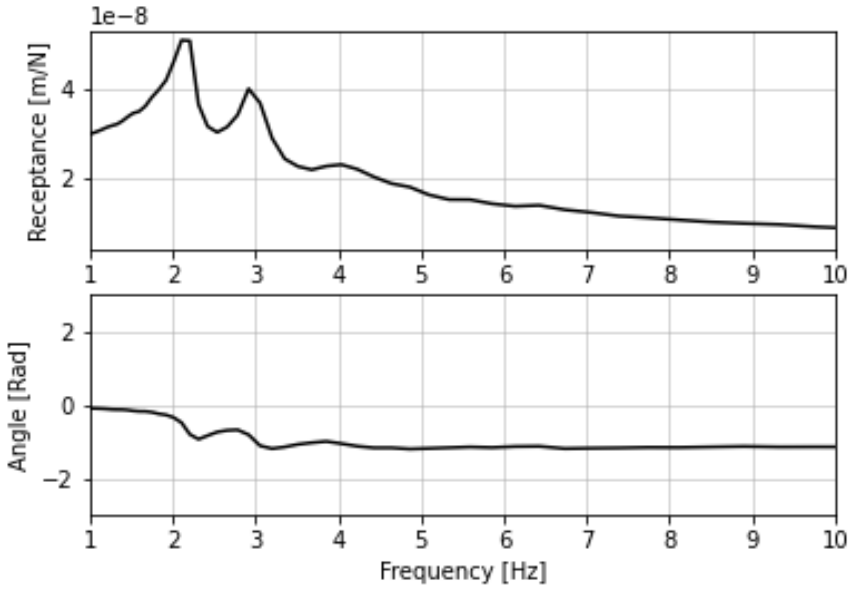


**Figure 5.1.5** Example of a calculated receptance for an analyzed case

*Assessment of the critical speed*

In this analysis, the critical speed is determined ($c_{cr}$) and compared to the lowest allowed critical speed according to *TK Geo* (see *Chapter 2.2.2.).* Also, the calculated displacement at the designed train speed ($v_{sth}$) is compared to the highest allowed displacement at the rail (see *Chapter 2.2.2.).* In this analysis, multiple simulations with different speeds are performed. *Figure 5.1.6* shows an example with maximum calculated peak-to-peak track displacement against the train speed. In *Figure 5.1.7,* another plot from the calculations is shown. Here, the initial soil properties are compared with the adjusted soil properties based on the calculated shear strain levels. Finally, in *Figure 5.1.8* an example from the calculated track displacements from a train set traveling at train speed of 70km/h is shown.

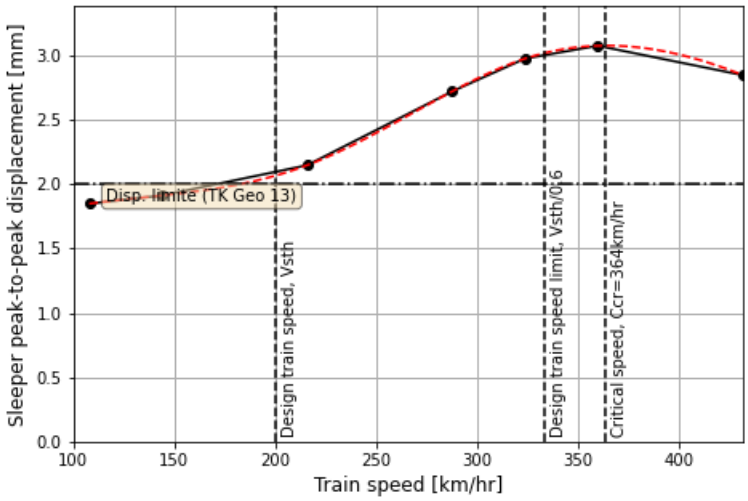


**Figure 5.1.6** Example of results for assessment of critical speed and comparisons with allowed lowest train speed ($v_{sth}/0.6$) and highest allowed displacement at rail for the designed train speed ($v_{sth}$).

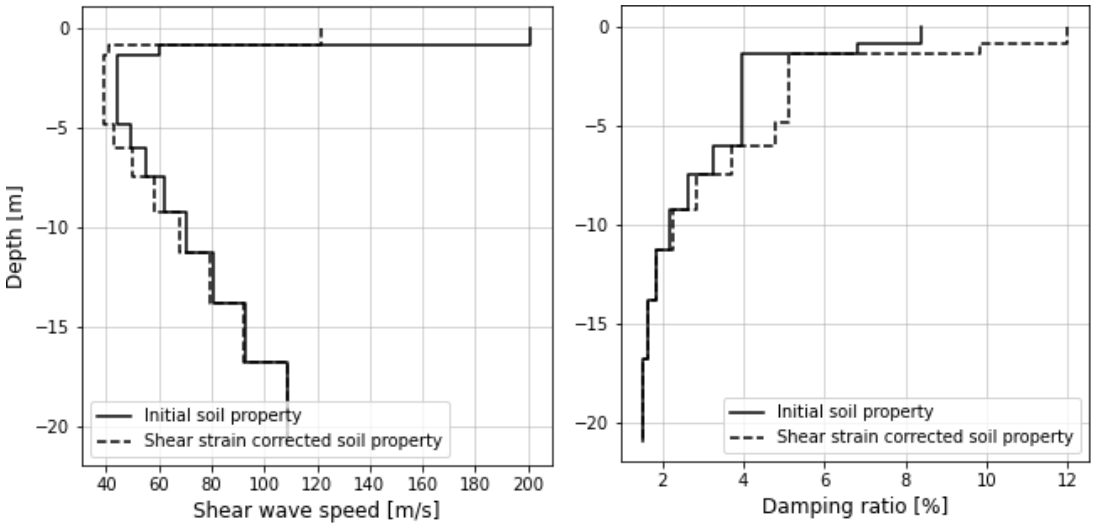


**Figure 5.1.7** Comparison of initial soil properties and shear strain correct soil properties at the designed train speed. This plot is made for all train speeds used for assessment of the critical train speed (here shows the example of V=70 km/h).

*Moving load*

The output from "Moving load" analysis is the same as the assessment of the critical speed, but only with one running train speed and without.

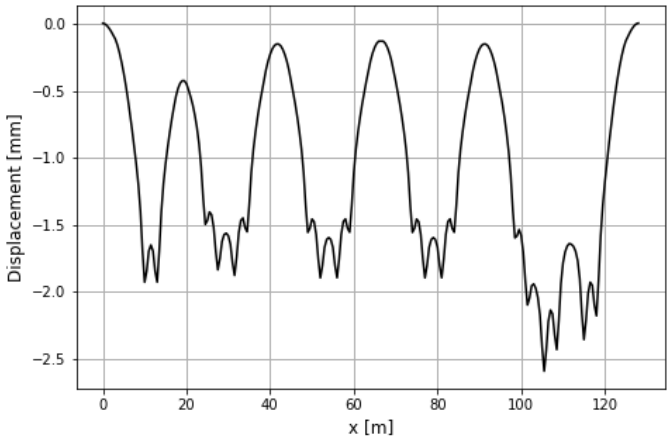


**Figure 5.1.8** Example of a calculated rail displacement from an analysis of X2000 train at train speed 70km/h.

## 5.2. Model Development

### 5.2.1. Element and Material Set-up

*Table 5.2.1* shows the element and material used in base model program. Beam with continuous support as Winkler foundation is used for the rail and rail-pad layer. Instead of using spring dashpot for modeling the rail-pad, a uniform thickness and height shell element is used to model the continuous support layer (Winkler foundation). According to *Shih (2017*), it gives the same results compared with the analytical results from Winkler foundation when an appropriate geometry is generated.

**Table 5.2.1** Element and material used in the base model program

| Model | Element type | Element index in Abaqus | Material |
|---|---|---|---|
| **Rail** | A 3-node quadratic beam in space. | B32 | Linear |
| **Railpad** | An 8-node doubly curved thick shell, reduced integration | S8R | Linear |
| **Sleeper** | A 20-node quadratic brick | C3D20 | Linear elastic orthotropic |
| **Ballast** | A 20-node quadratic brick | C3D20 | Linear elastic |
| **Embankment*** | A 20-node quadratic brick | C3D20 | Linear elastic |
| **Ground*** | A 20-node quadratic brick | C3D20 | Linear elastic |
| **Berm** | A 20-node quadratic brick | C3D20 | Linear elastic |
| **LCC*** | A 20-node quadratic brick | C3D20 | Linear elastic orthotropic /isotropic |

* effect of nonlinearity is considered using equivalent linear analysis

Discrete modeled sleepers (individual modeled sleeper with a spacing, see *Figure 5.2.1*) is not considered because the interested frequency is much lower than the sleeper passing frequency. Instead, continuous sleeper model (see *Figure 5.1.3.b)* using orthotropic material, which neglects the bending stress in the vertical direction, is used. Equivalent properties for the continuous sleeper model can, according to Shih (2017), be calculated based on the width of the sleeper

width and the sleeper spacing and the same track dynamics can be obtained compared to the results from the discrete sleeper model in the low frequency.

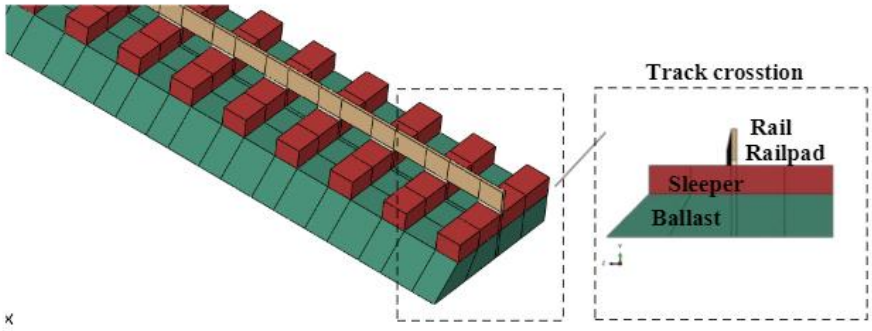


**Figure 5.2.1** Discrete sleeper model (*Shih, 2017*)

A quadratic brick element (as shown in *Figure 5.2.2)* is used for the foundation layer and reinforcement including ballast, embankment, ground, berm, and lime-cement columns (LCC.) Three different LCC designs are available:

- Longitudinal LCC-wall under the rail for vibrations reduction ($LCC_V$)
- LCC wall perpendicular to the rail for stability reinforcement ($LCC_{St}$)
- Single LCC for settlement reduction ($LCC_{Se}$)

are included in the program, as shown in *Figure 5.2.3.*

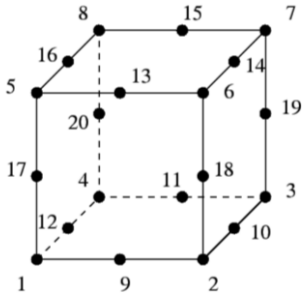


**Figure 5.2.2** Quadratic brick element

Except for the longitudinal LCC-wall under the rail ($LCC_V$), orthotropic material is used for the LCCs to account for the LCC movement. Equivalent parameters value can be calculated based on the real LCC geometry and to account for the spacing between the LCCs in the longitudinal direction, the equivalent properties is calculated based on the spacing between the LCCs and the diameter of the LCCs.

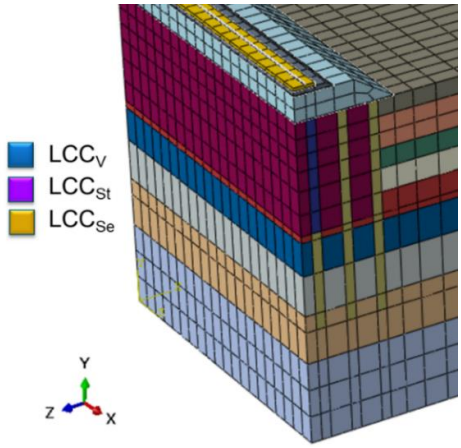


**Figure 5.2.3** LCC model in Base model program

### 5.2.2. Moving Load Simulation

A series of point loads are distributed between two beam elements (Rail) at the wheel position and the amplitude varies as a triangular between the nodes within the two elements to model the moving load, as shown in *Figure 5.2.4*. In order to minimize the noise caused by a sudden impulse load (see *Figure 4.4.3*) in the beginning, a transition zone (*Lt*), is applied which allows the load to increase gradually, as shown in *Figure 5.2.4*.

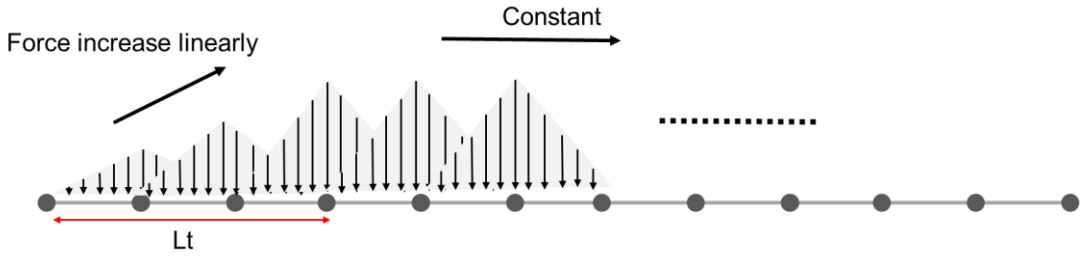


**Figure 5.2.4** Set-up of moving load analysis

### 5.2.3. Mesh Strategy

In order to improve the calculation efficiency, the mesh size has been stretched with factor of 1.2 in the far field in the transversal and vertical directions, as shown in *Figure 5.2.5*. Furthermore, according to *Shih (2017)*, the stretched mesh approach can help to attenuate the energy at the boundary more effectively. Mesh size requirement for the near field can be found in Section 4. Note here, due to the fact that the present study is focus on the near field responses, the mesh size in the transversal direction can be stretched. Otherwise, the uniform element is suggested for the far field results. Furthermore, the present study is focus on the moving load and if the vehicle dynamic is considered in the simulation, the mesh size for far field should follow the recommendation giving in *Chapter 4*.

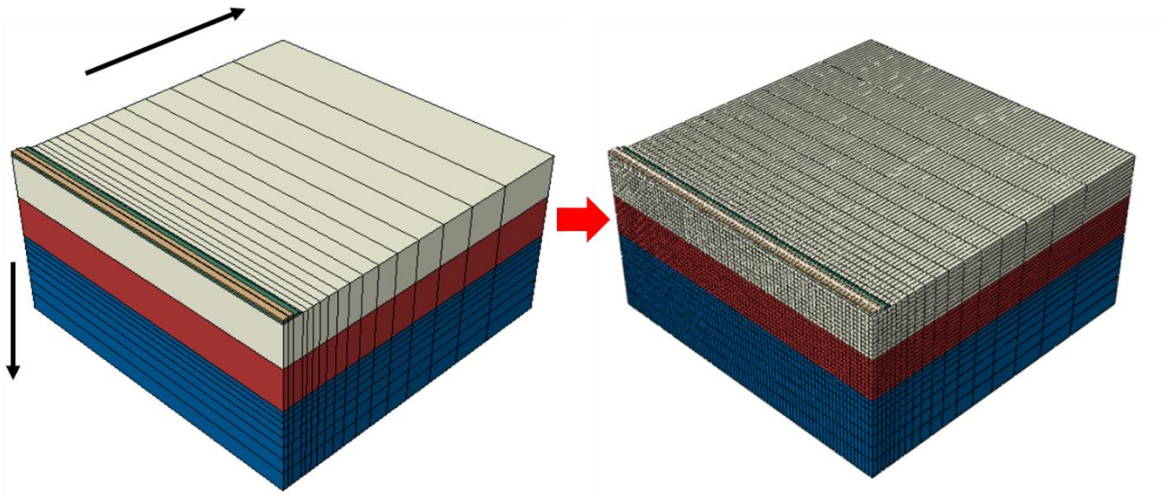

**Figure 5.2.5** Mesh strategy for the Base model

### 5.2.4. Soil Layers

To take account for that some material properties changes with depth, the soil layers have been divided into a number of sublayers based on the grid stretching factor 1.2 and the parameters are set-up based on the corresponding material properties changes with the depth as shown in *Figure 5.2.6*. The number of the sublayers varies with the thickness of the clay layer and for Ledsgård case study, 7 sublayers were generated for the clay layer.

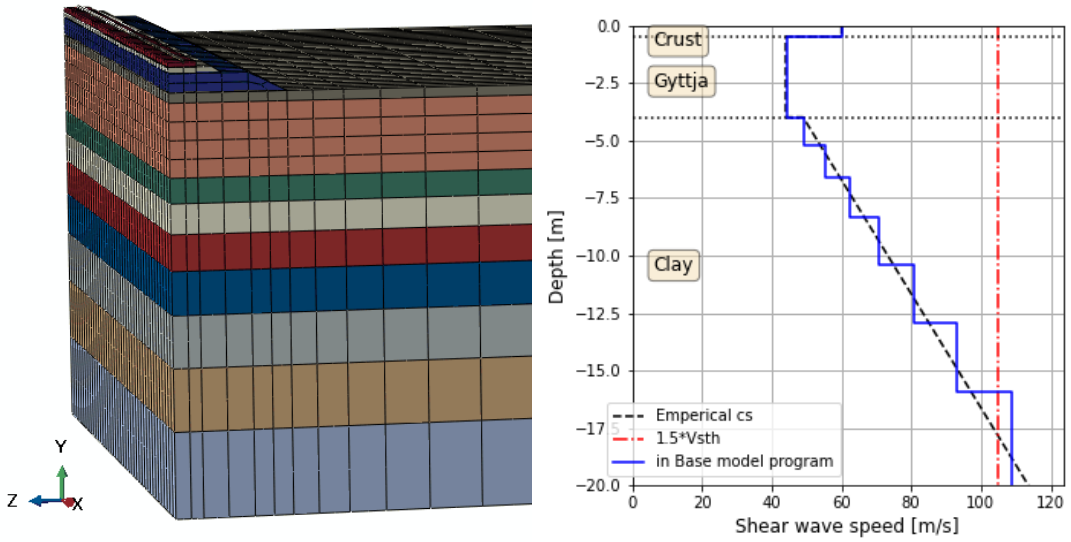


**Figure 5.2.6** Example of soil layer for Ledsgård case study

## 5.2.5. Boundary Set-Up

Symmetric constraint is applied at the symmetric plan of the model. A **periodic boundary condition** (PBC), according to *Wu et al (2014)*. is applied at the two longitudinal ends of the model, see *Figure 5.2.7.a.* This reduces the required size of model as mentioned in *Section 4.3.1.* Furthermore, although PBC has applied, the model size needs to be large enough for capturing the wavefront of a single moving load in the space domain. Therefore, an algorithm has been developed that assess the required model length for different speeds, as shown in *Figure 5.2.7.b.*

The cuboid model with appropriate Rayleigh damping with fixed boundaries was recommended in *Shih et al (2016)* for this application in terms of calculation efficiency. Therefore, the bottom and the plane at the far field side has been fixed in the base model. The required width for the model, which allows the incident wave to attenuate the energy before the wave reach the boundary is recommended in *Section 4.3.2* and *Section 4.3.3.*

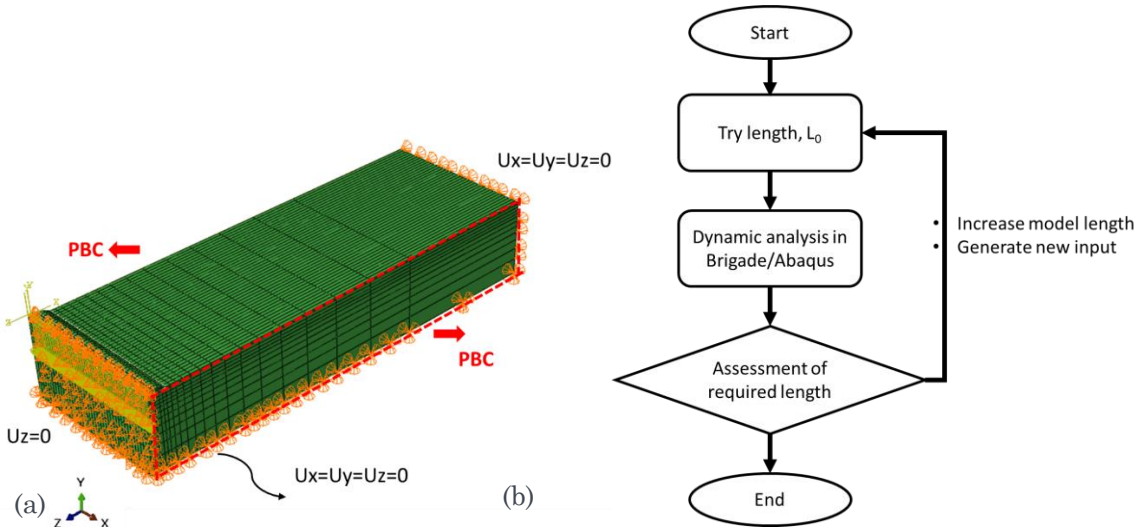


**Figure 5.2.7 (a)** Boundary set-up for the base model methodology. (b) Algorithm for assessing the minimum required model length

## 5.3. Model Validation

The numerical modeling using the base model methodology has been verified against the FE-PML model shown in *Chapter 4*. The PML model has similar track/ground model as the present base model. The material properties used in the analysis are shown in *Table 5.3.1* and the comparison of two the calculated responses are shown in *Figure 5.3.2*. As shown, very good agreement has been obtained for results from X2000 train traveling at a speed of 204 km/h.

**Table 5.3.1** Input parameters for validation of calculation with base model program and reference model of PML shown in chapter 4.

| Layer | Layers thickness h (m) | Total density ρ (kg/m³) | S-wave speed $c_S$ (m/s) | P-wave speed $c_P$ (m/s) | Damping ratio $D_0$ (%) |
|---|---|---|---|---|---|
| **Embankment** | 1.2 | 1800 | 210 | 340 | 4% |
| **Dry crust** | 1.1 | 1500 | 63 | 500 | 4% |
| **Organic clay** | 3.5 | 1260 | 41 | 500 | 2% |
| **Clay 1** | 4.5 | 1475 | 60 | 1500 | 5% |
| **Clay 2** | 6 | 1475 | 87 | 1500 | 5% |
| **Clay 3** | 30 | 1475 | 100 | 1500 | 5% |

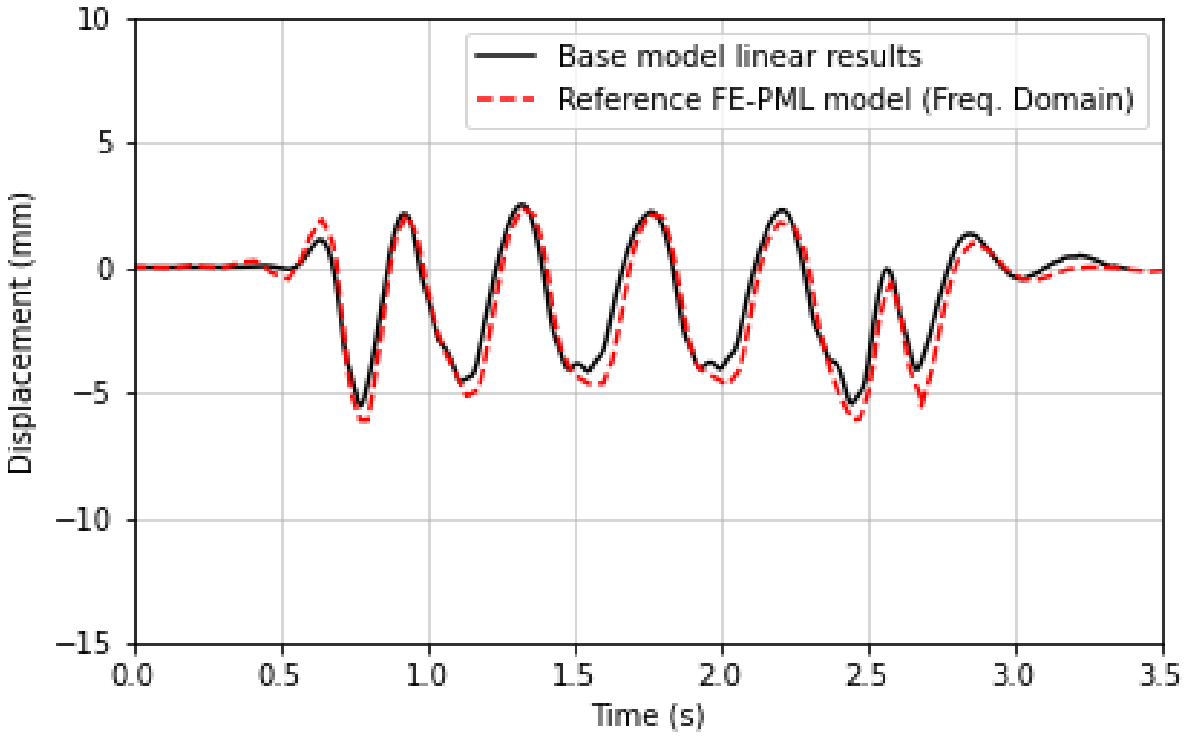


**Figure 5.3.1** Comparison of results from base model program and reference results for a X2000 train set traveling at train speed of 204 km/h.

## 5.4. Special Subroutines

### 5.4.1. Shear Strain Dependency

In this work, the effect of stiffness degradation with the strain level is considered in an approximate manner, by using an equivalent linear approach as described in *Chapter 3.2.2*. A few successive linear elastic analyses are performed through an iterative process, where the dynamic properties of the soil layers are modified based on the effective shear strain levels, until a certain convergence criterion is achieved.

The **effective shear strain** represents the strain level for a response time history. Usually, the effective shear strain is calculated from the maximum shear strain according to *Equation 3.2.1*. The calculated maximum shear strain level is then multiplied by a so-called strain reduction factor that, in soil dynamic analyses, usually has value about 0.65. In this way, the dynamic properties of the entire layer are roughly estimated based on the maximum strain level in the critical element of that specific layer. Since the interest of this work is focused on the region close to the track, relatively good predictions can be expected using this approach (*Madshus & Kaynia, 2000; Kaynia et al., 2000; Hall, 2003; Shih et al. 2017)*.

It should be noted that to evaluate the evolution of the shear modulus and damping for each iteration, the **octahedral shear strain**, $\gamma_{\mathrm{oct}}$, is used as the strain index, due to the complex 3D configuration of strains during train passages. This is given by:

$$\gamma_{\mathrm{oct}} = \frac{1}{3}\sqrt{(\varepsilon_{\mathrm{xx}} - \varepsilon_{\mathrm{yy}})^2 + (\varepsilon_{\mathrm{xx}} - \varepsilon_{\mathrm{zz}})^2 + (\varepsilon_{\mathrm{yy}} - \varepsilon_{\mathrm{zz}})^2 + 6(\gamma_{\mathrm{xy}}^2 + \gamma_{\mathrm{xz}}^2 + \gamma_{\mathrm{yz}}^2)} \qquad \text{(Equation 5.4.1)}$$

where $\varepsilon_{\mathrm{ii}}$ and $\gamma_{\mathrm{ij}}$ are respectively the normal and shear strains in three dimensions.

For this purpose, a python code is developed and used as a subroutine through the Abaqus Scripting Interface (ASI). The main steps of the computational procedure are below:

1. Assume low strain damping ratio ($\xi^i = \xi_0$) and shear modulus ($G^i = G_0$) for all elements as initial values.

2. Compute the time history of 6 strain components at the centroid of each element and evaluate the maximum value of the octahedral shear strain ($\gamma_{\mathrm{oct}}^i$) for each element.

3. Calculate the effective shear strain level ($\gamma_{\mathrm{eff}}^i$) for each specific layer, by choosing the maximum value of the octahedral shear strain at the critical element of each layer, reduced by a strain reduction factor $R_{\mathrm{r}}$. The factor $R_{\mathrm{r}}$ is set to 0.65 (*Costa, 2010*).

4. By using the estimated $\gamma_{\mathrm{eff}}^i$ into the degradation curves, choose a new value of damping ($\xi^{i+1}$) and shear modulus ($G^{i+1}$) for the next iteration.

5. Repeat steps 2 and 4 until the differences between the computed dynamic properties in two consecutive iterations becomes less than a certain tolerance. The convergence tolerance is set to 5 – 10 % (*Kramer, 1996*).

## 5.5. References


AMA AMA Anläggning 20. Published by *Svensk Byggtjänst*

COSTA PA, CALÇADA R, CARDOSO AS, BODARE A. (2010). "Influence of soil non-linearity on the dynamic response of high-speed railway tracks". *Soil Dyn Earthq Eng* 2010;30(4):221–35.

HALL L. (2003). "Simulations and analyses of train-induced ground vibrations in finite element models". *Soil Dyn Earthq Eng* 2003;23(5):403–13.

KRAMER SL, (1996). "Geotechnical earthquake engineering", Prentice-Hall Inc.1996.

KAYNIA AM, MADSHUS C, ZACKRISSON P. (2000). "Ground vibration from high-speed trains: prediction and countermeasure". *J Geotech Geoenviron Eng* 2000;126(6):531–7.

MADSHUS C, KAYNIA AM. (2000). "High-speed railway lines on soft ground: dynamic behaviour at critical train speed". J *Sound Vib 2000*;231(3):689–701.

REDA 2000 "Ballastless track System". *Rail One G*mbH.

SHIH, JY. (2017). "Models for vehicle/track/ground interaction in the time domain", PhD thesis, *Southampton University*. 2017.

SHIH J.Y., THOMPSON D.J., ZERVOS A., (2016). "The effect of boundary conditions, model size and damping models in the finite element modelling of a moving load on a track/ground system". *Soil Dynamics and Earthquake Engineering*, Volume 89, October 2016, Pages 12-27.

SHIH J.Y., THOMPSON D.J., ZERVOS A., (2017). "The influence of soil nonlinear properties on the track/ground vibration induced by trains running on soft ground". *Transportation Geotechnics* 2017 (11),1-16.

YOSHIDA N, KOBAYASHI S, SUETOMI I, MIURA K. (2002). "Equivalent linear method considering frequency dependent characteristics of stiffness and damping". *Soil Dyn Earthq Eng* 2002 (22) :205–222.

WU, W. & OWINO, GH, (2014) "Applying periodic boundary conditions in finite element analysis". *Simulia Commun Conf* (2014), pp. 707-719.

# 6. THE SIMPLIFIED CALCULATION TOOL – VIBTRAIN

## 6.1. Introduction

VibTrain was originally developed by NGI during the project "High Speed Lines on Soft Ground", conducted by Banverket in 1999. The program development was partly financed by Banverket and partly by NGI.

The Vibtrain program was developed when 3D FE analysis of ground vibrations would take weeks or months on regular computers. With the use of Green's functions for modeling the infinite extent of the soil beneath the embankment computational time could be reduced by several orders of magnitude. On a new laptop in 2021 the Vibtrain analysis takes about 30 seconds, and one or several train speeds does change the running time. While it has its limitations, e.g. horizontally layered ground and a simplified model of the embankment and rail, the speed of computations make it an attractive choice for e.g. screening of many sites. The computing time has reduced considerably over the years, the original version running an analysis for some 5 hours on Unix server in the late 1990's.

### 6.1.1. Vibtrain Versions

Since late 1990ies several versions of the Vibtrain tool has been developed. The original VibTrain model (*NGI, 1999*) computes only the response of the track and ground surface for moving train load. This version was extended to enable computation of motions and stresses in the ground. The extended version is denoted VibTrain-Stress (*NGI, 2004b*) and has been used for producing the Vibtrain results in this report.

There are also more versions/variations/extensions of Vibtrain. Preliminary studies with stochastic soil model have been performed (NGI, 2004b). In the Nordvib project (Phase 1 WP3), Vibtrain was extended to ExVibtrain in cooperation with Charmec (Chalmers University) for modeling track irregularities and interaction between track and train. ExVibtrain has in turn also been extended to be used in conjunction with the Track Load Vehicle (TLV-Vibtrain), for dealing with 1) Steady-state load at a stationary point on the rail, and 2) Wheel loads from a moving TLV (*NGI, 2003).*

The main difference between Vibtrain and the other two (ExVibtrain and Vibtrain-TLV) is that in the latter the embankment is modelled with solid continuum finite elements instead of an Eulerbeam. The infinite layered soil is modelled with Green's functions for all versions. Source code and graphical user interface in Matlab are available for these versions, but they have not been in much use in the last decade. These versions could possibly be "waken up" for future design projects when there is a need for a lot of analysis.

### 6.1.2. Modelling Theory

In VibTrain the ground consists of viscoelastic soil layers over a half-space and the substructure and tracks are modeled as separate beams with elastic elements between them to represent rail/sleeper pad flexibility. The interaction between the substructure beam and the ground is accounted for by use of Green's functions for layered media (see *Figure 6.1.1*).

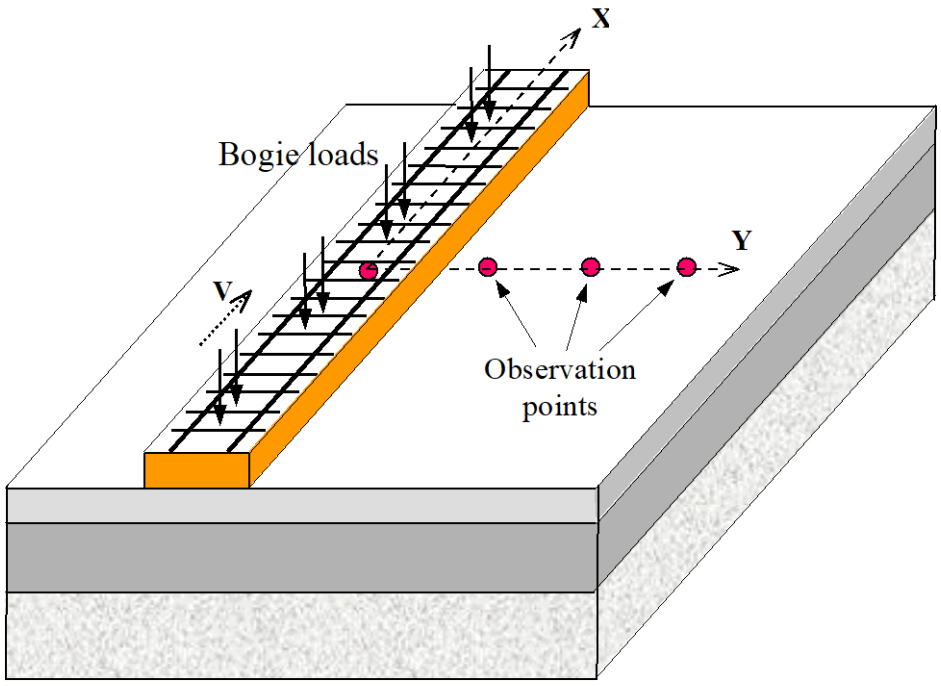


**Figure 6.1.1** Key features of VibTrain consisting of layered ground, embankment modelled as an equivalent beam, and rails.

## 6.2. Description of the Program

*VibTrain* is a numerical code for simulation of ground vibration from train loads moving over a 3-D track-ground medium. The ground is modeled as a layered visco-elastic halfspace, and the track (including the rail and embankment) is represented by a beam with equivalent mass and visco-elastic bending properties. The two substructures (i.e. ground and track) interact at discrete points, taken at the sleeper locations, along the track profile (*Figure 6.2.1*).

The excitation is a series of concentrated loads representing the axle loads of a train moving with constant speed *V*. To preserve the load distribution role of the rail, each concentrated axle load is distributed on the embankment according to the displacement variation under the rail, which can be most conveniently calculated using the theory of beam on elastic foundation. Procedures commonly known to railway engineers (for example, the Zimmerman method) can be used for this purpose. The loads are applied on the nodes with time shifts corresponding to the train speed.

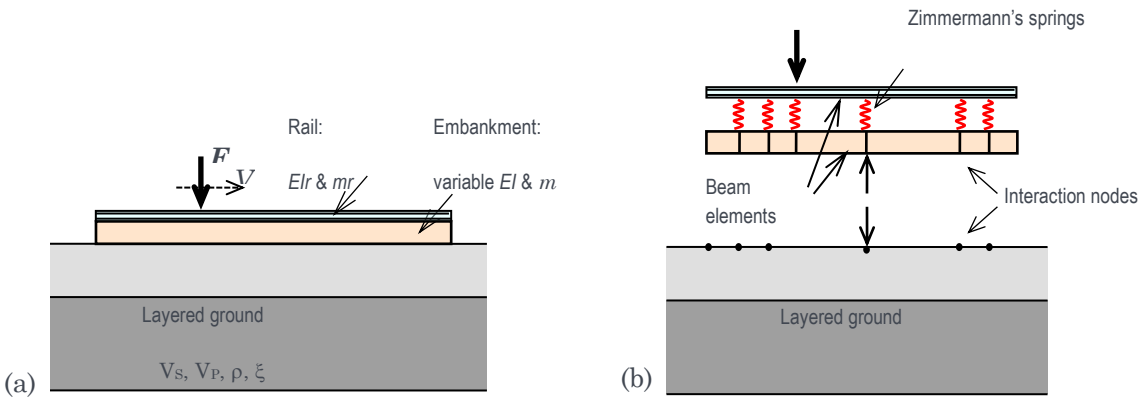


**Figure 6.2.1** Vibtrain model.

## 6.2.1. Modelling Aspects

*Figure 6.2.1* shows schematically the problem under investigation. The track/embankment structure is modeled as a beam resting on a layered half-space. The track/embankment is represented by its bending rigidity, *EI*, mass per unit length, *m*, and hysteretic damping ratio, $\beta$. Each soil layer is characterized by its shear-wave velocity, $c_S$, pressure-wave velocity, $c_P$ (or alternatively, the Poisson's ratio, $\nu$), mass density, $\rho$, and hysteretic damping ratio, $\xi$. It is assumed that the embankment is bonded to the supporting half-space at discrete points along the embankment, denoted as nodes. These points coincide with the location of the ties.

The excitation is a series of concentrated loads (Q) representing the wheel loads of a train moving with constant speed *V*. shows the static load of the X-2000 train used in the numerical simulations. The rail is not explicitly included in the calculation model, but its stiffness is included in bending stiffness of the embankment; However, to preserve its role in distributing the train load, each concentrated axle load is distributed on the embankment according to the displacement variation under the rail. Using the theory of beam on elastic foundation one can show that for a beam with bending rigidity *EI* and modulus of subgrade reaction *k,* the displacement of the beam can be calculated from the following expression (Timoshenko, 1926):

$$\varphi(x) = \frac{Q}{\sqrt{2}L} exp(-\left|\frac{x}{L}\right|) sin(\left|\frac{x}{L}\right| + \frac{\pi}{4}), \qquad \textit{(Equation 6.2.1)}$$

with $L = \sqrt[4]{\frac{4EI}{\kappa}}$, and $\kappa = k \cdot b$, where $b$ represents the equivalent width of the beam. This way of defining the load helps avoiding the extra computational effort required in representing the unnecessary high frequencies in the load variation. The loads are applied on the nodes with time shifts corresponding to the train speed. *Figure 6.2.2* shows the space variation of the nodal loads for $EI$ = 6.42E6 Nm², $\kappa$ = 5.25E7 N/m² and a tie spacing of 0.6m for .

Because the response of the layered ground and embankment is frequency dependent, the problem is formulated in the frequency domain. To this end, the loads are resolved into their frequency components by the Fourier transform method and the responses are calculated for the individual frequencies. The final time domain responses are then calculated by the inverse Fourier transform technique.

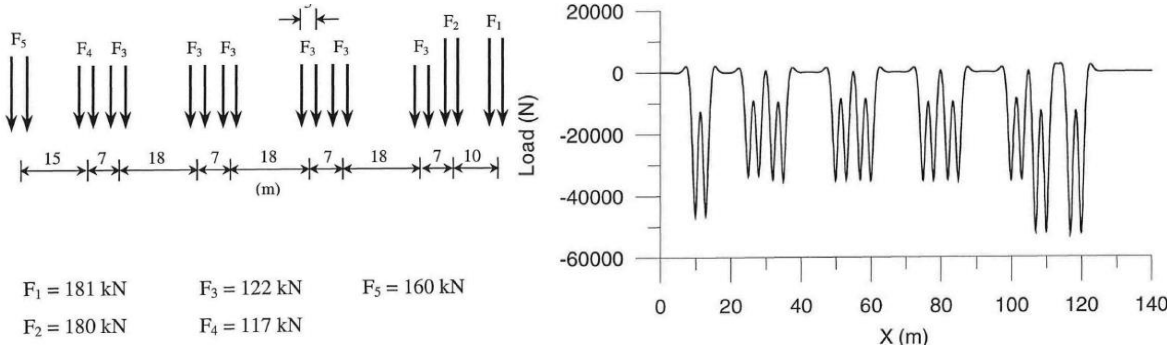


**Figure 6.2.2** Spatial variation of nodal loads used for modelling a X2000 train in Vibtrain.

## 6.2.2. Mathematical Formulation

As the loads travel along the track, interaction forces develop between the embankment (beam) and the supporting ground. The ground and the embankment can be considered as separate substructures under the nodal interaction forces, as illustrated in *Figure 6.2.1b*. If at a given frequency, ω, $\boldsymbol{P}$ denotes the vector of the interaction forces and $\boldsymbol{W}$ represents the associated vector of vertical ground-embankment displacements, then one can relate these vectors through the notion of Green's functions as:

$$\boldsymbol{W} = \boldsymbol{G}\,\boldsymbol{P} \qquad \textit{(Equation 6.2.2)}$$

where $\boldsymbol{G}$ is a symmetric matrix with frequency-dependent complex entries $\boldsymbol{G}_{ij}$ defining the ground response at node $i$ due to a unit load at node $j$. Inverting this relation, one can write:

$$\boldsymbol{P} = \boldsymbol{G}^{-1}\,\boldsymbol{W} = \boldsymbol{K}_S\,\boldsymbol{W} \qquad \textit{(Equation 6.2.3)}$$

where $\boldsymbol{K}_S$ is the stiffness matrix of the layered ground corresponding to the interaction nodes.

A similar relation can be established by considering the equilibrium of the embankment substructure. The stiffness matrix of the embankment can be assembled from the stiffness matrices of the individual beam elements. However, this matrix involves rotational degrees of freedom ($\boldsymbol{\theta}$) in addition to translational degrees. If the vector of these nodal motions is denoted by $\boldsymbol{U} = [\boldsymbol{W}\ \ \boldsymbol{\theta}]^T$, then one can write:

$$F - P = KB\,U \qquad \textit{(Equation 6.2.4)}$$

where $\boldsymbol{F}$ is the vector of applied forces and $\boldsymbol{K_B}$ is the dynamic stiffness matrix of the beam. This matrix is assembled from the classical stiffness matrix $\boldsymbol{K}^i$ and consistent mass matrix $\boldsymbol{M}^i$ of a generic element $i$ according to (*Chopra, 1995*):

$$\boldsymbol{K}^i{}_B = \boldsymbol{K}^i - \omega^2\,\boldsymbol{M}^i \qquad \textit{(Equation 6.2.5)}$$

Finally, eliminating the interaction force vector, one gets:

$$\boldsymbol{F} = (\boldsymbol{K}_S + \boldsymbol{K}_B)\,\boldsymbol{U} \qquad \textit{(Equation 6.2.6)}$$

where it is assumed that the matrix $\boldsymbol{K}_S$ has been augmented with necessary number of zero rows and columns to match the size of matrix $\boldsymbol{K}_B$. Alternatively, one could condense out the rotational degrees of freedom in $\boldsymbol{K}_B$ and directly assemble it with $\boldsymbol{K}_S$.

This formulation can accommodate “observation nodes” in the ground to obtain the responses at points other than those at the embankment-ground interface. In that case, it only suffices to include these additional nodes in the stiffness matrix of the ground without receiving any contribution from the beam stiffness matrix.

Essential to the above formulation is the implementation of a routine for the derivation of the Green's functions. In the present study, the Kausel-Roësset Green's functions for disk loads in layered media (*Kausel and Roësset, 1981*) have been used. The radius of the disk is taken such that the area of the disk is equal to the contact area at the embankment-ground interface between two adjacent nodes. For completeness, a brief account of the theory is incorporated in the following.

## 6.2.3. Green's Functions

The solution technique by *Kausel and Roësset (1981)* is based on the application of Fourier and Hankel transforms to the wave equations in each layer to reduce them to a series of ordinary differential equations. These equations are then solved by the imposition of the appropriate stress and kinematic boundary conditions at layer interfaces and the free surface. This is

achieved through a stiffness matrix approach in which each layer is represented by a stiffness matrix that relates the Fourier transform of stresses and displacements at the upper and lower surfaces of the layer. For the half space, this relation is obtained for the upper surface only. Stiffness expressions derived by *Kausel & Roësset (1981*) are incorporated here for completeness. The reader is referred to the original reference for more details.

If $k$ denotes the wavenumber, $G$ is the shear modulus, and $q$ and $s$ are defined as

$$q = \sqrt{1-(\omega/kc_P)^2} \qquad \textit{(Equation 6.2.7)}$$

$$s = \sqrt{1-(\omega/kc_S)^2} \qquad \textit{(Equation 6.2.8)}$$

then the symmetric layer stiffness matrix for the "SV-P wave" case is given by

$$\boldsymbol{K}_L^{SV-P} = 2kG \begin{Bmatrix} \boldsymbol{K}_{11} & \boldsymbol{K}_{12} \\ \boldsymbol{K}_{21} & \boldsymbol{K}_{22} \end{Bmatrix} \qquad \textit{(Equation 6.2.9)}$$

where

$$\boldsymbol{K}_{11} = \frac{1-s^2}{2D}\begin{Bmatrix} \frac{1}{s}(C^qS^s - qsC^sS^q) & -(1-C^qC^s+qsS^qS^s) \\ -(1-C^qC^s+qsS^qS^s) & \frac{1}{q}(C^sS^q - qsC^qS^s) \end{Bmatrix} - \frac{1+s^2}{2}\begin{Bmatrix} 0 & 1 \\ 1 & 0 \end{Bmatrix}$$

$\boldsymbol{K}_{22}$ = same as $\boldsymbol{K}_{11}$, with off-diagonal signs changed

$$\boldsymbol{K}_{12} = \boldsymbol{K}_{21} = \frac{1-s^2}{2D}\begin{Bmatrix} \frac{1}{s}\left(qsS^q - S^s\right) & -\left(C^q - C^s\right) \\ C^q - C^s & \frac{1}{q}\left(qsC^s - S^q\right) \end{Bmatrix}$$

and the stiffness matrix of the half-space is:

$$\boldsymbol{K}_H^{SV-P} = 2kG\left[\frac{1-s^2}{2(1-qs)}\begin{Bmatrix} q & 1 \\ 1 & s \end{Bmatrix} - \begin{Bmatrix} 0 & 1 \\ 1 & 0 \end{Bmatrix}\right] \qquad \textit{(Equation 6.2.10)}$$

where

$C_q = \cosh kqh \qquad S^q = \sinh kqh$

$C\,s = \cosh ksh \qquad S = \sinh ksh$

$D = 2(1-C^qC^s) + \left(\frac{1}{qs} + qs\right)S^qS^s$

The stiffness matrices for each layer and half-space for the "SH-wave" case are

$$\boldsymbol{K}_L^{SH} = \frac{ksG}{\sinh ksh}\begin{Bmatrix} \cosh k\,sh & -1 \\ -1 & \cosh k\,sh \end{Bmatrix} \qquad \textit{(Equation 6.2.11)}$$

$$\boldsymbol{K}_H^{SH} = ksG \qquad \textit{(Equation 6.2.12)}$$

The stiffness matrices are assembled in a finite element sense and the displacements in the transformed domain are obtained for the desired forces. The steady-state responses (Green's functions) are then evaluated by applying the appropriate inverse Hankel transforms. For instance, the vertical response due to a disk load with radius $R$ at a distance $r$ can be expressed as

$$u_Z(r,z) \;=\; \frac{1}{\pi}\int_0^{\infty} \bar{u}_2\, J_0(kr)\frac{J_1(kR)}{kR}\, kdk \qquad \textit{(Equation 6.2.13)}$$

where $J_0$ and $J_1$ are the zeroth order and first order Bessel functions of the first kind, respectively, and $\bar{u}_2$ is the vertical component of the Hankel transformed displacement.

The integrals derived above for the various components of Green's functions have to be evaluated numerically. For this purpose, one needs to use a robust procedure to make sure that the sharp peaks in the variation of the integrands are captured within the wavenumber step $\Delta k$. Discretization of the integrals introduces an artificial spatial periodicity of the load which is another potential source of inaccuracy. Therefore, $\Delta k$ has to be small enough to ensure an accurate representation of the load. These guidelines and rules have formed the basis for the numerical integration implemented in the present work.

Using the above solution, the following expression can be established:

$$\begin{bmatrix} u_u^{int} \\ u_u^{ob} \end{bmatrix}(\omega_f) \begin{bmatrix} R(\omega_f) \\ \underline{\rightleftarrows\ 0} \end{bmatrix} \qquad \textit{(Equation 6.2.14)}$$

where the vector $u_u^{int}$contains displacements of the nodes at the embankment-ground interface while $u_u^{ob}$ contains nodal displacements for the additional observation points. $R(\omega_f)$ is the vector of interaction forces on the embankment-ground interface. Taking the inverse of this relation, which is possible since $\boldsymbol{G}(\omega_f)$ is non-singular, one obtains

$$\boldsymbol{S}_u(\omega_f) \begin{bmatrix} u_u^{int} \\ u_u^{ob} \end{bmatrix} \begin{bmatrix} R(\omega_f) \\ \underline{\leftarrow\ 0} \end{bmatrix} = \left(\boldsymbol{G}(\omega_f)\right)^{-1} = \begin{bmatrix} \boldsymbol{S}_u^{11}(\omega_f) & \boldsymbol{S}_u^{12}(\omega_f) \\ \boldsymbol{S}_u^{21}(\omega_f) & \boldsymbol{S}_u^{22}(\omega_f) \end{bmatrix} \qquad \textit{(Equation 6.2.15)}$$

Both $G\ (\omega_f)$ and $S_u(\omega_f)$ are densely populated matrices, i.e. they are matrices where all elements are non-zero. However, the matrices have a clear band-structure with a dominant main-diagonal. In addition the matrices are complex and frequency dependent. For these reasons the number of matrix elements and the computational effort of obtaining these elements grow rapidly with the number of interaction points. A powerful aspect of this formulation, however, is the rigorous modeling of the ground as a semi-infinite medium with no artificial boundaries, which is often a problem in commercially available codes based on finite elements or finite differences.

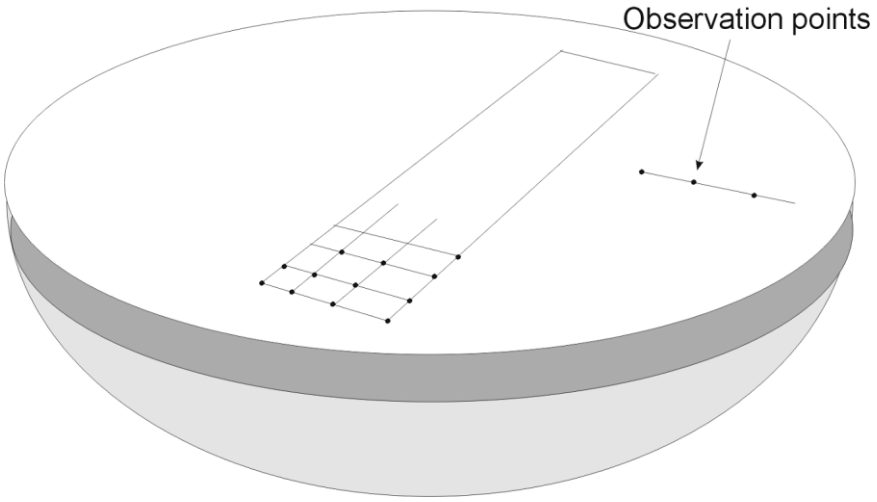


**Figure 6.2.2** Model of the unbounded domain.

## 6.3. Input file description

In *Appendix D*, an example of input file for the Vibtrain program is shown. A python "wrapper" for creating input, running, and plotting results have recently been created by *Håård (2022)*.-

## 6.4. Verification of Vibtrain

Several of the different Vibtrain versions have been recompiled with Intel Fortran compiler (2019 version) within the development environment Visual Studio 2017. The recompiled executables were tested by running the same input files and comparing the results. Results were indistinguishable from the executables compiled with older and other versions of Fortran compilers.

### 6.4.1. Receptance Analysis (dynamic non-moving load)

For further verification of Vibtrain, receptance values have been compared with the ones computed with EDT toolbox (*Schevenels et al., 2009*), and also for the Track load Vehicle receptance results for the Ledsgård site. Figure 6.4.1 shows Vibtrain computed receptance for Ledsgård for a model with a half space (absorbing boundary) and for a model with a rigid base at the bottom of the soil profile. The results match well with values at Ledsgård measured with the Track Load Vehicle (*Holm et. al. 2010*) shown in *Figure 7.2.1*. The TLV applies loads to the track using hydraulic actuator coupled to the central part of the car body. The car body first resonance influences the measurements frequencies 5 Hz resulting in low force is applied to the track. This car body effect is not accounted for in the Vibtrain nor in the base model, thus it is not possible to obtain a match for these frequencies around 5 Hz in the field measurements.

Both the Vibtrain and base model matches relatively well the frequency of the peak value in the receptance curve, indicating the models have well calibrated soil properties, while they underestimate the response with some 20%. Numerical methods often over-predict radiation damping, e.g. due to the homogenous horizontal layering in the models compared to the in-situ profile (e.g. *Johansson & Kaynia, 2021*).

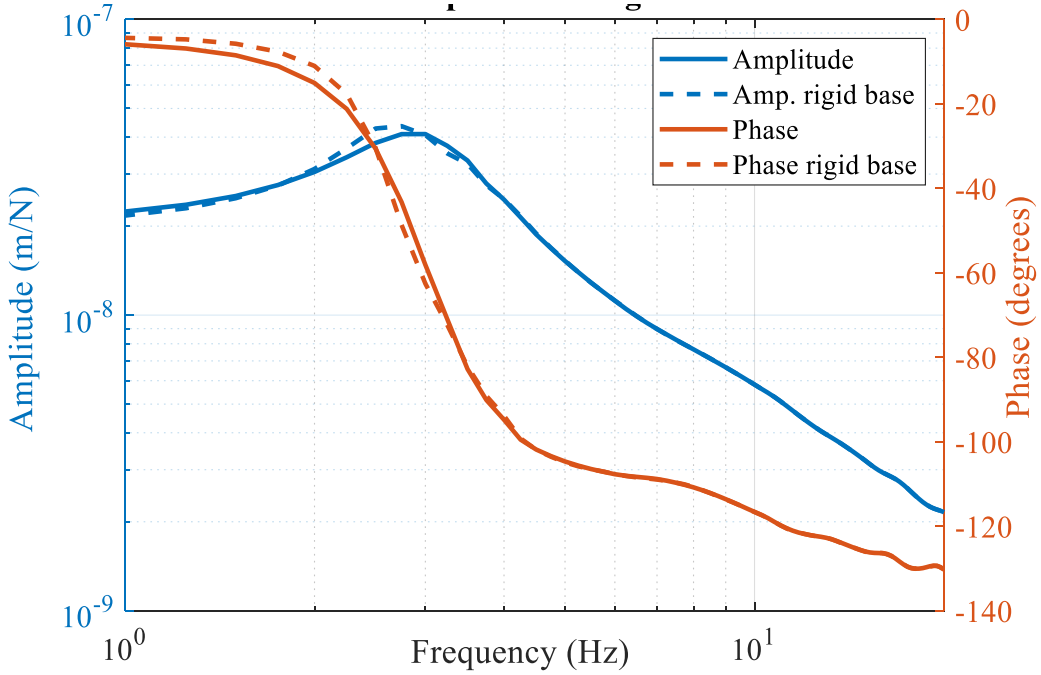


**Figure 6.4.1** Vibtrain computed receptance for Ledsgård for model with half space (absorbing boundary) and for model with rigid base.

### 6.4.2. Train Vibration Comparison with EDT and the Base Model Program

A Vibtrain model without a beam, and the embankment modeled as a soil layer is compared in *Figure 6.4.2* with similar model computed with the EDT toolbox (*Schevenels et al., 2009*). The yellow curve in *Figure 6.4.2 a*) is for the same parameters used in the EDT and Comsol FE-model shown in b). Results are satisfactory with Comsol and EDT giving slightly larger displacement. The difference is likely due to slight differences in input parameters in Vibtrain, EDT toolbox and the FE-model.

Finally the base model results shown in *Figure 5.3.1* are compared with Vibtrain results shown in *Figure 6.4.3* for a train speed of 204 km/h. The soil properties are given in *Table 5.3.1*. The Vibtrain results in larger downward displacements than the Comsol reference model and the base model, 9mm compared to 6 mm, the upward displacements are of similar amplitude. The reason for the discrepancy has not been further investigated.

It is worth mentioning the Vibtrain results are somewhat sensitive to the choice of bending-stiffness and mass of the beam representing embankment. Further evaluations of selection of these parameters are recommended. By using two models in Comsol one with the embankment with solid elements and one with beam element and match results can allow for better understanding how to better select beam properties in the Vibtrain model.

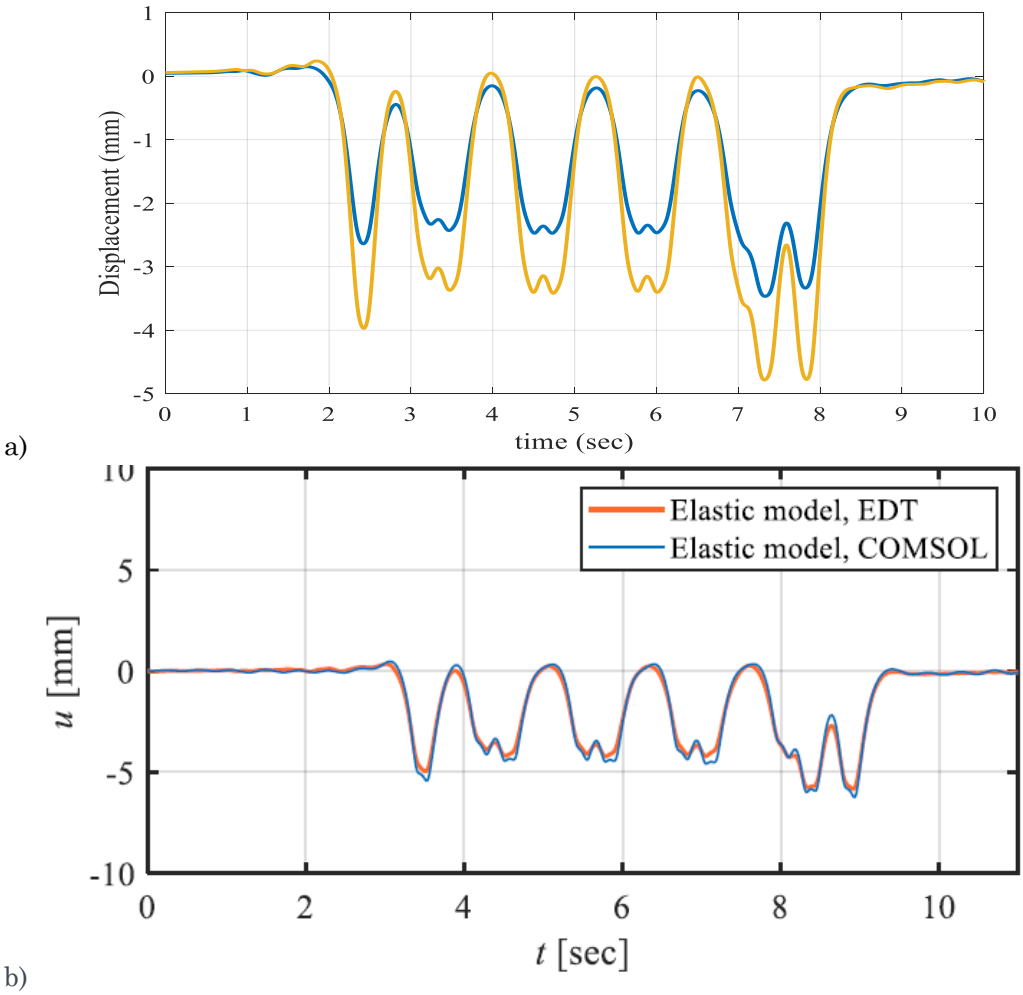


**Figure 6.4.2** Track displacement at Ledsgård for a 70 km/h train speed with a) Vibtrain and b) EDT (Green's functions) and COMSOL (Finite Element).

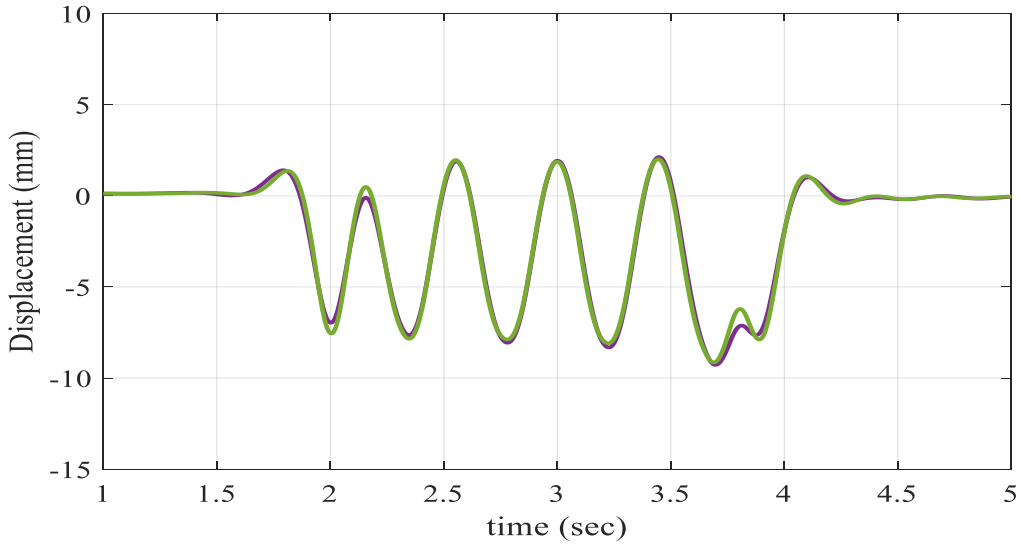


**Figure 6.4.3** Displacement for a velocity of 204 km/h for a base model input. For comparisons with Figure 5.3.1.

## 6.5. Summary

The several Vibtrain models developed since the late 1990's and the following decade have been presented and compared with the Abaqus base model, the reference Comsol model, and the EDT toolbox. Results are satisfactory, while there is some more experience needed for selection of best estimate properties of the beam representing the embankment. One benefit of the Vibtrain is the speed and ease of use. A typical run for computing train vibrations for one train speed is about half a minute. Thus a critical speed analysis with 20 train speeds takes about 10 minutes. The tool is suitable for screening procedures, as shown in the implementation for use in combination with the Track Load Vehicle. In the next section the Vibtrain is used compute rail displacements for the Ledsgård case.

## 6.6. References


ADOLFSSON, K., ANDRÉASSON, B., BENGTSSON, P.E. & ZACKRISSON, P. (1999). High speed train X2000 on soft organic clay - measurements in Sweden. *Proc. XIIth Europ. Conf. Soil Mech. Geotech. Engng*, Amsterdam, Netherlands, 3, 1713-1718.

AUBRY, D., CLOUTEAU, D. & BONNET, G. (1994). Modeling of wave propagation due to fixed or mobile dynamic sources. *Proc. Of workshop Wave'94*, Ruhr Univ., Berg-Verlag, Bochum, 79-93.

BENGTSSON, P.E .(1998). Mätningar i samband med passage av X2-tåg, 1997-10-03 1997-10-04, Ledsgård Gbdl 3 km 24+265,Report no. Dnr 2-9708-405, Appendix 11 SGI-

BENGTSSON, P.E .(1998). Swedish Geotechnical Institute (1999). High speed lines on soft ground: Evaluation and analyses of measurements from the West Coast Line. Report no. Dnr 2-9710-502, 48p + Appendix 1 through 15. *SGI.*

CHOPRA, A. K. (1995). Dynamics of Structures. *Prentice Hall*, New Jersey.

COLE, J. & HUTH, J. (1958). Stress produced in a half-space by moving loads. *J. Appl. Mech.* 25, 433-436.

DE BARROS, F. C. P. & LUCO, J. E. (1994). Response of a layered viscoelastic half-space to a moving point load. *Wave Motion*, 19, 189-210.

DIETERMAN, H. A. AND METRIKINE, A. V. (1997). Steady-state displacements of a beam on an elastic half-space due to a uniformly moving constant load. *Eur. J. Mech., A/Solids*, 16 (2), 295-306.

HOLM, G., ANDRÉASSON, B., BENGTSSON, P.-E., BODARE, A., ERIKSSON, H (2010). Mitigation of Track and Ground Vibrations by High Speed Trains at Ledsgård, Sweden. Svensk Djupstabilisering report 10.

HÅÅRD. J (2022). Train-indued ground vibrations using the VibTrain program. Master thesis. *KTH.*

JOHANSSON, J., & KAYNIA, A. 2021. Equivalent linear pseudostatic and dynamic modelling of vertically vibrating monopile. *Marine Structures,* 75: 102870. Elsevier.

JONES, C.J.C. (1994). Use of numerical models to determine the effectiveness of anti-vibration systems for railways. *Proc. Instn Civ. Engrs Transp*. 105, 43-51.

KARLSRUD, K. (1999). General aspects of transportation infrastructure. *Proc. XIIth Europ. Conf. Soil Mech. Geotech. Engng*, Amsterdam, Netherlands, 1, 17-30.

KAUSEL, E. & ROESSET, J.M. (1981). Stiffness matrices for layered soils. Bull. Seism. Soc. Am., 71 (6), 1743-1761.

KAYNIA, A.M. (1999). VibTrain: A computer code for numerical simulation of train-induced ground vibration. *NGI Research Report* 514063-2

KAYNIA, A.M. (2002). NordVib Phase 1. Report: WP3 VibTrain. Theory and User's Manual (for ExVibtrain). For Swedish National Railway Administration (*Banverket).*

KAYNIA, A.M. (2004). Computation of motion and stress in ground. Report no 20041519-2. 30 December 2004. Project:Extension of VibTrain for stress computation and stochastic soil parameters.. For Swedish National Railway Administration (*Banverket).*

KAYNIA, A.M., & EKEVID, T. (2002) “NordVib Phase 1. Report: WP3 - research and Development. 3C Tools for track and environmental vibration”. VibTrain development. Rapport utarbeidet av NGI og Chalmers. For Swedish National Railway Administration (*Banverket)*.

KAYNIA, A.M., & EKEVID, T. (2003), "Extension of VibTrain for modelling track response to Banverket's TLV ", *NGI Report* No. 20031253-1, 12 December 2003

KRYLOV, V. V. (1995). Generations of ground vibrations from superfast trains. *Appl. Acoustics*, 44, 149-164.

LIEB, M. & SUDRET, B. (1998). A fast algorithm for soil dynamics calculations by wavelet decomposition. *Archive of Appl. Mech*., 68, 147-157.

MADSHUS, C.M. (2004). Stochastic Vibration Generation - Pilot Study. Report no 20041519-1. 30 December 2004. Project:Extension of VibTrain for stress computation and stochastic soil parameters.. *Banverke*t. BV - 3469 002

MADSHUS, C. & KAYNIA, A.M. (1999). Dynamic ground interaction; a critical issue for high speed train lines on soft soil. *Proc. XIIth Europ. Conf. Soil Mech. Geotech. Eng.,* Amsterdam, Netherlands, 3, 1829-1836.

MADSHUS, C. & KAYNIA, A.M., (1998), High Speed Railway Lines on Soft Ground: Dynamic Behavior at Critical Train Speed, P*roceedings of the Sixth International Workshop on Railway Noi*se, Ile des Embiez, France.

MADSHUS, C. & KAYNIA, A.M., (1998), “High speed lines on soft ground: Soil behaviour. Laboratory test results. Ledsgård and Peppared at the West Coast Line”. *NGI Report* 515177-2. September 1998.

NAZARIAN, S. & STOKOE, K.H. (1984). In situ shear wave velocities from spectral analysis of surface waves. *Proc. 8th World Conf. on Earthquake Engng*, San Francisco, USA, 3, 31-38.

PAYTON, R.G. (1964). An application of the dynamic Betti-Rayleigh reciprocal theorem to moving point load in elastic media. Quart. *Appl. Math.,* 21, 299-313.

TIMOSHENKO, S.P., (1926), “Method of analysis of statical and dynamical stress in rails”, Proceedings, 2nd International Congress of Applied Mechanics, pp. 407-418, Zürich, Switzerland

VERRUIJT, A. (1999). Dynamics of soils with hysteretic damping. *Proc. XIIth Europ. Conf. Soil Mech. Geotech. Eng*., Amsterdam, Netherlands, 1, 3-14.

WOLDRINGH, R.F., NEW, B.M. (1999). Embankment design for high speed trains on soft soils. *Proc. XIIth Europ. Conf. Soil Mech. Geotech. Eng*., Amsterdam, Netherlands, 3, 1703-1712.

WOLFERT, A.R.M., DIETERMAN, H.A. & METRIKINE, A.V. (1997). Passing through the "elastic wave barrier" by a load moving along a waveguide. *J. Sound & Vibr.,* 203(4), 597-606.

# 7. CASE STUDIES

## 7.1. The Ledsgård Case History

The Ledsgård case history is one of the most well documented case histories concerning measurements of train induced ground vibrations. Vibration measurements have been performed here at different times, both before and after the installed ground reinforcements. The measurements were performed on sleepers, in the railway embankment and at different depths below the embankment, and also on ground surface at different distances away from embankment. Unfortunately, some data from the vibration measurements have been lost and others are not very well documented, or just available in pdf-format. For this study, the data found are considered to be sufficiently comprehensive.

In the chapter, previously performed soil investigations, ground reinforcements and vibration measurements are summarized. The case history has, in this study, been analyzed with the base model methodology, using the developed base model program, and the results from the calculations have been compared with the previously performed vibration measurements. Calculation results with the VibTrain program are also shown.

### 7.1.1. Background

Ledsgård is a small village located just north of Kungsbacka and about 25 km south of Göteborg. Through this village, the west coast line passes, i.e. the railway line between Göteborg and Copenhagen. The railway embankment here (the eastern track), were built in the end of the 19th century. In the 1990, the embankment was broadened to the west, to make room for two new tracks and to manage train speeds up to 200km/h. The high-speed train X2000 started operating on the track in early 1997 and shortly afterwards, excessive ground vibrations were measured at the railway embankment in Ledsgård. According to *Adolfsson et al (1999),* the vibration levels were about 10 times higher than normal. To further analyze the problem, seismic ground investigations and extensive vibration measurements were carried out in October 1997. Thereafter, the allowed train speed for the railway line through Ledsgård was reduced. In the summer of 2000, lime-cement columns were installed under the northbound (western) track as a ground reinforcement measure against the high-speed ground vibrations. Additional vibration measurements were performed in December 2000, i.e., the after the installation of the lime-cement columns. After this, the train speeds were again allowed up to 200 km/h for the railway line.

### 7.1.2. Geotechnical Conditions

In Ledsgård, there is lens of very soft organic soil (gyttja) with a thickness up to 3.5 m under an about 1.3m thick layer of crust (see *Andréasson, 1999 and 2000*). The lens of gyttja extends about 200m along and under the railway embankment. Under the gyttja lens, a thicker clay layer follows down to depth of about 50m. The embankment from 1990 had thickness of 1.4m and consisted of 0.52m ballast with sleepers and 0.9m thick subballast, se *Figure 7.1.1.* The track consists of UIC 60 rail placed on Pandrol rubber pads (10 mm) and concrete sleepers with a spacing of 0.67 m,

In 1997, in connection with the extensive ground vibrations measurements, seismic field tests were performed at the site by KTH (*Hall, 2000*) and laboratory tests on soil samples from the gyttja layer were performed by NGI (*Madhus & Hårvik, 1999*). As seen in *Figure 7.1.2,* the shear wave propagation speed determined with seismic field and laboratory tests, agreed very well with the empirical relationship of the undrained shear strength and the liquid limit (plasticity index). NGI (*Madhus & Hårvik, 1999*) also performed cyclic compression tests (CAUCcy) on gyttja specimens. The evaluated shear modulus reduction curves for the gyttja layer, based on

the results from the cyclic compression tests, showed less good agreement with empirical relationships, see comparison in *Figure 7.1.2*.

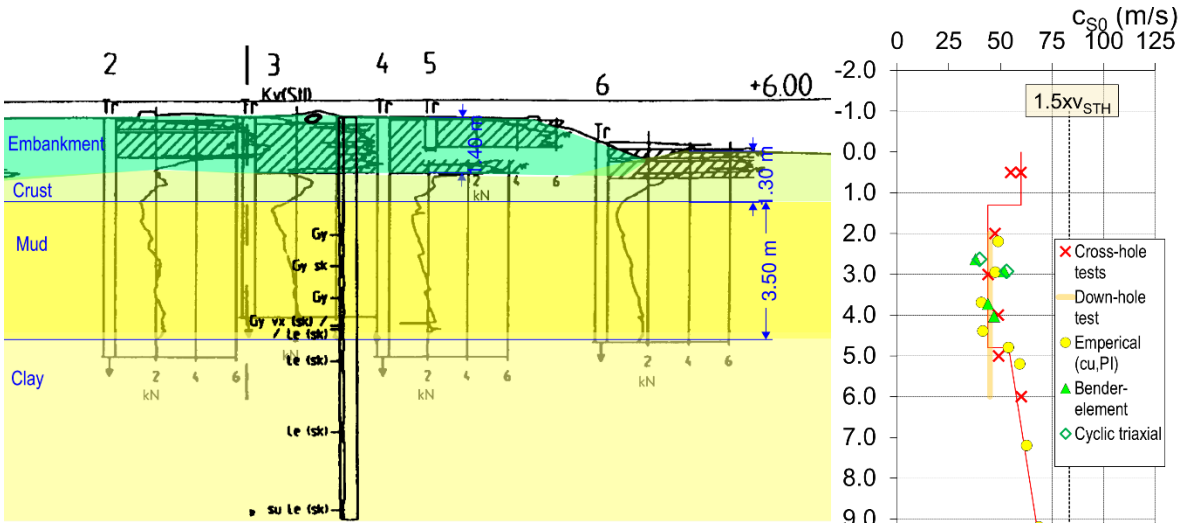


**Figure 7.1.1** Geotechnical soil profile in Ledsgård and comparisons of results from seismic tests field and laboratory tests, and empirical relationships with the undrained shear strength.

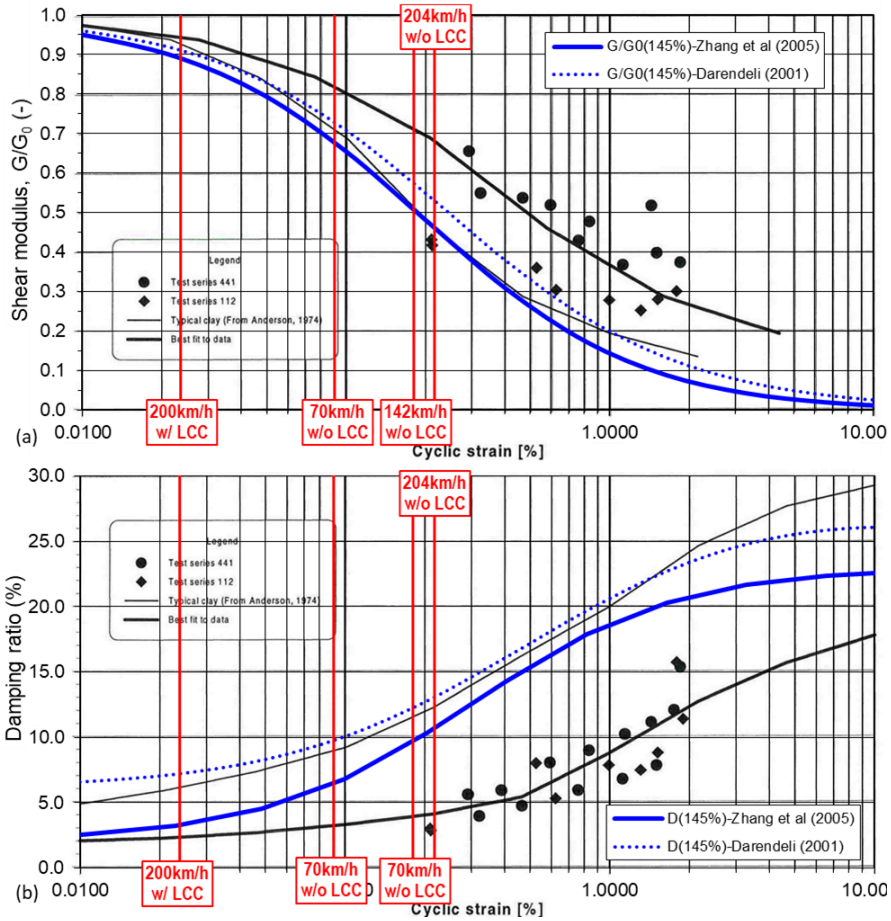


**Figure 7.1.2** (a) Shear modulus reductions curve and (b) damping ratio versus cyclic shear strain from dynamic triaxial tests on gyttja specimens from depths of 3.4 m (test series 441) and 3.7 m (test series 112) below the rail (RUK) in Ledsgård (*Madshus & Hårvik, 1999*) and comparison with empirical relationship of *Zhang et al (2005)*, *Darendeli (2001)* and *Andersson (1974)* for the same effective confining pressure and plasticity index as for the tested soil specimens.

### 7.1.3. Lime-Cement Column Reinforcement

The main cause to the large ground vibrations at Ledsgård, were found to be the soft soils and especially the soft gyttja layer. It was decided that lime-cement columns under the railway embankment, would be an effective measure to stiffening the soft ground. The design of the ground reinforcement was performed by the consulting firm J&W AB (*Andréasson, 2000*) and the lime-cement columns were installed by contractor Hercules Grundläggning AB (*Hansson, 2000*). Only the north-going track (the western embankment) were reinforced with lime-cement columns. The ground reinforcement measures, were performed during the summer of 2000.

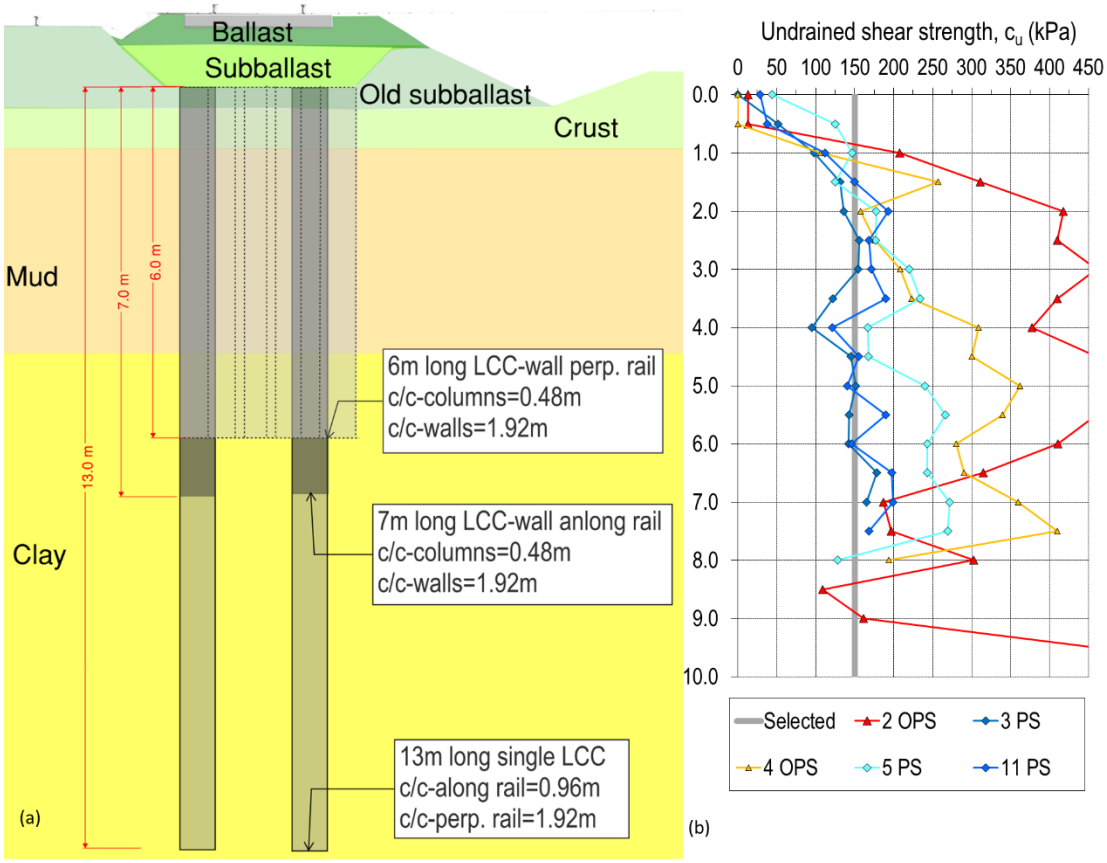


**Figure 7.1.3** (a) The pattern of the LCC ground reinforcement in Ledsgård. (b) Results from column sounding tests on the test LCCs (data from *Hansson, 2000*).
Note: PS= traditional column sounding, OPS= reversed column sounding

The lime-cement columns with a diameter of 600mm were installed in pattern as shown in *Figure 7.1.3.a.* The LCC pattern in Ledsgård was "ladder shaped" with of LCC walls along and under track (longitudinal LCC walls) with a spacing of 1.9m, and LCC walls perpendicular to longitudinal LCC walls with a spacing of about 1.9m. The lime-cement columns within in the LCC walls were installed with an overlap of about 0.1m. The longitudinal LCC walls were installed with a length of 7m and perpendicular LCC walls were installed with a length of 6m. Where the longitudinal and perpendicular LCC walls connects, lime-cement columns with a length of 13m were installed. It's unclear whether the longer single lime-cement columns were installed with a purpose of reducing settlement and if the perpendicular LCC walls were installed to increase the stability of the embankment.

Before the installation of LCC, the old embankment was excavated about 1m and left only 0.4m of the old subballast. After the LCC were installed, a new subballast of 0.7m and ballast with sleepers of 0.52m were laid out. The level of the embankment was thus increased by about 0.2m and gave the new embankment a total thickness of about 1.6m.

To verify that the chosen lime-cement binding recipe would create LCC with sufficient undrained shear strength, 12 different test columns were installed in May 2000. Three of these columns were tested after 5 days and another 2 columns were tested after 14 days since installation. Two columns were tested with reversed column sounding (OPS) and three columns were tested with traditional column sounding (PS). For descriptions of the different lime-cement column sounding methods, see *Larsson (2006).* The results from the column sounding tests, can be read in the report by *Hansson (2000)* and are summarized in *Figure 7.1.3.b.* According to *Hansson (2000)*, the first meter should not be considered in the evaluation. This because disturbances in testing columns close to ground surface and because no lime-cement mixing were discharged closer than 0.5m of the ground surface. As can be seen *Figure 7.1.3.b,* there is a very large spread in the results with an undrained shear strength that varied between 95 and 450kPa. The used methods to determine the shear strength of LCC are also very crude. In this study, an undrained shear strength of 150kPa was chosen as representative value. The shear strength of the columns can also have increased even more with time.

## 7.1.4. Vibration Measurements

### *Measurements before the ground reinforcement*

The extensive vibration measurements in Ledsgård took place during the night between October 3 and 4, 1997. For this purpose, a X2000 train of was chartered. The train was driven at different speeds back and forth past the site, while different types of ground movements were measured in the railway embankment and its surrounding. The X2000 train consisted of a power car, followed by three passenger cars and a driving trailer. The train had a total length of 114.7 m. The weights of the separate cars in the order given above were as follows: 74.3, 48.8, 50.2, 48.8 and 57.3 tons. The wheel load for the train is shown in *Figure 7.1.4.*

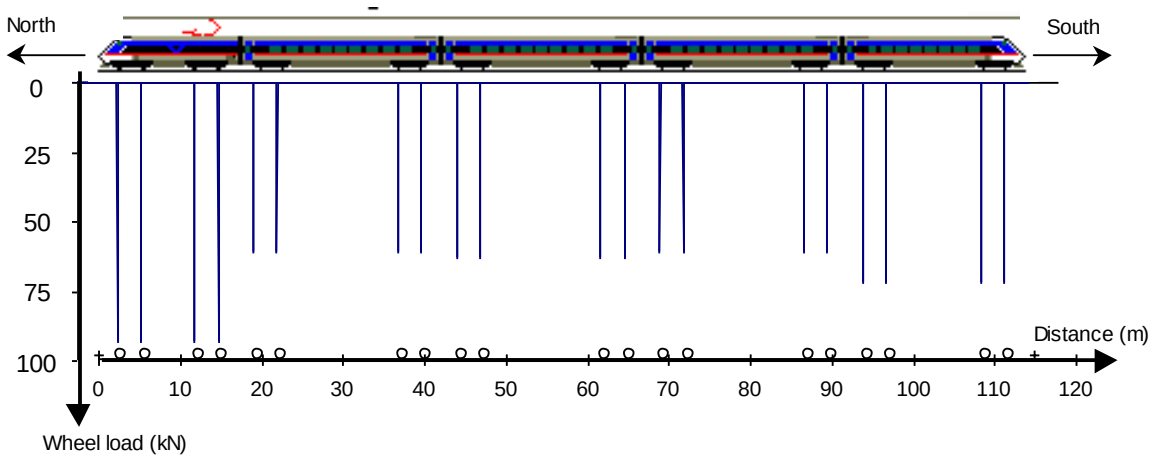


**Figure 7.1.4** Wheel load of the X2000 train used in the Ledsgård tests (*Hall, 2000*).

In the measurements of the train-induced ground vibrations, many different methods were used. These included measurement of vertical displacement of the railway embankment with extensometers (supervised by SGI), measurements of vertical particle acceleration in the railway embankment with accelerometers (supervised by Banverket) and measurements of particle velocity in the surroundings with geophones (supervised by KTH). The test set-up for the various measuring methods used at Ledsgård is shown in *Figure 7.1.5.* For more details of the vibration measurements, see *Bengtsson et al (1998)* or *Hall (2000).* The results from the vibrations measurements are available digitally by Trafikverket (formerly Banverket) together with a report prepared by *Bengtsson et al (1998).*

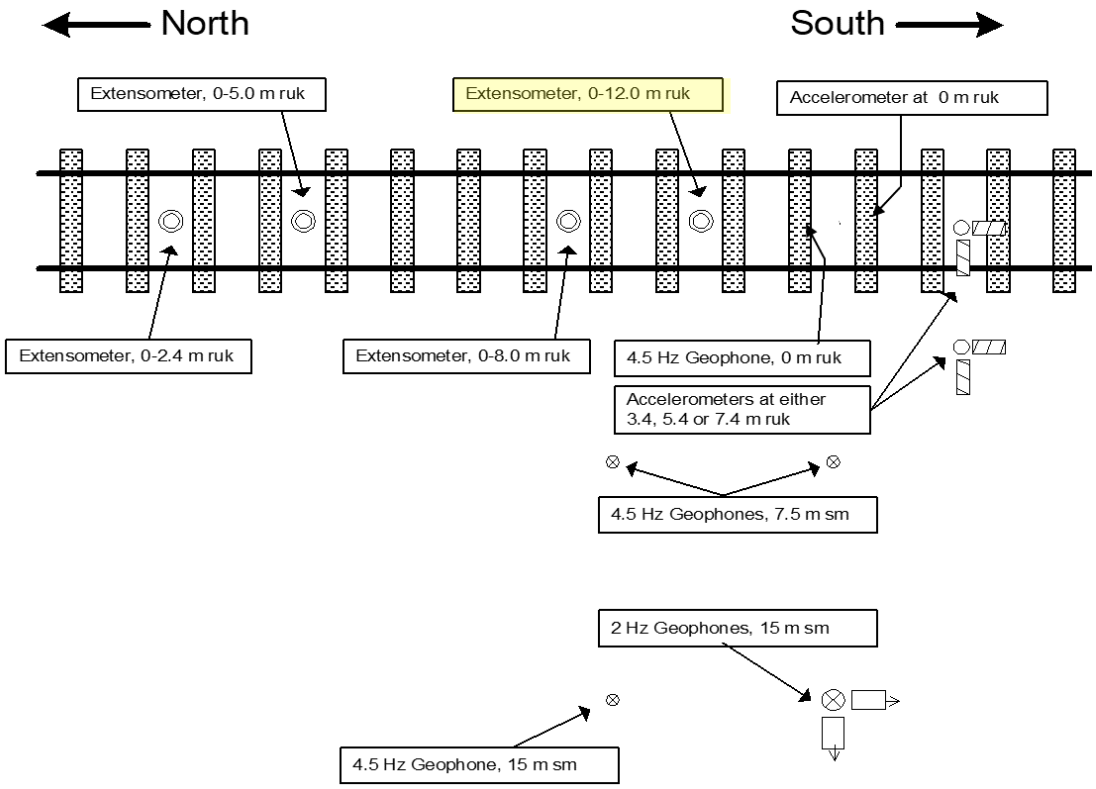


**Figure 7.1.5** Test set-up for ground motion measurements of train-induced ground vibrations at Ledsgård in October 1997 for the northbound (western) track. Note: ruk indicates depth below rail and sm distance from the track center. The geophones at 22,5, 30, 37.5 and 50 m from the track are not shown in the figure (*Hall, 2000*).

In *Figure 7.1.6*, the measured vibrations in the railway embankment are shown from train passages at speeds of (a) 70km/h, (b) 142km/h and (c) 204km/h. The measured **track displacements** in the figures are from the extensometer between 0-8m depth and from the accelerometers at the sleeper minus the accelerometer at depth 7.4m. The results from the extensometer and the accelerometers, shows similar results. The difference is that the results from the accelerometers, consists of double integrated signals (to obtain the displacements) and are only correct when looking on the peek-to-peek values. In *Figure 7.1.6.d*, the measured maximum displacements from the extensometer 0-12m are compiled from train passages at different speeds. Up to train speeds of about 70km/h, the measured vibrations are basically constant and doesn't increase much with train speed. Also, up to this train speed, there are mainly downward displacement with a maximum value about 6.5mm. At higher train speeds (>70km/h), both the downward and upward displacement increase with increasing train speed. Especially after train speeds of 140km/h, there is a significantly increase of vibrations. According to the vibration measurements, the **critical speed** of the railway embankment seems to be slightly higher than the highest measured train speed (204km/h). The measured displacement at train speed 204km/h had a maximum a peek-to-peek value about 21mm, where the maximum downward displacements were about 13.5m and the maximum upward displacements were about 7.5mm.

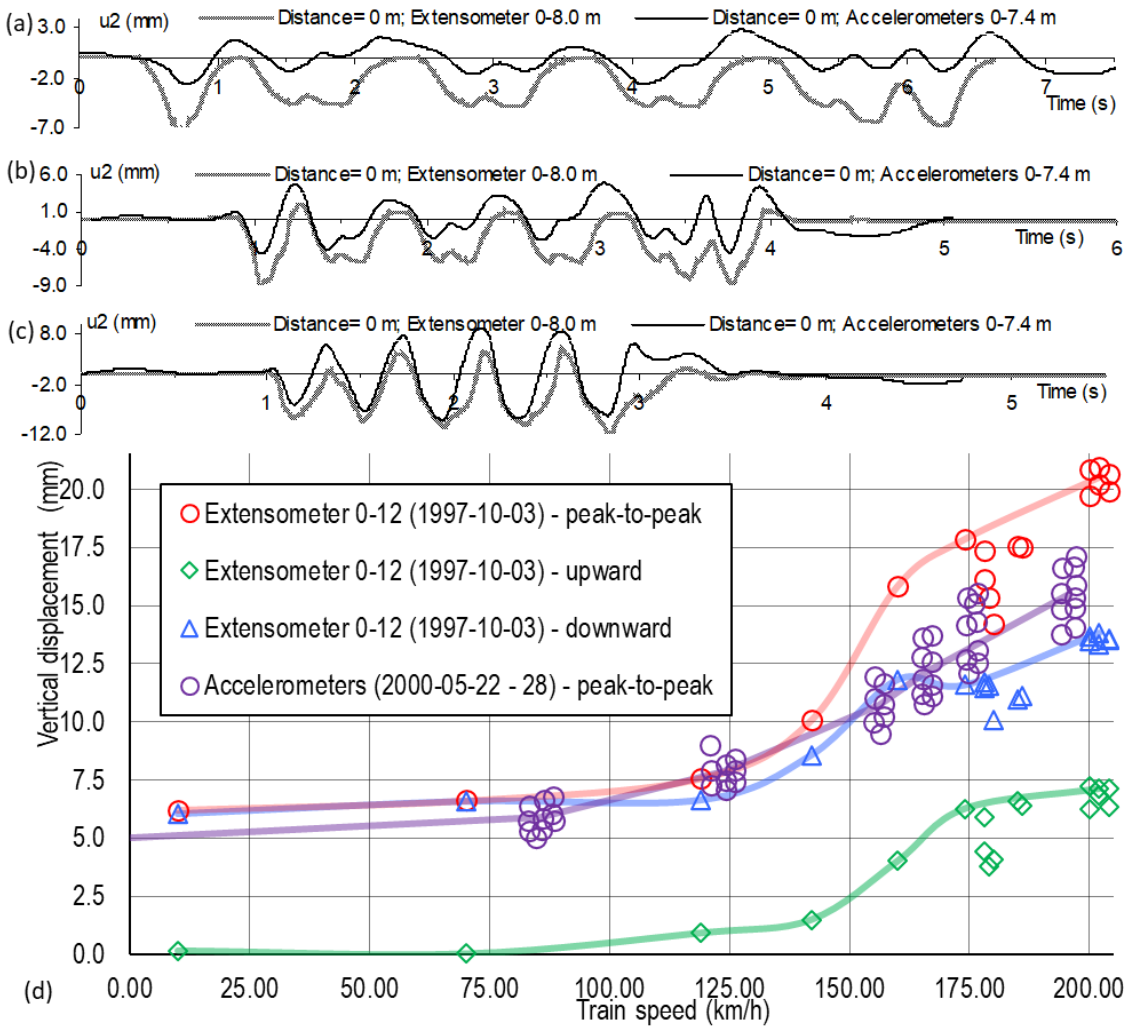


**Figure 7.1.6** Measured displacements at train speeds (a) 70km/h (b) 142km h and (c) 204km/h embankment with extensometer 0-8m and accelerometers (on sleeper and 7.4m depth) from the vibration measurements in October. (*Hall, 2000*) (d) Measured maximum displacements at different train speeds with extensometer 0-12m and accelerometer from the vibration measurements in October 1997 and May 2000 -, respectively.

In the measurements with extensometers, there is a glitch in the measurements under the first bogie. After that the extensometers seems to work fine. The glitch in measurements were more prominent at the lower train speeds and especially for the extensometer 0-12m. When evaluation the measurements from the extensometers, the downward displacement under the first bogie should not be considered.

Additional vibration measurements were performed by Banverket (*Johansson, 2001*) in May 2000 (22-28/5-2000) on passing of different X2000 trains. During these measurements, accelerometers were mounted on sleepers with a set-up as shown in the *Figure 7.1.7*. The double integrated peek-to-peek values from these measurements are shown in *Figure 7.1.6.d* together with the extensometer measurements from October 1997. The measured vibrations (peek-to-peek values) with the accelerometer are, at higher speeds (>150km/h), a bit lower compared to the measured vibrations with the extensometer.

*Measurements performed after the ground reinforcement*

In December 2000, Banverket (*Johansson, 2001*) performed vibration measurements on the ground reinforced railway embankment. Measurements consisted of accelerometers mounted on 6 different sleepers as seen in *Figure 7.1.7*. Measurements were performed during train passages of different X2000 trains. The results, see *Figure 7.1.8*, showed that the lime-cement reinforcement had decreased the **track displacements** to about 2mm peek-to-peek value (double integrated signals) and there was no sign of increased vibrations with train speed. The **critical speed** is thereby, by experience, at least at a train speed that is higher than 280km/h (≥1.4·200km/h). Hence, the effect of the ground reinforcement with the lime-columns can be concluded to be significant.

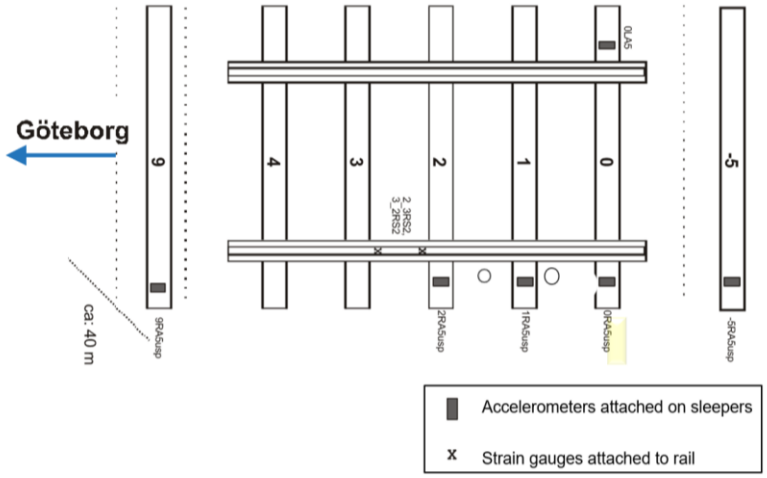


**Figure 7.1.7** Test set-up for ground motion measurements on the of train-induced ground vibrations at Ledsgård in May and December 2000 and March 2001 for the northbound (western) track before and after the ground reinforcement(*Johansson, 2001*).

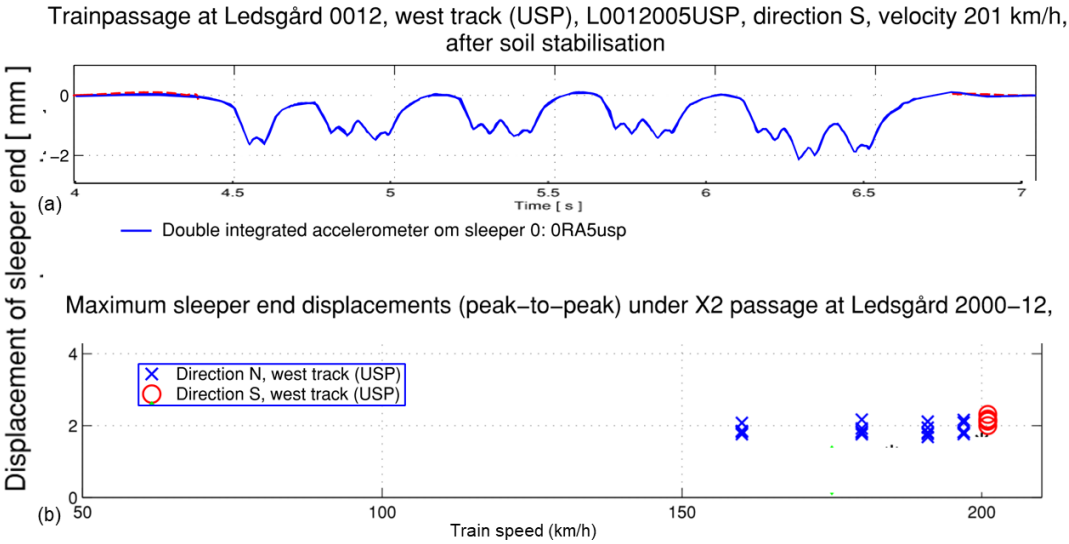


**Figure 7.1.8** Measured maximum displacements at different train speeds with accelerometers at the northbound (western) ground reinforced track (*Johansson, 2001*).

*Track receptance measurements*

Banverket (*Johansson, 2001*) also performed track reception measurements with a track-loading vehicle (TLV). The measurements before the ground reinforcement were carried out in May 2000 (22- 28/5-2000) and the measurements after the ground reinforcement took place in March 2001 (12-16/3-2001). The track-loading vehicle excites the tracks during tests, using hydraulic jacks with two oscillating masses above middle of a rebuild freight wagon. The responses were measured by accelerometers mounted on the sleepers as shown in *Figure 7.1.7*. The results from track receptance measurements, with a static preload of 90kN and a dynamic load of 10kN, before and after ground reinforcement, are shown *Figure 7.1.9*.

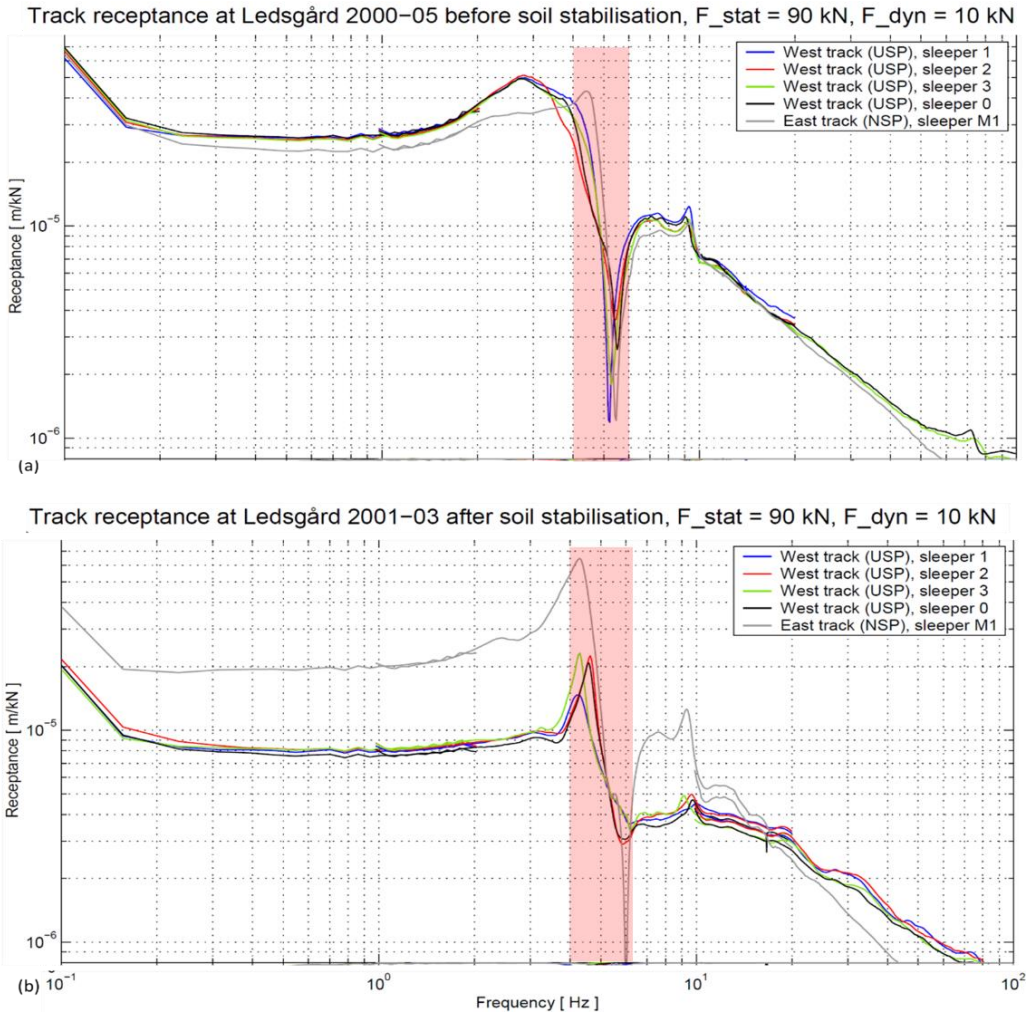


**Figure 7.1.9** Track receptance measurements with a track loading vehicle before and after the ground reinforcement (*Johansson, 2001).* The measurements in the frequency span between 4 and 6Hz may, according to *Berggren (2010*), be disturbed by the vibration source.

Before the ground reinforcement, very high receptance were measured with a value of about $27 \cdot 10^{-5}$m/kN at 1Hz. After the ground reinforcement, the measured receptance were decreased to about $8 \cdot 10^{-6}$m/kN at 1Hz. A resonance around 3Hz and a clear antiresonance around 5Hz were observed in all the measurements. The anti-resonance frequency observed in the measurements is, according to *Berggren (2010*), the TLV vehicle's own resonance frequency that is transmitted back to the track. The measured response between 4Hz and 6Hz should therefore not be considered when evaluating the results from track receptance measurements. It unclear if the measured resonance frequencies also were affected by the vehicle's resonance frequency.

The inverse of the receptance, is a value of the **track stiffness**. This means that the stiffness of the western track was around 47MN/m before the ground reinforcement and were measured to be around 125MN/m after the ground reinforcement. According to Johnsson (2001), a "normal" Swedish track has, for static preload of 90kN, have approximately a track stiffness of 200MN/m.

## 7.2. Calculations with the Base Model Methodology

Calculations using the developed base model program was applied to the Ledsgård case history for the two cases - before and after the ground reinforcement. The results from the calculations were compared with the vibrations measurements from October 1997 (*Bengtsson et al, 1997*) and from December 2000 (*Johansson, 2001*) for the unreinforced and reinforced case respectively.

### 7.2.1. Input

In *Appendix B1*, the input file to base model program is shown with values for the embankment and ground conditions that existed before the ground reinforcement. *Appendix C1* shows the corresponding values in the input file, for the conditions that exists after that the lime-cement columns were installed.

### 7.2.2. Results

The results from the analyses are shown in *Appendix B2* and *Appendix C2* for the unreinforced and reinforced case, receptively. In this chapter the results from the calculations are compared with the results from the vibration measurements.

#### *Receptance analyses*

Track receptance analyses were first performed to capture the overall **track stiffness** of the numerical models. Track receptance is commonly used to assess the track stiffness, which can be derived by inverse of the track receptance value at very low frequencies. The calculations were performed with the initial soil properties as the shear strains in these calculations are very small. The calculations were performed in the frequency domain for a harmonic load applied on the track in the middle of the model. The calculations were performed for the frequency span 1Hz to 10 Hz.

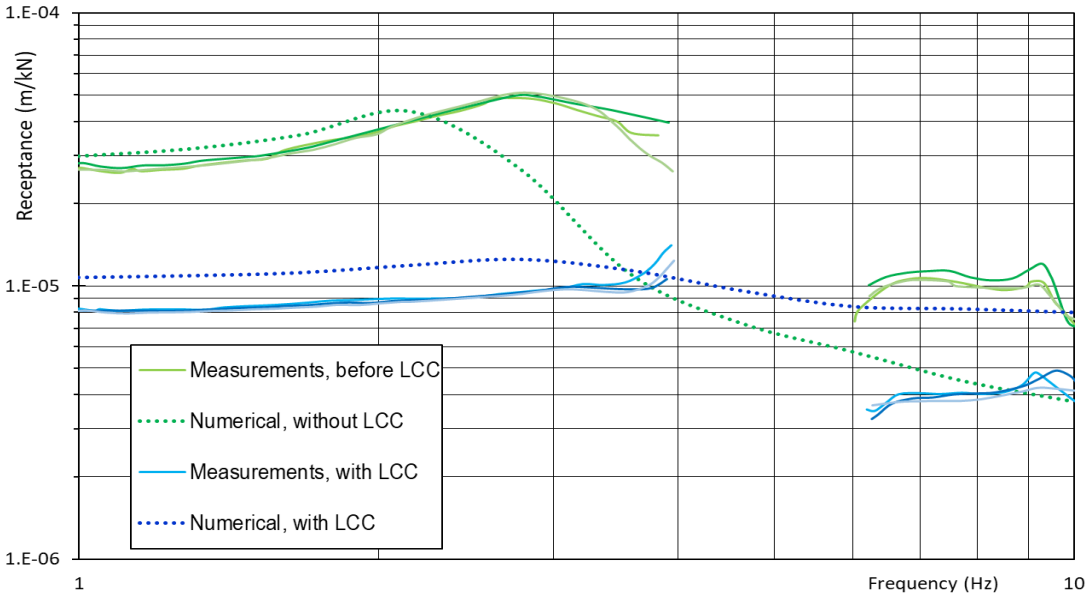


**Figure 7.2.1** Comparison between the calculated track receptance from the numerical models and the measured track receptance from the loading vehicle for the two cases before and after the ground reinforcement.

In *Figure 7.2.1*, the calculated track receptance from the numerical models (from the base model program) are compared with the measured track receptance from the track-loading vehicle (TLV (see *Chapter 7.1.2*) for the two cases - before and after the ground reinforcement. The results from the numerical calculations showed reasonably good agreement with the measurements. There are some differences though. The resonance frequency is around 2Hz in the calculation and around 3 Hz in the measurements. Also, in the numerical models seems a have slightly softer track stiffness compared to what is indicated by the measurements.

### *Moving load analyses*

Moving load analyses were performed in developed base model program and the calculated response curves of the **track displacements** for train speeds of 70, 142 and 204km/h for the unreinforced case, were compared with corresponding measurements from the extensometer. For the reinforced case, calculation of train speed of 200km/h were compared with corresponding measurements from accelerometer. The comparisons are shown in *Figure 7.2.2*. For the unreinforced case, the calculations and measurements show good agreement for the train speeds 70km/h and 142km/h. At train speed 204km/h, the calculations show on a bit smaller and broader displacement compared to the measurements. For reinforced case, at train speed 200km/h, the calculations show on very good agreement with the measurements.

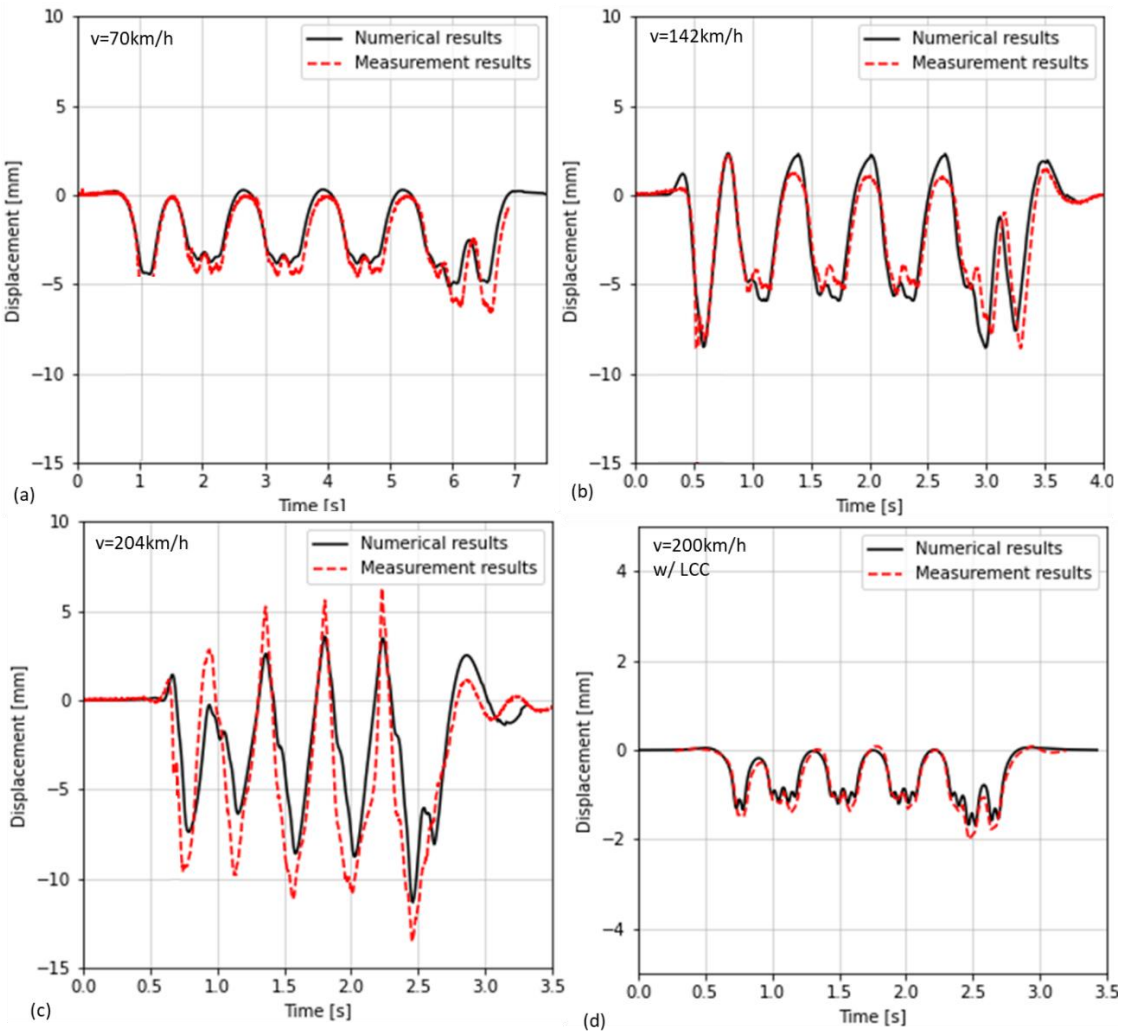


**Figure 7.2.2** Comparisons of the calculated displacement with measured displacement with extensometer 0-12m for the unreinforced cases at train speeds (a) 70km/h, (b) 142km/h and (d )204km/h, as well as calculated displacement and measured displacement with accelerometer at train speed (d) 200km/h on the ground reinforced embankment.

In *Figure 7.2.3,* the calculated and measured maximum peek-to-peek value are compared against train speed. For the unreinforced case, the calculations and measurements show good agreement up to a train speed of about 185km/h. According to the calculation with the base model methodology, the **critical speed** is obtained at 185km and the calculated displacements starts to decrease at higher train speed. The measurements showed that the critical speed was higher than 204km/h and this explains the difference in displacement between the calculations and measurements at train speed 204km/h. The critical speed for the reinforced case was determined to about 405km/h. Hence, the lime-column ground reinforcement increased the critical speed with a factor around 2.

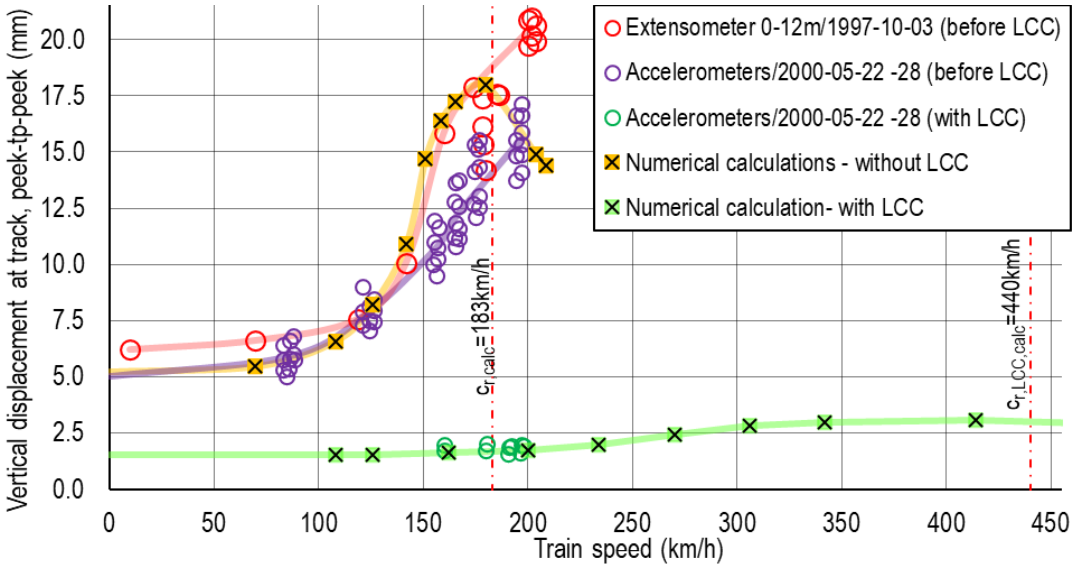


**Figure 7.2.3** Comparisons of the maximum calculated and measured peek-to-peek displacement against train speed for both the unreinforced and reinforced cases.

As seen the comparisons in *Figure 7.2.3*, the numerical calculation, with automated subroutine for adjusting the shear strain dependent properties, can capture the deformations quite well. In *Figure 7.2.4.a,* the **adjusted shear wave propagations speed** for the calculated unreinforced cases (train speeds 70, 142 and 204km/h) and the calculated reinforced case (200km/h), are compared to the initial shear wave propagations speed. The adjusted shear wave propagation speeds shows that shear modules reduction is especially high in the embankment (the subballast). At higher train speeds (>140km/h), there are also a significant reduction of the shear speeds for the soil layers down to a depth of 7m below the ground surface.

In *Figure 7.2.4.b*, the **calculated shear strain**, in the different calculations used for adjusting the shear strain dependent soil properties, are shown. As seen in the figure, the calculated shear strains are highest in the gyttja layer and then decreases with depth. A significant increase in shear strain occurs, for the unreinforced case, between train speed 70km/h and 142km/h. For the reinforced case, the shear strain levels are dramatical decreased in the upper soil profile (<7m depth) and have instead slightly increased shear strain in the lower soil profile (>7m). Also, in the *Figure 7.2.4.b*, the linear and **volumetric threshold shear strains,** are shown according to the plasticity index in the different soil layers (see *Chapter 3.1*). According to this, the volumetric threshold shear strains are exceeded in the embankment and in the crust layer for all analyzed cases. At train speeds higher than 140km/h for the unreinforced case, the volumetric threshold shear strain is also exceeded for the gyttja layer. When comparing the calculated effective shear strains with the **linear threshold shear strain**, see *Figure 7.2.4.b*, shear strain, it can be evaluated that the soil all the analyzed cases only behave as linear elastic material at depths greater than 15m below the ground surface.

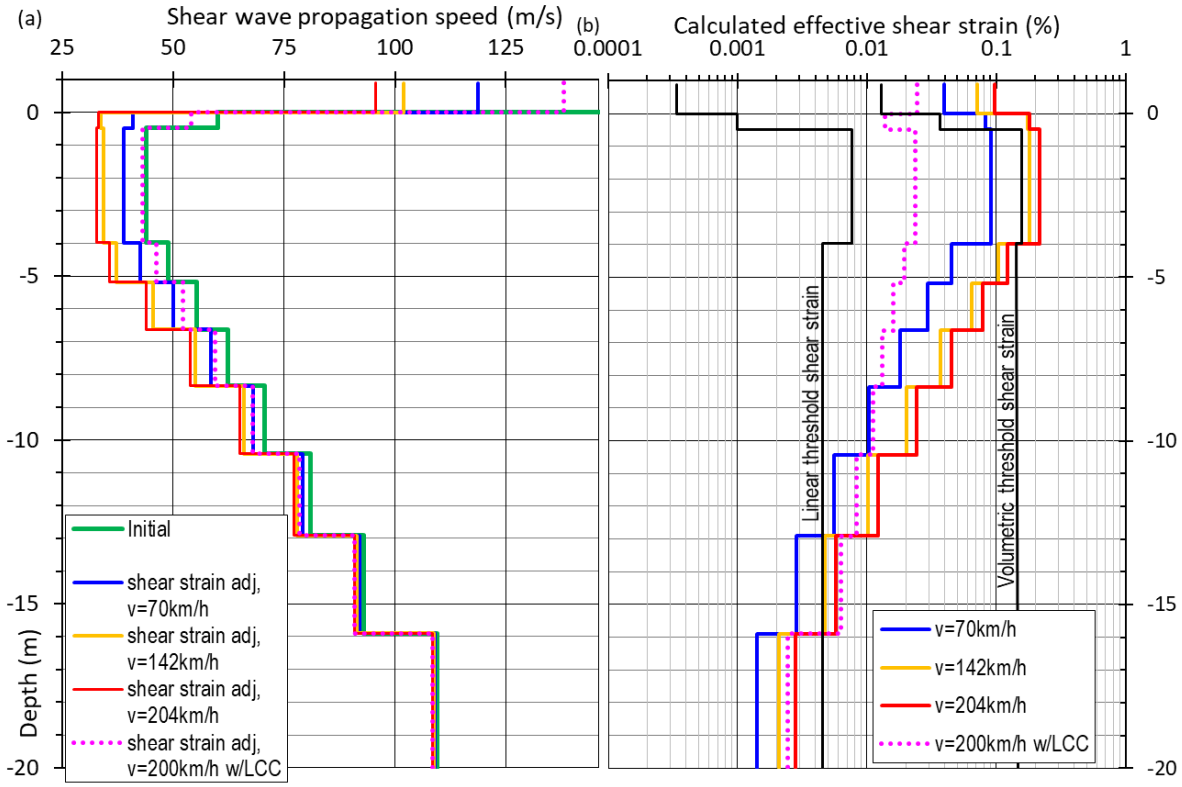


**Figure 7.2.4** (a) Initial shear wave propagation speed and shear strain adjusted shear wave speed for the different calculations b) The calculated shear strain in the different calculation used for adjusting the shear strain dependent soil properties and comparison to linear and volumetric threshold shear strain according to *Vucetic (1994*) for the respectively plasticity index in the different soil layers.

## 7.3. Calculations with the VibTrain Program

To compare calculations using the Vibtrain program with results the from the developed base model program, Vibtrain analysis have been performed for the same shear strain adjusted soil properties as shown *Figure 7.2.4.a* for the analyzed train speeds without ground reinforcement. The corresponding shear modulus, from the calculations with the base model program, are shown with green and blue curves in *Figure 7.3.1* for trains speed of 70 and 204 km/h. The shear modulus for 142 km/h lies in between these two curves. The shear modulus used the analysis by *Kaynia et. al (2000*) for 200 km/h, is shown with a red curve in the same figure.

The Vibtrain results for all three train speeds (show in *Figure 7.3.2, Figure 7.3.3* and *Figure 7.3.4*), using the shear modulus calculated in the base model program, have about a factor 2 larger calculated **track displacements** than the vibrations measurements (shown in *Figure 7.2.*2). A better match with the measurements is obtained with Vibtrain using the shear modulus profile by *Kaynia et. al (2000*). This shows the importance of calibrating the specific computational model used and the applying it to the problem at hand.

For the train speed of 70 km/h, the effect of the stiffness of the beam representing the embankment and the rail was investigated. Comparing with measurements and also the results of the base model (*Figure 7.2.2.)* it seems a relatively soft beam of 50-100 MNm$^2$ is good choice. For this stiffness, the upward deflection shape of the last boogie under the locomotive is better captured. The assumption of how the beam distributes the axle loads smoothens out the results for the other boogies and the relative upward deflections between the axle loads seen in measurements and the base model is not captured.

Finally, calculation of the **critical speed**, using the two soil profiles for train speed of 70 km/h and 204 km/h from the base model calculations, are shown in *Figure 7.3.5.* The stiffer soil profile (train speed of 70 km/h) gives a critical speed of about 210 km/h and the softer soil profile (train speed of 204km/h) results in critical speed of 190 km/h. Thus, even though the calculated displacement is much larger with Vibtrain compared with the results from the base model program for the same soil profiles, the critical speed estimate of the base model program and Vibtrain are fairly close.

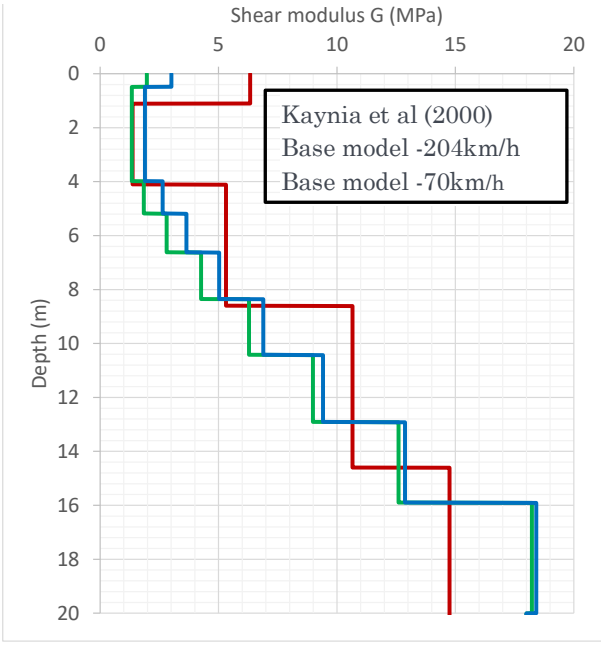


**Figure 7.3.1** Soil shear modulus used in the Vibtrain analysis. Blue and green curves are shear modulus calculated in the base model program for train speeds 70km/h and 204km/h, respectively. The red curve with and compared with shear modulus used by *Kaynia (2000)*.

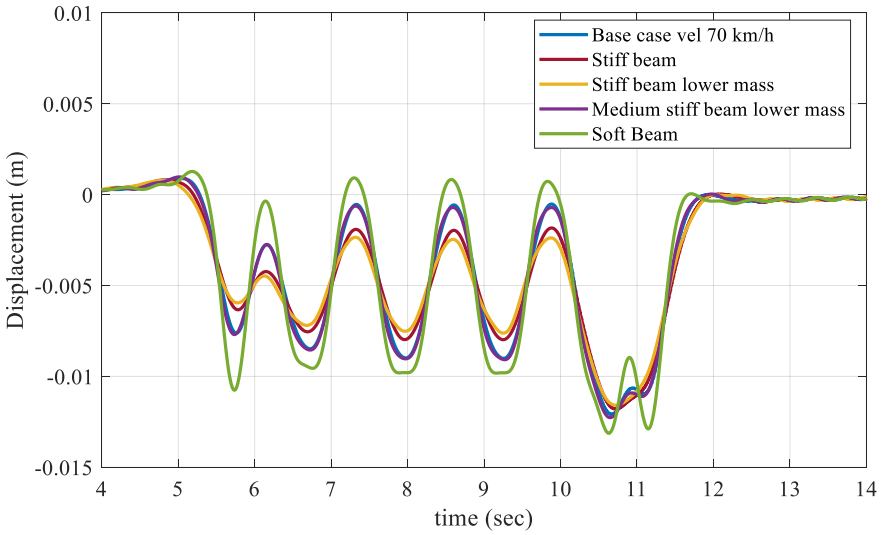


**Figure 7.3.2** Base model train speed 70 km/h. Three different stiffness of the embankment beam

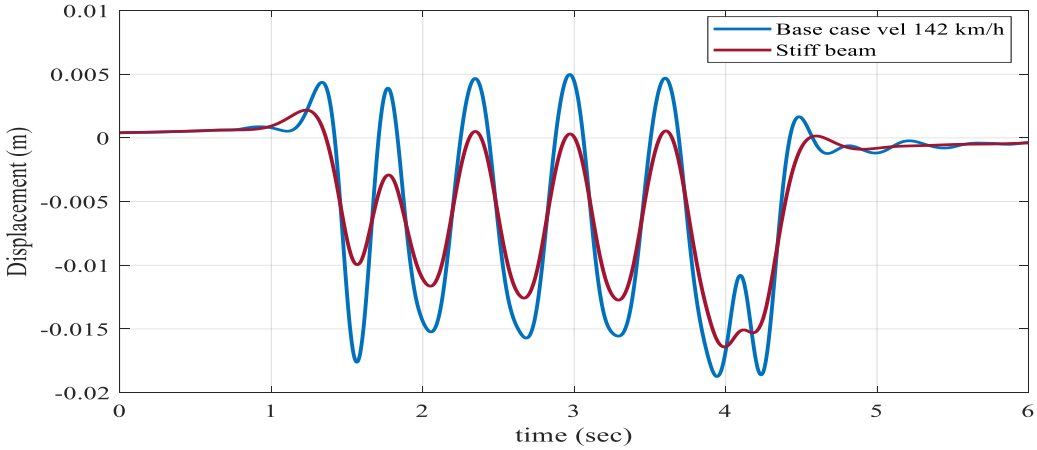


**Figure 7.3.3** Base model train speed 142 km/h.

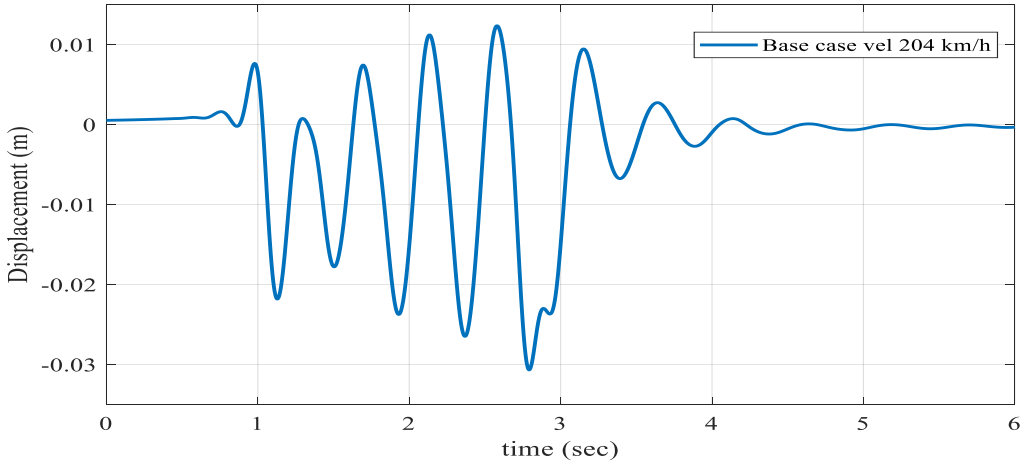


**Figure 7.3.4** Base model train speed 204 km/h.

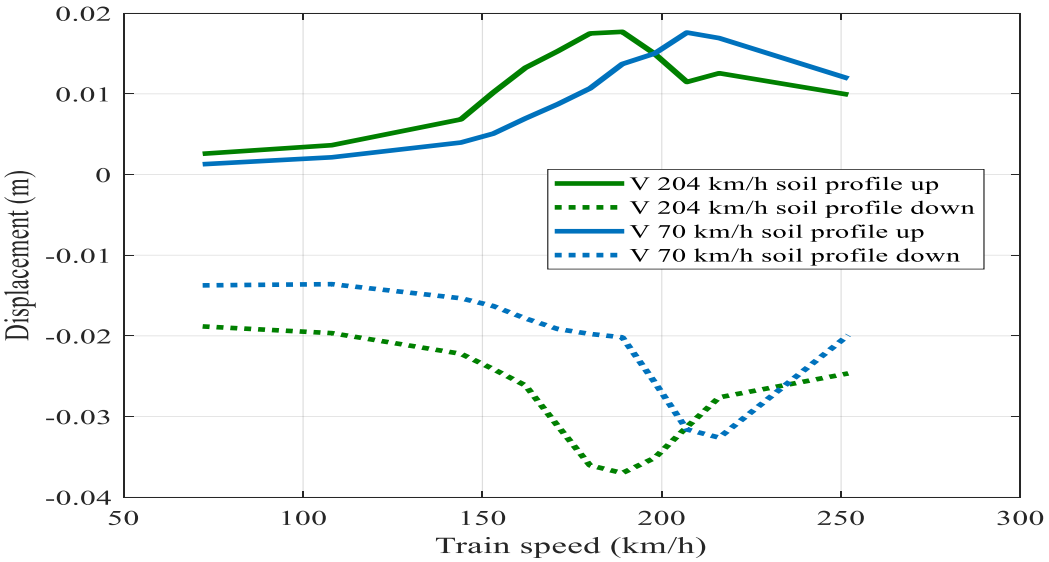


**Figure 7.3.5** Critical speed plot. Maximum upward and downward displacement for the two soil profiles shown in Figure 7.3.1 constant for all speeds.

## 7.4. Discussion

The developed base model methodology seems to work well, and the calculations gives good agreement with the measurements. The major difference between the calculations and the vibrations measurement, was that critical speed was determined to be lower than what the measurements indicated. An explanation to this is given in this chapter. Some other aspects in the vibrations measurements and the numerical modeling are also discussed.

The soil properties non-linearity with shear strain

The dynamic triaxial tests performed on soil samples from the organic mud (gyttja) layer shows, as seen in *Figure 7.1.2*, a much stiffer behavior at higher shear strains levels than what is typical according to literature and empirical equations for the same confining pressure and plasticity index. In this study, the shear modulus reduction with shear strain according to equations by Zhang et (2005) was used. Time has not allowed to, in the numerical calculations, test the use of the shear strain dependency of the gyttja layer according to the laboratory tests. However, it is also unclear why there is discrepancy between results from laboratory tests for shear-dependent soil properties compared to typical values according to the literature. Some additional notes on this are given in *Appendix A*.

The effective shear strain in the equivalent linear method

In the equivalent linear method, an effective shear strain is used when adjusting the soil properties (see *Chapter 3.2.2* and *Chapter 5.4.1*). The effective shear strain is calculated by multiplying the maximum calculated shear strain, from the numerical calculations, with factor $R_f$. The value of factor $R_f$ is based on recommendation in the literature. The results in the numerical calculations appears, especially for the lower train speed results, to be influences by the chosen value of $R_f$, A more sophisticated approach, which identifies the shear strain levels based on the statistics analyses, might have given an even better match with the measurements.

The adjustment of the shear dependency by soil layers

The shear strain depended soil properties were adjusted, based on calculated shear strain under the embankment, for the whole horizontal soil layers. It's believed that this does no effects the results on the calculated response in the railways embankment. To study this, a more advanced equivalent linear subroutine needs to be developed, which can divide the horizontal soil layers into a number of zones depending on the different ranges of calculated shear strain levels.

Non-linearity of the material properties in the ballast layer

In the numerical modeling, the material properties of the ballast layer are assumed to be linear elastic. Consideration of ballast nonlinearity may improve the results and is something that needs to be evaluated in coming studies. The stiffness of the ballast might, see *Appendix A,* be affected by both cyclic shear strain and the increased confining pressure due to the train loads.

The vibration measurements

Generally, the calculated displacement in the moving load analyses, showed on good agreement with all the measurements up to a train speed of about 150km/h. At higher train speeds, the accelerometers showed on slightly less vibrations levels than compared to measurements with extensometers.

It is assumed that the vibrations measurements from extensometer are more correct in measuring displacement than accelerometers. This as they measure the displacement directly. As a method for measuring ground vibration, however, this method is very uncommon. Vibration measurements with accelerometers are, on the other hand, used regularly. In order to obtain displacements from accelerometer measurements, however, a double integration of the signal is necessary, and this might be a source to some uncertainties.

The vibration measurements can also be affected by the heterogenous properties in ground. Especially the results from receptance tests, where the loading is local, are more prone to be affected by local discrepancies in the ground.

Simplifications of the geometry

In the numerical modeling, symmetry of the railways embankment's geometry is used. Only one track is thereby modeled, and the railway embankment is therefore not as broad as the actual railway embankment with three tracks. Another simplification of the geometry in the numerical modelling, is that the soil layer under the embankment has the same thickness outside the embankment. For the analyzed case in Ledsgård, this means that the ground surface outside the embankment is about 0.8m lower than the actual ground surface. The thickness of the different material layers in the embankments and the thickness of the different the soil layers under the embankment is correct. It is believed that this will not affect the results in the calculations, but this is something that needs to be evaluated in further studies.

The receptance analyses

The receptance analyses need some more studies concerning both the measurements and the numerical modeling. Especially concerning the resonances that were seen in the measurements with track-loading vehicle (TLV), but not in the numerical calculations.

The lime-cement column reinforcement

The LCC walls along the track (longitudinal) were, in the numerical calculations, modelled with its actual geometry and soil properties. The perpendicular LCC walls and the single lime-cement columns were also modelled as walls in the longitudinal direction, but with equivalent material properties of the LCC and the unreinforced soil in-between the columns. The equivalent material properties were calculated based on the coverage degree of the LCC. This averaging technique is commonly used in the calculation for design of required LCC reinforcement for stability and settlement problems, see *Larsson (2003).*

The stiffness of the lime-cement columns seems, according to literature, have's strong empirical relationship with its shear strength (see *Chapter 3.3.4*). Shear strength of the lime-cement columns determined in by field tests have, as seen in *Figure 7.1.3*, has a large spread. The shear strength was chosen conservatively, but when comparing calculations results with measurements, this might be too conservative.

The Rayleigh damping model

In the present work, the Rayleigh damping is used in the numerical calculations to model the damping ratio (see *Chapter 4.4.5*). As the Rayleigh damping is frequency dependent, the parameters in the Rayleigh damping model are calculated based on the dominating frequency range in the numerical model. However, the dominating frequencies decreases when the stiffness of the ground decreases with increasing train speed (as the shear strain increases). When updating parameters, α and ß, in the Rayleigh damping model for increasing damping ratio with shear strain, the changes in dominating frequencies is not considered in the current the equivalent linear subroutine. Therefore, a slightly higher damping may have been used in the numerical calculations. This might have some effects on the results at the higher train speeds.

Exceeding the volumetric threshold shear strain

When the volumetric threshold shear strain is exceeded, there is a risk of permanent microstructure changes in unsaturated soils and risk of build of excess porewater pressure in saturated soils. In both cases this can lead to loss in shear strengths and may thereby affect the stability of the railway embankment. To check if the effective calculated shear strain exceeds the volumetric threshold shear strains, may be a simple method to evaluate if the cyclic loading from train traffic may affect the overall stability of railway embankments.

Exceeding the linear threshold shear strain

In analyzed case history, the calculated shear strain exceeds the linear threshold shear strain down to depth of 15m below the ground surface. Below this depth (≥15m), the linear threshold shear strain was not exceeded. This was valid for both the unreinforced and reinforced case. Thereby, when analyzing train-induced ground vibrations of trains with axle loads up to 250kN, soil properties at depth 15m below the railway embankment can be assumed to be linear-elastic.

The critical speed

In this study, there was no time analyze why he calculated critical speed, determined with base model methodology, was lower than what the measurements showed. It might be caused by the fact that the selected material model did not describe the shear strain dependence in the gyttja layer correctly. Further studies are needed to investigate this.

Vibtrain

The track response pattern is captured quite well with VibTrain. The magnitude of the calculated displacements was, however, a factor 2 higher than the measurements for the shear strain adjusted shear modulus from to the base model program. Some time is probably needed to calibrate the stiffness of the beam (representing the embankment) to be able to get a better fit. There is also a need for a subroutine to, directly in the program, be able to take account for the shear strain dependency of the stiffness and damping for materials in both the embankment and the ground. Also, some further studies and development of the program, are needed to be able to model ground reinforcements with VibTrain.

## 7.5. References


ADOLFSSON, K., ANDREASSON, B., BENGTSSON, P.E. & ZACKRISSON, P. (1999). High speed train X2000 on soft organic clay – measurements in Sweden. *Proc. XIIth Europ. Conf. Soil Mech. Geotech. Engng*, Amsterdam, Netherlands, 3, 1713-1718.

ANDERSON, D.G. (1974). "Dynamic modulus of cohesive soils." Doctoral Thesis. University of Michigan.

ANDREASSON, B., (1999), "Geotechnical investigation in Ledsgård," Appendix 1, in Bengtsson, P.E., ed., High Speed Lines on Soft Ground, Evaluation and Analyses from the West Coast Line, Dnr 2-9710-502, *Swedish National Rail Administration*,.

ANDRÉASSON, B. (2000). "Geotekniska undersökningar, Rapport RGeo" Projekt VBK Förstärkningsåtgärder Ledsgård, km 24+000 till 24+400. Datum 2000-03-10. Upprättad av J&W AB på uppdrag av *Banverket*.

BENGTSSON, P.E., (1999), "High Speed Lines on Soft Ground, Evaluation and Analyses from the West Coast Line", Dnr 2-9710-502, *Swedish National Rail Administration*-

HALL, L. (2000). "Simulations and analyses of train-induced ground vibrations". Doctoral Thesis, Division of Soil and Rock Mechanics, *KTH-Royal Institute of Technology*.

HALL L. (2003). "Simulations and analyses of train-induced ground vibrations in finite element models". *Soil Dyn Earthq Eng* 2003;23(5):403–13.

HANSSON, T. (2000). "Utvädering Provpelare , Provyta öst, Ledsgård. *Hercules Grundläggning*

JOHANSSON E. (2001). "Track Stiffness and Track Vibrations at Ledsgård 2000-2001, before and after soil stabilization,".BBS 2001/03, *NordVib 4A4*, published 2001-05-30.

KAYNIA AM, MADSHUS C, ZACKRISSON P. (2000). Ground vibration from high-speed trains: prediction and countermeasure. *J Geotech Geoenviron Eng*; 126(6): 531–7.

LARSSON L. (2006) "Djupstabilisering medbindemedelsstabiliserade pelare och masstabilisering– En vägledning". *Svensk Djupstabilisering*. Rapport 16.

MADSHUS, C. & HÅRVIK, L., (1999), "Laboratory test results. Ledsgård and Peppared"., Dnr 2-9710-502, *Swedish National Rail Administration.*

ZHANG, J., ANDRUS, R. D., & JUANG, C. H. (2005). "Normalized shear modulus and material damping ratio relationships". ASCE J. *Geotech & GeoEn Eng,* 131(4), 453-464.

# 8. CONCLUSIONS

The intention of this project was to develop a user-friendly methodology for efficient numerical calculations of train-induced ground vibrations in the railway embankments. A methodology has been developed and it has been proven that it works. This was made by developing an input file with a database to set-up the problem and by developing a shell program that reads the input file, creates, and runs the model of the problem on a commercial numerical software, and also extracts the results from the calculation of the problem and saves the results in an output file. Through this, the calculations could be automated and thus made them easy to use.

The developed methodology was applied to published reference case and to a case history with vibrations measurements before and after a ground reinforcement with lime-cement columns. From these results, it has been showed that the developed methodology:

- can be used calculate ground vibrations that show very good agreement (almost identical) with results in published analyzes and good agreement with vibration measurements for analyzed case studies.
- can be used to determine required lime-cement columns ground reinforcement based on permissible vibration requirements.

Also, in analyses of the case history, the following observations were made:

- In the analyses, it's important to have the correct geometry and good estimates of the material and soil properties.
- For the dynamic soil properties:
    - It is useful to use the strong empirical relationships, with the undrained shear strength ($c_u$) plasticity index (PI) and effective stress ($\sigma'$), to estimate the initial soil properties.
    - The equivalent linear method, to take account for the shear strain dependency of the material and soil properties, seems to work very well.

The results in the calculations are thus strongly influenced by input to the analyzes. In this report, guidance is given on how to evaluate soil properties necessary for soil dynamic analyzes. The report also provides guidance on how to optimize the numerical calculations in order to minimize the computing time with sufficient accuracy in the results.

The developed methodology is self-instructive, and less time and work are needed in performing numerical calculations of train induced ground vibrations. The need to have high knowledge to use advanced numerical computer programs decreases. This form of analyses thus becomes more user-friendly, more people can perform these analyses and thereby increases the understanding the knowledge for this kind of problem. The developed methodology will decrease calculations and designing errors, as well as creating more time in optimizing any required ground reinforcement. This methodology can therefore be very useful in the design of the forthcoming major infrastructure projects with the expansion of the new planned railways lines in the Nordic countries.

# Appendix A

## Soil behavior under cyclic loading: NGI:s approach

# A1 INTRODUCTION

NGI has long tradition in investigating the soil's behavior from cyclic loads. These experiences are shortly summarized in this appendix. The methods to handle cyclic loading developed at NGI have focused on (offshore) foundation capacity (ultimate limit state, ULS), and thus aimed at larger strains and displacements. In recent years the methods have been adopted to Offshore wind structures where typically serviceability limit state (SLS), and soil stiffness and damping are as important as it is for train induced vibrations.

For train induced vibrations it is desirable keep the strain in the geomaterial below a level where large non-linearity starts degrading the stiffness quickly. Thus for modelling dynamic train induced vibrations it commonly considered enough to account for stiffness and damping at small to intermediate strain levels, which can be well approximated with modulus reduction and damping curves as described in the main report. For completeness of the report the NGI approach to deal with large stresses and strains, and also some more recent findings on stiffness and damping are included below.

# A2 EQUIVALENT LINEAR MODELS

The concept of equivalent linear models to account for cyclic loading is described in the main report. A brief literature review was performed to evaluate which model to select. There are several empirical models for shear modulus reduction and damping curves in the literature. Often used are the ones described by Darendeli (2001), Vardanega & Bolton (2013), Vucetic and Dobry (1991), and *Zhang et. al. (2005).* Kishida (2016) does thorough comparison of the four these models. The controlling parameters in the models are the cyclic shear strain, $\gamma_c$, effective vertical overburden or mean pressure, $\sigma_v'$ or $\sigma_m^{'}$, and plasticity index, PI. The more recent models also operate with a reference strain $\gamma_r$. When the cyclic shear strain is equal to the reference strain the shear modulus, $G$ is equal to 50% of the maximum shear modulus $G_0$.

The over consolidation ratio, OCR, is not accounted for in Zhang's model. However, some researchers (e.g. *Vucetic Dobry 1991, Kokusho 1982*) have shown OCR has only a small effect on the shape of the modulus reduction curve. Experience at NGI from working with the Darendeli (2001) model show that the effect of overburden stress and OCR counteract such that modulus reduction curves for shallow and deeper soil layers become relatively similar if other parameters are similar. In the *Darendeli (2001)* model the damping factor also increases with increasing loading frequency. Thus, the loading frequency must be determined carefully to compute the damping, making the Darendeli formulation requiring more input from the user.

Therefor to avoid the issue of the frequency dependency in Darendeli's model it was decided to adopt the modulus reduction and curves based on Zhang et. al. (2005) in the project. For critical applications the resulting shear modulus reduction and damping curves should be verified with cyclic lab tests on site specific soils.

One aspect not accounted for in the above empirical models for shear modulus reduction and damping is the effect of a so-called average stress, which is described in the following sections.

# A3 NGIs APPROACH TO CYCLIC LOADING

The NGIs approach to cyclic loading (is described in many publications, see e.g. *Andersen 2015*) can be considered an advanced version of the equivalent linear approach described above, where the effect of both cyclic stress and average stress in the soil are considered for evaluating both cyclic strains and also permanent strains. *Figure A3.1* visualizes how a soil element is subjected to cyclic stress beneath the gray box representing an individual sleeper or the embankment (man-made) resting on top of natural soil. There is an average shear stress component due to the masses in the system, the weight of the train, the weight of track and sleepers, and the weight of the embankment etc. Depending on the location of the soil element with respect to the sleeper/embankment it will be subject to different "modes" of cyclic behavior. By modes we refer to how cyclic testing is performed in the laboratory. Advanced tests are usually triaxial test (compression or extension tests) or DSS (" direct simple shear" tests). As shown in *Figure A3.2*, the passing of the train over point will give rise to both an average displacement (approximately shown with the red line) and cyclic displacement.

In addition, traffic load (road and rail) causes cyclic stresses with rotation of principle stresses in the embankment and soil materials (e.g., *Powrie 2007, Xu 2018*), which induces more volumetric strain in drained/dry materials or pore pressure build up in undrained materials (such as clay and silt, and possibly lime cement). The closer to the track the larger the rotation of principal stress. For soils larger depths the weight become the dominating load and the stress rotation is less. Thus, for evaluating cyclic behavior of materials such as the ballast and the embankment, laboratory tests with rotation of stress such as direct simple shear or DSS may be more suitable. For the soils at larger depths triaxial tests (cyclic compression or extension) are more suitable.

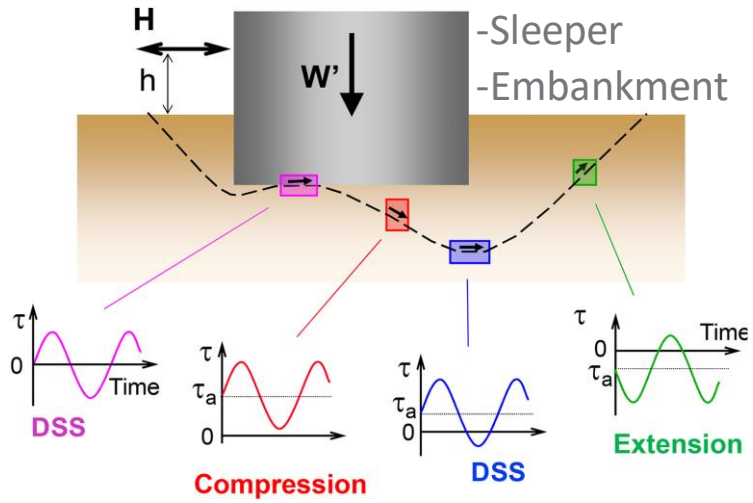


**Figure A3.1** Conceptual visualization of the behavior of soil elements beneath a foundation. This can also be considered on different scales. The gray box could e.g., represent an individual sleeper beneath the track or the embankment resting on natural ground beneath.

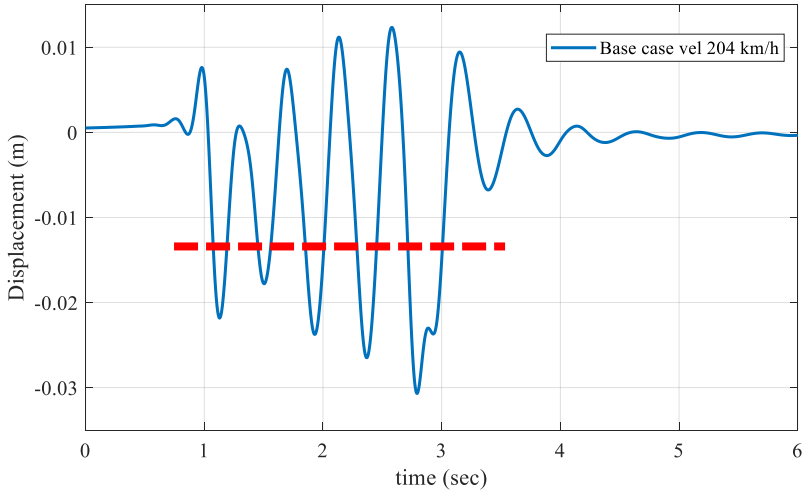


**Figure A3.2** Example of cyclic displacement beneath train track. Red line indicating an approximate average displacement.

Typical soil behaviour subjected to monotonic or cyclic shear stresses are shown in *Figure A3.3.a*. *Figure A3.3.b* shows how cyclic and average parameters (shear stress $\tau_{cy}, \tau_a$ , pore pressure, $u_p$ and shear strain, $\gamma_{cy}, \gamma_a$) vary with time. The cyclic and average shear stresses cause an increase in pore pressure and shear strain with each load cycle. *Figure A3.4* shows further how the inclination of the shear stress-strain loop decreases with the number of load cycles, i.e., the cyclic shear stiffness (shear modulus) decreases with number of load cycles. The stiffness reduction is mainly related to an increase in pore pressure but also other effect such as change in grain contacts etc. The table given in *Figure A3.4* show how the ratio between cyclic and average shear stress is important for the cyclic soil behavior. The smaller the cyclic shear stress $\tau_{cy}$ is relative to average shear stress $\tau_a$, the larger number of cycles, N, are needed for developing permanent pore pressure, $u_p$ and accumulating shear strain.

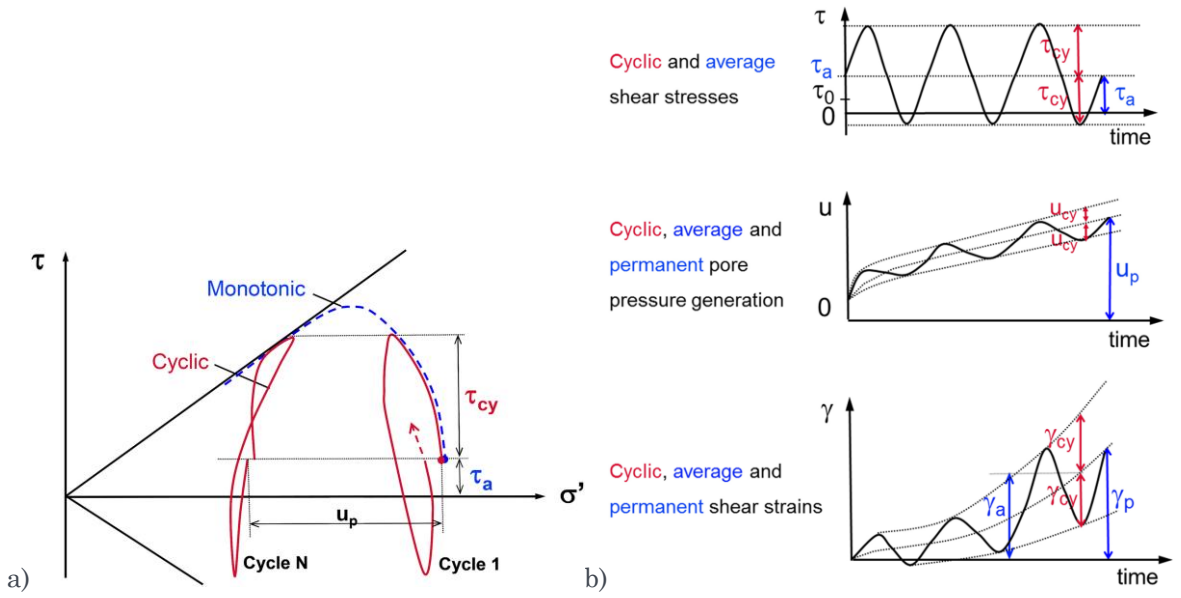


**Figure A.3.3** a) stress path plot showing a monotonic and cyclic shear stress test. b) Cyclic and average parameters (shear stress, pore pressure and shear strain)

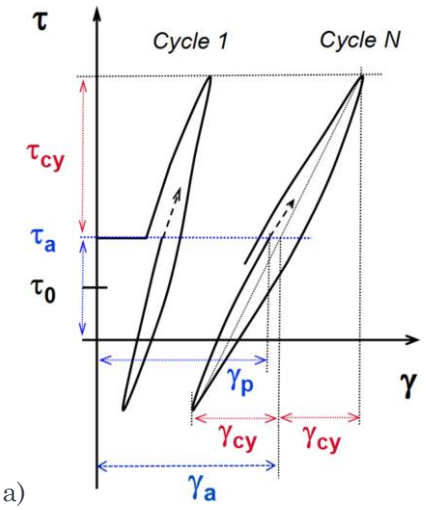


a)

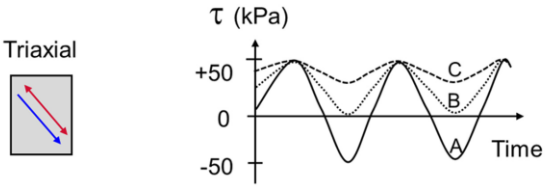


b)

| Test | $\tau_{max}$ | $\tau_a$ | $\tau_{cy}$ | Result |
|---|---|---|---|---|
| A | 50 | 0 | 50 | Failure ($\gamma$=15%) 10 cycles |
| B | 50 | 25 | 25 | $\gamma_p$=0.8%, $\gamma_{cy}$=0.3% 2500 cycles |
| C | 50 | 42.5 | 7.5 | $\gamma_p$=0.03%, $\gamma_{cy}$=0.02% 2500 cycles |

**Figure A3.4** Effect of number of cycles and ratio between average shear stress and cyclic shear stress**.**

# A4 CYCLIC BEHAVIOR OF DENSE SAND

An important aspect of the cyclic soil behaviour is the effect of an average (or static) shear stress on the behaviour, as shown with the example in *Figure A3.* The effect of an average stress on the cyclic stress strain curves (and modulus reduction) are relatively well understood (Andersen 2015). However, the effect of average stress on the soil damping behaviour has not been investigated very much. Some initial findings are given in Løvholt et al. (2017) indicating that material damping may increase with increasing average shear stress. Below we see that the average stress has stabilizing effect on undrained dense sand (like a pretensioning) which also change the damping considerably.

*Figure A4.1* and Figure *A4.2* show the effect of increasing average shear stress and increasing the cyclic shear stress on the stress-strain response for a dense sand in cyclic DSS tests (performed at NGI) with a static vertical pressure of 200 kPa. The results are presented in form of modulus reduction and damping curves (MRD). Typical curves from the literature are also shown with thick dashed lines based on *Darendeli (2001).*

Figure A4.1 shows how the response (stiffness and damping) for a cyclic shear stress of 120 kPa changes when increasing the average shear stress from 0 to 60 and 120 kPa. The normalized secant stiffness increases from 0.01 to 0.2. The average shear stress has a "stiffening" and a "stabilizing" effects on the material, i.e., the stiffness increases with number of cycles. This is thought to be related that reversal of shear stress is reduced with increasing average shear stress. The same effect is also seen for the tests with cyclic shear stress, $t_{cy}$ of 60 kPa and average shear stress, $t_a$ increases from 0 to 60 kPa.

Figure A4.2 shows the results of three test with different cyclic shear stress amplitude. Typically, the shear modulus and damping variation with shear strain is shown for an equal number of cycles, e.g., N=1 or N=10. For the shear modulus of the dense sand this would become a smooth curve not very different from the curve based on *Darendeli (2001*). Even though the induvial soil element subjected to approximately a constant cyclic stress amplitude would follow a slightly different path than given by the Darendeli curve, it seems rational to use shear modulus reduction curves for accounting for soil nonlinearity with increasing loading/straining.

However, a damping curve for the dense sand for N=1 or N=10 would deviate considerably from the damping curve from damping curve based on *Darendeli (2001)* shown with dashed violet curve in *Figure A4.1* and *Figure A4.2*.

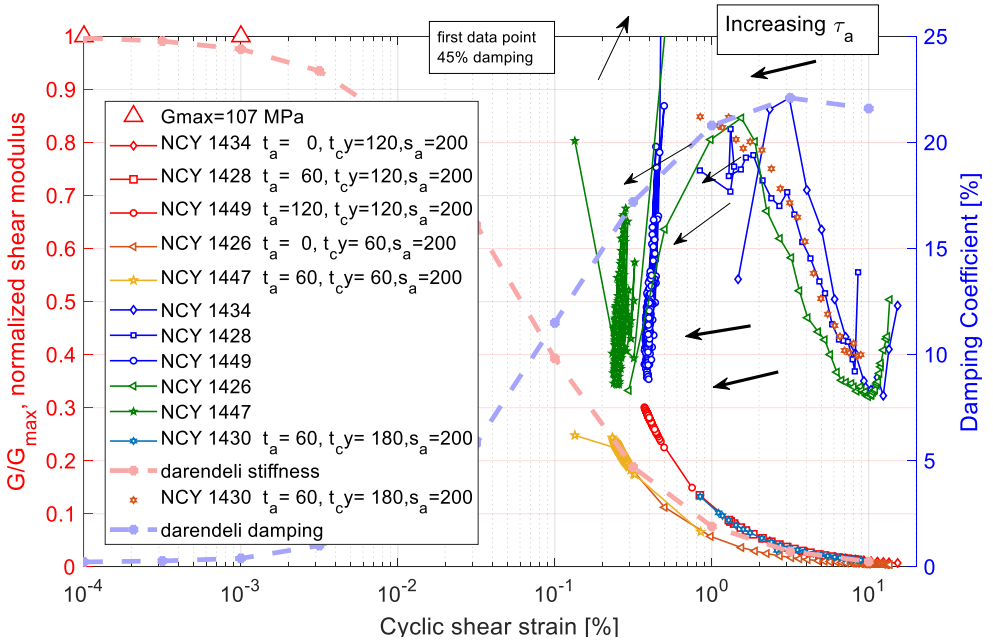


**Figure A4.1** Modulus reduction and damping curves for dense sand based on cyclic DSS tests. An average shear stress imposed on the cyclic loading. Red and yellow curves show stiffness, blue and green curves show damping.

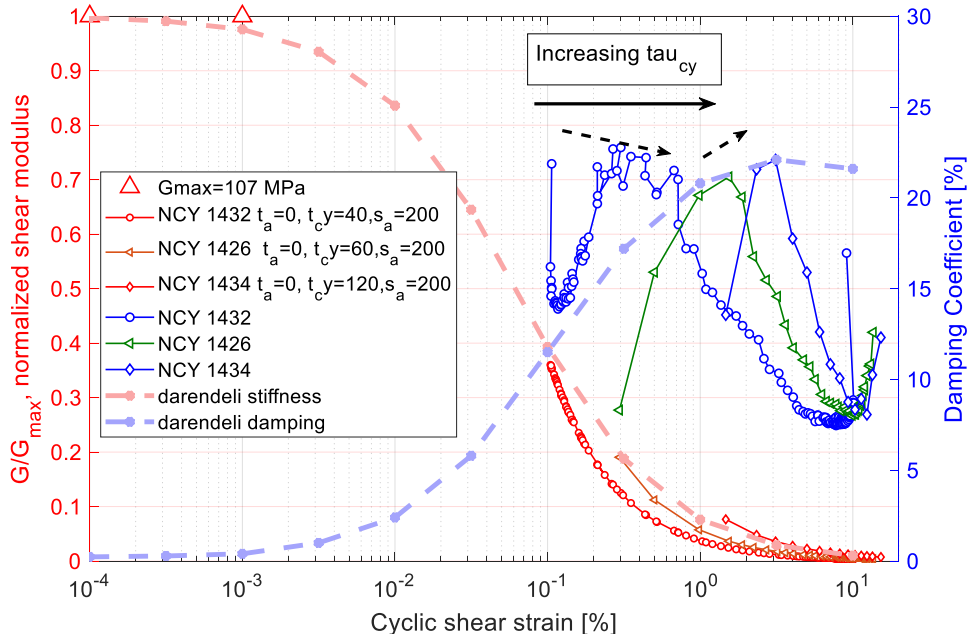


**Figure A4.2** Modulus reduction and damping curves for dense sand based on cyclic DSS tests

# A5 EFFECT OF NON-PLASTIC FINES CONTENTS

Some lab-test at NGI (Figure A5.1) on a sand with non-plastic fines have shown unusually low material damping in the intermediate strain range (0.01% to 0.5%) compared to the damping curves in the literature (*Darendeli 2001, Zhang 2005,* and *Seed & Idriss, 1970*). The low damping is believed to be due to the 10% non-plastic fines content of the sand.

The effect of fines content on the shear modulus and the damping factor of sand has been studied by e.g., *Wichtmann et. al. (2015*), who observed a factor of 6 lower damping at confining pressures of 50 kPa and factor of 1.5 at 400 kPa for a sand with about 10% fines content. The grain size distributions tested by Wichtmann et al. is similar to sand as seen in *Figure A5.2* and *Figure A5.4*. The NGI lab test were performed at 340 kPa and suggest a factor of 3-4 lower than the damping given by Darendeli (2001). The lower damping caused by increasing fines content is also observed to some extent for Doggerbank sand (*Blaker & Andersen 2019*).

*Whichtmann et. al. (2013*) suggests a micromechanical explanation for the lower damping with increasing fines content. The smaller silt grains will act as a kind of lubricant (or "roller bearing") for the larger sand grains. Rolling of grains involves a smaller dissipation of energy than the sliding mechanism, i.e., damping ratio decreases. Similar observations of the lubricant effect of smaller grains on larger grains have been observed in numerical simulation with the DEM method (de *Frias Lopez, 2020*). The smaller grains work as roller bearings for the larger grains, resulting in both lower stiffness and damping of the material.

The above observations suggest it is important to have information about the grain size distribution for non-cohesive materials.

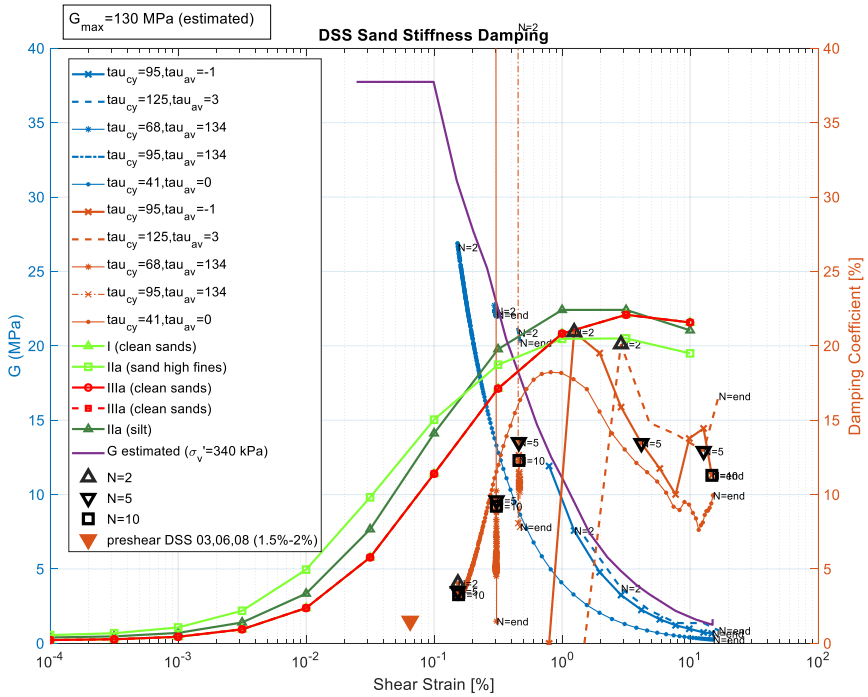


**Figure A5.1** Stiffness and damping curves for sand based on lab tests (*NGI, 2020*) and *Darendeli (2001*)**.**

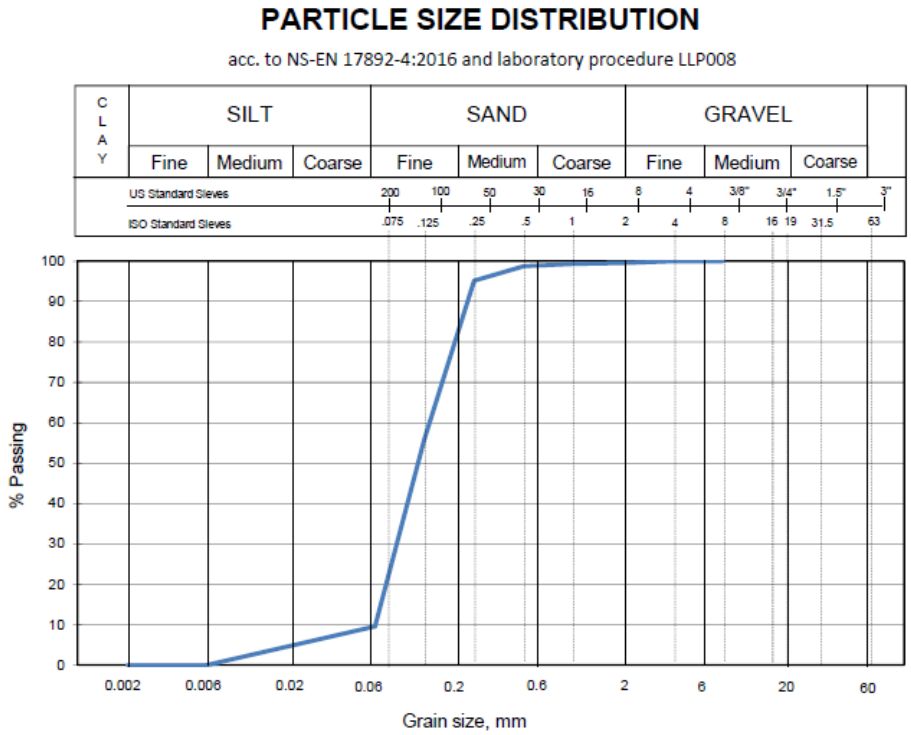


**Figure A.5.2** Grain size distribution of sand with about 10% non-plastic fines.

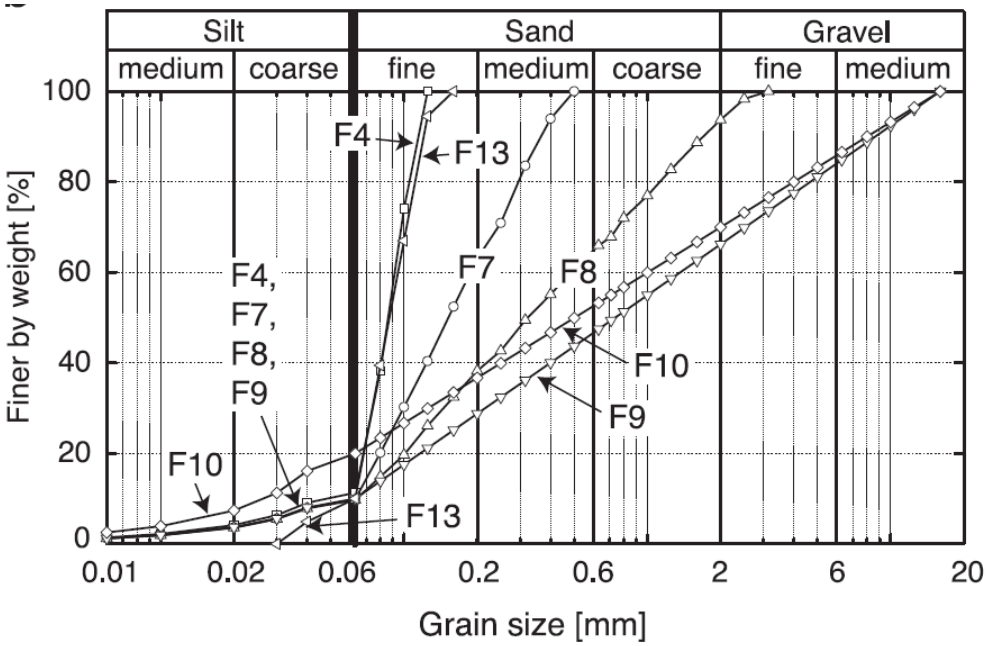


**FigureA.5.3** Grain size distribution in *Wichtman et. al. (2015).* Curve F7 is fairly similar to Batch A.

# A6 RATE EFFECTS ON STIFFNESS, STRENGTH AND DAMPING

It is well known that stress-strain-pore pressure response of clayey soils are strain rate dependent (e.g. *Coelho/Dijkstra, Nallathamby, Lunne Andersen, Lefebvre Pendler, Shibuya/Tatsuoka*).

The strain rates induced by the train loading evaluated in simplified manner as follows. Considering under normal operation large non-linearities should be avoided in the railway embankment and foundation soil, therefore shear strains much larger than 0.1% should likely be avoided. Based on this strain an estimate of shear strain rate is of the order of 0.1%/s assuming the response giving the largest strains has a 1 Hz vibration frequency. This shear strain rate corresponds to 6%/min or 360%/hour. For the Ledsgård case the strain level in the soft clay was estimated to an order of magnitude larger (~1%) and thus also strain rate also order of magnitude larger. It is important to be aware of the potential effect of strain rates when planning and interpreting field and laboratory tests for evaluating input parameters for numerical analysis. Below follows some observations based on the literature.

The undrained strength of clay increases with factor on the order of 20% per log-cycle strain rate increase (e.g. Lunne and Andersen 2007). However, the effect of strain rate on shear modulus is not conclusive as shown in *Figure A6.1. Brown and Robinson (2013*) observe a 10% reduction of shear modulus per log-cycle increase in shear strain rate for a reconstituted Speswhite Kaolin clay (which agrees with observations by Sorensen et. al. (2010). They suggest the test with low strain rate allows for creep/bonding effects ("ageing") which increases the stiffness with time.

On the other hand, based on combination of resonant column, monotonic and cyclic torsional shear tests, D'Onofrio et. al. shows the opposite trend with shear modulus increasing with about 5 % for each log-cycle increase in shear strain rate for a natural over-consolidated stiff clay. They also report tests by other researchers on natural silty clay and compacted silty sand showing similar increase in shear modulus with strain rate.

*D'Onofrio et. al. (1999)* also discusses the effect of strain rate (*Figure A6.2*) on the small strain damping factor obtained in laboratory tests. For an intermediate strain rate the damping has a minimum value and then increases for lower and higher strain rates. The higher damping for very small strain rates is attributed to creep during the test. For strain rates relevant for train vibration (1%/min-10%/min) the damping factor seem to be of similar magnitude as other researchers report based on e.g., Resonant column tests.

A database of cyclic direct shear tests performed on quick clay at NGI indicate on the order 50% less pore pressure build up when reducing the load period from 10 s to 1s for the same number of load cycles. This seem to be consistent with *Brown and Robinsons' (2013*) observation that the threshold strain for when pore pressure builds up due to cyclic loading (as described in *Section A3*), also increases with strain rate. For Kaolin they suggest an elastic threshold shear strain of $\gamma_{el} = 0.003\dot{\gamma}^{0.2}$, where $\dot{\gamma}$ is the shear strain rate.

The above observations suggest that undrained shear strength increases, and pore pressure build up decreases with increasing strain rate. However, regarding the effect of strain rate on shear modulus and damping there are not many studies and would merit further research.

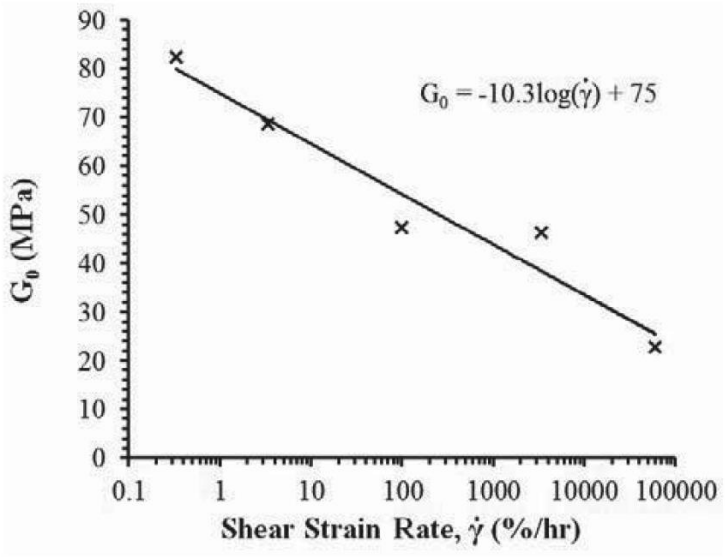


a)

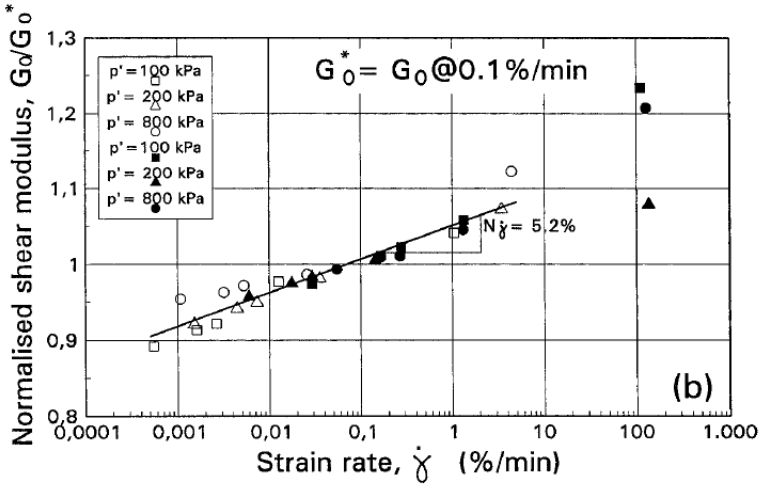


b)

**Figure A6.1** Opposite effect of shear strain rate on shear modulus, a) from Brown and Robinson, and b) From D'Onofrio et. Al (1999).

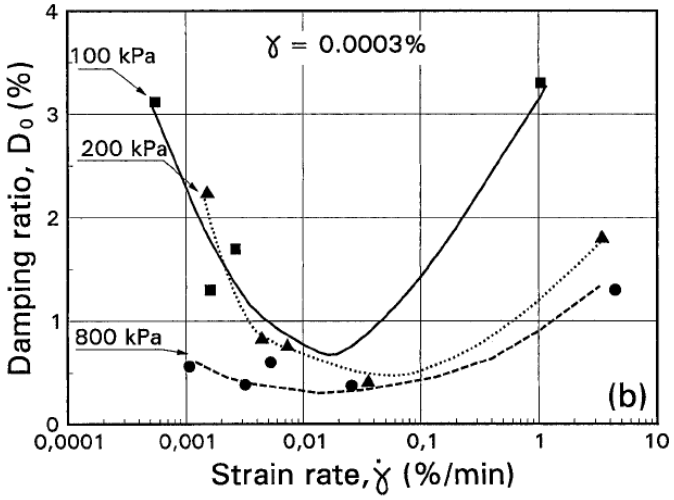


**Figure A.4.2** Effect of strain rate on damping factor

# A7 SOME OBSERVATIONS ON THE STIFFNESS OF THE GYTTJA LAYER FROM LEDSGÅRD

NGI performed static and cyclic triaxial tests and bender element tests to characterize the gyttja layer in Ledsgård. The main part of this report (also *NGI 1998*) showed a spread in the normalized shear modulus reduction curves. The initial shear modulus values for Test 7 and 8 (on tubes 441 and 112) show approximately 70% higher initial shear modulus value for test 7 compared to test 8. However, the secant shear modulus of the two samples are very similar (as show in *Figure A7.1* below). Thus the spread in the normalized curves are due to the different initial shear modulus of the two samples. Similar observations have also been made for other clays tested at NGI. A larger a spread in the initial shear modulus then in the secant shear modulus has also been observed in tests on other clays at NGI. This indicates the importance of using site specific laboratory test results and carefully evaluating the initial shear modulus and corresponding shear modulus reduction curve of the different soil layers.

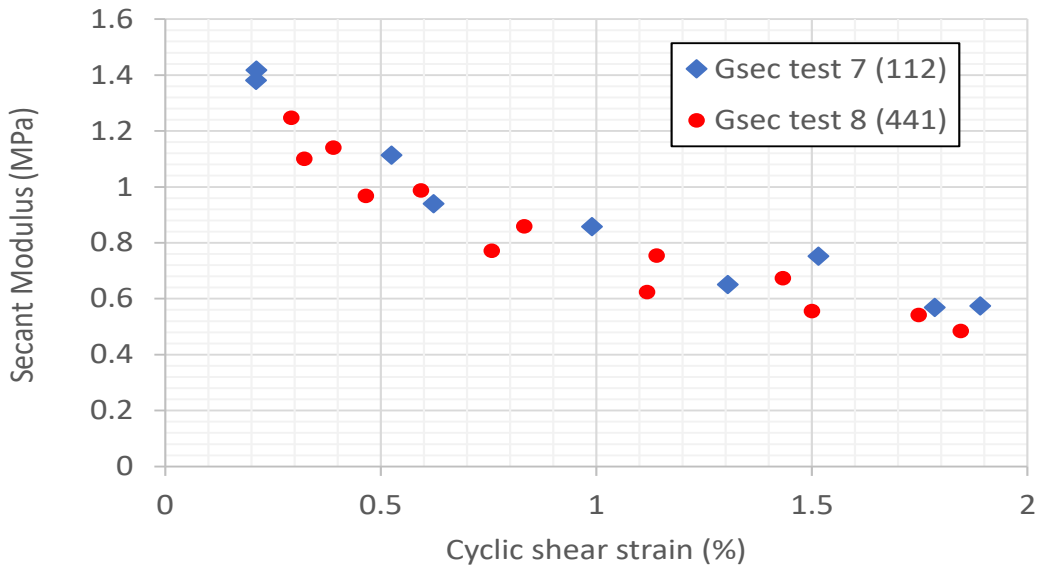


**Figure A7.1** Secant shear modulus for two samples from Ledsgård (NGI, 1998)

In the numerical modelling of Ledsgård with the base models and Vibtrain, the shear strains reach up to 0.3% in the embankment and upper clay layers. The tests on the Ledsgård clay (NGI, 1998) give larger secant modulus and lower damping than e.g. the empirical model from *Zhang et al (2005)*. There may be a few potential causes of this. The fitting parameters in most empirical models are not based on laboratory tests on Scandinavian soils and thus may not be fully captured their cyclic behaviour. Furthermore, an average stress was applied in the tests performed on Ledsgård clay (*NGI, 1998*) and thus the "stabilizing effect" described above may contributed to a larger stiffness and smaller damping than the empirical curves. In addition principal stress rotation, which is accounted for in the modulus reduction curves by Zhang et. al, but not in the triaxial tests of the Ledsgård clay may also contribute to the difference.

# A8 GRAVEL AND BALLAST MATERIALS

The current section focuses on cyclic (dynamic) shear and bulk moduli, and also damping, of ballast and underlying coarse granular materials (gravels) for use in numerical modelling train induced vibrations. The permanent straining/compaction of these materials due to cyclic loading (e.g. *Suiker et al. 2005 , Indraratna 2005*) is out of scope here. However, it is expected the choice of cyclic/dynamic stiffness and damping is important for evaluating train induced cyclic stresses that contribute to the long term degradation of these materials.

Train induced stress levels in the ballast and subgrade depend on the axle load and vary with depth in the ballast and subgrade. Typical peak stress levels in the ballast under a railway sleeper is on the order of 150 kPa (vertical) and 50 kPa (horizontal). The stress increase due to the train load diminishes quickly with distance from the point of application on the rail. Stresses return to in-situ "at rest" values some 20 cm to the side of the load (*Lenart, S. et.al. 2014*). Principal stress rotation is also important for the cyclic behavior, specially the long term permanent deformations. Gräbe and Clayton (2014) report principal stress rotation angles (deviation first principal stress from vertical) of less than ±45 degrees for horizontal to vertical stress ratio, K0, of 0.5-1.0 and up to 90 degrees for higher K0 values. Powrie et. al (2007) report ±20 degree rotation for K0 of 0.5. Ionescu (2004, sited by Guo 2010) have shown the field measured K0 values increase with horizontal stress, from 0.2 for a horizontal stress below 100 kPa and reaching 0.4 for horizontal stress of 400 kPa. Thus, the principal stress rotation are often between around ± 20 degrees. Further study with field measurements combined with modern constitutive models to accounting for increase in stiffness with increasing confining pressure can give more detailed understanding of how cyclic stiffness and damping varies for different loading conditions.

One issue with evaluation of dynamic properties of coarse geomaterials is the large grain size of gravels, which require large laboratory equipment, minimum sample size should be 5 times the largest grain size according to the Eurepean standard *EN 13286-7*. Thus commonly tested sample diameters are on the order of 30 cm.

*Rollins (1998, 2020),* often referred to, have proposed equations for modulus reduction and damping curves based on a database of some 17 plus studies with large scale diameter triaxial and torsional shear test performed on gravels and rock fill materials with loading frequencies up to 0.2 Hz. *Rollins et. al. (2020*) writes there is little difference in shear modulus reduction curves ($G/G_0$) from cyclic triaxial tests (CTX) and cyclic torsional simple shear (CTSS), with the latter type of test have principal stress rotation. While principal stress ratio has a large effect on the cumulative deformation of geomaterials (see e.g. Gräbe and Clayton 2014), the cyclic stiffness (and possibly also damping) seems to be less dependent on the principal stress rotation. However, interpretation of shear modulus reduction and damping from triaxial test may be more complicated due to increase in confining pressure for increasing deviator stress, as shown in next section.

*Yasuda and Matsumoto (1994*) compared monotonic and cyclic deformation characteristics of rockfill materials with field measurements and concluded shear wave speeds measured in the field compared reasonably well with large scale laboratory triaxial tests.

The dependency on rate of loading for clay and to some extent sand materials are well documented (*D'Onofrio, 1999, Stokoe, 1995, Shibuya 1995, Darendeli 2001*) as described in a previous section. There are less studies on the effect of loading frequency on the stiffness and damping of coarse materials. Araei et. al. have showed the frequency is importance for damping and to some extent also for the stiffness for gravel and rock fill materials.

## A8.1 EARLIER TEST PERFORMED AT NGI

Bellow follows a summary of earlier tests performed by NGI and conclusions important with respect railway embankment and ballast performance.

The data presented below for six different materials shown in *Table A8.1* are from large scale vacuum static and cyclic triaxial tests performed by NGI in 1994-1995 for "Kvalitet av pukk og grusindustriens produkter, KPG", now part of "Norsk Bergindustri". Stiffness in terms of Young's modulus and shear modulus are given first and then some few reprocessed data for establishing modulus reduction and damping curves are presented.

These triaxial test samples had extra-large dimensions with a diameter of 625 mm and a height of 1250 mm. Due to the size, the tests were performed without a pressure chamber, and a "suction" (under-pressure) was applied inside the sample so that the lateral stress (enveloping pressure) was approximately 80 kPa in all experiments. Each triaxial test was performed in 3 phases with different water content (1: Natural, 2: Almost water saturated and 3: Drained condition). The results for rock and gravel with natural water content are summarized in Table A8.1.

The loading in each phase was applied in stages with 1000 cycles in each stage and with the same cyclic deviator stress amplitude. The deviator stress amplitude was increased with 20 kPa from one stage to the next starting at 20 kPa and ending at 420 kPa or higher for some stronger materials. Each load cycle consisted of sinusoidal impulse of 0.1 s duration, corresponding to a 10 Hz loading.

**Table A8.1** Measured cyclic E-moduli for different deviator stress at natural water content (phase 1). Radial pressure is constant 80 kPa in all experiments.

| Type of material | Particle size (mm) | Place | E q=120 kPa (MPa) | E q=220 kPa (MPa) | E q=320 kPa (MPa) |
|---|---|---|---|---|---|
| Gravel with sand hump (A) | | Hovinmoen gravel quarry | 305 | 270 | 385 |
| Gravel without sand hump (D) | 0-32 | | 270 | 360 | 392 |
| Crushed stone (B) | 0-32 | Åndalen crushing plant (class 2 stone) | 259 | 418 | 572 |
| Crushed stone (E) | 25-50 | | 413 | 514 | 648 |
| Crushed stone (F) | 0-120 | | 415 | 475 | 574 |
| Crushed stone (C) | 0-120 w/some fines | Garderfjell, lower quality stone (class 3-4) | 335 | 572 | Na |

The cyclic shear and bulk moduli were modelled based on the test results with the equations from *Dawson (1994)*

$$G(p) = G_a \left(\frac{p}{p_a}\right)^{1-n}$$

$$K(p) = \frac{K_1\left(\frac{p}{p_a}\right)^{1-n}}{1-\beta\left(\frac{q}{p}\right)^2}, \qquad \text{where } \beta = \frac{K_1(1-n)}{6G_a}$$

$G_a$ and $K_1$ are reference moduli given together with the fitting parameter $n$ in Table A8.1. The other parameters in the equations is the mean effective pressure $p$, the deviatoric stress, $q$ and a reference pressure, $p_a$, of 100 kPa.

The Poisson's value are reported to vary between 0.15 -0.45, which larger values for highly mobilized material.

The Dawson's formulation given above are only one of many equations for modelling the shear and bulk modulus of granular materials. Lekarp et. al. gives a good overview of several formulations for modulus and Poisson's ratio and important parameters affecting the behaviour of coarse materials.

**Table A8.1** Parameters for Dawson's model of for cyclic moduli based on large scale triaxal tests.

| **Materiale** | **$G_a$ [MPa]** | **n** | **$K_1$ [MPa]** |
|---|---|---|---|
| Gravel Hovinmoen 0-32 mm, 1994 | 116 | 0.83 | 193 |
| Gravel Hovinmoen 0-32 mm, 1995 | 98 | 0.59 | 223 |
| Garderfjell 0-120 mm | 99 | 0.0 | 85 |
| Crushed stone Åndalen 25-50 mm | 109 | 0.0 | 98 |
| Crushed stone Åndalen 20-120 mm | 159 | 0.3 | 168 |
| Crushed stone Åndalen 0-120 mm | 141 | 0.25 | 144 |

## A8.2 MODULUS REDUCTION AND DAMPING

Dynamic stiffness and damping values for very coarse materials such as ballast and gravel presented above are much less common in the literature than for soils with smaller grain sizes. With the purpose of understanding better how moduli and specifically the damping for these coarse materials tested in triaxial stress condition, older test data files were recovered and for some of the cyclic tests data have been reprocessed to determine the shear modulus reduction and damping curves shown in *Figure A8.1, A8.2 and A8.3* or Hovinmoen gravel 0-32 mm and the Åndalen 0-120 mm crushed stone, respectively.

The results for Hovinmoen show the secant shear moduli increase from 75 MPa to 100 MPa with increasing deviator stress due to an increase in mean pressure (from 88 kPa to 165 kPa), while the damping decreases from a high value of some 15% at small strains of 0.03%. The results for the Åndalen crushed stone show a similar trend to the Hovinmoen, of increasing stiffness and reduction of damping with increasing deviator stress (and mean pressure).

The stress strain loops have the shape of a concave lens for lower deviatoric stress however at higher deviator stress, the stress strain loops become banana shaped as shown in *Figure A8.* This also the cause of the large reduction in damping with increasing strain. The area within the banana-shaped loop is relatively much smaller than the oval shape for lower deviator stress.

The large damping (of about 15%) observed at lower deviator stresses may be due to the high loading frequency of 10 Hz, similar to the observations by *Araei et. al. (2012),* who report very large damping values of up to 40% for a cyclic shear strain of 0.01% and loading frequency of 10 Hz for different lime stone rock fill materials. Such large damping values have not been reported by other investigators (see refs in *Rollins 2020* and *Araei 2012*). Further evaluation of the large scale test data is necessary to interpret appropriate damping values for use in numerical analysis.

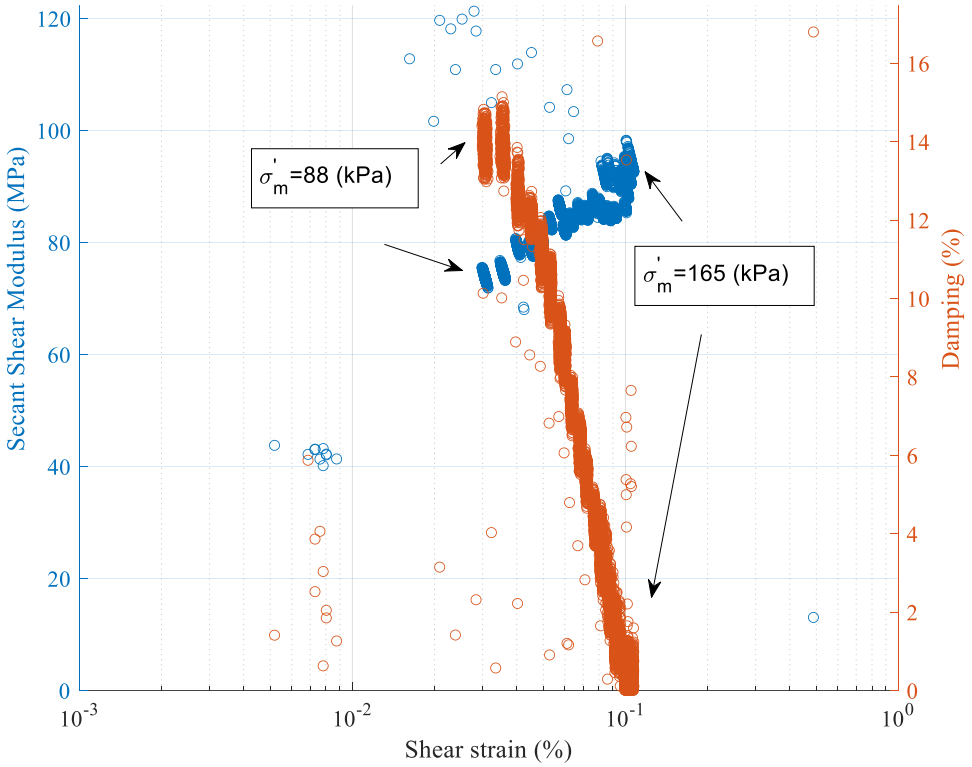


**Figure A8.1** Shear modulus reduction and damping curves for Hovinmoen gravel 0-32 mm. Secant shear modulus shown with blue rings and damping coefficients with red rings.

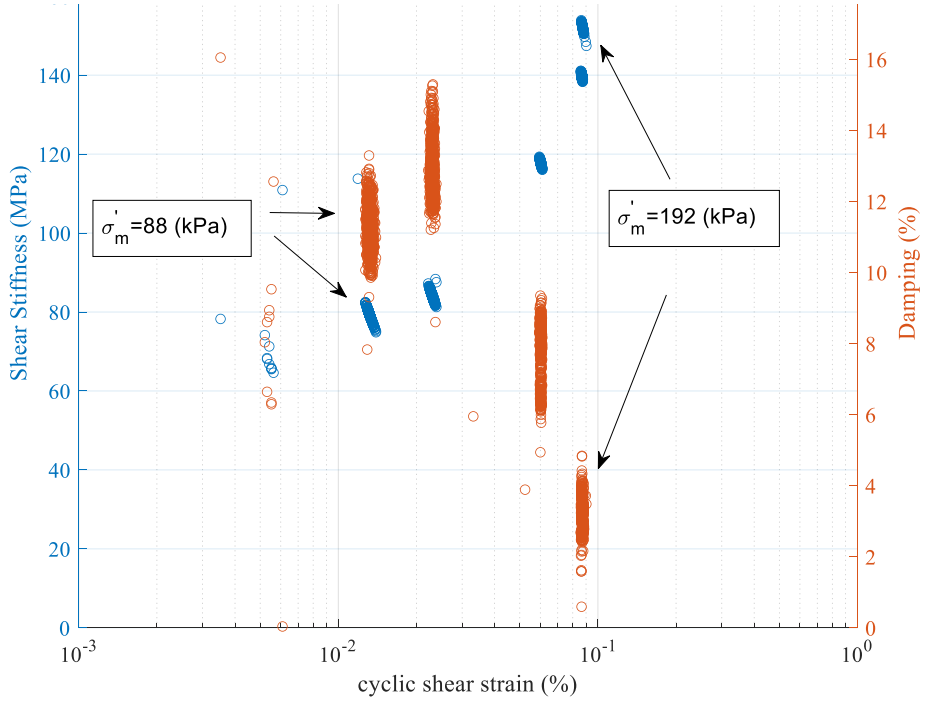


**Figure A8.2** Shear modulus reduction and damping curves for Åndalen 0-120 mm crushed stone. Secant shear modulus shown with blue rings and damping coefficient with red rings.

The material behaviour shown in the three figures below, as interpreted from the large scale triaxial tests, indicate the response of the material will be dependent to some extent on the vertical load magnitude exerted by the train axle on the track, ballast and fill material. Thus, for large axle loads the possible stiffening of the ballast may be beneficial and the response may be less than if stiffness did not increase. Further evaluation of the ballast response with FE-models are needed to link the ballast properties to dynamic performance under more realistic stress conditions. E.g., if the ballast horizontal confinement in the embankment is likely somewhere in between triaxial and oedometer conditions. In addition, the train loading induced principal stress rotation.

*Dyvik and Kaynia (2018)* presents modulus and reduction on some results also performed at NGI in a similar setup as described above, but with lower confining pressures. The results presented here are similar to the results presented by Dyvik and Kaynia.

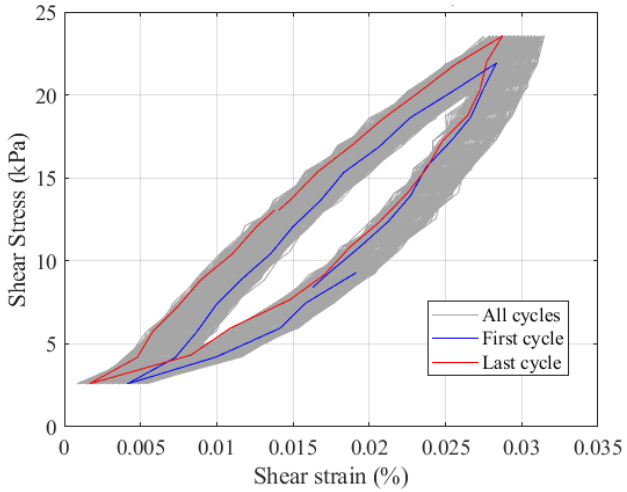


**Figure A8.3** Åndalen 0-120 mm shear stress strain loops for deviator stress of 40 kPa and mean stress at peak shear stress is 88 kPa.

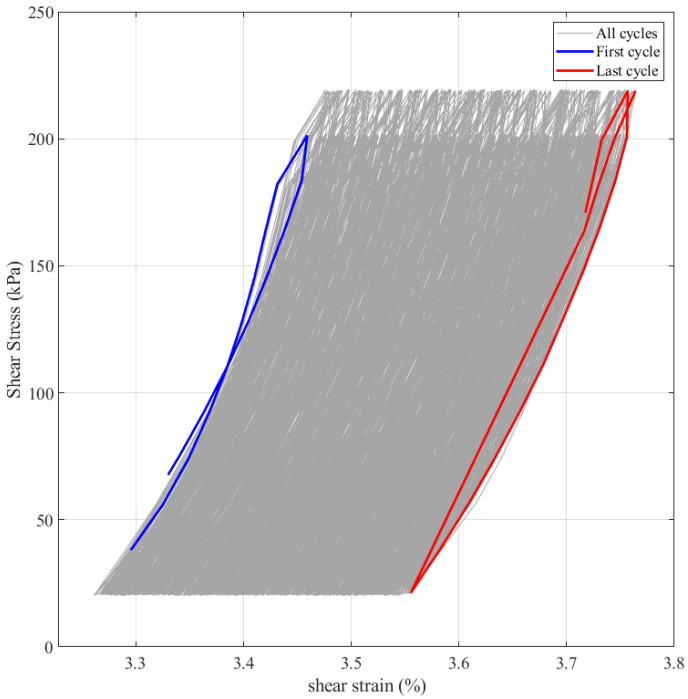


**Figure A8.4** Hovinmoen 0-32 mm shear stress strain loops for deviator stress of 440 kPa and mean stress at peak shear stress is 230 kPa.

## A8.3 SUMMARY GRAVEL AND BALLAST MATERIAL

In general, the lowest E-moduli are obtained for weak rock material, sharp-edged stones (angular) and well-sorted (poorly graded material), and reversely, the highest E-moduli are observed for good quality stone material, rounded stone and well-graded stone material.

Cyclic E-moduli are higher than static E-moduli. Recommended values for input for modelling of train vibrations should therefore be based on the cyclic (vacuum) tests. High estimate values should be chosen from well-graded material with good stone quality, while low estimate value should be chosen from well-sorted material with poor stone quality.

The vacuum triax tests are limited in number and the range of modules may be greater than that recommended. Stone strength, grain shape, degree of sorting and initial packing can have a big impact. The empirical formula for the cyclic shear modulus gives a good fit for well compacted dense materials.

The experiments at NGI, in agreement with reviewed more recent literature (e.g. Suiker et. al) have shown that the cyclic E-modulus of the different materials in is virtually independent of the number of cycles. Up to 1000 cycles were run for each voltage level, and even with a high degree of mobilization (large shear stresses), the module remained almost constant. This also justifies that the expression of the cyclic shear modulus is independent of the number of cycles.

Very large damping values have been measured for low strains. This may be due to high frequency impulse loading used in the test. Further interpretation of test results are necessary to conclude on this issue and how to determine appropriate damping values for use in numerical analysis.

# A9 CYCLIC LOADING OF LIME-CEMENT MIXED SOIL

Cyclic loading of lime cement strengthened clay material have almost exclusively been done on materials outside of Scandinavia. Resonant column experiments on stabilized clay show that stiffness and damping are dependent on stress and strain levels and vary with different amounts of added lime cement and chemical properties of the clay (*Tsai et al, 2012*). With increasing number of load cycles, the earth can be degraded (e.g. *Fonseca et al, 2013*). Wave propagation in piled soil can give vibration patterns similar to bending modes which is a possible breaking mode in KC columns (*Larsson et al, 2008*). Field measurements in combination with numerical calculations provide a basis for determining how stabilized soil in the field is affected by cyclic train loads with many load cycles, how great the stresses are and what the deformations look like.

# A10 REFERENCES

AINGARAN S. (2014) Experimental investigation of static and cyclic behaviour of scaled railway ballast and the effect of stress reversal PhD thesis University of Southampton; 2014.

ARAEI, A. A., RAZEGHI, H. R., TABATABAEI, S. H., & GHALANDARZADEH, A. (2012). Loading frequency effect on stiffness, damping and cyclic strength of modeled rockfill materials. Soil Dynamics and Earthquake Engineering, 33, 1–18. https://doi.org/10.1016/j.soildyn.2011.05.009

BIAN, X., JIANG, J., JIN, W., SUN, D., LI, W., AND LI, X. (2016). Cyclic and Postcyclic Triaxial Testing of Ballast and Subballast. Journal of Materials in Civil Engineering, 28: 4016032. American Society of Civil Engineers (ASCE). doi:10.1061/(asce)mt.1943-5533.0001523.

COELHO, B. Z., DIJKSTRA, J., & KARSTUNEN, M. (2021). Viscoplastic cyclic degradation model for soft natural soils. Computers and Geotechnics, 135, 104176.

DARENDELI, M. B. 2001. "Development of a new family of normalized modulus reduction and material damping curves." PhD thesis, Dept. of Civil Engineering, Univ. of Texas at Austin.

DAWSON, A.R., CORREIA, A.G, JOUVE, P., PAUTE, J-L. AND GALJAARD, P.J (1994). Modeling resilient and permanent deflections in granular and soil pavement layers. Proc.4, Int. Conf on the Bearing Capasity of Roads and Airfields, Vol. 2, pp 847-861 Minnestota, USA

DE FRIAS LOPEZ, R. (2020). DEM Modelling of Unbound Granular Materials for Transport Infrastructures : On soil fabric and rockfill embankments. In TRITA-ABE-DLT (No.205; Number 205, p. 89). KTH, Soil and Rock Mechanics.

DYVIK, R., & KAYNIA, A. M. (2018). Large-Scale Triaxial Tests on Railway Embankment Material. In Railroad Ballast Testing and Properties (pp. 173–190). ASTM International. https://doi.org/10.1520/stp160520170031

GRÄBE, P. J., & CLAYTON, C. R. I. (2014). Effects of Principal Stress Rotation on Resilient Behavior in Rail Track Foundations. Journal of Geotechnical and Geoenvironmental Engineering, 140(2), 4013010. https://doi.org/10.1061/(asce)gt.1943-5606.0001023

GUO, P. (2010). Effect of density and compressibility on K 0 of cohesionless soils. Acta Geotechnica, 5, 225–238. https://doi.org/10.1007/s11440-010-0125-0

HARDIN, B.O. & DRNEVICH, V.P. (1972a). Shear modulus and damping in soils: design equations and curves. Journal of the Soil Mechanics and Foundations Division, ASCE, 98(SM7):667-692, 1972.

HARDIN, B.O. & DRNEVICH, V.P. (1972b). Shear modulus and damping in soils: measurement and parameter effects. Journal of the Soil Mechanics and Foundations Division, ASCE, 98(SM6):603-624, 1972.

INDRARATNA, B., LACKENBY, J., & CHRISTIE, D. (2005). Effect of confining pressure on the degradation of ballast under cyclic loading. Géotechnique, 55, 325–328. https://doi.org/10.1680/geot.2005.55.4.325

IONESCU, D. (2004) Evaluation of the engineering behaviour of railway ballast. Ph.D. thesis, University of Wollongong, p 435.

KISHIDA, T. (2017). Comparison and Correction of Modulus Reduction Models for Clays and Silts. Journal of Geotechnical and Geoenvironmental Engineering, 143(4), 4016110.

LEKARP, F., ISACSSON, U., & DAWSON, A. (2000). State of the Art.1emI: Resilient Response of Unbound Aggregates. Journal of Transportation Engineering, 126, 66–75. https://doi.org/10.1061/(asce)0733-947x(2000)126:1(66)

LENART, S., KOSEKI, J., MIYASHITA, Y., & SATO, T. (2014). Large-scale triaxial tests of dense gravel material at low confining pressures. Soils and Foundations, 54, 45–55. https://doi.org/10.1016/j.sandf.2013.12.005NGI, Soil behaviour. Laboratory test results. Ledsgård and Peppared at The West Coast Line. Project: High speed lines on soft ground. Report 515177-2, Rev 1. 22 June 1998.

NORÉN-COSGRIFF, K., DAHL, B. M., PARK, J., & KAYNIA, A. M. (2021). FE Modelling as a Design Tool for Mitigation Measures for Railway Vibrations. In Notes on Numerical Fluid Mechanics and Multidisciplinary Design (pp. 429–436). Springer International

ROBINSON S., BROWN M.J., Rate effects at varying strain levels in fine grained soils, Proceedings of the 18th International Conference on Soil Mechanics and Geotechnical Engineering, Paris 2013.

ROLLINS, K. M., SINGH, M., & ROY, J. (2020). Simplified Equations for Shear-Modulus Degradation and Damping of Gravels. Journal of Geotechnical and Geoenvironmental Engineering, 146(9), 4020076. https://doi.org/10.1061/(asce)gt.1943-5606.0002300

SENETAKIS, K., PAYAN, M., LI, H., & ZAMANIAN, M. (2021). Nonlinear stiffness and damping characteristics of gravelly crushed rock: Developing generic curves and attempting multi-scale insights. Transportation Geotechnics, 31, 100668. https://doi.org/10.1016/j.trgeo.2021.100668

SHIH, J.-Y., GROSSONI, I., & BEZIN, Y. (2019). Settlement analysis using a generic ballasted track simulation package. Transportation Geotechnics, 20, 100249. https://doi.org/10.1016/j.trgeo.2019.100249

SHI X. (2009) Prediction of permanent deformation in railway track PhD thesis University of Nottingham; 2009.

SORENSEN, K. K., BAUDET, B. A., & SIMPSON, B. (2010). Influence of strain rate and acceleration on the behaviour of reconstituted clays at small strains. Géotechnique, 60(10), 751–763.

SUIKER, A. S. J., SELIG, E. T., AND FRENKEL, R. (2005). Static and Cyclic Triaxial Testing of Ballast and Subballast. Journal of Geotechnical and Geoenvironmental Engineering, 131: 771–782. American Society of Civil Engineers (ASCE). doi:10.1061/(asce)1090-0241(2005)131:6(771).

WICHTMANN, T. & TRIANTAFYLLIDIS, T. (2013). Effect of Uniformity Coefficient on G/Gmax and Damping Ratio of Uniform to Well-Graded Quartz Sands Journal of Geotechnical and Geoenvironmental Engineering, American Society of Civil Engineers (ASCE), 2013, 139, 59-72

WICHTMANN, T., HERNÁNDEZ, M. A. N., & TRIANTAFYLLIDIS, T. (2015). On the influence of a non-cohesive fines content on small strain stiffness, modulus degradation and damping of quartz sand. Soil Dynamics and Earthquake Engineering, 69, 103–114.

YASUDA, N., & MATSUMOTO, N. (1994). Comparisons of deformation characteristics of rockfill materials using monotonic and cyclic loading laboratory tests and in situ tests. Canadian Geotechnical Journal, 31, 162–174. https://doi.org/10.1139/t94-022

ÅHNBERG & LARSON, 2011, Nedbrytning av odränerad skjuvhållfasthet i lera på grund av cyklisk belastning, SIG Varia 617. (Degradation of undrained shear strenght of clay caused by cyclic loading, in Swedish)

# Appendix B

## The base model program: input and output files - Ledsgård prior LCC

# DESIGN OF GROUND FOUNDATION FOR HIGH-SPEED RAILWAYS

## Input variables to the base model program

Case: **Ledsgård prior LCC reinforcement**

## A Design of railway

| **A1. Vechicle type** | | **Selected vechicle type** | | **Guideline** |
|---|---|---|---|---|
| A1.1 Vehicle type | VT= | X2000 | | |
| A1.3 Design train speed | $V_{STH}$= | 200 | km/h | |

| **A2. Track structure** | | **Selected track stucture** | | **Guideline** |
|---|---|---|---|---|
| A2.1 Rail type | RT= | 60E1 | | |
| A2.2 Rail pad | RP= | medium | | |
| A2.2 Track system | TS= | Concrete sleepers with ballast | | AMA DCH.311 |

| **A3. Track foundation** | | **Selected track foundation** | | **Guideline** |
|---|---|---|---|---|
| A3.1 Subballast | SB= | 800 mm | | AMA DCH.15 |
| A3.2 Frost insulation, thickness | SBf= | 100 | mm | Figure RA DCH.1/1 + AMA DCH.16 |
| A3.3 Subgrade | SG= | Crushed rock fill | | AMA CEB.321 |

| **A4. Embankment geometry** | | **Geometry** | | | **Guideline** | | | | | | |
|---|---|---|---|---|---|---|---|---|---|---|---|
| A4.1 Level of rail top | RÖK= | +5.772 | m.s.l. | | | | | | | | |
| A4.2 Level of ground surface | GS= | +5.000 | m.s.l. | | | | | | | | |
| A4.3 Slope of embankment | S: | 1: 1.5 | | | BVS 1585:005 | | | | | | |
| A4.4 Vegetation soil removal | VR= | 200 | mm | | | | | | | | |
| Height over GS | H= | 0.60 | m | | Width at top= | $W_T$= | 7.40 | m | $W_T/2$= | 3.70 | m |
| Thickness below GS | D= | 0.82 | m | | Width at GS= | $W_{GS}$= | 9.20 | m | $W_{GS}/2$= | 4.60 | m |
| Level of embankment bottom | EB= | +4.18 | m.s.l. | | Width at bottom= | $W_B$= | 11.66 | m | $W_B/2$= | 5.83 | m |

## B Ground conditions

| **B1 Ground & Material Models** | | | **Guideline** |
|---|---|---|---|
| B1.1 Ground model | GM | Layered half-space | Choose "fixed bottom" when frictional soil layer or bedrock is at depth less than 30m |
| B1.2 Material model | MM | Equivalent linear | Choose "Equivilent linear" to consider shear strain dependent stiffness and damping |
| B1.2.1 Strain reduction factor | $R_f$= | 0.65 | $\gamma_{eff}=R_f \cdot \gamma_{max}$, - a value of 0.65 is recommended |

| **B1 Soil geometry and properties** | | **B1 Soil layer 1** | | | **B2 Soil layer 1** | | | **B3 Soil layer 1** | | |
|---|---|---|---|---|---|---|---|---|---|---|
| B1.1 Soil type | | Layer #1 | Crust | | Layer #2 | Gyttja | | **Layer #3** | **Clay** | |
| B1.1 Levels | top | $L_{1t}$= | +5.00 | m.s.l. | $L_{2t}$= | +3.70 | m.s.l. | $L_{2t}$= | +0.20 | m.s.l. |
| | bottom | $L_{1t}$= | +3.70 | m.s.l. | $L_{2t}$= | +0.20 | m.s.l. | $L_{3t}$= | -45.00 | m.s.l. |
| | grund water table | GWT= | +3.70 | m.s.l. | | | | | | |
| B1.3 Total density | top | $\rho_{1t}$= | 1.80 | t/m$^3$ | $\rho_{2t}$= | 1.25 | t/m$^3$ | $\rho_{3t}$= | 1.45 | t/m$^3$ |
| | bottom | $\rho_{1b}$= | 1.80 | t/m$^3$ | $\rho_{2b}$= | 1.25 | t/m$^3$ | $\rho_{3b}$= | 1.70 | t/m$^3$ |
| B1.2 S-wave propagation speed | top | $c_{S0,1t}$= | 60.0 | m/s | $c_{S0,2t}$= | 44.0 | m/s | $c_{S0,3t}$= | 54.0 | m/s |
| | bottom | $c_{S0,1b}$= | 60.0 | m/s | $c_{S0,2b}$= | 44.0 | m/s | $c_{S0,3b}$= | 195.0 | m/s |
| B1.2 P-wave propagation speed | whole | $c_{P0,1}$= | 300.0 | m/s | $c_{P0,2}$= | 570.0 | m/s | $c_{P0,3}$= | 1050.0 | m/s |
| B1.4 Damping ratio | whole layer | $D_{0,1}$= | 4.00 | % | $D_{0,2}$= | 4.00 | % | $D_{0,3}$= | 4.00 | % |
| B1.5 Plasticity index | top | $PI_{1t}$= | 20 | % | $PI_{2t}$= | 165 | % | $PI_{3t}$= | 70 | % |
| | bottom | $PI_{1b}$= | 20 | % | $PI_{2b}$= | 165 | % | $PI_{3b}$= | 70 | % |
| B1.6 Earth pressure at rest | whole layer | $K_{0,1}$= | 0.50 | - | $K_{0,2}$= | 0.60 | - | $K_{0,3}$= | 0.55 | - |

**Tabel B1.1** Summary of selected material and propeties for the embankment and ground. The ground water table is located between soil layer 1 and 2.

| Type | Material | Levels part | Levels Level (m.s.l.) | Depth d (m) | Thick. t (m) | Stiffness ρ (t/m$^3$) | Stiffness $G_0$ (MPa) | Stiffness ν (-) | Koefficients $D_0$ (%) | Koefficients PI (%) | Koefficients $K_0$ (-) (-) |
|---|---|---|---|---|---|---|---|---|---|---|---|
| A2.1 Rail type | 60E1 | top | +5.77 | -0.77 | 0.172 | 7.80 | 76 923 | 0.2270 | 4.0 | | |
| | | bottom | +5.60 | -0.60 | | | | | | | |
| A2.2 Rail pad | medium | | +5.60 | -0.60 | 0.000 | | | | | | |
| A2.2 Track system | Sleepers | top | +5.60 | -0.60 | 0.220 | 2.50 | 13 000 | 0.1500 | 4.0 | 0.0 | 1.00 |
| | | bottom | +5.38 | -0.38 | | | | | | | |
| | Ballast | top | +5.38 | -0.38 | 0.300 | 1.70 | 93.1 | 0.3000 | 4.0 | 0.0 | 1.00 |
| | | bottom | +5.08 | -0.08 | | | | | | | |
| A3.1 Subballast | Subballast | top | +5.08 | -0.08 | 0.800 | 1.90 | 76.6 | 0.3000 | 4.0 | 0.0 | 1.00 |
| | | bottom | +4.28 | 0.72 | | | | | | | |
| A3.2 Frost insulation | Frost insulation | top | +4.28 | 0.72 | 0.100 | 1.90 | 76.6 | 0.3000 | 4.0 | 0.0 | 1.00 |
| | | bottom | +4.18 | 0.82 | | | | | | | |
| A3.3 Subgrade | Crushed rock fill | top | +4.18 | 0.82 | 0.000 | 2.00 | 92.1 | 0.3000 | 4.0 | 0.0 | 1.00 |
| | | bottom | +4.18 | 0.82 | | | | | | | |
| B1.1 Soil layer 1 | Crust | top | +5.00 | 0.00 | 1.300 | 1.80 | 6.5 | 0.4750 | 4.0 | 20.0 | 0.50 |
| | | bottom | +3.70 | 1.30 | | 1.80 | 6.5 | 0.4750 | 4.0 | 20.0 | 0.50 |
| B1.2 Soil layer 2 | Gyttja | top | +3.70 | 1.30 | 3.500 | 1.25 | 2.4 | 0.4750 | 4.0 | 165.0 | 0.60 |
| | | bottom | +0.20 | 4.80 | | 1.25 | 2.4 | 0.4750 | 4.0 | 165.0 | 0.60 |
| B1.3 Soil layer 2 | Clay | top | +0.20 | 4.80 | 45.200 | 1.45 | 4.2 | 0.4750 | 4.0 | 70.0 | 0.55 |
| | | bottom | -45.00 | 50.00 | | 1.70 | 64.6 | 0.4750 | 4.0 | 70.0 | 0.55 |

# DESIGN OF GROUND FOUNDATION FOR HIGH-SPEED RAILWAYS

## Input variables to the base model program

Case: **Ledgård prior ground reforcement**

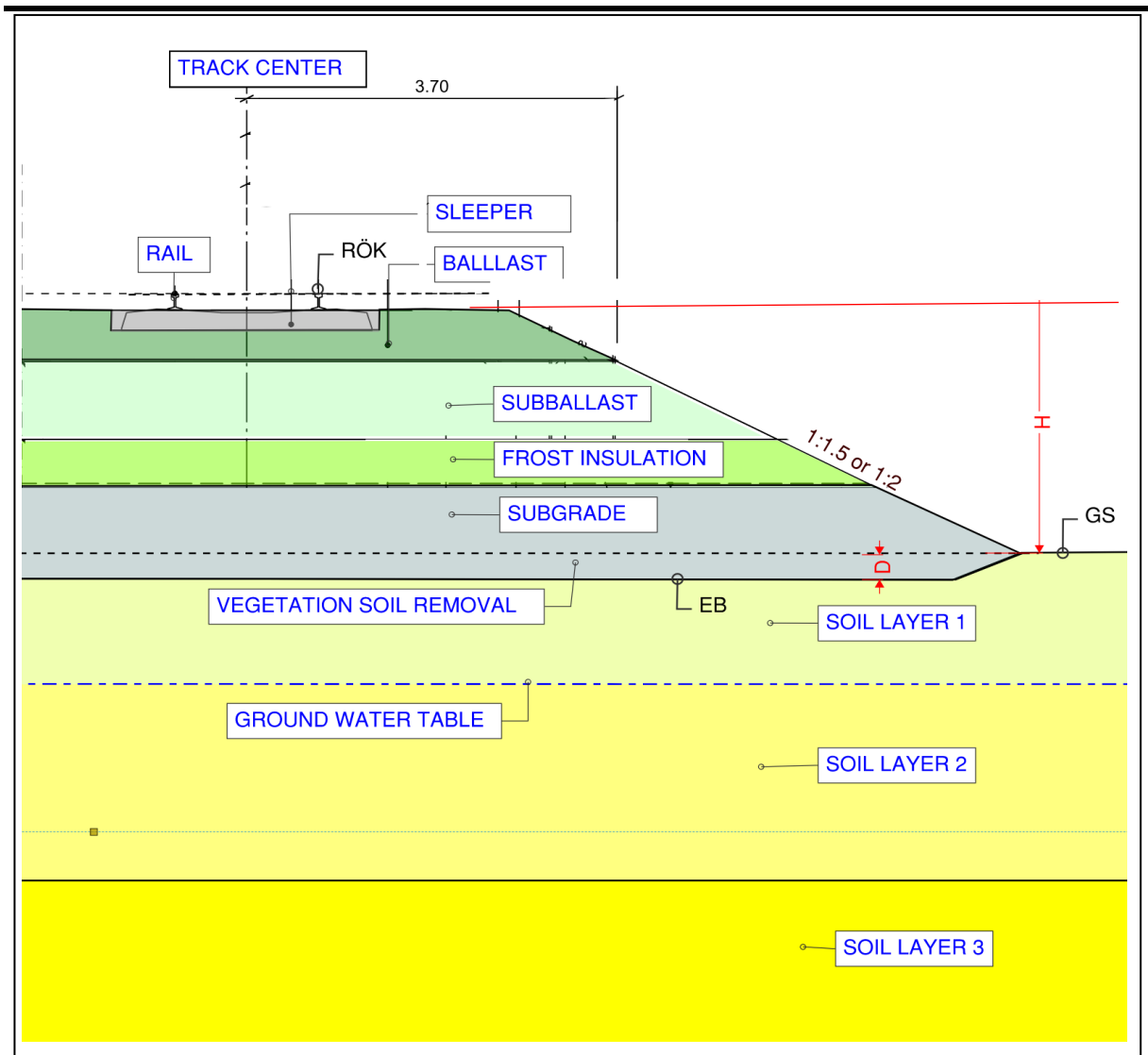


**Figure A2.1** Embankment with ballast (*Source: BVS 1585:005*)

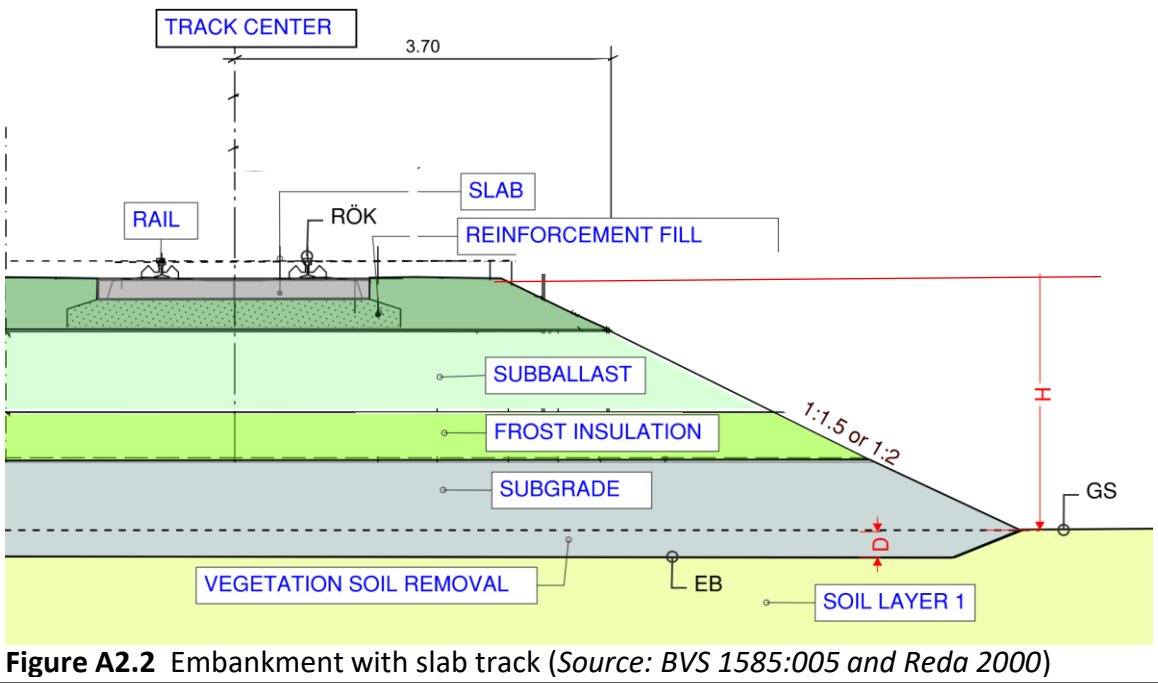


**Figure A2.2** Embankment with slab track (*Source: BVS 1585:005 and Reda 2000*)

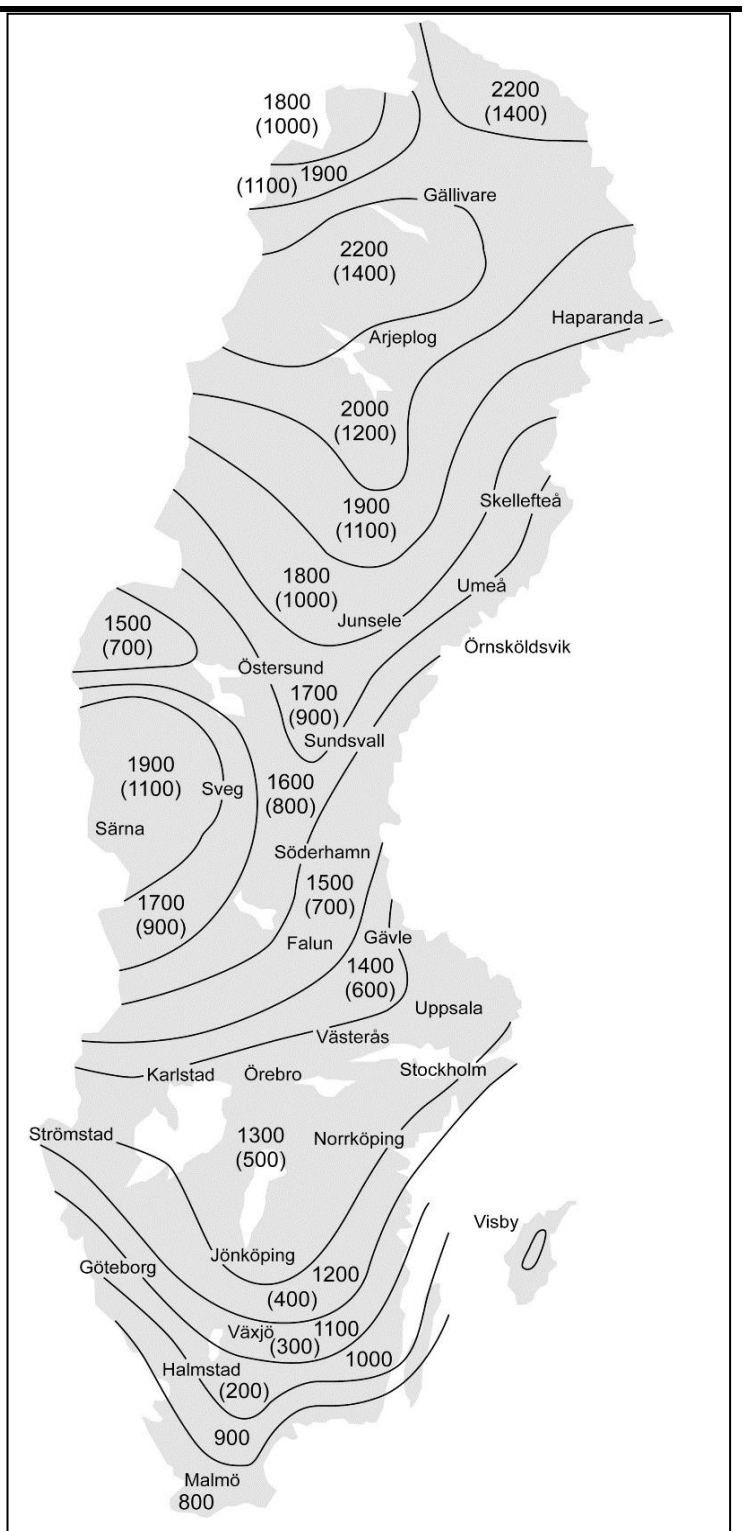


**Figure A3.1** Thickness of subballast when underground consist of frost heave sensitve soil.
The values in parantesis is required thickness of the frost insulation layer, when ballast has a thickness of 500mm and the subblast has a thickness of 800mm.

*Source: RA DCH.1/1 in AMA Anläggning 2020*

**Tabel B1.2** Summary of selected material and propeties under embankment (E) and ground surface (G), respectively.

| Levels | | Depth | | Density | | Shear modulus | | Poisson's ratio | | Damping ratio | | Plasticity index | | Lateral ratio | | Effectiv stress | |
|---|---|---|---|---|---|---|---|---|---|---|---|---|---|---|---|---|---|
| $L_E$ (m.s.l.) | $L_G$ (m.s.l.) | $d_E$ (m) | $d_G$ (m) | $\rho_E$ (t/m$^3$) | $\rho_G$ (t/m$^3$) | $G_{0,E}$ (MPa) | $G_{0,G}$ (MPa) | $\nu_E$ (-) | $\nu_G$ (-) | $D_{0,E}$ (%) | $D_{0,G}$ (%) | $PI_E$ (%) | $PI_E$ (%) | $K_{0,E}$ (-) | $K_{0,G}$ (-) | $p'_E$ (kPa) | $p'_G$ (kPa) |
| +5.77 | | -0.77 | | 7.80 | | 76 923 | | 0.2270 | | 4.00 | | 0.00 | | | | | |
| +5.60 | | -0.60 | | 7.80 | | 76 923 | | 0.2270 | | 4.00 | | 0.0 | | | | | |
| +5.60 | | -0.60 | | | | | | | | | | | | | | | |
| +5.60 | | -0.60 | | 2.50 | | 13 000 | | 0.1500 | | 4.00 | | 0.0 | | 1.00 | | 0.0 | |
| +5.38 | | -0.38 | | 2.50 | | 13 000 | | 0.1500 | | 4.00 | | 0.0 | | 1.00 | | 5.5 | |
| +5.38 | | -0.38 | | 1.70 | | 93.1 | | 0.3000 | | 4.00 | | 0.0 | | 1.00 | | 5.5 | |
| +5.08 | | -0.08 | | 1.70 | | 93.1 | | 0.3000 | | 4.00 | | 0.0 | | 1.00 | | 10.6 | |
| +5.08 | | -0.08 | | 1.90 | | 76.6 | | 0.3000 | | 4.00 | | 0.0 | | 1.00 | | 10.6 | |
| +4.28 | | 0.72 | | 1.90 | | 76.6 | | 0.3000 | | 4.00 | | 0.0 | | 1.00 | | 25.8 | |
| +4.28 | | 0.72 | | 1.90 | | 76.6 | | 0.3000 | | 4.00 | | 0.0 | | 1.00 | | 25.8 | |
| +4.18 | | 0.82 | | 1.90 | | 76.6 | | 0.3000 | | 4.00 | | 0.0 | | 1.00 | | 27.7 | |
| +4.18 | | 0.82 | | 1.90 | | 76.6 | | 0.3000 | | 4.00 | | 0.0 | | 1.00 | | 27.7 | |
| +4.18 | | 0.82 | | 1.90 | | 76.6 | | 0.3000 | | 4.00 | | 0.0 | | 1.00 | | 27.7 | |
| +4.18 | +5.00 | 0.82 | 0.00 | 1.80 | 1.80 | 6.5 | 6.5 | 0.4750 | 0.4750 | 4.00 | 4.00 | 20.0 | 20.0 | 0.50 | 0.50 | 27.7 | 0.0 |
| +3.70 | +3.70 | 1.30 | 1.30 | 1.80 | 1.80 | 6.5 | 6.5 | 0.4750 | 0.4750 | 4.00 | 4.00 | 20.0 | 20.0 | 0.50 | 0.50 | 27.7 | 15.6 |
| +3.70 | +3.70 | 1.30 | 1.30 | 1.25 | 1.25 | 2.4 | 2.4 | 0.4750 | 0.4750 | 4.00 | 4.00 | 165.0 | 165.0 | 0.60 | 0.60 | 27.7 | 17.2 |
| +0.20 | +0.20 | 4.80 | 4.80 | 1.25 | 1.25 | 2.4 | 2.4 | 0.4750 | 0.4750 | 4.00 | 4.00 | 165.0 | 165.0 | 0.60 | 0.60 | 30.7 | 23.6 |
| +0.20 | +0.20 | 4.80 | 4.80 | 1.45 | 1.45 | 4.2 | 4.2 | 0.4750 | 0.4750 | 4.00 | 4.00 | 70.0 | 70.0 | 0.55 | 0.55 | 30.7 | 23.6 |
| -45.00 | -45.00 | 50.00 | 50.00 | 1.70 | 1.70 | 64.6 | 64.6 | 0.4750 | 0.4750 | 4.00 | 4.00 | 70.0 | 70.0 | 0.55 | 0.55 | 206.2 | 204.4 |

# DESIGN OF GROUND FOUNDATION FOR HIGH-SPEED RAILWAYS

## Input variables to the base model program

Case: **Ledsgård prior LCC reinforcement**

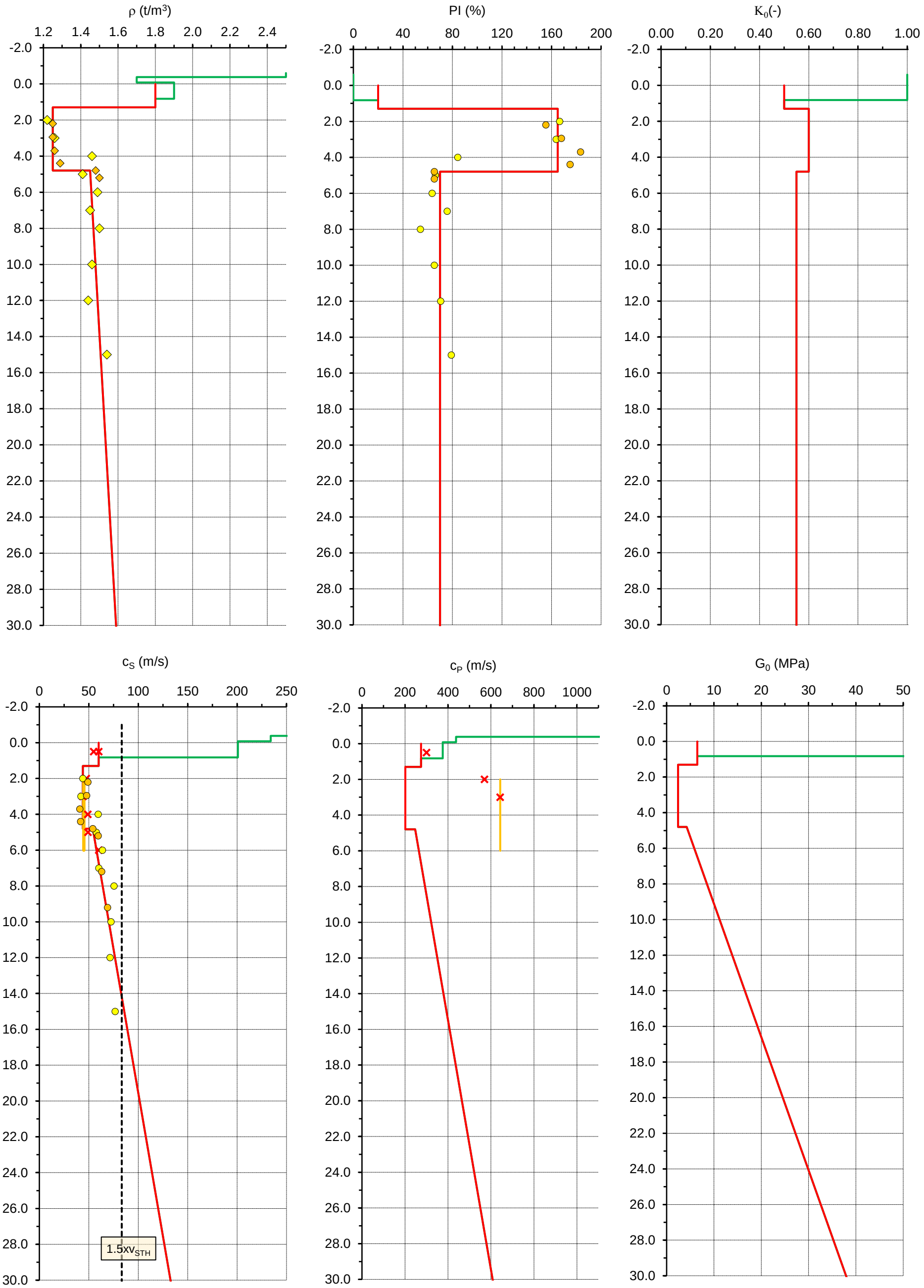


**Figure B1.1** Summary of selected material and propeties for the embankment and ground

# DESIGN OF GROUND FOUNDATION FOR HIGH-SPEED RAILWAYS

## Input variables to the base model program

Case: **Ledgård prior ground reforcement**

| | |
|---|---|
| Scale depth | -2.00 |
| | 30.00 |

**Ledsgård - 1997**

| d | soil type | ρ | $w_L$ | PI | $c_{u,k}$ | $c_{S0,emperi}$ |
|---|---|---|---|---|---|---|
| 2 | Mud | 1.22 | 258 | 167 | 12.1 | 44.0 |
| 3 | Mud | 1.26 | 254 | 164 | 11.2 | 42.0 |
| 4 | Mud/Cla | 1.46 | 118 | 84 | 12.1 | 59.5 |
| 5 | Clayey m | 1.41 | 97 | 66 | 9.0 | 57.7 |
| 6 | Clayey m | 1.49 | 94 | 64 | 11.3 | 63.8 |
| 7 | Clayey m | 1.45 | 108 | 76 | 11.2 | 60.1 |
| 8 | Clayey m | 1.50 | 83 | 54 | 14.1 | 75.6 |
| 10 | Clay | 1.46 | 96 | 65 | 14.6 | 72.5 |
| 12 | Clay | 1.44 | 102 | 71 | 14.9 | 71.5 |
| 15 | Clay | 1.54 | 112 | 79 | 20.1 | 76.6 |

**Ledsgård - JW4 (1999)**

| d | soil type | ρ | $w_L$ | PI | $c_{u,k}$ | $c_{S0,emperi}$ |
|---|---|---|---|---|---|---|
| 2.2 | Mud | 1.25 | 242 | 155 | 14.4 | 49.0 |
| 2.95 | Mud | 1.25 | 260 | 168 | 14.7 | 47.7 |
| 3.7 | Mud | 1.26 | 282 | 183 | 11.8 | 40.9 |
| 4.4 | Mud | 1.29 | 270 | 175 | 12.0 | 41.7 |
| 4.8 | Clay | 1.48 | 96 | 65 | 8.2 | 54.0 |
| 5.2 | Clay | 1.50 | 96 | 65 | 10.1 | 59.5 |
| 7.2 | Clay | 1.49 | 110 | 77 | 12.9 | 63.0 |
| 9.2 | Clay | 1.49 | 100 | 69 | 14.1 | 68.9 |

**Ledsgård -seismic tests (1997)**

| Test | d | $c_{S0}$ | $c_{P0}$ | $D_0$ |
|---|---|---|---|---|
| Surface | 0.5 | 55 | | |
| Surface | 0.5 | 60 | 300 | |
| Cross-hole tests | 2 | 47.4 | 570 | 4.3 |
| Cross-hole tests | 3 | 44 | 643 | 4.9 |
| Cross-hole tests | 4 | 49 | | 2.6 |
| Cross-hole tests | 5 | 49.1 | | 2.55 |
| Cross-hole tests | 6 | 60.1 | | 2.5 |
| Down-hole | 2 | 45 | 643 | |
| - "- | 6 | 45 | 643 | |
| Bender-element | 3.728 | 44 | | |
| Bender-element | 2.928 | 52 | | |
| Bender-element | 2.628 | 38 | | |
| Bender-element | 4.028 | 47 | | |
| Cyclic triaxial | 2.928 | 52.987 | | |
| Cyclic triaxial | 2.628 | 39.936 | | |

# DESIGN OF GROUND FOUNDATION FOR HIGH-SPEED RAILWAYS

## Input variables to the base model program

Case: **Ledsgård prior LCC reinforcement**

## D Finite-element modelling

| D1.Numerical Modelling | | | | |
|---|---|---|---|---|
| D1.1 Case name | | Ledsgård prior LCC reinforcement | | |
| D1.2 Type of analysis | NA | Moving load | | |
| D1.3 Maximum frequency of interest | $f_{max}$= | 5 | Hz | |

| D2. Numerical Calculations | | | | |
|---|---|---|---|---|
| D2.1 FE Software | FEP | Brigade | | |
| D2.2 Number of cores in PC | CORES | 6 | st | |

**Moving load analysis – train speed 70km/h**

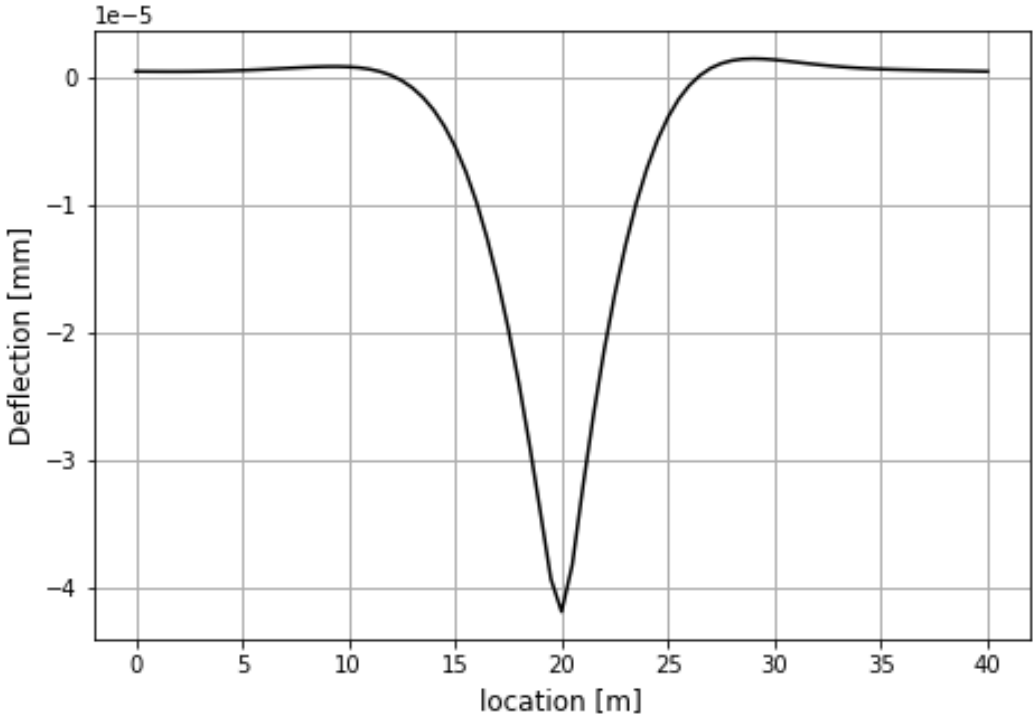


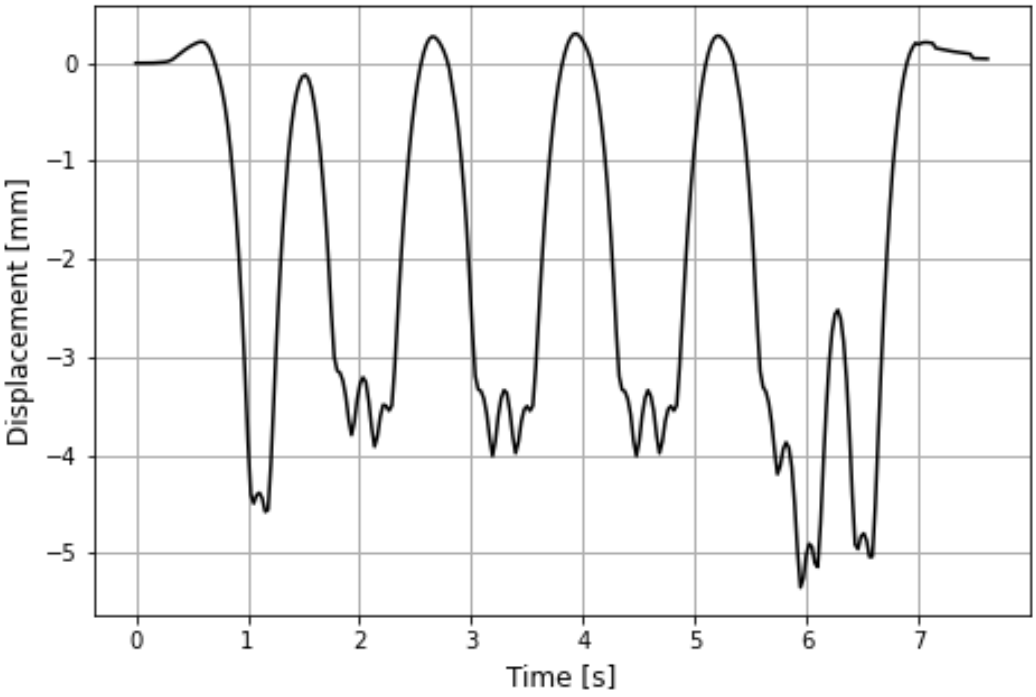

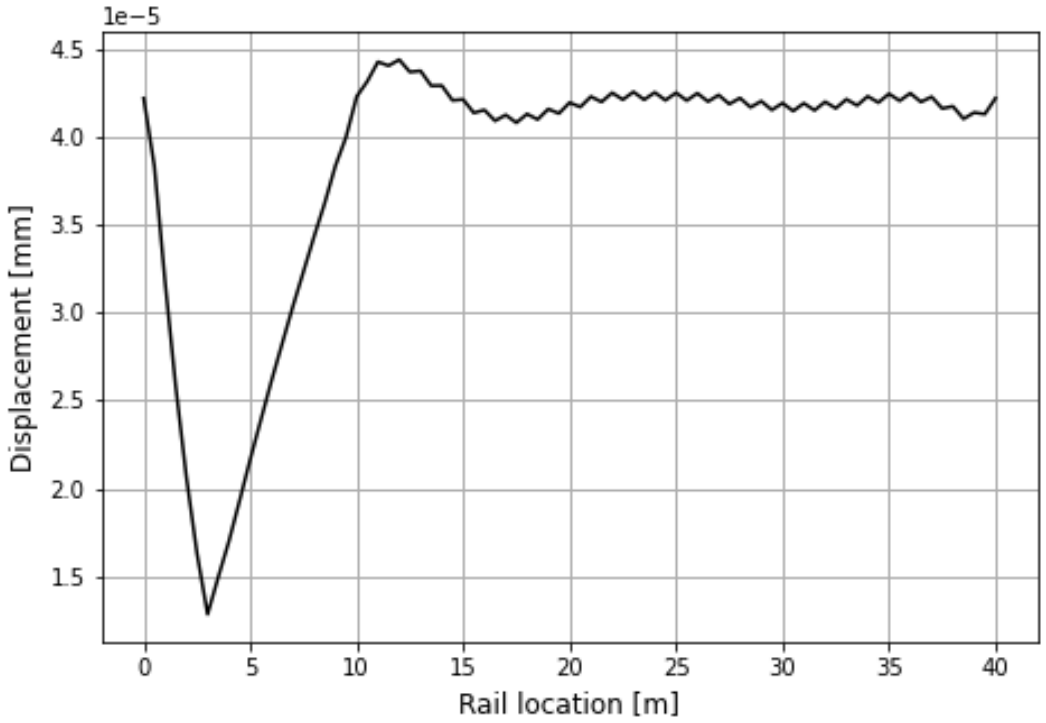
1e−5
4.5
4.0
3.5
3.0
2.5
2.0
1.5
Displacement [mm]
0
5
10
15
20
25
30
35
40
Rail location [m]

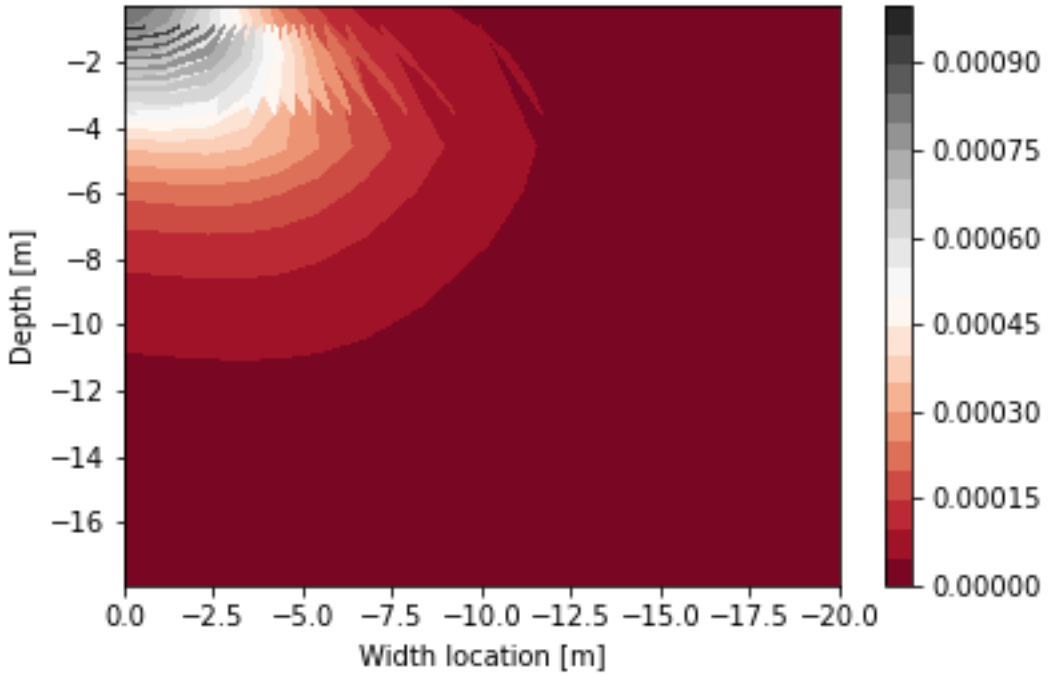
−2
−4
−6
−8
−10
−12
−14
−16
Depth [m]
0.0
−2.5
−5.0
−7.5
−10.0
−12.5
−15.0
−17.5
−20.0
Width location [m]
0.00090
0.00075
0.00060
0.00045
0.00030
0.00015
0.00000

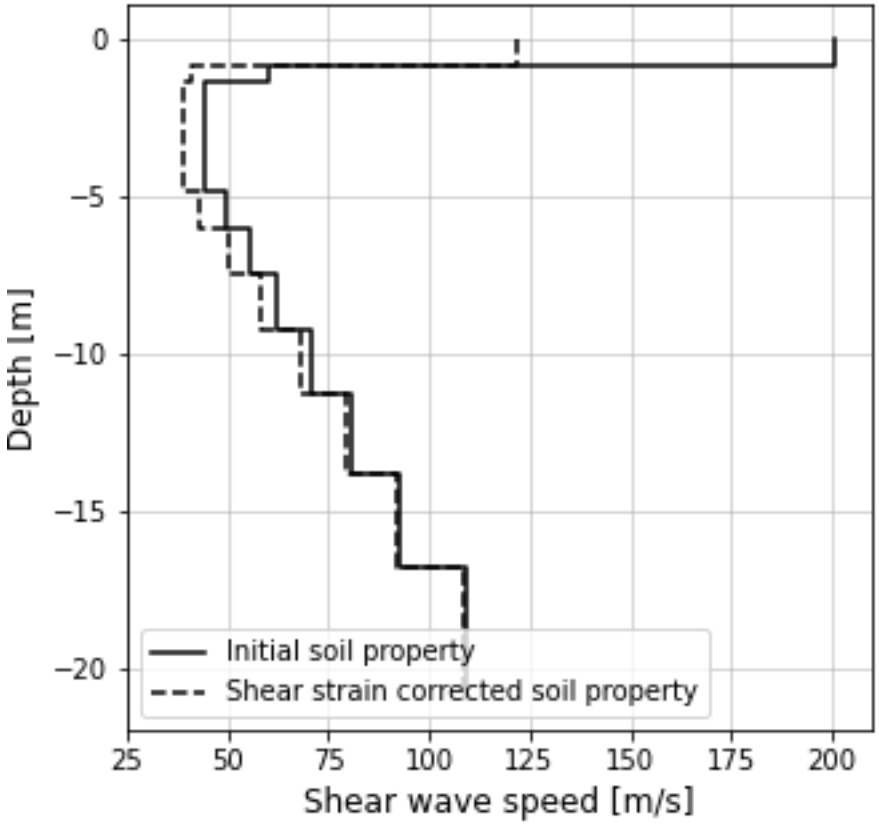
0
−5
−10
−15
−20
Depth [m]
25
50
75
100
125
150
175
200
Shear wave speed [m/s]
Initial soil property
Shear strain corrected soil property

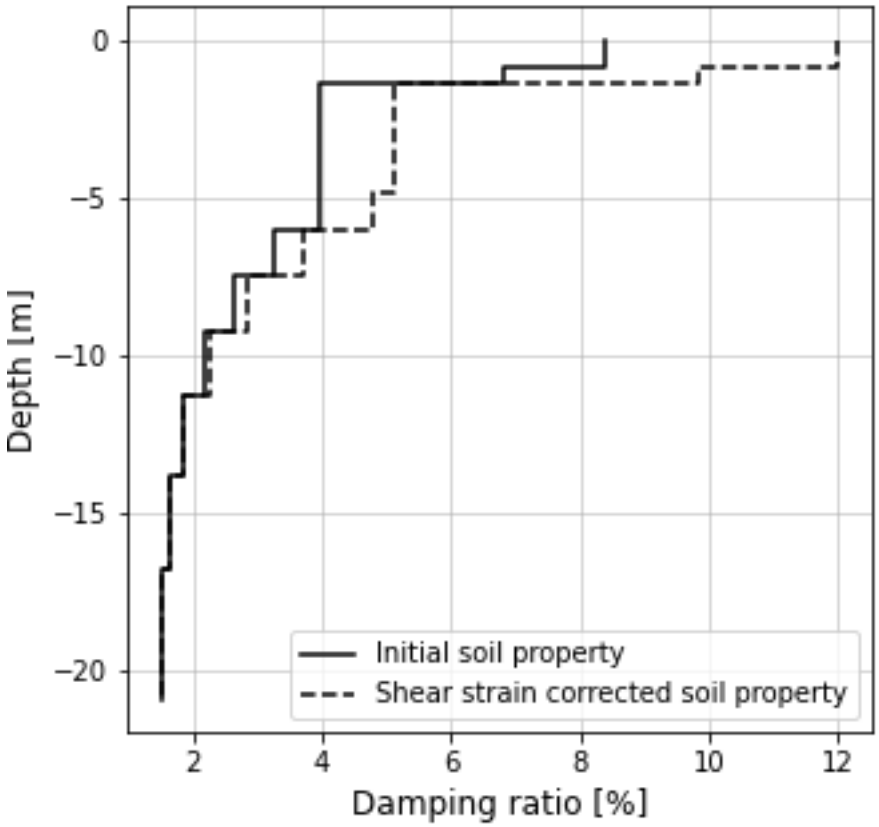
0
−5
−10
−15
−20
Depth [m]
2
4
6
8
10
12
Damping ratio [%]
Initial soil property
Shear strain corrected soil property

**Moving load analysis – train speed 142km/h**

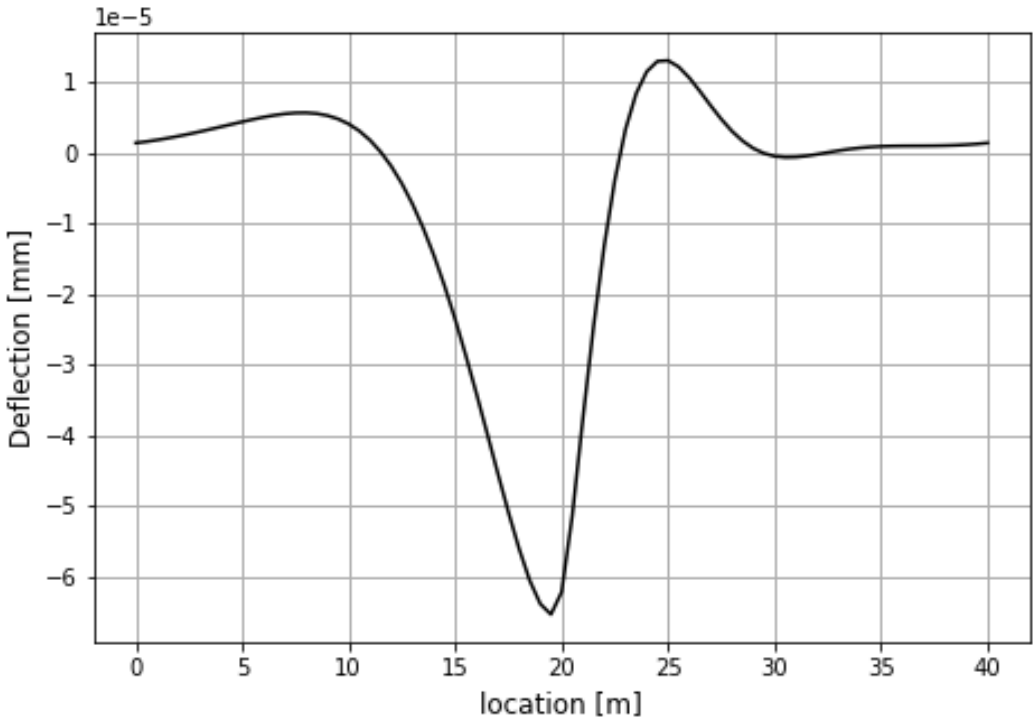


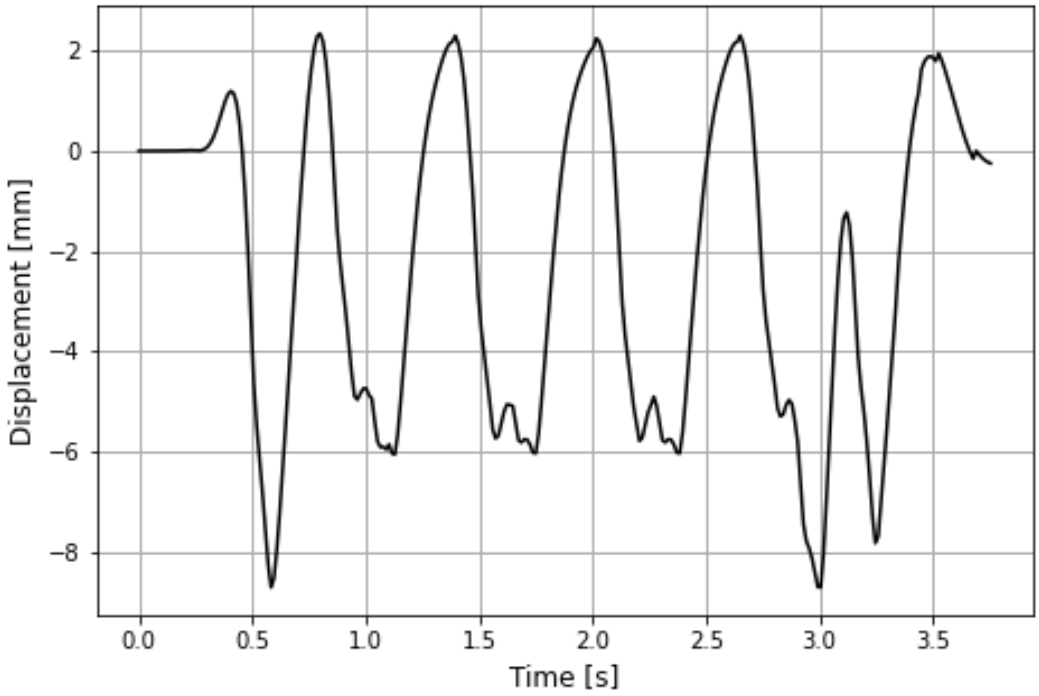

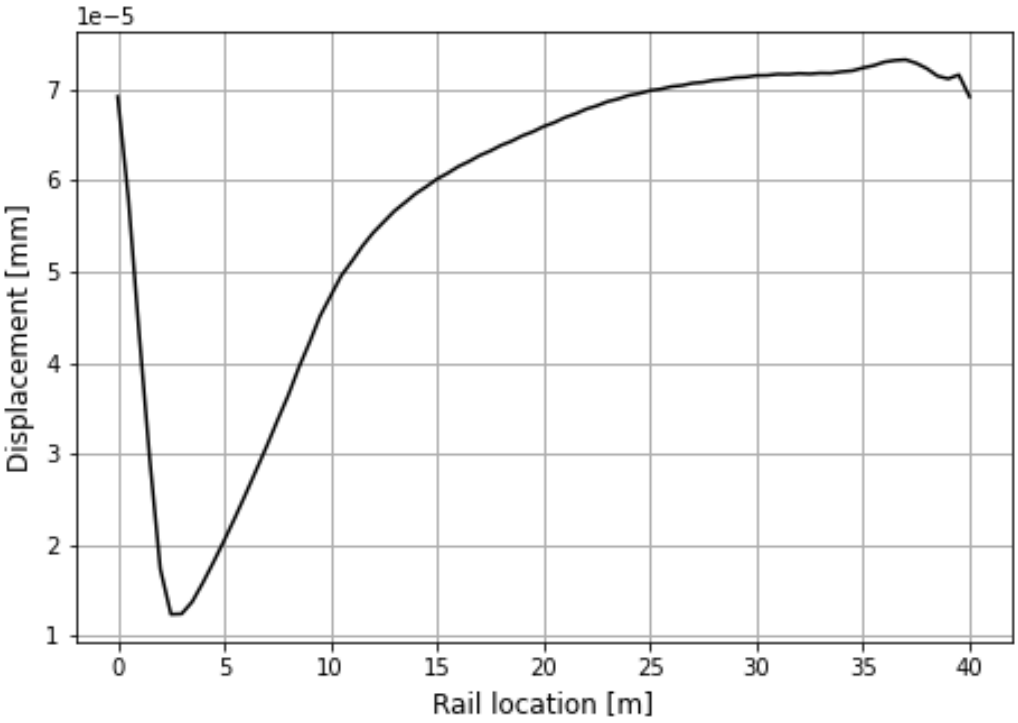
1e−5
Displacement [mm]
Rail location [m]

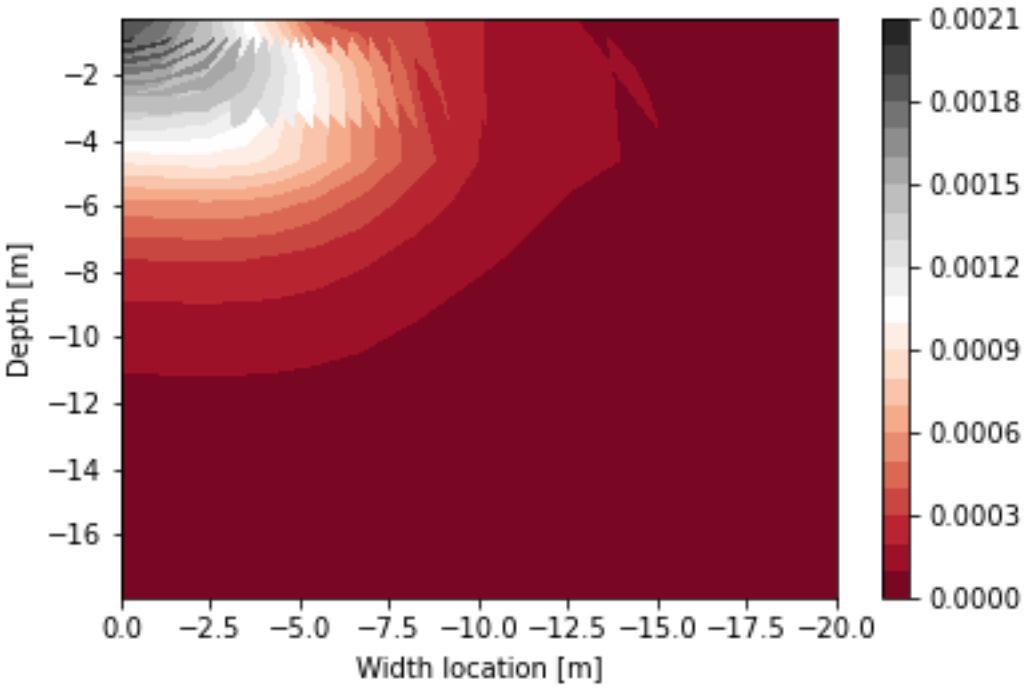
Depth [m]
Width location [m]

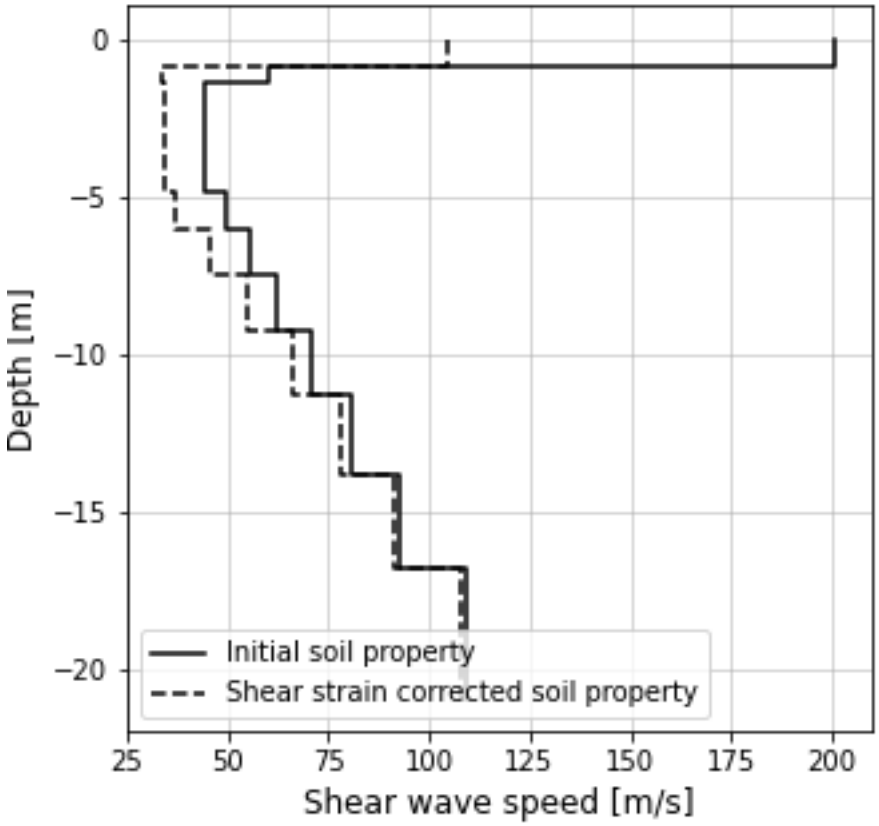
0
−5
−10
−15
−20
Depth [m]
25
50
75
100
125
150
175
200
Shear wave speed [m/s]
Initial soil property
Shear strain corrected soil property

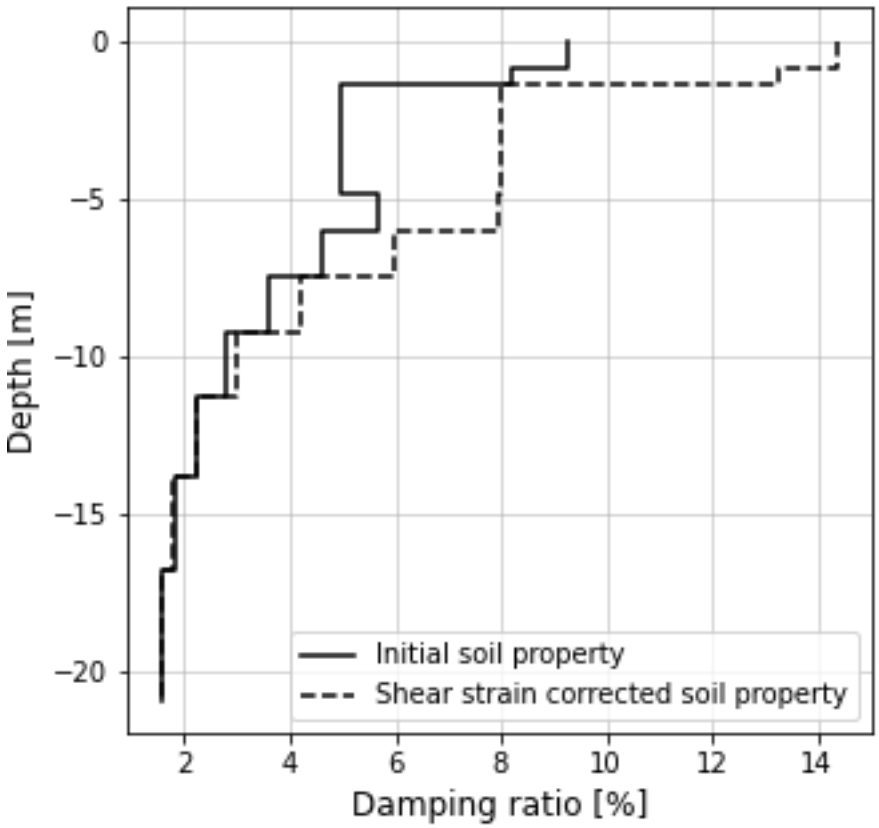
0
−5
−10
−15
−20
Depth [m]
2
4
6
8
10
12
14
Damping ratio [%]
Initial soil property
Shear strain corrected soil property

**Moving load analysis – train speed 204km/h**

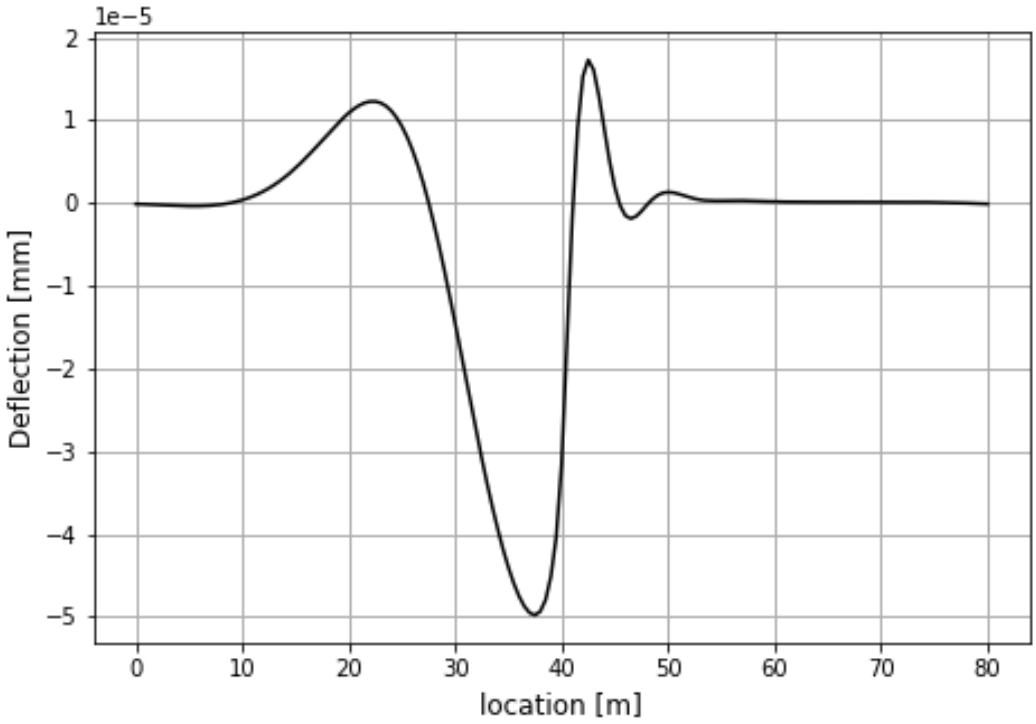


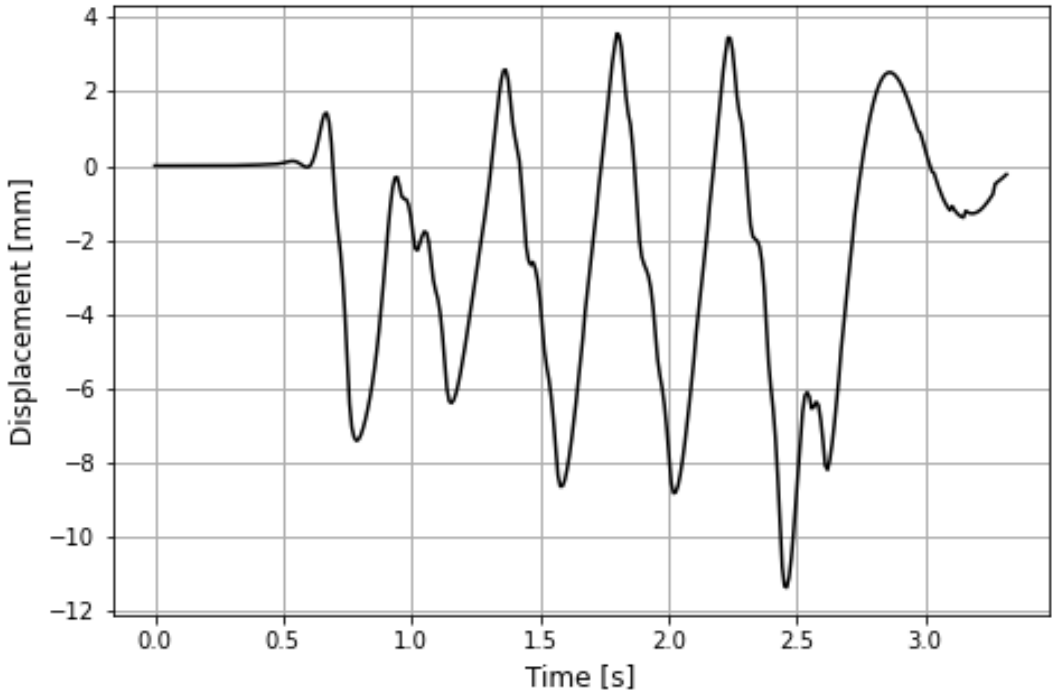

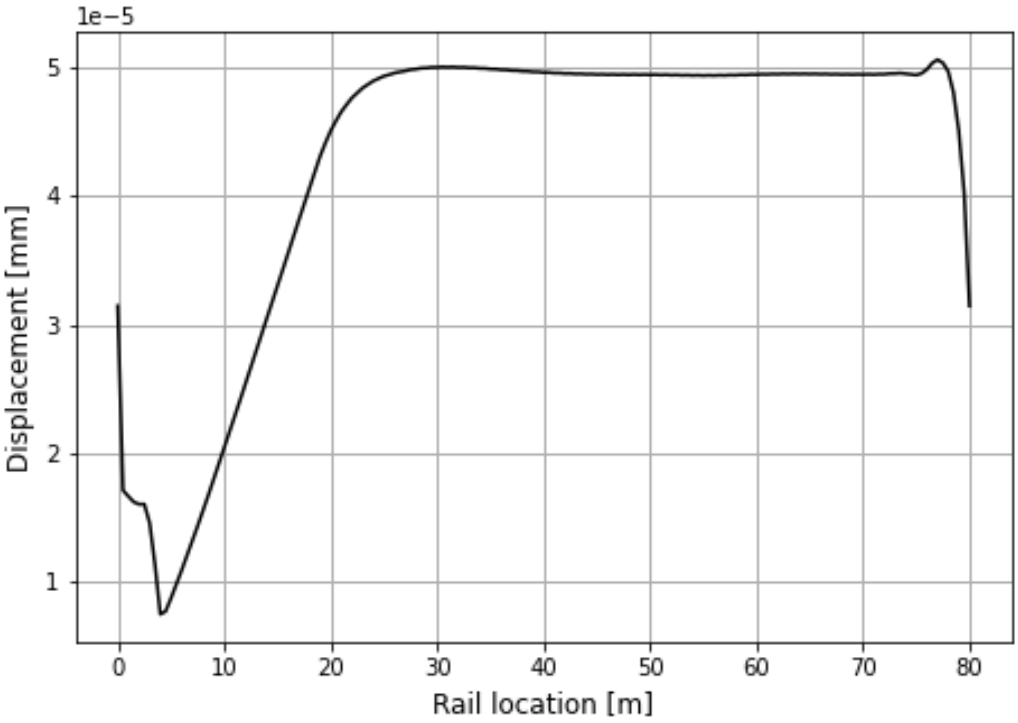
1e−5
5
4
3
2
1
Displacement [mm]
0
10
20
30
40
50
60
70
80
Rail location [m]

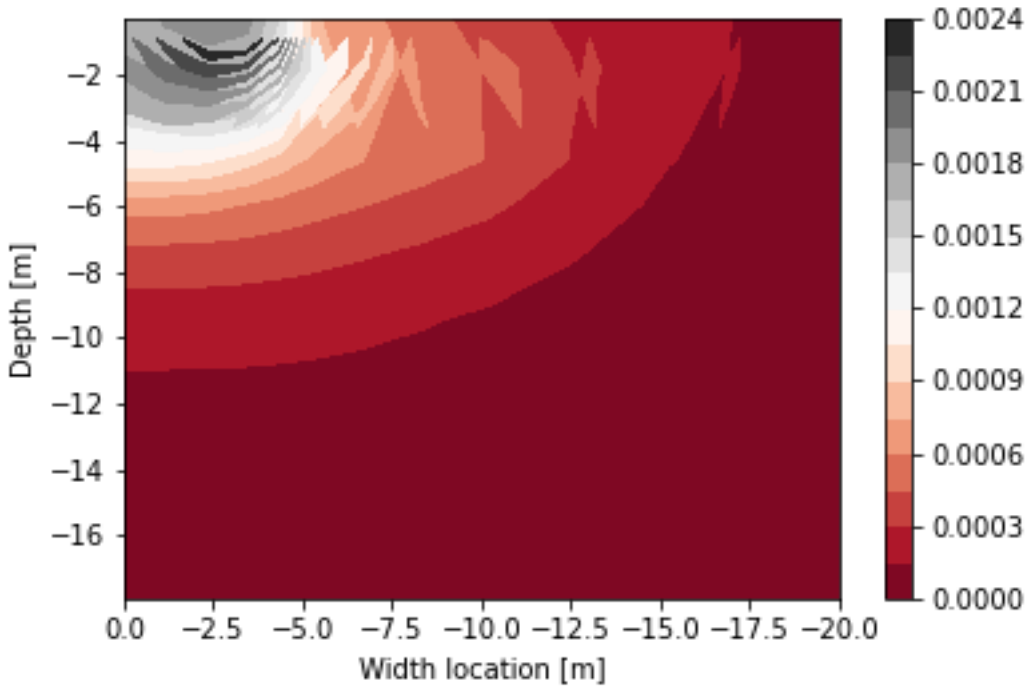
−2
−4
−6
−8
−10
−12
−14
−16
Depth [m]
0.0
−2.5
−5.0
−7.5
−10.0
−12.5
−15.0
−17.5
−20.0
Width location [m]
0.0024
0.0021
0.0018
0.0015
0.0012
0.0009
0.0006
0.0003
0.0000

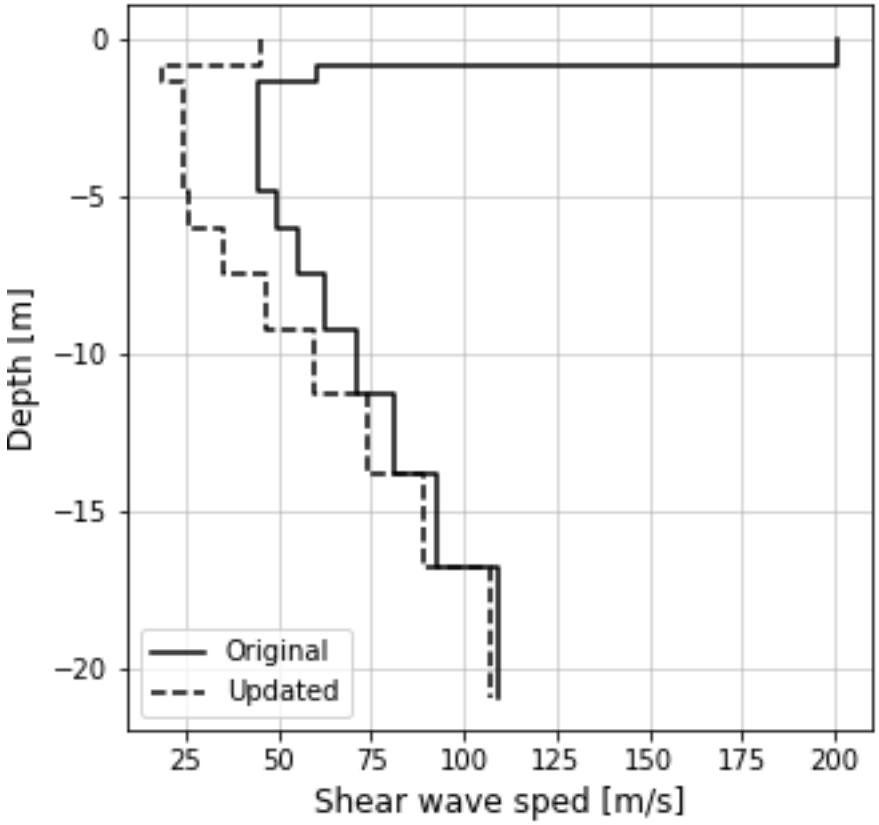
0
−5
−10
−15
−20
Depth [m]
Original
Updated
25
50
75
100
125
150
175
200
Shear wave sped [m/s]

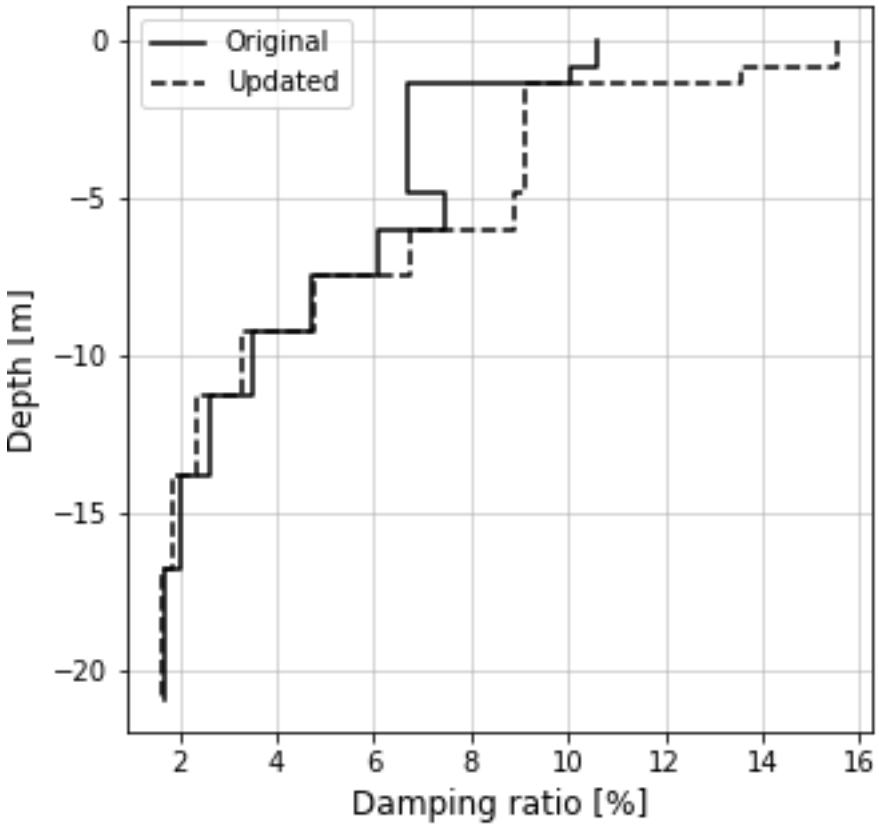
0
−5
−10
−15
−20
Depth [m]
Original
Updated
2
4
6
8
10
12
14
16
Damping ratio [%]

**Assessment of critical speed**

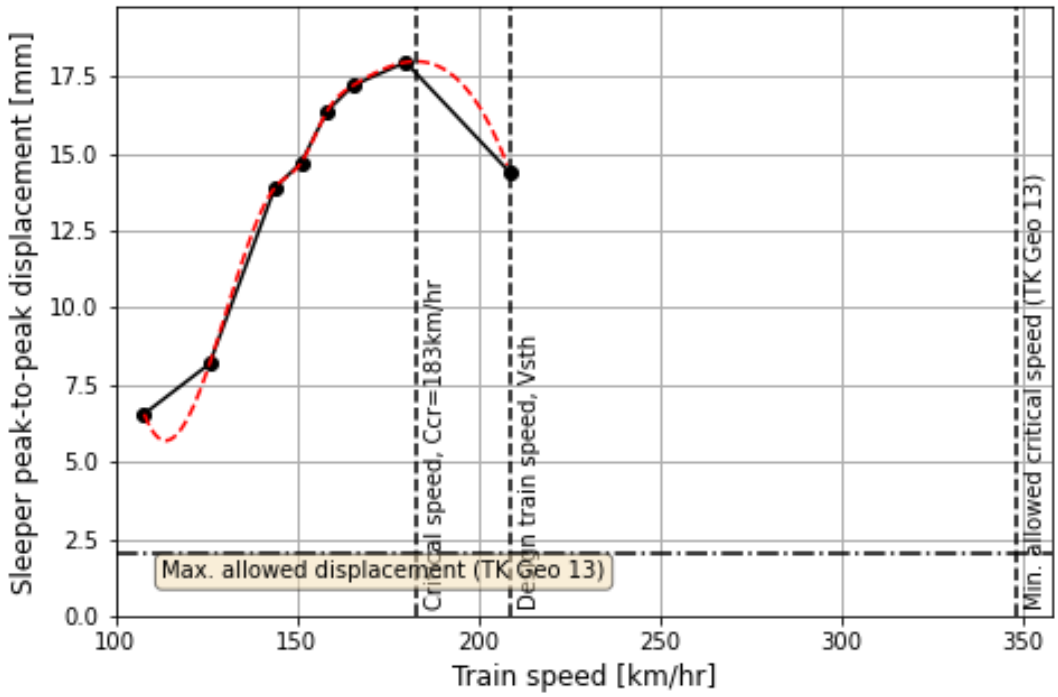


**Receptance analysis**

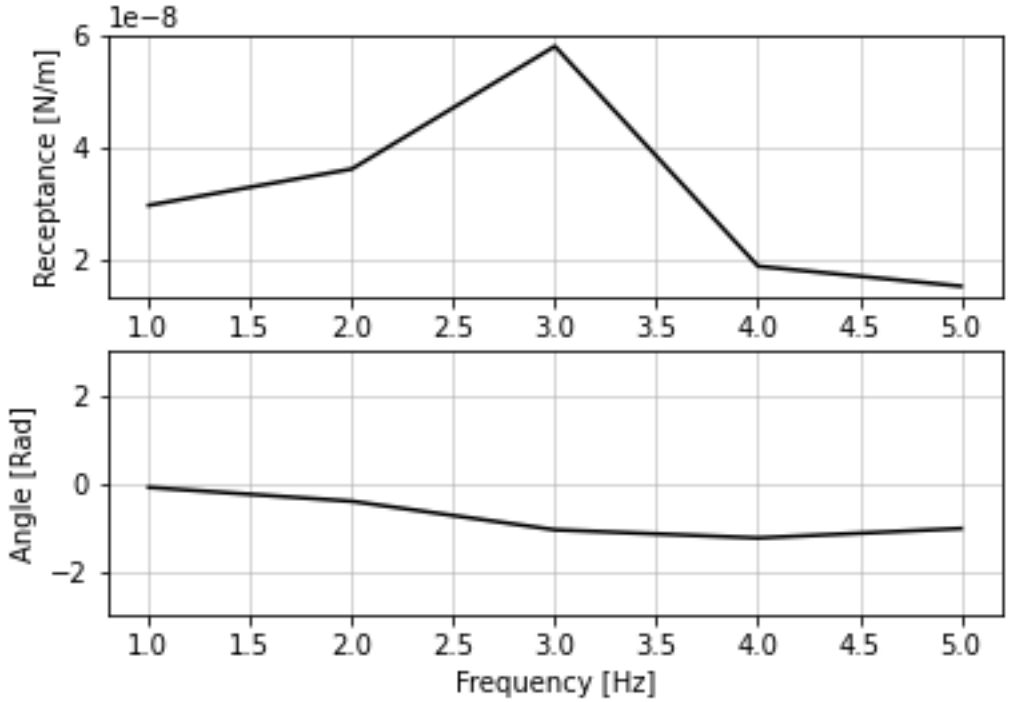

# Appendix C

## The base model program: input and output files - Ledsgård with LCC

# DESIGN OF GROUND FOUNDATION FOR HIGH-SPEED RAILWAYS

## Input variables to the base model program

Case: **Ledsgård with LCC reinforcement**

## A Design of railway

| **A1. Vechicle type** | | **Selected vechicle type** | | **Guideline** |
|---|---|---|---|---|
| A1.1 Vehicle type | VT= | X2000 | | |
| A1.3 Design train speed | $V_{STH}$= | 200 | km/h | |

| **A2. Track structure** | | **Selected track stucture** | | **Guideline** |
|---|---|---|---|---|
| A2.1 Rail type | RT= | 60E1 | | |
| A2.2 Rail pad | RP= | medium | | |
| A2.2 Track system | TS= | Concrete sleepers with ballast | | AMA DCH.311 |

| **A3. Track foundation** | | **Selected track foundation** | | **Guideline** |
|---|---|---|---|---|
| A3.1 Subballast | SB= | 800 mm | | AMA DCH.15 |
| A3.2 Frost insulation, thickness | SBf= | 300 | mm | Figure RA DCH.1/1 + AMA DCH.16 |
| A3.3 Subgrade | SG= | Crushed rock fill | | AMA CEB.321 |

| **A4. Embankment geometry** | | **Geometry** | | | **Guideline** | | | | | | |
|---|---|---|---|---|---|---|---|---|---|---|---|
| A4.1 Level of rail top | RÖK= | +5.972 | m.s.l. | | | | | | | | |
| A4.2 Level of ground surface | GS= | +5.000 | m.s.l. | | | | | | | | |
| A4.3 Slope of embankment | S: | 1: 1.5 | | | BVS 1585:005 | | | | | | |
| A4.4 Vegetation soil removal | VR= | 200 | mm | | | | | | | | |
| Height over GS | H= | 0.97 | m | | Width at top= | $W_T$= | 7.40 | m | $W_T/2$= | 3.70 | m |
| Thickness below GS | D= | 0.82 | m | | Width at GS= | $W_{GS}$= | 10.32 | m | $W_{GS}/2$= | 5.16 | m |
| Level of embankment bottom | EB= | +4.18 | m.s.l. | | Width at bottom= | $W_B$= | 12.78 | m | $W_B/2$= | 6.39 | m |

## B Ground conditions

| **B1 Ground & Material Models** | | | **Guideline** |
|---|---|---|---|
| B1.1 Ground model | GM | Layered half-space | Choose "fixed bottom" when frictional soil layer or bedrock is at depth less than 30m |
| B1.2 Material model | MM | Equivalent linear | Choose "Equivilent linear" to consider shear strain dependent stiffness and damping |
| B1.2.1 Strain reduction factor | $R_f$= | 0.65 | $\gamma_{eff}=R_f \cdot \gamma_{max}$, - a value of 0.65 is recommended |

| **B1 Soil geometry and properties** | | **B1 Soil layer 1** | | | **B2 Soil layer 1** | | | **B3 Soil layer 1** | | |
|---|---|---|---|---|---|---|---|---|---|---|
| B1.1 Soil type | | Layer #1 | Crust | | Layer #2 | Gyttja | | Layer #3 | Clay | |
| B1.1 Levels | top | $L_{1t}$= | +5.00 | m.s.l. | $L_{2t}$= | +4.00 | m.s.l. | $L_{2t}$= | +0.50 | m.s.l. |
| | bottom | $L_{1t}$= | +4.00 | m.s.l. | $L_{2t}$= | +0.50 | m.s.l. | $L_{3t}$= | -45.00 | m.s.l. |
| | grund water table | GWT= | +4.00 | m.s.l. | | | | | | |
| B1.3 Total density | top | $\rho_{1t}$= | 1.80 | t/m$^3$ | $\rho_{2t}$= | 1.25 | t/m$^3$ | $\rho_{3t}$= | 1.45 | t/m$^3$ |
| | bottom | $\rho_{1b}$= | 1.80 | t/m$^3$ | $\rho_{2b}$= | 1.25 | t/m$^3$ | $\rho_{3b}$= | 1.70 | t/m$^3$ |
| B1.2 S-wave propagation speed | top | $c_{S0,1t}$= | 60.0 | m/s | $c_{S0,2t}$= | 44.0 | m/s | $c_{S0,3t}$= | 55.0 | m/s |
| | bottom | $c_{S0,1b}$= | 60.0 | m/s | $c_{S0,2b}$= | 44.0 | m/s | $c_{S0,3b}$= | 195.0 | m/s |
| B1.2 P-wave propagation speed | whole | $c_{P0,1}$= | 300.0 | m/s | $c_{P0,2}$= | 570.0 | m/s | $c_{P0,3}$= | 1050.0 | m/s |
| B1.4 Damping ratio | whole layer | $D_{0,1}$= | 4.00 | % | $D_{0,2}$= | 4.00 | % | $D_{0,3}$= | 4.00 | % |
| B1.5 Plasticity index | top | $PI_{1t}$= | 20 | % | $PI_{2t}$= | 165 | % | $PI_{3t}$= | 70 | % |
| | bottom | $PI_{1b}$= | 20 | % | $PI_{2b}$= | 165 | % | $PI_{3b}$= | 70 | % |
| B1.6 Earth pressure at rest | whole layer | $K_{0,1}$= | 0.50 | - | $K_{0,2}$= | 0.60 | - | $K_{0,3}$= | 0.55 | - |

**Tabel B1.1** Summary of selected material and propeties for the embankment and ground. The ground water table is located between soil layer 1 and 2.

| Type | Material | Levels | | Depth | Thick. | Stiffness | | | Koefficients | | |
|---|---|---|---|---|---|---|---|---|---|---|---|
| | | part | Level (m.s.l.) | d (m) | t (m) | ρ (t/m$^3$) | $G_0$ (MPa) | ν (-) | $D_0$ (%) | PI (%) | $K_0$ (-) (-) |
| A2.1 Rail type | 60E1 | top | +5.97 | -0.97 | 0.172 | 7.80 | 76 923 | 0.2270 | 4.0 | | |
| | | bottom | +5.80 | -0.80 | | | | | | | |
| A2.2 Rail pad | medium | | +5.80 | -0.80 | 0.000 | | | | | | |
| A2.2 Track system | Sleepers | top | +5.80 | -0.80 | 0.220 | 2.50 | 13 000 | 0.1500 | 4.0 | 0.0 | 1.00 |
| | | bottom | +5.58 | -0.58 | | | | | | | |
| | Ballast | top | +5.58 | -0.58 | 0.300 | 1.70 | 93.1 | 0.3000 | 4.0 | 0.0 | 1.00 |
| | | bottom | +5.28 | -0.28 | | | | | | | |
| A3.1 Subballast | Subballast | top | +5.28 | -0.28 | 0.800 | 1.90 | 80.3 | 0.3000 | 4.0 | 0.0 | 1.00 |
| | | bottom | +4.48 | 0.52 | | | | | | | |
| A3.2 Frost insulation | Frost insulation | top | +4.48 | 0.52 | 0.300 | 1.90 | 80.3 | 0.3000 | 4.0 | 0.0 | 1.00 |
| | | bottom | +4.18 | 0.82 | | | | | | | |
| A3.3 Subgrade | Crushed rock fill | top | +4.18 | 0.82 | 0.000 | 2.00 | 98.2 | 0.3000 | 4.0 | 0.0 | 1.00 |
| | | bottom | +4.18 | 0.82 | | | | | | | |
| B1.1 Soil layer 1 | Crust | top | +5.00 | 0.00 | 1.000 | 1.80 | 6.5 | 0.4750 | 4.0 | 20.0 | 0.50 |
| | | bottom | +4.00 | 1.00 | | 1.80 | 6.5 | 0.4750 | 4.0 | 20.0 | 0.50 |
| B1.2 Soil layer 2 | Gyttja | top | +4.00 | 1.00 | 3.500 | 1.25 | 2.4 | 0.4750 | 4.0 | 165.0 | 0.60 |
| | | bottom | +0.50 | 4.50 | | 1.25 | 2.4 | 0.4750 | 4.0 | 165.0 | 0.60 |
| B1.3 Soil layer 2 | Clay | top | +0.50 | 4.50 | 45.500 | 1.45 | 4.4 | 0.4750 | 4.0 | 70.0 | 0.55 |
| | | bottom | -45.00 | 50.00 | | 1.70 | 64.6 | 0.4750 | 4.0 | 70.0 | 0.55 |

# DESIGN OF GROUND FOUNDATION FOR HIGH-SPEED RAILWAYS

## Input variables to the base model program

Case: **Ledsgård with LCC reinforcement**

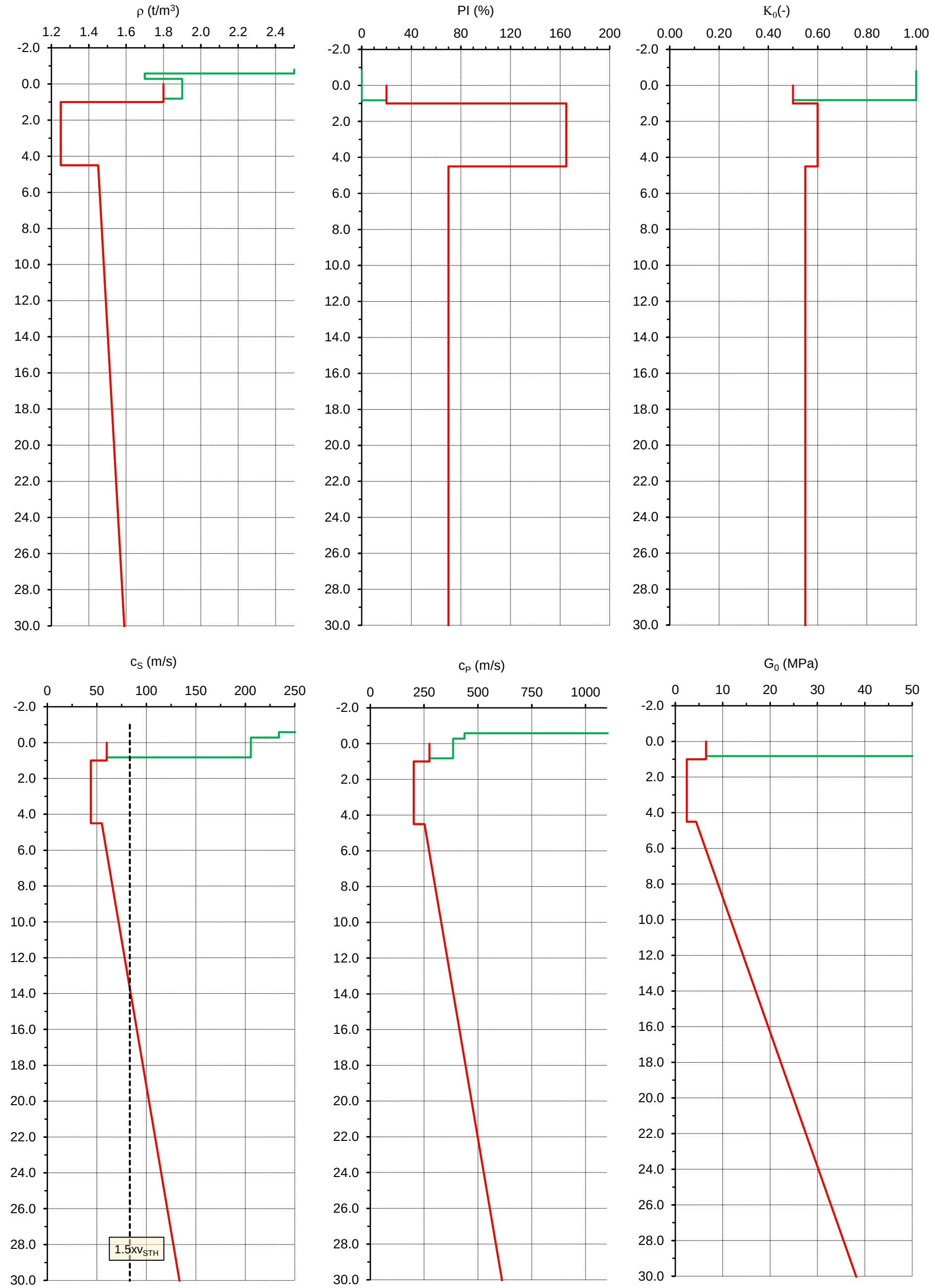


**Figure B1.1** Summary of selected material and propeties for the embankment and ground

# DESIGN OF GROUND FOUNDATION FOR HIGH-SPEED RAILWAYS

## Input variables to the base model program

Case: **Ledsgård with LCC reinforcement**

## C Ground Reinforcement

### C1. Berms (stability increment)

| | | | | | |
|---|---|---|---|---|---|
| A4.1 Berm | | none | | | |
| A4.1 Height | $H_B$= | 1.00 | m | Hb < 0.97m | |
| A4.2 With | $W_B$= | 5.00 | m | | |
| A4.3 Slope | $S_B$= | 1: 2 | - | | |
| A3.3 Filling material | SG= | Fill of coarse-grained mixed soil | | AMA CEB.74 | |

### C2. Lime-cement columns (LCC)

#### C2.1 Continues LCC-wall under rail, set V (vibration reduction)

| | | | | |
|---|---|---|---|---|
| C2.1.1 LCC, Set V | Set V= | yes - a set lengt | | None, set length or optimize length |
| C2.1.2 Diameter | $D_{LCC}$= | 0.60 | m | $D_{LCC1}$= 0.6 or 0.8m |
| C2.1.3 Length below EB | $L_{LCC-V}$= | 7.00 | m | When Set V="yes - a optimized length", then LCC1= 3 - 10m |
| C2.1.4 Spacing, perp. direct | $s_{LCC-V,P}$= | 1.92 | m | Choose s=1.44 or 1.92m for $D_{LCC}$=0.6 and s=1.44 or 2.16 $D_{LCC}$=0.8 |
| C2.1.5 Spacing, long. direct. | $s_{LCC-V,L}$= | 0.48 | m | s=0.48m for $D_{LCC}$=0.6 and s=0.54 for $D_{LCC}$=0.8 |

#### C2.2 Continues LCC-wall perpendicular rail, set St (total stability reinforcement)

| | | | | |
|---|---|---|---|---|
| C2.1.1 LCC, Set St | Set St= | yes - a set lengt | | When Set V="yes - a optimized length", then Set S1="none" |
| C2.1.2 Diameter | $D_{LCC}$= | 0.60 | m | Same as set V |
| C2.1.3 Length below EB | $L_{LCC-St}$= | 7.00 | m | Same as set V |
| C2.1.4 Spacing, perp. direct | $s_{LCC-St,P}$= | 0.48 | m | s=0.48m for $D_{LCC}$=0.6 and s=0.54 for $D_{LCC}$=0.8 |
| C2.1.5 Spacing, long. direct. | $s_{LCC-St,L}$= | 1.92 | m | Choose s=1.44, 1.92,2.4 or 2.88m for $D_{LCC}$=0.6 and s=1.44, 2.16, 2.88 or 3.6m $D_{LCC}$=0.8 |

#### C2.3. Long single LCC under rail, set Se (settlement reduction)

| | | | | |
|---|---|---|---|---|
| C2.2.1 LCC, Set Se1 | Set S1= | yes - a set lengt | | When Set V="yes - a optimized length", then Set S1="none" |
| C2.2.3 Diameter | $D_{LCC=}$ | 0.60 | m | Same as set V |
| C2.2.3 Length below EB | $L_{LCC-Se}$= | 13.00 | m | Up to 22m |
| C2.2.4 Spacing, perp. direct. | $s_{LCC-Se1,P}$= | 1.92 | m | Same as $s_{LCC-V,P}$ |
| C2.2.5 Spacing, long. direct. | $s_{LCC-Se1,L}$= | 1.92 | m | Same as $s_{LCC-St,P}$ |

#### C2.5. LCC properties

| | | | | |
|---|---|---|---|---|
| C2.5.1 Shear strength | $c_{u,LCC}$= | 150.00 | kPa | |
| C2.5.2 S-wave prop. speed | $c_{S0,LCC}$= | 279.61 | m/s | |
| C2.5.3 P-wave prop. speed | $c_{P0,LCC}$ | 448.66 | m/s | |
| C2.5.4 Damping ratio | $D_{0,LCC}$= | 4.00 | % | |

**Tabel C1.1** Summary of selected geometery and propeties for the berm

| Reinforcement: Berm | | Berm dimension and location | | | | | Stiffness | | | Koefficients | | | Eff. Stress | |
|---|---|---|---|---|---|---|---|---|---|---|---|---|---|---|
| | | Level (m.s.l.) | d (m) | H (m) | W (m) | S (-) | ρ (t/m³) | $G_0$ (MPa) | ν (-) | $D_0$ (%) | PI (%) | $K_0$ (-) (-) | p' (kPa) | p'$_{av}$ (kPa) |
| none | Fill of coarse-grained mixed soil | +5.00<br>+5.00 | 0.00<br>0.00 | 0.000 | 0.000 | | 2.00 | 48.9 | 0.3000 | 4.0 | 0.0 | 0.50 | 0.00<br>0.00 | 0.00 |

**Tabel C2.1** Summary of selected geometery and propeties for the LCCs

| Reinforcement: Lime-cement columns (LCC) | | | LCC dimensions and locations | | | | | | | | | | Stiffness | | | Koefficients | |
|---|---|---|---|---|---|---|---|---|---|---|---|---|---|---|---|---|---|
| | | | Level | | | Depth | | $L_{LCC}$ | $W_{LCC}$[1] | $y_{cord}$ | $s_{LCC,L}$ | $s_{LCC,P}$ | a[2] | ρ | $G_0$ | ν | $D_0$ | PI |
| | | | Up | Low | Averge | Up(m) | Low(m) | (m) | (m) | (m) | (m) | (m) | (-) | (t/m³) | (MPa) | (-) | (%) | (%) |
| C2.1 Continues LCC-wall | set V | rail | +4.18 | -2.82 | +0.68 | 0.82 | 7.82 | 7.00 | 0.53 | 0.96 | 0.48 | 1.92 | 1.00 | 1.46 | 114.4 | 0.1825 | 4.00 | 0.0 |
| C2.1 Continues LCC-wall | set St | perp. rail | +4.18 | -2.82 | +0.68 | 0.82 | 7.82 | 7.00 | 0.53 | perp. | 1.92 | 0.48 | 1.00 | 1.46 | 114.4 | 0.1825 | 4.00 | 0.0 |
| C2.2. Single LCC | set Se1 | center | -2.82 | -8.82 | -5.82 | 7.82 | 13.82 | 6.00 | 0.27 | 0.00 | 1.92 | 1.92 | 0.14 | 1.48 | 15.7 | 0.4545 | 4.00 | 60.3 |
| C2.3. Single LCC | set Se2 | rail | -2.82 | -8.82 | -5.82 | 7.82 | 13.82 | 6.00 | 0.53 | 1.92 | 1.92 | 1.92 | 0.28 | 1.48 | 25.6 | 0.4285 | 4.00 | 50.6 |
| C2.3. Single LCC | set Se3 | emb | -2.82 | -8.82 | -5.82 | 7.82 | 13.82 | 6.00 | 0.53 | 3.84 | 1.92 | 1.92 | 0.28 | 1.48 | 25.6 | 0.4285 | 4.00 | 50.6 |
| C2.3. Single LCC | set Se4 | none | -2.82 | -2.82 | -2.82 | 7.82 | 7.82 | 0.00 | 0.00 | 5.76 | 1.92 | 1.92 | 0.00 | 1.47 | 5.7 | 0.4750 | 4.00 | 95.0 |

Footnotes

[1] Effective width for LCC corrsponding almost to square columns with the same volume as circular columns

[2] Coverage degree of LCC rows over the width in the longitudinal direction.

# DESIGN OF GROUND FOUNDATION FOR HIGH-SPEED RAILWAYS

## Input variables to the base model program

Case: **Ledsgård with LCC reinforcement**

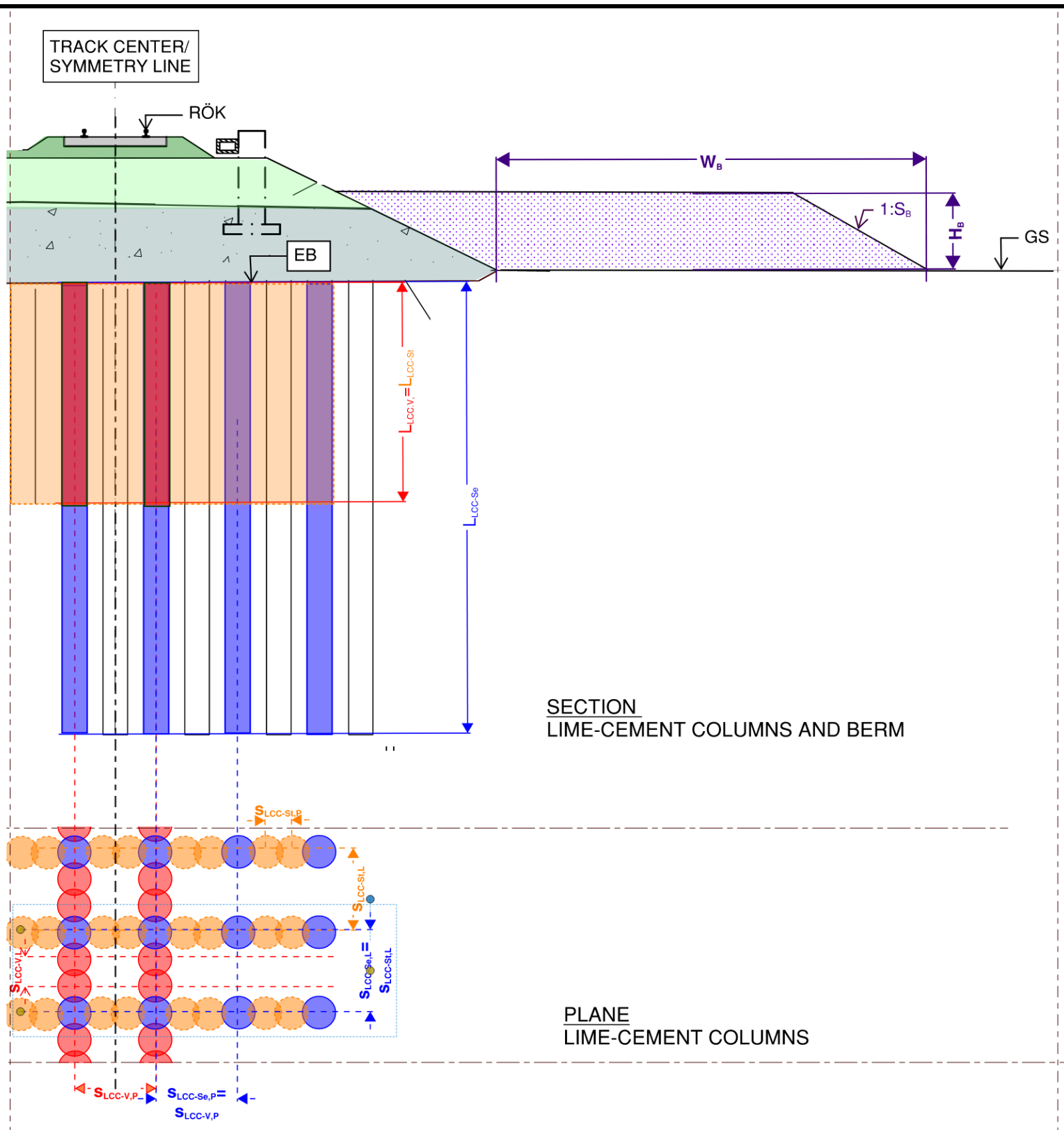


**Figure C1.1** Geometry of reinforcement with berm and lime-cement columns.

**Tabel C2.1** Cont.

| Wave speed | | Eff. Stress |
|---|---|---|
| $c_{S0}$ (m/s) | $c_{P0}$ (m/s) | $p'_{average}$ (kPa) |
| 279.6 | 448.7 | 31.50 |
| 279.6 | 448.7 | 31.50 |
| 102.8 | 356.0 | 52.39 |
| 131.2 | 370.9 | 52.39 |
| 131.2 | 370.9 | 52.39 |
| 62.4 | 285.8 | 40.99 |

# DESIGN OF GROUND FOUNDATION FOR HIGH-SPEED RAILWAYS

## Input variables to the base model program

Case: **Ledsgård with LCC reinforcement**

## D Finite-element modelling

| D1.Numerical Modelling | | | | |
|---|---|---|---|---|
| D1.1 Case name | | Ledsgård with LCC reinforcement | | |
| D1.2 Type of analysis | NA | Moving load | | |
| D1.3 Maximum frequency of interest | $f_{max}$= | 5 | Hz | |

| D2. Numerical Calculations | | | | | | | | | | | | | | | |
|---|---|---|---|---|---|---|---|---|---|---|---|---|---|---|---|
| D2.1 FE Software | FEP | Brigade | | | | | | | | | | | | | |
| D2.2 Number of cores in PC | CORES | 6 | st | | | | | | | | | | | | |

**DESIGN OF GROUND FOUNDATION FOR HIGH-SPEED RAILWAYS**

**Output - diagrams from the base model program** Case: **Ledsgård with LCC reinforcement**

**Moving load analysis – train speed 200km/h**

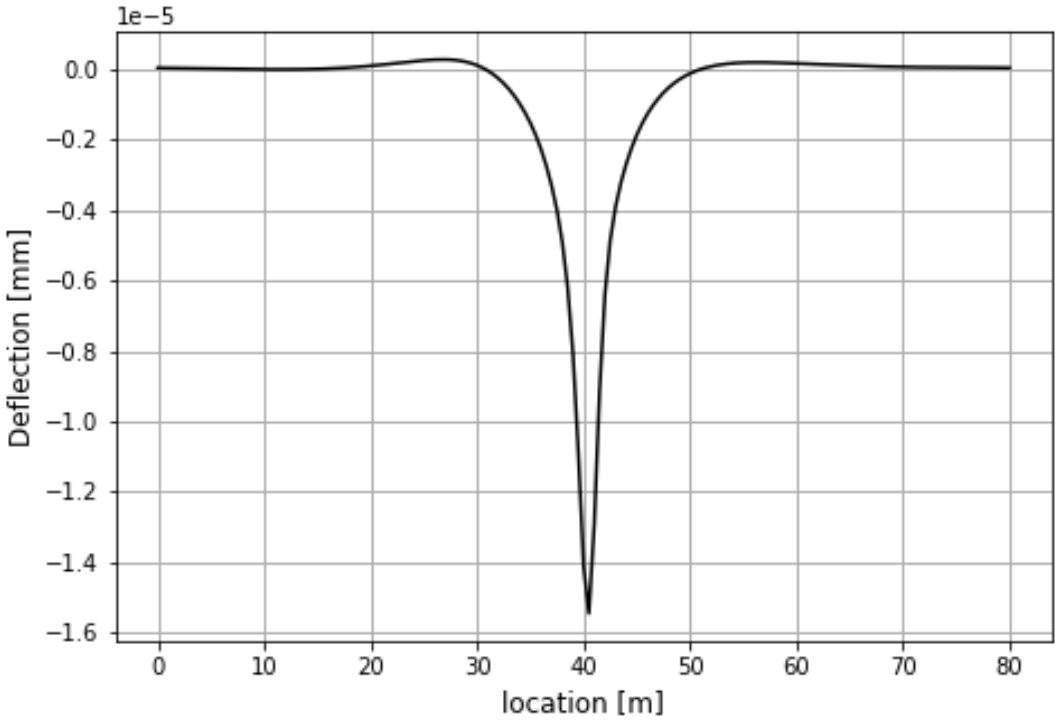


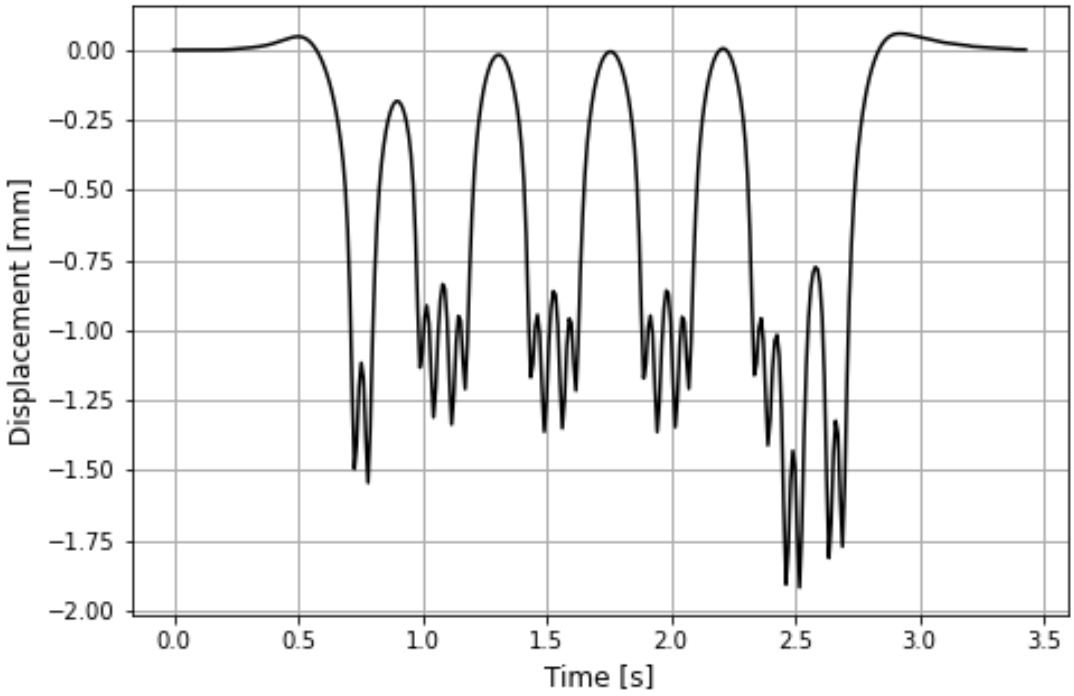

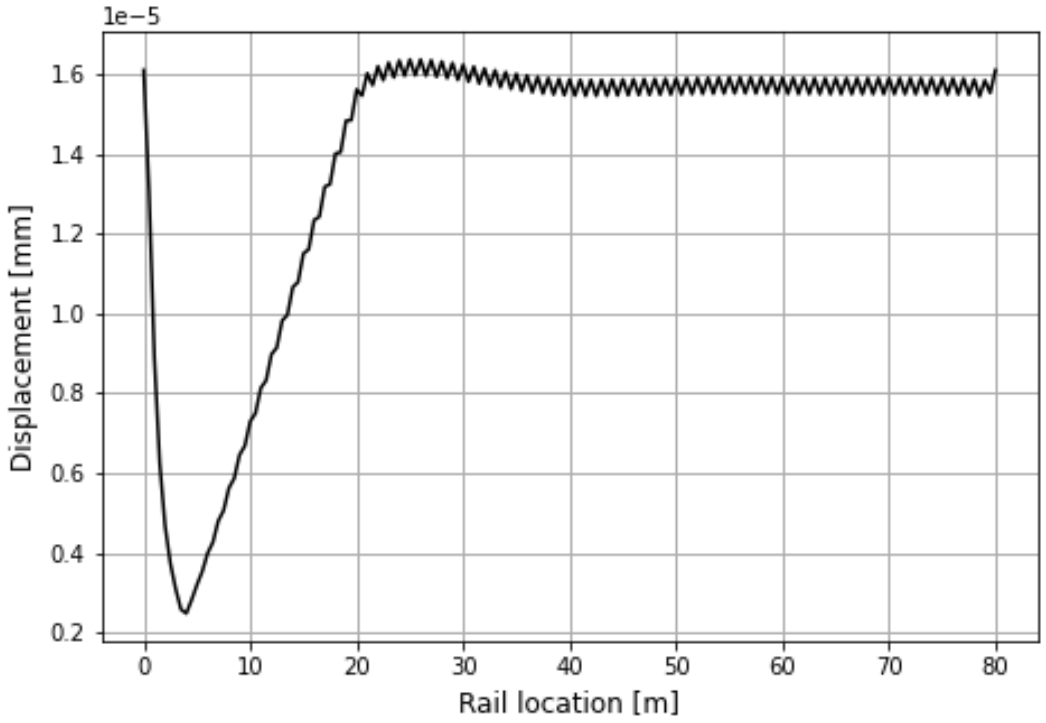
1e−5
1.6
1.4
1.2
1.0
0.8
0.6
0.4
0.2
Displacement [mm]
0
10
20
30
40
50
60
70
80
Rail location [m]

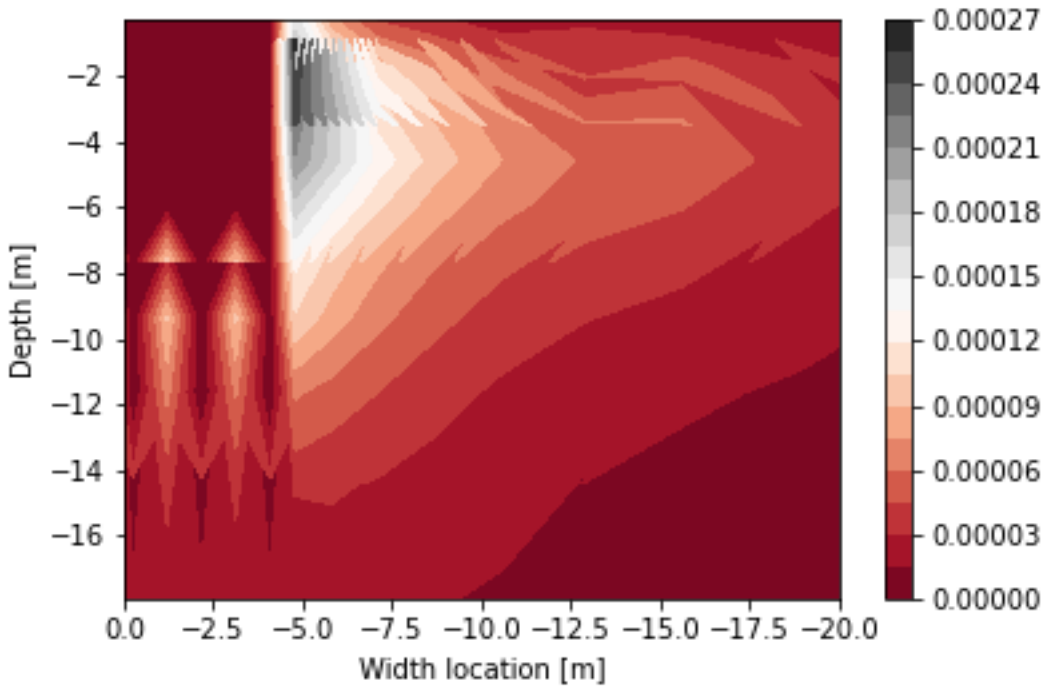
−2
−4
−6
−8
−10
−12
−14
−16
Depth [m]
0.0
−2.5
−5.0
−7.5
−10.0
−12.5
−15.0
−17.5
−20.0
Width location [m]
0.00027
0.00024
0.00021
0.00018
0.00015
0.00012
0.00009
0.00006
0.00003
0.00000

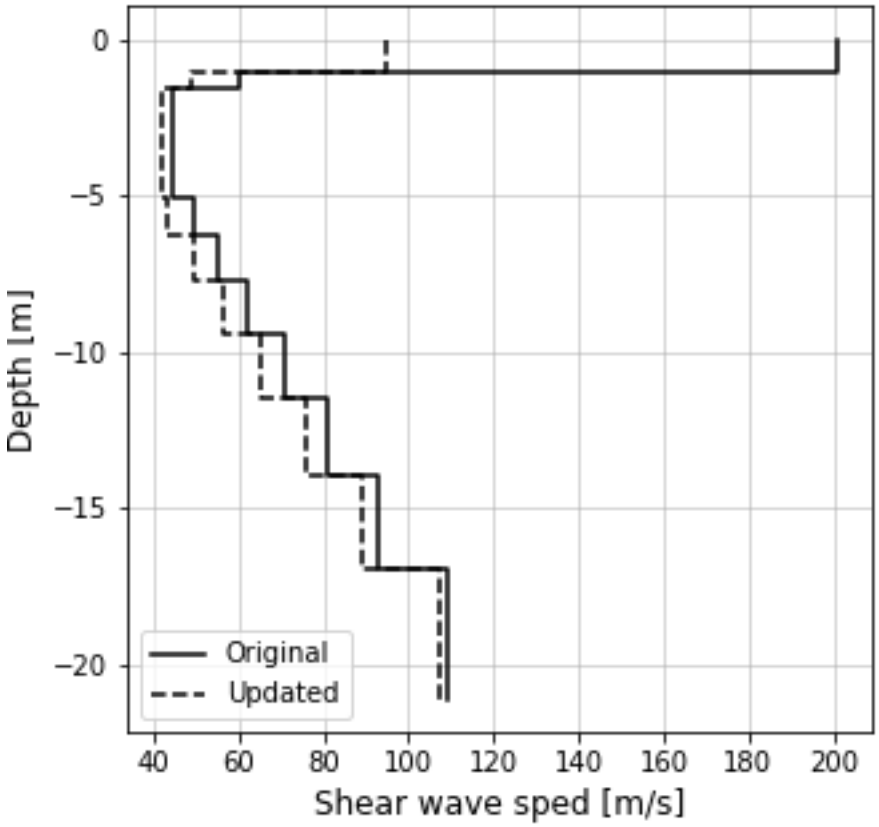
0
−5
−10
−15
−20
Depth [m]
Original
Updated
40
60
80
100
120
140
160
180
200
Shear wave sped [m/s]

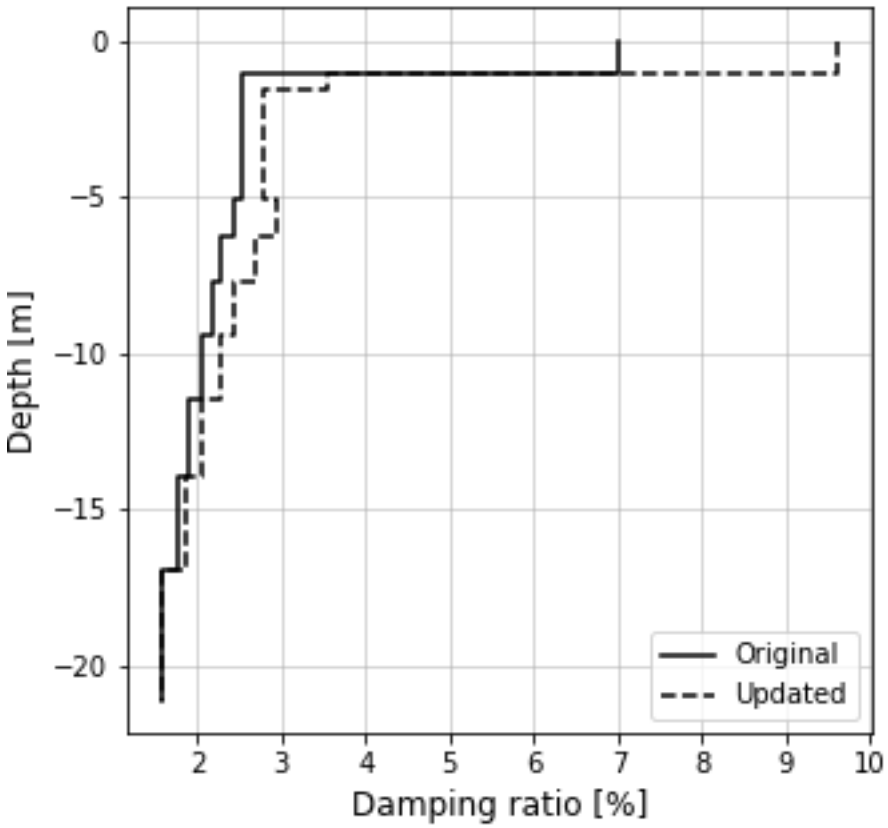
0
−5
−10
−15
−20
Depth [m]
Original
Updated
2
3
4
5
6
7
8
9
10
Damping ratio [%]

# DESIGN OF GROUND FOUNDATION FOR HIGH-SPEED RAILWAYS

**Output - diagrams from the base model program** Case: **Ledsgård with LCC reinforcement**

## Assessment of critical speed

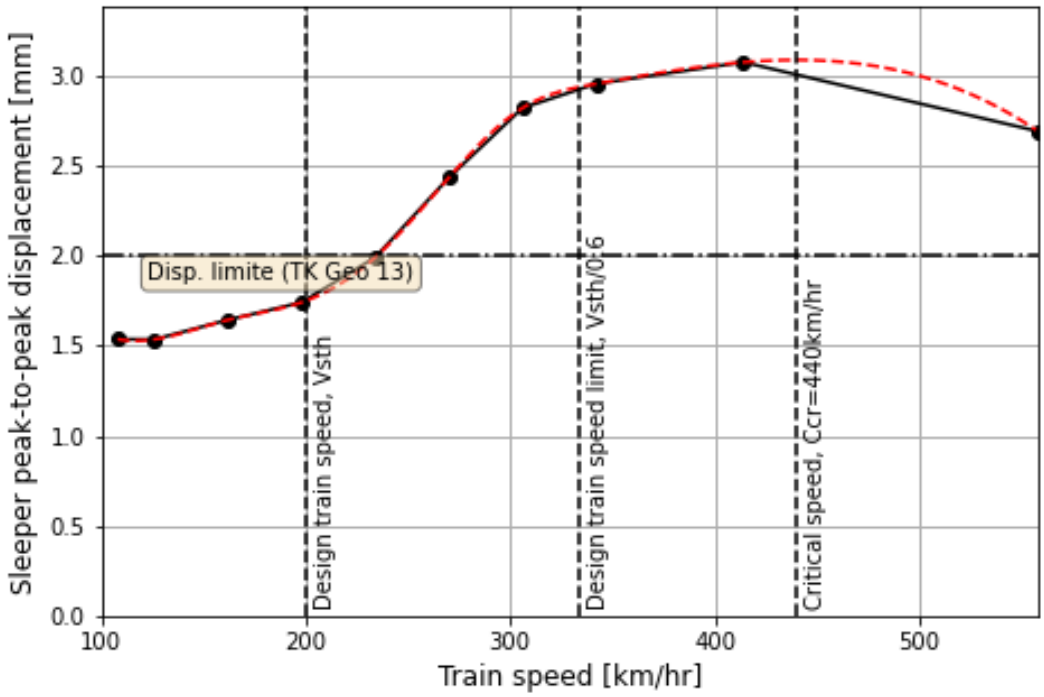


## Receptance analysis

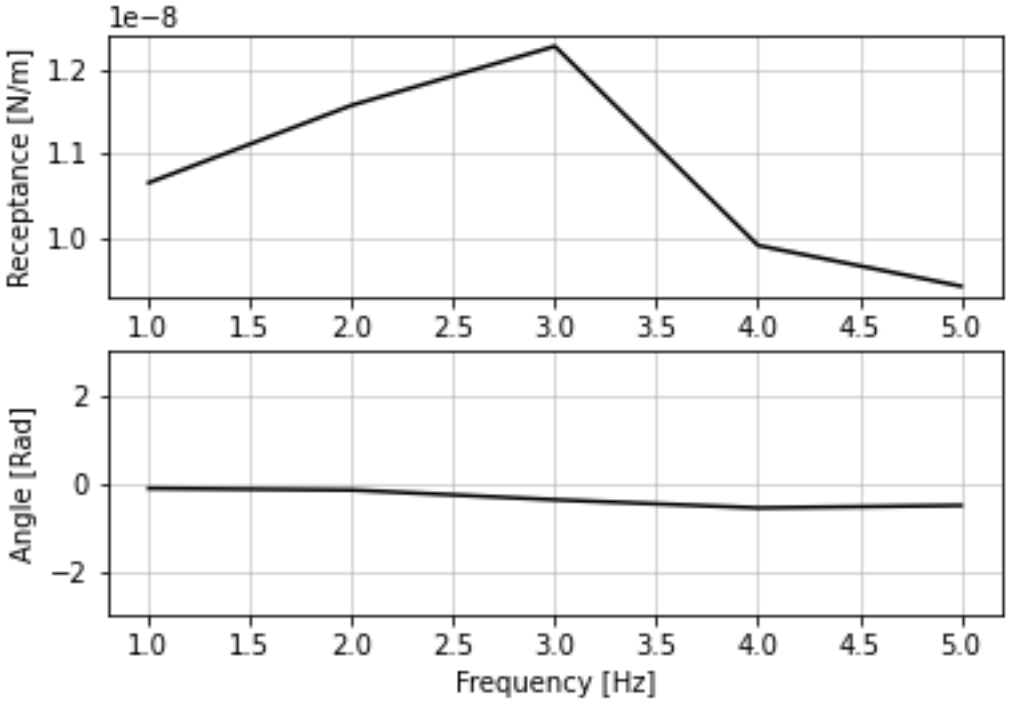

# Appendix D
## VibTrain: input file

The following is an example of input file for the Vibtrain program.

# D1 INDATA

## D1.1 Track data

Line 1

```
NEL,EL,EI,EM,DAMP
300   0.60   3.0E8   32400.0   0.08
```

NEL= Number of track elements (or sleepers) to define the total length of track

EL= Distance between sleepers (m)

EI= Total bending rigidity of track/embankment ($N.m^2$)

EM= Mass per unit length of embankment (kg)

DAMP = Damping ratio of embankment (typical values 0.04 for low vibration, 0.08 for extensive vibration)

## D1.2 Rail data

Line 2

```
EI1, BK1
```

EI1= Rail bending rigidity ($N.m^2$)

BK1= Zimmermann's subgrade modulus ($N/m^3$)

```
6.42e6   5.25e7
```

## D1.3 Extra points outside track for monitoring

(Not used in Vibtrain Stress):

Line 3

```
(NPNT), ELMAX
```

ELMAX= Maximum length to be considered in modeling interaction between sleepers (m) – typically 0.5- 0.8 times total length of track (NEL*EL).

NPNT = No. of side points (for displacement evaluation), Maximum influence distance between nodal points. Nodal points beyond 60, in this example, are not interacting. Could be set to about one third to half of the model length (NEL*EL).(Not used in Vibtrain-Stress version)

```
3   50.0
```

```
(X)
```

X= x-coordinates of observation points on ground surface in m. The x-axis runs along the track with origin at the start of track. Start of model, 0,0 node 1. (Last node on other end of model.). Model is 300x0.6m=180 m long. Middle node of the track is then at 90m.

```
90.0 90.0 90.0
```

```
(Y)
```

Y= y-coordinates of observation points on ground surface in m. The y-axis lies on the ground surface and is normal to the x-axis. Must be smaller than ELMAX. Points located at 5m,.10m, and15m from center of track.

```
5.0 10.0 15.0
```

## D1.4 Soil data

Line 4

```
NLAY, NBASE
```

NLAY= No. of soil layers (maximum 11 layers)

NBASE= 0: bedrock under soil layers ("fixed base"), = 1: half-space under layers

```
7 1
```

Line 5-12

```
T(I),CS(I),RHO(I),B(I),POIS(I)
```

T= Thickness (m) (put 0.0 for half-space)

CS= Shear-wave velocity (m/s)

RHo= Mass density (kg/m$^3$)

B= Damping ratio

POIS= Poisson's Ratio

```
0.5  150.0  1800.0  0.04  0.49
1.0  127.0  1800.0  0.04  0.49
2.0  103.0  1700.0  0.04   0.49
3.0  127.0  1700.0  0.03   0.49
3.0  145.0  1700.0  0.03   0.49
2.0  150.0  1700.0  0.03   0.49
4.5  300.0  1700.0  0.03   0.49
0.0  600.0  1800.0  0.03   0.49
```

## D1.5 Parameters for Green's function:

Line 13

`RP,NTYPE,NKK`

`RP`= Radius of disk load for Greens functions computations under each sleeper (m): set equal to height of embankment times half the sleeper distance. *(RP not to be taken less than half the sleeper spacing).*

`NTYPE`= Type of requested output for motions:

1 = displacement, 2 = velocity, 3 = acceleration

`NKK`= Number of integration points: set equal to 2500

```
0.4  1  2500
```

## D1.6 Axle load data

(position line 14, amplitude line 15):

Line 14

`NAXLE,(AXLE(I),I=1,NAXLE) (iii)` ==> (1 line or more)

`NAXLE`= No. of axle loads

`AXLE(I)` = `NAXLE` values defining the position of the axle loads along an x-axis, starting with 0.0 for the first axle load. If necessary, continue entering values on several lines as shown example below for 20 axle load positions. (Comment: This is old Fortran style may not be necessary to break lines for new code.)

```
20 0.0 3.0 15.0 18.0 22.0 25.0 40.0 43.0 47.0 50.0
65.0 68.0 72.0 75.0 90.0 93.0 97.0 100.0 107.0 110.0
```

Line 15

`(FMOVLD(I),I=1,NAXLE) (iii)` ==> (1 line or more)

- `FMOVLD(I)` = `NAXLE` values giving the axle loads. If necessary, continue entering values on several lines (see example).(should be same number loads as positions above)

```
1.61e5 1.61e5 1.17e5 1.17e5 1.22e5 1.22e5 1.22e5 1.22e5 1.22e5 1.22e5
1.22e5 1.22e5 1.22e5 1.22e5 1.22e5 1.22e5 1.80e5 1.80e5 1.81e5 1.81e5
```

## D1.7 Frequency domain analysis (FFT) data

Line 16

```
NTIM, DT, FMAX,
```

NTIM= Number of time steps, should be a power of 2, typical value = 4096. Used to compute number of frequencies to perform analysis for.

DT= Time step in the time histories (s) – typical values 0.003-0.005.

FMAX= Maximum frequency of interest (Hz) – typical values: 20-30 Hz. "Cut-off frequency".

```
4096  0.004  20.0
```

## D1.8 Train speed data:

Line 17

```
NVEL,VEL
```

NVEL= No. of train speeds (maximum 12 speeds in one run)

VEL= NVEL values defining the train speeds

```
12   34.7   41.7   48.6   55.6   62.5   69.4   76.4   83.3   90.3   97.2
104.2   111.1
```

## D1.9 Monitoring points

(Not used in Vibtrain Stress):

Line 18

```
(NOBS,NUMOBS)
```

NOBS= No. of locations where output is required

NUMOBS = Node number for output points. The point numbering starts with 1 for the first node on the track. Then follow the points on the ground surface (see example below).
Comment:

This is a *bit cumbersome since here the nodal number has to be given. Has to be computed from no. nodal points in the track =no. elements + (300+1 in this example). First nodal point outside the track is then 302, the next 303, and the 3rd point is 304.*

```
1  151 302 303 304
```

# D2 TLV-VIBTRAIN SPECIFIC INPUT DATA CHANGES

For TLV version of Vibtrain a few extra input parameters are needed as marked with red below and some input lines for train axle loads and train speed should be deleted.

The input format is the same as the VibTrain-Stress program (NGI Rep. 20041519-2) except for the following changes:

Rail data:

Line 2

`EI1,BK1,EMR,DAMP1` **`(i)`** `==>` (1 line)

The additional parameters EMR and DAMP1 are the mass (per unit length, in kg) and damping in rail.

Delete input lines for train axle load (load locations and loads) and lines for train speed and replace with the following new lines:

`Nfreq` (1 line)

`FREQ` (in Hz) (Nfreq lines)

# D3 SELECTION OF ZIMMERMANN'S TRACK PARAMETER

Assuming the width of the sleeper (the dimension parallel to the rail – typical 0.15m) is w, the height of the embankment is h, and the average elastic modulus of the embankment is E. Then the Zimmermann stiffness is computed from Ksl = E (w + 0.5h)/h; then BK1 = Ksl (see line 2. above)

If there exists a pad under the rail with stiffness Kp then the equivalent stiffness BK1 is calculated from

$$\frac{1}{BK1} = \frac{1}{K_{sl}} + \frac{1}{K_p} \qquad \textit{(Equation D3.1)}$$